Univerzita Karlova

1. lékařská fakulta

Studijní program: Biochemie a patobiochemie

Studijní obor: YBICH18

Ing. Anna Mengr (roz. Zmeškalová)

Neuroprotektivní účinky nových anorektických analogů peptidu uvolňujícího prolaktin (PrRP) v modelech neurodegenerace *in vitro* a *in vivo*

Neuroprotective effects of novel anorexigenic analogs of prolactin-releasing peptide (PrRP) in models of neurodegeneration *in vitro* and *in vivo*

Disertační práce

Školitelka: RNDr. Lenka Maletínská, CSc.

Praha, 2022

Prohlášení:

Prohlašuji, že jsem závěrečnou práci zpracovala samostatně a že jsem řádně uvedla a citovala všechny použité prameny a literaturu. Současně prohlašuji, že práce nebyla využita k získání jiného nebo stejného titulu.

Souhlasím s trvalým uložením elektronické verze mé práce v databázi systému meziuniverzitního projektu Theses.cz za účelem soustavné kontroly podobnosti kvalifikačních prací.

V Praze, dne 25. 7. 2022

Anna Mengr

Identifikační záznam:

MENGR, Anna. *Neuroprotektivní účinky nových anorektických analogů peptidu uvolňujícího prolaktin (PrRP) v modelech neurodegenerace in vitro a in vivo. [Neuroprotective effects of novel anorexigenic analogs of prolactin-releasing peptide (PrRP) in models of neurodegeneration in vitro and in vivo.* Praha, 2022. 140 stran, 4 přílohy. Disertační práce. Univerzita Karlova, 1. lékařská fakulta, Klinika / Ústav 1. LF UK 2008. Ústav organické chemie a biochemie Akademie věd České republiky, v.v.i. Vedoucí disertační práce Maletínská, Lenka.

ABSTRAKT

Alzheimerova choroba (AD) je progresivní mozková porucha charakterizovaná extracelulárními beta amyloidními (Aβ) plaky, intracelulárními neurofibrilárními klubky tvořenými hyperfosforylovaným proteinem Tau a zánětem. Vzhledem k tomu, že obezita a diabetes mellitus 2. typu (T2DM) byly stanoveny jako rizikové faktory pro rozvoj neurologických poruch, anorexigenní a antidiabetické peptidy, jako je peptid uvolňující prolaktin (PrRP), se zdají být potenciálními neuroprotektivními látkami.

V první části práce byly studovány molekulární mechanismy účinku přirozeného PrRP31 a jeho lipidovaného analogu palm^{11}-PrRP31 v buněčné linii lidského neuroblastomu SH-SY5Y. Oba peptidy významně aktivovaly signální dráhy typické pro insulin podporující přežití a růst buněk. Kromě toho PrRP31 a palm^{11}-PrRP31 zvýšily životaschopnost buněk a potlačily apoptózu v buňkách SH-SY5Y stresovaných methylglyoxalem.

Druhá část práce byla zaměřena na neuroprotektivní a protizánětlivé účinky v mozku APP/PS1 myší, modelu Aβ patologie, po subkutánním podávání palm^{11}-PrRP31 po dobu 2 měsíců. Palm^{11}-PrRP31 signifikantně snížil množství Aβ plaků a mikrogliózu v hipokampech, kortexech a mozečku. Kromě toho palm^{11}-PrRP31 zvýšil synaptogenezi a zmírnil centrální zánět a apoptózu v hipokampu myší APP/PS1.

Ve třetí části práce byl sledován potenciální vztah mezi insulinovou rezistencí a AD v mozcích a periferii myší APP/PS1 krmených dietou s vysokým obsahem tuků (HFD), modelu spojujícím obezitu a patologii podobnou AD. HFD zhoršila Aβ patologii v hipokampech a významně ovlivnila jak centrální, tak periferní zánět. Kromě toho se u myší na HFD vyvinula výrazná periferní inzulínová rezistence vedoucí k centrální inzulínové rezistenci. Studie odhalila škodlivý vliv zánětu souvisejícího s obezitou a prediabetem na rozvoj Aβ patologie a zánětu v mozku a potvrdila periferní a centrální zánět a inzulínovou rezistenci jako potenciální mediátory mozkové dysfunkce u AD.

Závěrem je možné konstatovat, že PrRP a jeho analog palm^{11}-PrRP31 potlačují patologii podobnou AD, díky snižování zánětu v periferii i v mozku, aktivaci insulinové signalizační kaskády, tvorbě nových synapsí, redukci Abeta plaků a snižování hyperfosforylace proteinu Tau.

KLÍČOVÁ SLOVA

Alzheimerova choroba, obezita, zánět, centrální zánět, APP/PS1 myši, Aβ plaky, Tau, inzulinová rezistence, buňky SH-SY5Y, peptid uvolňující prolaktin

ABSTRACT

Alzheimer´s disease (AD) is a progressive brain disorder characterized by extracellular beta amyloid (Aβ) plaques, intracellular neurofibrillary tangles formed by hyperphosphorylated Tau protein and neuroinflammation. Since obesity and type 2 diabetes mellitus (T2DM) have been established as risk factors for the development of neurological disorders, anorexigenic and antidiabetic peptides, such as prolactin-releasing peptide (PrRP) seem to be potential neuroprotective agents.

In the first part of the study, the molecular mechanisms of action of natural PrRP31 and its lipidized analog palm^{11}-PrRP31 was studied in the human neuroblastoma cell line SH-SY5Y. Both compounds significantly activated the signaling pathways typical for insulin promoting cell survival and growth. Moreover, PrRP31 and palm^{11}-PrRP31 increased cell viability and suppressed apoptosis in methylglyoxal-stressed SH-SY5Y cells.

The second part of the thesis was focused on the neuroprotective and anti-inflammatory effects of 2-month-long subcutaneous administration of palm^{11}-PrRP31 in the brains of APP/PS1 mice, model of Aβ pathology. Palm^{11}-PrRP31 significantly reduced the Aβ plaque load and microgliosis in the hippocampi, cortices, and cerebella. Furthermore, palm^{11}-PrRP31 increased the synaptogenesis and attenuated neuroinflammation and apoptosis in the hippocampus of APP/PS1 mice.

In the third part of the thesis, a potential relationship between insulin resistance and AD was followed in the brains and periphery of APP/PS1 mice fed with high-fat diet (HFD), the model connecting obesity and AD-like pathology. HFD worsened the Aβ pathology in hippocampi and significantly affected both central and peripheral inflammation. Furthermore, mice on HFD developed substantial peripheral insulin resistance leading to central insulin resistance. The study revealed a deleterious effect of obesity-related inflammation and pre-diabetes on the development of Aβ pathology and neuroinflammation and confirmed peripheral and central inflammation and insulin resistance as potential mediators of brain dysfunction in AD.

In conclusion, my thesis proves beneficial effect of PrRP in the AD-like pathology, suggesting palm^{11}-PrRP31 as a promising agent for the treatment of AD.

KEY WORDS:

Alzheimer´s disease, obesity, inflammation, neuroinflammation, APP/PS1 mice, Aβ plaques, Tau, insulin resistance, SH-SY5Y cells, prolactin-releasing peptide

ACKNOWLEDGEMENT

Firstly, I would like to express my gratitude to my PhD thesis supervisor, Dr. Lenka Maletínská for giving me the opportunity to work in her group and also for her guidance and sharing her expertise during the elaboration of my thesis. I would like to thank the whole team of Antiobesity peptides of Dr. Maletínská from the Institute of Organic Chemistry and Biochemistry, Czech Academy of Sciences, especially to Dr. Blanka Železná, Dr. Andrea Pačesová and Dr. Jaroslav Kuneš for their valuable advice during my research and comments during my thesis writing, Aneta Stružová, MSc. and Lucie hrubá, MSc. for their help with the experimental part of my thesis, Martina Kojecká, MSc. for RIA and ELISA measurement, Dr. Veronika Strnadová for liver histology and Hedvika Vysušilová for her excellent technical assistance. Furthermore, I would like to acknowledge Miroslava Blechová, MSc. for peptide synthesis.

I would also like to thank the whole team of Dr. Luc Buée for a warm welcome to their group Alzheimer&Tauopathies from INSERM UMR-S-1172 in Lille, France, especially to group of Dr. Marie-Christine Galas, namely to Marine Denéchaud, MSc., Thomas Comptdaer, MSc., Sarra Kraïem, MSc. and Raphaelle Caillierez, MSc. for extending my knowledge in immunohistochemistry, their helpful approach and kindness.

I would like to thank Lucia, Alena and Lucie for their cooperation throughout my studies.

Finally, I would like to thank my awesome family and especially my husband Miroslav, who kept me strong, supported me lovingly and encouraged me throughout my studies.

The PhD theses was supported by the Grant Agency of the Czech Republic No. 20-00546S, Technology Agency of the Czech Republic (PerMed) No. TN01000013, the Academy of Sciences of the Czech Republic RVO:61388963 and RVO:67958523 and from European Regional Development Fund; OP RDE; Project: „IOCB Mobility II“ No. CZ.02.2.69/0.0/0.0/18_053/0016940.

CONTENTS

ABBREVIATIONS 12

1. INTRODUCTION 14

1.1 CURRENT STATE OF KNOWLEDGE 14

1.1.1 Alzheimer´s disease (AD) 14

1.1.2 AD discovery 14

1.1.3 AD and the brain 14

1.1.4 AD staging 17

1.1.5 Hallmarks of AD 17

1.1.5.1 Aβ plaques 17

1.1.5.2 Neurofibrillary tangles 19

1.1.5.3 Neuroinflammation 21

1.1.5.3.1 Microglia 21

1.1.5.3.2 Astrocytes 22

1.1.5.4 Brain insulin signaling 24

1.1.5.5 Loss of synapses 27

1.1.5.6 Diagnosis of AD 27

1.1.6 Current AD treatment 28

1.1.6.1 AD risk factors 29

1.1.6.1.1 Ageing 29

1.1.6.1.2 Obesity 29

1.1.6.1.3 Type 2 diabetes mellitus (T2DM) 31

1.1.6.1.4 Disrupted blood-brain barrier 32

1.2 Models of neurodegeneration, obesity and T2DM 33

1.2.1 Models of neurodegeneration 33

1.2.1.1 Cellular models of neurodegeneration 33

1.2.1.1.1 SH-SY5Y cell line 33

1.2.1.1.2 Primary neuronal culture 34

1.2.1.2 Mouse models of AD 35

1.2.1.2.1 APP/PS1 transgenic mouse model 35

1.2.1.2.2 3xTgAD mouse model 36
1.2.1.2.3 5xFAD mouse model 36
1.2.2 Mouse models of obesity and T2DM 36
1.2.2.1.1 Model of diet-induced obesity 36
1.3 Food intake regulating peptides as a potential treatment of AD 37
1.3.1 GLP-1 analogs 37
1.3.1.1 Exenatide 38
1.3.1.2 Liraglutide 39
1.3.1.3 Semaglutide 39
1.3.2 Prolactin-releasing peptide analogs 40
2. AIMS OF THE THESIS 42
3. METHODS 43
3.1 Peptides 43
3.2 *In vitro* studies 43
3.2.1 Cell lines 43
3.2.2 Cellular signaling triggered by PrRP and palm^{11}-PrRP 44
3.2.3 Western blotting 45
3.2.4 Cell Viability Measurement 45
3.2.4.1 Activation of apoptic pathways by MG and its prevention by PrRP31 and palm^{11}-PrRP31 46
3.2.5 Analysis of data and statistics 46
3.3 Animal models – study designs, housing, and treatment 46
3.3.1 Treatment of APP/PS1 mice on standard diet 46
3.3.2 Impact of HFD on metabolic parametres and AD-related pathology in APP/PS1 and WT mice 48
3.4 Oral glucose tolerance test 49
3.5 Blood sampling 49
3.5.1 Determination of hormonal and biochemical parameters in fasting plasma 49
3.5.2 Determination of CRP 50

3.6 Organ dissections 50
3.6.1 Brains 50
3.6.1.1 Immunohistochemistry 50
3.6.1.2 Tissue Preparation for WB 52
3.6.2 Livers 54
3.6.2.1 Liver histology 54
3.6.2.2 Tissue preparation for WB 54
3.6.3 eWAT 55
3.6.3.1 Tissue preparation for WB 55
3.6.4 Muscles 55
3.6.4.1 Tissue Preparation for WB 55
3.6.5 Quantification of cytokine level 56
3.6.6 Statistical analyses 56
4. RESULTS 57
4.1 Cellular signaling and anti-apoptotic effects of PrRP and its lipidized analog palm^{11}-PrRP31 on SH-SY5Y cells 57
4.1.1 PrRP31 and palm^{11}-PrRP31 activated the PI3K/Akt signaling pathway in SH-SY5Y cells 57
4.1.2 PrRP31 and palm^{11}-PrRP31 activated the ERK-CREB signaling pathway in SH-SY5Y cells 57
4.1.3 Specific inhibitors of signaling proteins confirmed that PrRP31 and palm^{11}-PrRP31 activated m-Tor, ERK and GSK-3β in SH-SY5Y cells 59
4.1.4 PrRP31 and its lipidized analog attenuated methylglyoxal-induced cytotoxicity in SH-SY5Y cells and rat cortical neurons 61
4.1.4.1 PrRP31 and palm^{11}-PrRP31 prevented SH-SY5Y cells from the cytotoxic effects of MG 61
4.1.4.2 PrRP and palm^{11}-PrRP31 increased the viability of SH-SY5Y cells after 16 h of exposure to MG 62
4.1.4.3 PrRP31 and palm^{11}-PrRP31 induced anti-apoptotic signaling in SH-SY5Y cells 63

4.1.4.4 PrRP31 and palm^{11}-PrRP31 attenuated Tau hyperphosphorylation at different epitopes in SH-SY5Y cells 65

4.2 Effect of palm^{11}-PrRP31 analog on pathological markers connected to AD in APP/PS1 mice on standard diet..... 65

4.2.1 Effects of palm^{11}-PrRP31 on body weight and metabolic parameters 66

4.2.2 Palm^{11}-PrRP31 reduced the Aβ plaque load, microgliosis and astrocytosis in the hippocampi and cortices of APP/PS1 mice 66

4.2.3 Palm^{11}-PrRP31 reduced the Aβ plaque load and microgliosis in the cerebella of APP/PS1 mice 68

4.2.4 Palm^{11}-PrRP31 reduced neuroinflammation in the hippocampi of APP/PS1 mice 70

4.2.5 Palm^{11}-PrRP31 decreased apoptosis in the hippocampi of APP/PS1 mice 71

4.2.6 Palm^{11}-PrRP31 increased synaptogenesis in APP/PS1 mice..... 71

4.2.7 Palm^{11}-PrRP31 improved the glymphatic system in APP/PS1 mice... 74

4.2.8 Palm^{11}-PrRP31 decreased the protein levels of p-m-Tor and LRP1 in the brains of APP/PS1 mice 76

4.3 Impact of HFD on metabolic parametres and neurodegeneration in APP/PS1 and WT mice 78

4.3.1 Effect of HFD on BW, eWAT weight and metabolic parametres 78

4.3.2 HFD caused peripheral inflammation 81

4.3.3 HFD caused liver steatosis 81

4.3.4 Markers related to peripheral insulin resistance 83

4.3.4.1 HFD and age attenuated the PI3K/Akt signaling pathway in the liver 83

4.3.4.2 HFD reduced the PI3K/Akt signaling pathway in eWAT 83

4.3.4.3 HFD attenuated the PI3K/Akt signaling pathway in the skeletal muscle 86

4.3.5 Effects of HFD on the development of AD-like pathology 89

4.3.5.1 HFD exacerbated the Aβ plaque load in the hippocampi and cortices of APP/PS1 mice 89
4.3.5.2 HFD worsened neuroinflammation in the brains of APP/PS1 mice ……...90
4.3.5.3 Increased Tau phosphorylation in the hippocampi and cortices of APP/PS1 mice ……..92
4.3.5.4 HFD and age attenuated the PI3K/Akt signaling pathway in the hippocampus 93
4.3.5.5 Decreased neuronal density and neurogenesis with age of mice . 93
4.3.5.6 HFD decreased synaptogenesis in the hippocampus of APP/PS1 mice 97
4.3.6 Decrease in markers connected to disrupted BBB in APP/PS1 mice... 98
5. DISCUSSION..... 101
5.1 Cell signaling pathways induced by PrRP31 and palm^{11}-PrRP31 in SH-SY5Y cells..... 101
5.2 Potential neuroprotective and anti-apoptotic effects of PrRP31 and palm^{11}-PrRP31 in SH-SY5Y cells and rat cortical neurons..... 104
5.3 Effect of palm^{11}-PrRP31 analog on pathological markers connected to AD in APP/PS1 mice on standard diet..... 106
5.4 Impact of HFD on metabolic parametres and development of AD-like pathology in APP/PS1 and WT mice..... 111
5.4.1 Peripheral effects of HFD..... 111
5.4.2 Central effects of HFD..... 113
6. SUMMARY..... 117
7. CONCLUSIONS..... 118
8. REFERENCES..... 120

ABBREVIATIONS

Aβ	amyloid β
Ab	antibody
AD	Alzheimer´s disease
APP	amyloid precursor protein
AQ4	aquaporin-4
AT	adipose tissue
AUC	area under curve
Bad	Bcl-2-associated death promoter
Bax	Bcl-2-associated X protein
BBB	blood-brain barrier
BMI	body mass index
BW	body weight
CA	cornu ammonis
CNS	central nervous system
CRP	c-reactive protein
CSF	cerebrospinal fluid
DCX	doublecortin
DIO	diet-induced obesity
DMSO	dimethyl sulfoxid
ERK	extracellular regulatory kinase
eWAT	epididymal white adipose tissue
FDG	fluorodeoxyglucose
GAPDH	glyceraldehyde 3-phosphate dehydrogenase
GFAP	glial fibrillary acidic protein
GIP	glucose-dependent insulinotropic peptides
GLP-1	glucagon-like peptide 1
GLUT	glucose transporter
GSK-3β	glycogen-synthase kinase-3beta
HF/HFD	high-fat/high-fat diet
HOMA-IR	homeostatic model assessment for insulin resistance
IAPP	islet amyloid polypeptide
Iba1	ionized calcium-binding adapter molecule 1
IDE	insulin degrading enzyme
IFN	interferon
IHC	immunohistochemistry
IL	interleukin
IR	insulin resistance
IRβ	insulin receptor β
JNK	c-Jun N-terminal kinase
LRP1	low-density lipoprotein receptor-related protein 1
MAP	mitogen-activated protein
MAPK	mitogen-activated protein kinase
MG	methylglyoxal

MRI	magnetic resonance imaging
MSG	monosodium glutamate
m-Tor	mammalian target of rapamycin
MWM	Morris water maze
NFT	neurofibrillary tangles
NMDA	N-methyl-d-aspartate
NO	nitric oxide
OGTT	oral glucose tolerance test
PBS	phosphate-buffered saline
PET	positron emission tomography
PI3K	phosphoinositide 3-kinase
PrRP	prolactin releasing peptide
PSD95	postsynaptic density protein
RT	room temperature
s.c.	subcutaneous
ST/STD	standard/standard diet
TBS	Tris-buffered saline
T2DM	type 2 diabetes mellitus
TNF	tumor necrosis factor
TREM2	triggering receptor expressed on myeloid cells 2
WB	western blot
WT	wild-type

1. INTRODUCTION

1.1 CURRENT STATE OF KNOWLEDGE

1.1.1 Alzheimer´s disease (AD)

Alzheimer's disease (AD) is an age-associated neurological disorder, and it is the most common type of dementia globally, accounting for 60 - 80% of all dementia cases. AD is a progressive disease with gradually worsening symptoms that deteriorate life quality not only of the patients, but also of their caregivers (Duong et al., 2017).

1.1.2 AD discovery

In 1906, German psychiatrist Dr. Alois Alzheimer firstly described "a peculiar severe disease process of the cerebral cortex", later known as AD in the case of Auguste Deter, a 51-year-old woman, whom he had monitored for 5 years from her admission for paranoia, progressive sleep and memory disturbance, aggression, and confusion, until her death. Alzheimer´s report noted abnormally thinner cerebral cortex, distinctive plaques and neurofibrillary tangles (NFT) in the brain histology. Despite the significance of the discovery, little importance was given to his report at that time. A few years later his colleague Emil Kraepelin proposed to name the disease as Alzheimer´s disease (Hippius and Neundörfer, 2003, Berchtold and Cotman, 1998).

1.1.3 AD and the brain

The brain consists of 100 billion neurons, each of them connected to many others, forming communication networks. The brain areas differ in the neuronal types they contain, input they receive, and types of connections they make with other brain areas. These structural differences result in functional differences making the brain areas specialized for different processes (Ackerman, 1992).

In AD, neurons are injured and die throughout the brain, connections between neurons break down and brain regions begin to shrink, which results in significant loss of brain volume in the final stages of AD, mainly in the brain regions important for the memory formation and language (Bloom, 2014).

One of the most vulnerable brain areas damaged during AD and one of the earliest to be affected by the disease is hippocampus (shown in Figure 1) (Braak et al., 1993). Hippocampus is part of a limbic lobe and has a critical role in learning and memories forming (Squire, 1992) by long-term potentiation and synaptic remodeling (Bliss and Lomo, 1973, Matsuzaki et al., 2004). Hippocampus consists of Cornu ammonis 1-3 (CA) and dentate gyrus (DG), separated by hippocampal sulcus (Anand and Dhikav, 2012, Mu and Gage, 2011).

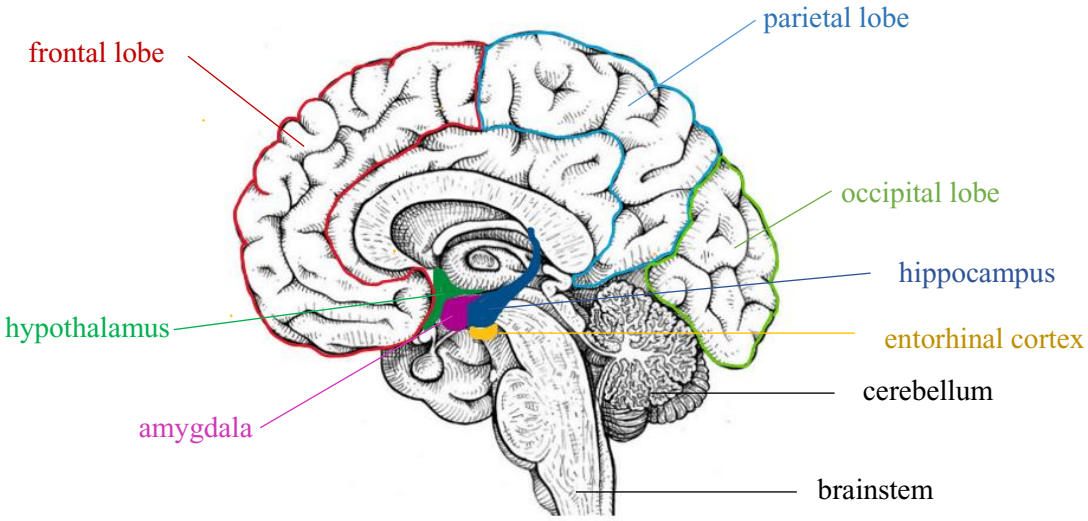

Figure 1. Brain structures.

Besides the hippocampus, the entorhinal cortex is the first area of the brain, which is affected with AD. The entorhinal cortex is located in the medial temporal lobe between the hippocampus and neocortex and plays an important role in memory formation, memory consolidation, and memory optimization in sleep (Khan et al., 2014, Van Hoesen et al., 1991).

Brainstem may be a part of an important pathologic core in AD progression as brainstem nuclei are interconnected with several cortical structures and regulate several autonomic, cognitive, and behavioral functions. During the early stages of AD, brainstem neurodegeneration might result in the erratic sleep patterns and emotional disturbances (Montplaisir et al., 1995) and in the later stages in autonomic dysfunctions, such as difficulties in swallowing, breathing and arrhythmia (Rüb et al., 2001, Lee et al., 2015).

Another important brain region early and severely affected in AD is amygdala, which is responsible for the experiences and expressions of emotion. The amygdala is located in the medial temporal lobe, just anterior to the hippocampus and in AD patients shows a considerable shrinkage, distortion, neuronal loss, and widespread gliosis. If this region is attacked, personality changes and the disruption in fear and pleasure responses could occur (Cuénod et al., 1993, Schafe et al., 2005).

Cerebellum, brain region affected in later stages of dementia, is linked to coordination of voluntary movement, gait, posture, speech, and motor functions. It is also believed to help with control of cognition and behavior. The role of the cerebellum in AD has been neglected for a long time, but recent studies have demonstrated that cerebellum is affected via synaptic transmission and plasticity (Hoxha et al., 2018, Singh-Bains et al., 2019).

Metabolic and non-cognitive manifestations of AD such as feeding, sleep and circadian rhytm disorders can occur even before the onset of cognitive symptoms and worsen with disease progression (Saper and German, 1987). A major culprit of these signs could be a substantial decrease in the neuronal number and a loss of dendritic branches in the hypothalamus. Hypothalamus is a brain region critical for integrating peripheral signals with essential homeostatic physiological functions (Baloyannis et al., 2015, Hiller and Ishii, 2018).

Frontal lobe, which handles executive functions, such as planning, judgement, motivation, and behaviour, is also often damaged by AD. The result is a loss of motivation, making the person becoming tired, lethargic, and struggling to get out of bed (Hirono et al., 1998).

Also, parietal lobe, responsible for spatial relationships, perception and magnitude and for the sense over the body could be attacked in AD. This results in forgetting of common movements, not recognising objects, faces or surroundings (Jacobs et al., 2012).

The occipital lobe participates in processing and interpreting of the vision. Pathology of the occipital lobe may occur in sporadic late onset AD and if, the patients may misinterpret their environment through illusions, misperceptions, and misidentification. Damage to this region may also result in hallucinations (Holroyd et al., 2000).

1.1.4 AD staging

Heiko Braak observed that AD pathology in the brain can be distinguished with respect to the location of the tangle-bearing neurons and the severity of changes into six stages of the disease propagation that could be according to the degree of cognitive impairment further subdivided into 3 stages: entorhinal, limbic, and isocortical (Braak et al., 2011). The first transentorhinal stage of AD is clinically silent, with no apparent symptoms in patient's behavior. There is starting pathology in entorhinal cortex and in CA1 of the hippocampus. Further, in the incipient AD in the phase called limbic stage, the disease spreads to other hippocampal regions and to the centers such as amygdala and thalamus. In this phase clinical symptoms of cognitive decline occur manifested by problems with recognizing, speaking and forgetting. Later, alternations in the person´s behavior such as apathy, aggression, and psychosis are observed. In the last stage that is called the isocortical stage, pathology in neocortex, widened brain ventricles and reduced brain weight are noticed. The patients get disoriented and unable to take care of themselves (Serrano-Pozo et al., 2011, Braak et al., 2011).

1.1.5 Hallmarks of AD

Two major histopathological hallmarks of AD are intracellular NFTs formed by hyperphosphorylated Tau protein and extracellular senile plaques formed by amyloid-β (Aβ) peptide. In addition to the two major hallmarks, AD is characterized by neuroinflammation, extensive loss of synapses, loss of neurons in vulnerable regions and subsequent structural changes in the brain, including hippocampal volume loss, brain atrophy and disturbed glucose metabolism in the brain (Bloom, 2014, Serrano-Pozo et al., 2011, Zilberter and Zilberter, 2017). As shown in Figure 2, Aβ plaques are obvious in preclinical stage of AD, and precede manifestation of dementia, while NFT formation increases later during the AD progression.

1.1.5.1 Aβ plaques

Although the number of NFT correlates more strongly with the degree of dementia than does the number of plaques, genetic and pathologic findings indicate that Aβ peptide

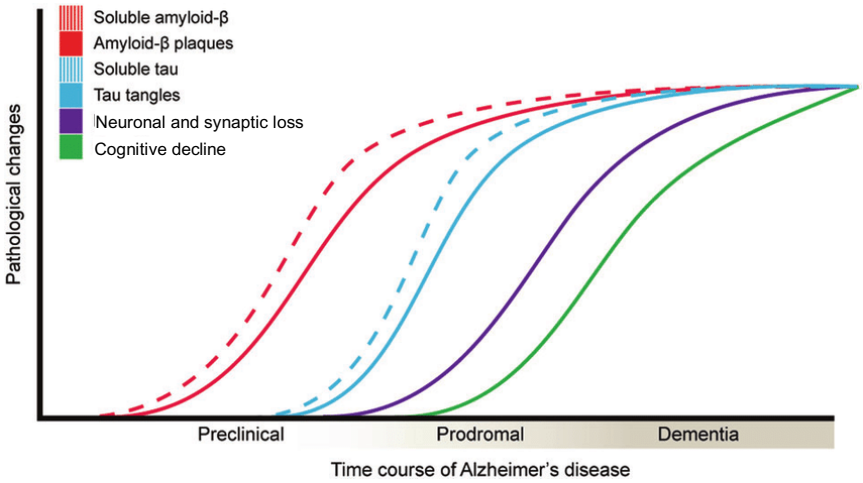

Figure 2: Development of pathogenesis of AD. Hypothetical time course of pathological changes in Alzheimer's disease (AD), in which biomarkers for amyloid-β become abnormally increase, followed by abnormal increase in Tau tangles, synaptic and neuronal loss, and cognitive decline (Leuzy et al., 2019).

plays a central role in the risk, onset, and progression of AD (Rukmangadachar and Bollu, 2022). Aβ plaques are extracellular deposits of Aβ peptides, products of proteolyticcleavage of amyloid precursor protein (APP), that is present most abundantly in the brain, but also in the periphery. APP can be cleaved by α-, β- and γ-secretase. In the physiological state, Aβ peptide is believed to be a nontoxic player in neuronal cell survival and is a product of sequential α- and γ-secretase cleavage of APP (Pearson and Peers, 2006). However, under pathophysiological conditions, APP starts to be cleaved in amyloidogenic pathway by β- and γ-secretase, which results in the production of Aβ peptides with 40 (Aβ40), or 42 (Aβ42) amino acids as shown in Figure 3 (Newcombe et al., 2018). Aβ40, but mainly Aβ42 form toxic oligomers, which polymerize into fibrils and finally are stored as senile plaques, highly variable in shape and size (Tabaton et al., 2010, Špolcová, 2015). Misfolded and aggregated Aβ, especially in its oligomeric state is also thought to be neurotoxic and play an important role in the onset of AD pathology (Haass and Selkoe, 2007). Small number of senile plaques can be developed in the ageing brain as a result of their senescence, but abnormally large numbers are characteristic feature for AD pathology (Ballard et al., 2011). An excessive cummulation of Aβ peptide can contributte to imbalance between its production and clearance (Mawuenyega et al., 2010).

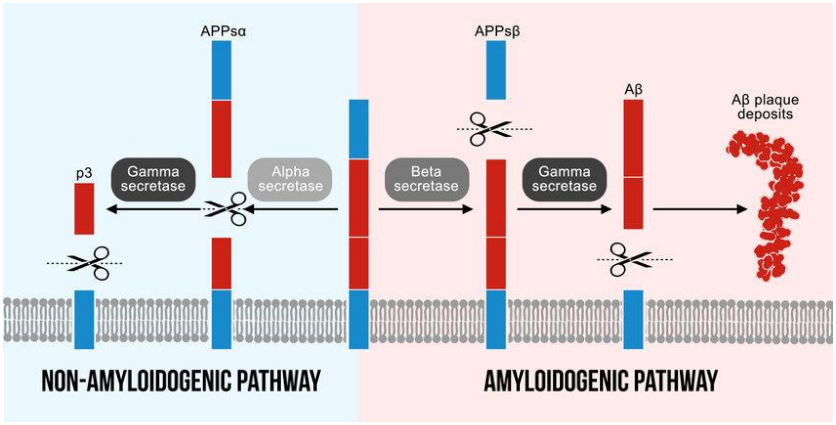

Figure 3: Non-amyloidogenic and amyloidogenic pathways diagram. Visualization of amyloid precursor protein (APP) and its role in both pathways; physiological non-amyloidogenic pathway, and amyloidogenic pathway which leads to production of toxic Aβ oligomers, and subsequently to Aβ plaque formation (Sasmita, 2019).

1.1.5.2 Neurofibrillary tangles

NFT are intracellular aggregates of Tau protein, which is naturally expressed by neurons, localized into axons and at low level into dendrites (Laurent et al., 2018), but it is also found in peripheral tissues such as muscles, heart, or kidney (Goedert et al., 1989). Tau belongs to the group of microtubule-associated proteins (MAPs) and is responsible for microtubule stability through the interactions with α- and β-tubulin and thus for stabilization of the axons of neurons (Weingarten et al., 1975, Ding et al., 2006). Furthermore, Tau protein participates in the maintenance of synaptic plasticity (Bukar Maina et al., 2016).

Tau protein can undergo several post-translational modifications, such as phosphorylation, O-GlcNAcylation, or glycation, which are important for its biological functions. Tau is a phosphoprotein with almost 80 potential serine (Ser) and threonine (Thr) phosphorylation sites. Phosphorylation of Tau is regulated by many protein kinases and protein phosphatases which can either directly or indirectly phosphorylate or dephosphorylate the Tau protein. The most important kinases implicated in Tau hyperphosphorylation are glycogen-synthase kinase-3beta (GSK-3β) (Cho and Johnson, 2004, Takashima, 2006), c-Jun N-terminal kinase (JNK) (Atzori et al., 2001), cyclin-dependent kinase 5 (Alvarez et al., 2001, Jicha et al., 1999), mitogen-activated protein kinase/extracellular regulatory kinase (MAPK/ERK) (Ekinci and Shea, 1999), or protein

kinase A (Lee and Leugers, 2012).The main role in Tau dephosphorylation has protein phosphatase 2A that comprises more than 70 % of the brain phosphatase activity, the others are protein phosphatase 1 and 5 etc (Martin et al., 2013).

Physiological phosphorylation of Tau protein is crucial for its function, however, increased phosphorylation negatively influences its function in microtubule assembly and stabilization (Lindwall and Cole, 1984). For example, phosphorylation at epitope Thr231 reduces the ability to bind to microtubules, phosphorylation at Ser396 turns Tau to more fibrillogenic protein, and phosphorylation of Ser422 results in an increased aggregation of the Tau protein (Johnson and Stoothoff, 2004, Alonso et al., 2010) (Alonso et al., 2010, Andrea). Moreover, hyperphosphorylated Tau does not bind to microtubules but instead of that dimerizes into paired helical fillaments that aggregate into NFT, as shown in Figure 4 (Grundke-Iqbal et al., 1986).

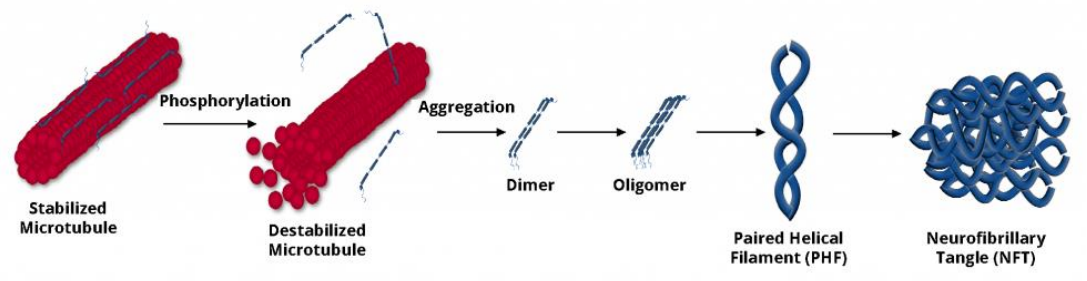

Figure 4: Formation of neurofibrillary tangles. Tau dissociates from microtubules, leading to their destabilization. It then aggregates into dimers, oligomers, paired helical filaments, and ultimately neurofibrillary tangles (www.stressmarq.com).

Another post-translational modification affecting Tau is O-GlcNAcylation. Glycosylation sites are the same as the phosphorylation sites. Brain glucose metabolism, which is essential for proper brain function, is impaired in AD and can lead to decrease in O-Glc-NAcylation of Tau protein. In the brains of AD patients and type 2 diabetes mellitus (T2DM) patients, decreased numbers of glucose transporters 1 and 3 (GLUTs) were observed. Decreased brain intracellular glucose level subsequently caused attenuation of hexosamine biosyntetic pathway, resulting in decreased O-GlcNAcylation of the Tau protein. Decrease in O-GlcNAcylation positively correlated with increased

hyperphosphorylation of the Tau protein at epitopes implicated in AD development (Gong et al., 2006, Liu et al., 2009, Špolcová, 2015).

1.1.5.3 Neuroinflammation

Microglia and astrocytes are key regulators of inflammatory responses in the central nervous system (CNS) and are associated with neurodegenerative diseases, such as AD. Glial cell activation may occur early in AD, even before Aβ peptide deposition (Kummer et al., 2014).

1.1.5.3.1 Microglia

Microglia are resident phagocytes of the CNS, ubiquitously distributed throughout the brain that act as the first and the main form of active immune defense. At the same time, microglia contribute to the protection and remodeling of synapses for proper neuronal plasticity (Ji et al., 2013).

Microglia exhibit multiple phenotypes reflective on their response to the local environment, including physical interaction with other cells and their physiological activity in the brain. Activation of classical pro-inflammatory (M1) phenotype is characterized by elevated pro-inflammatory cytokines such as tumor necrosis factor alpha (TNF-α) and interleukins IL-1β, IL-6, IL-12, IL-23, production of toxic nitric oxide (NO) and is accompanied by impaired phagocytic capacity (Mantovani et al., 2002). In contrast, alternative activation of non-inflammatory (M2) phenotype is characterized by secretion of the anti-inflammatory cytokines, such as IL-4, IL-10, and IL-6, transforming growth factor (Bamberger et al., 2003, Sierra-Filardi et al., 2011) without the production of NO. The M1/M2 activation states represent the polar extremes of myloid cell activation. There is a large diversity and graduation of phenotypic states in peripheral monocyte-derived macrophages, particularly under the conditions of chronic inflammation (Xue et al., 2014).

Microglias, which are once activated due to pathological triggers, such as neuronal death or protein aggregates, extend their processes to the site of injury, start to migrate to the lesions and initiate an innate immune response (Heneka et al., 2015). Binding of microglia to Aβ oligomers and fibrils results in activating microglia, which starts to

produce pro-inflammatory cytokines and chemokines (El Khoury et al., 2003, Stewart et al., 2010) and to engulf Aβ fibrills by phagocytosis. These fibrils enter consequently the endosomal/lysosomal pathway. Fibrillar Aβ peptide is largely resistant to enzymatic degradation, however the soluble Aβ peptide can be degraded by a variety of extracellular proteases (Lee and Landreth, 2010). In the microglial context, two proteases, neprilysin and insulin degrading enzyme (IDE) are of major importance and their disability can lead to an inefficient clearance of Aβ peptide (Mawuenyega et al., 2010).

Increased cytokine production downregulates Aβ peptide phagocytosis receptors of microglia (Hickman et al., 2008). Rare mutations of triggering receptor expressed on myeloid cells 2 (TREM2), microglia membrane receptor functioning in immune response that may be involved in chronic inflammation by triggering the production of constitutive pro-inflammatory cytokines (Frank et al., 2008, Hickman et al., 2013). TREM2 is also detected on reactive astrocytes surrounding Aβ plaques and on damaged neurons and oligodendrocytes (Hsieh et al., 2009).

After exposure to Aβ peptide, the acute microglial reaction aims at the removal of the recognized abnormality or pathology. However, in AD, the ongoing formation of Aβ peptide and positive feedback loops between inflammation and APP processing compromises abatement of the inflammation. Instead, the sustained accumulation of Aβ peptide and neuronal debris and exposure to chemokines, cytokines and other inflammatory mediators establish a chronic, non-resolved inflammation with the persistent functional impairment of microglia (Krabbe et al., 2013, Heneka et al., 2015, Shahidehpour et al., 2021).

1.1.5.3.2 Astrocytes

Astrocytes are star-shaped macroglial cells in the CNS with wide range of functions, such as biochemical control of endothelial cells forming the blood-brain barrier (BBB) (Rothermundt and Arolt, 2007), provision of nutrients to the nervous tissue and regulation of cerebral blood flow. Astrocytes are crucial regulators of innate and adaptive immune responses in the injured CNS (Freeman and Rowitch, 2013) and they are central for maintaining synaptic transmission thereby contributing to cognitive deficits (Beauquis et

al., 2013). Together with pericytes, astrocytes play an important role in the formation of tight junctions between endothelial cells of the BBB, which protects the brain against the infiltration of peripheral pathogens, leukocytes or undesirable molecules. When the BBB fails, reactive astrocytes regulate leukocyte and humoral transit to the brain by forming tight junctions of their own (Newcombe et al., 2018, Horng et al., 2017).

Similarly, to macrophages, astrocytes can exist in two states: reactive A1 astrocytes and neuroprotective A2 astrocytes (Liddelow et al., 2017, Marttinen et al., 2018). In neurodegenerative diseases, a greater number of A1 astrocytes than A2 astrocytes was registered (Liddelow et al., 2017). Astrocytes reponses to pathological agents are represented by reactive astrogliosis, a complex, multi-stage and pathology-specific remodeling of astrocytes generally aimed at neuroprotection and recovery of injured neural tissue (Sofroniew, 2009, Sofroniew and Vinters, 2010). Next to activated microglia, hypertrophic reactive astrocytes accumulate around Aβ plaques are commonly found in post-mortem human AD tissue (Medeiros and LaFerla, 2013) as well as in AD animal models (Olabarria et al., 2010). Reactive astrocytes are characterized by increased expression of glial fibrillary acidic protein (GFAP) and signs of functional impairment (Olabarria et al., 2011).

Similarly, to microglia, astrocytes release cytokines, interleukins and other potentially cytotoxic molecules upon exposure to Aβ peptide and thereby exacerbate neuroinflammatory response. Astrocytes have a potential role in internalizing and degrading Aβ peptide (Wyss-Coray et al., 2003). Furthermore, adult astrocytes up-regulate expression of extracellular soluble-Aβ-degrading proteases (Saido and Leissring, 2012), such as neprilysin or IDE and others upon exposure to native Aβ deposits (Pihlaja et al., 2011). Astrocytes with impaired function and/or atrophy produce less proteolytic enzymes mentioned and thus contribute less to Aβ peptide clearance. In addition to the above mentioned clearing pathways, astrocytes are involved in the clearance of soluble Aβ peptide from the brain parenchyma by glymphatic paravenous drainage (Iliff et al., 2012). This pathway is believed to depend on the astrocytic water channel aquaporin-4 (AQ4), since its deletion resulted in a strong decrease in Aβ peptide clearance.

The emerging role of microglial and astroglial activation in AD progression makes these cells a legitimate therapeutic target. However, since microglial activation can appear in both beneficial and detrimental guises and may act differently in different stages of the disease, in different animal models and in different brain regions, it is crucial to understand both the normal trajectory of pro- and anti-inflammatory molecules and signaling mechanisms as well as the extent to which the activation of microglia and other immune cells represents a compensatory mechanism in the disease process (Heneka et al., 2015).

1.1.5.4 Brain insulin signaling

Insulin was detected in various brain areas under physiological conditions, especially in the cortex, hippocampus, and hypothalamus and its role in AD is currently of major interest (Tabassum et al., 2020). Insulin is primarily of blood origin and is transported to the brain via insulin binding sites present on brain endothelial cells (Hersom et al., 2018). Insulin receptors are widely present in various brain areas, especially those regions that regulate olfaction, cognition, appetite, and autonomic activity (Pomytkin et al., 2018). Several studies have consistently shown that insulin is linked to cognitive functions (Plum et al., 2005, Tabassum et al., 2020).

Hyperinsulinemia leading to insulin resistance (IR) is a pathological condition, in which target tissues are not physiologically responsive to insulin (Kim and Reaven, 2008). Insulin is hypothesized to decrease the IDE-mediated Aβ peptide degradation via the competitive inhibition, but this statement needs to be qualified. The central IR leads to the impairment of insulin signaling in the brain, which induces the hyperphosphorylation of Tau protein and formation of Aβ oligomers by the multiple mechanisms. Particularly, IR lowers the IDE expression and, in this way, decreases IDE-mediated Aβ peptide degradation.

Additionally, IR inhibits the non-amyloidogenic pathway by reducing the expression of α-secretase and increased expression of β-secretase (Gasparini et al., 2001), which triggers the excessive accumulation of Aβ peptides and neuritic plaques which can in turn aggravate IR in the brain. All these molecular events finally lead to the formation of Aβ

plaques and NFT disturbing the neuronal organization and function (Pivovarova et al., 2016).

After insulin binding to the insulin receptor, autophosphorylation of the tyrosine kinase domain of insulin rceptor causes phosphorylation of insulin receptor substrate 1 (IRS-1), which further activates downstream signaling pathways, including the phosphoinositide 3-kinase (PI3K) and Ras/ERK cascades that directly regulate various physiological processes (Takeda et al., 2011).

Phosphorylation of regulatory subunit of PI3K p85 further leads to phosphorylation of 3-phosphoinositide-dependent protein kinase 1 (PDK-1) at Ser241 and downstream activation of Akt. Akt is fully activated by phosphorylation at both Thr308 and Ser473. Activated Akt phosphorylates GSK-3β at Ser9, or GSK-3α at Ser21, which inhibits the kinase activity of GSK-3 and the mammalian target of rapamycin (m-Tor). Phosphorylation of Ras leads to phosphorylation of ERK and further to phosphorylation of cAMP response element binding protein (CREB) a direct downstream target of ERK. The Ras/ERK cascade is thought to play a role in synaptic plasticity and memory formation.

As shown in Figure 5, in case of central IR, activation of the insulin signaling cascade is impaired, which is manifested by decreased phosphorylation of the implicated kinases and finally by a decreased phosphorylation of CREB, leading to worsened memory formation, and GSK-3β at its inhibitory site Ser9 that leads to an increase of GSK-3β kinase activity as GSK-3β is one of the most important kinases implicated in Tau hyperphosphorylation of Tau and accumulation of NFTs (Liu et al., 2011, Jolivalt et al., 2008, Tabassum et al., 2020), this points to a link between IR and AD.

Glucose metabolism and insulin signaling are essential for the proper functioning of the brain. Increasing evidence suggests that hypometabolism of glucose might be a key player in dementia pathology (Kuehn, 2020, Tabassum et al., 2020). Remarkably, changes in glucose metabolism are also associated with AD since imaging studies typically show decreased glucose metabolism in the temporal and parietal brain regions

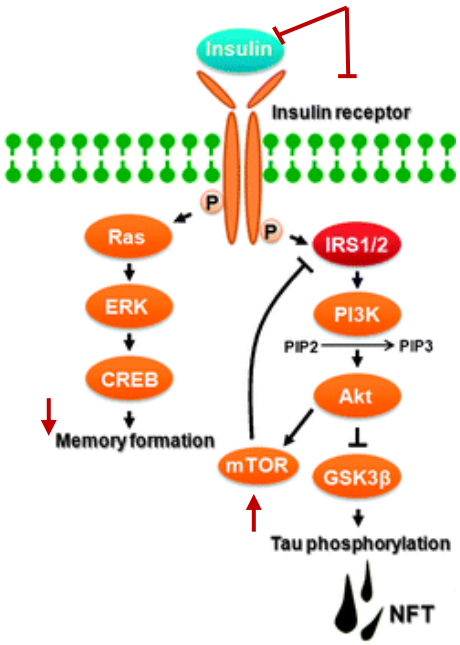

Figure 5: Impaired insulin signaling pathway leading to Tau hyperphosphorylation (Takeda et al., 2011). Insulin resistance leads to decreased phosphorylation of kinases implicated in insulin signaling that further leads to decrease in memory formation and abnormally phosphorylated tau forming NFT.

of AD patients and individuals at risk of developing this disease (Figure 6) (Small et al., 2000). Moreover, intravenous administration of insulin or glucose in AD patients and healthy elderly adults, improves their cognitive function (Watson and Craft, 2004).

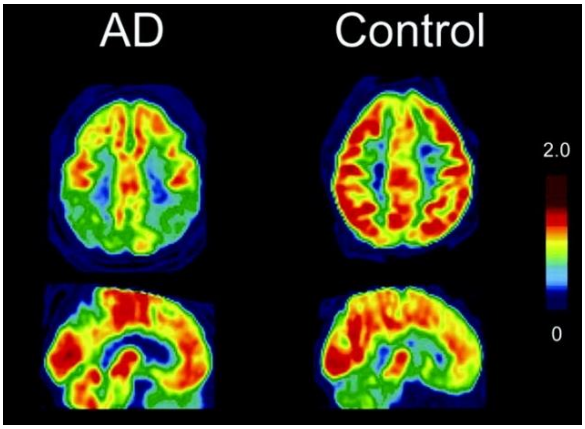

Figure 6: Glucose hypometabolism in the brain of mild-AD patient. Fluorodeoxyglucose (FDG)-positron emission tomography (PET) images of a normal control subject and a patient with AD with severe hypometabolism (yellow and blue cortical regions) (Boxer et al., 2007).

1.1.5.5 Loss of synapses

Loss of synapses, which is associated with the disruption of neuronal plasticity, is implicated in early AD pathology and may be robust even before overt neurodegeneration and brain atrophy (Scheff et al., 2006, Jack et al., 2010). Despite the fact that Aβ plaques colocalize with approximately one-third of synapses in AD patients, the exact mechanism of synaptic loss induced by Aβ peptide and Tau is not fully understood (Walsh et al., 2002, Fein et al., 2008). However, many direct and some indirect effect, such as inflammation and IR, have been suggested to play an important role in pathological synaptic dysfunction. Activated microglia have been shown first to engulf and then excessively reduce the number of synapses in AD mouse models through a complement-dependent mechanism (Hong et al., 2016). Released pro-inflammatory cytokines, such as TNF-α and IL-1, from activated microglia can have indirect excitotoxic effects on synapses (Jackson et al., 2019, Wang et al., 2015c).

1.1.5.6 Diagnosis of AD

Until recently, AD was diagnosed by a microscopic analysis of Aβ plaques and NFT in brain tissue at autopsy, or it relied on documenting of worsened mental health, at which point severe brain damage had been already caused (Thal et al., 2019). Furthermore, an Alzheimer's Questionnaire was developed to screen quickly and accurately the cognitive impairment due to AD (Malek-Ahmadi and Sabbagh, 2015).

Neuroimaging is regularly used today for the early detection of AD. Structural imaging, including the magnetic resonance imaging (MRI) and the computed tomography, provides information about the shape, morphology, or volume of the brain tissue, revealing shrinkage in specific brain regions, such as hippocampus that indicates presence or progression of the disease.

Functional imaging, such as positron emission tomography (PET) and functional MRI (fMRI), reveals cells in various brain regions actively use glucose or oxygen, suggesting that individuals with AD have typically reduced brain cell activity in certain regions. For example, studies with fluorodeoxyglucose (FDG)-PET indicate that AD is

often associated with reduced use of glucose in the brain areas ivolved in memory and learning.

Molecular imaging, including PET, fMRI, and single photon emission computed tomography uses highly targeted radiotracers to detect cellular or chemical changes, such as changes in Aβ peptide and Tau developing, linked to specific diseases. However, single evaluation of Aβ peptide, or Tau cannot be used for the AD diagnosis.

For AD diagnosis cerebrospinal fluid (CSF) biomarkers can also be used. CSF is a clear fluid that bathes and cushions the brain and the spinal cord. CSF can be sampled by physicians, through a minimally invasive procedure called a lumbar puncture, or a spinal tap. Research suggests that changes in CSF levels of Tau and Aβ peptide can be detected in early stages. Neurofilament light chain is another potential marker reflecting axonal damage in neurodegenerative diseases such as AD.

Scientists also identified genetic risk profiling; APP, PSEN1 and PSEN2 genes with rare variations cause AD and several genes that increase risk but don't guarantee that a person will develop the disease that are also used in the mouse models modelling AD pathology decribed in 1.2.1.2.3 (https://www.alz.org/alzheimers-dementia/research_progress/ earlier -diagnosis).

1.1.6 Current AD treatment

Alzheimer's disease is the seventh-leading cause of death worldwide. On average, a person with AD lives 4 to 8 years after diagnosis but can live 20 years (https://www.who.int/news-room/fact-sheets/detail/dementia). Even though there is a worldwide effort underway to find ways to diagnose, or to treat AD, delay its onset and prevent it from developing, currently no sufficient cure is available. However, there are treatments and drug and non-drug options that may change the disease progression and temporarily reduce the symptoms (Cummings, 2021, Winslow et al., 2011).

One of the main used medicines are acetylcholinesterase inhibitors, such as donepezil, galantamine and rivastigmine. These prevent enzyme acetylcholinesterase from breaking down neurotransmitter acetylcholine, resulting in higher level of acetylcholine in the brain helping nerve cells to communicate better with each other (Marucci et al., 2021, Winslow et al., 2011).

Another available medicine is memantine, N-methyl-d-aspartate (NMDA) receptor antagonist. Memantine blocks current flow through NMDA receptors, a glutamate receptor subfamily broadly involved in brain function (Johnson and Kotermanski, 2006).

Newly approved treatment by the U.S. Food and Drug Administration (June 2021) in the United States is aducanumab. It is monoclonal antibody against Aβ peptide, one of the AD hallmarks, suggesting reduction of cognitive and functional decline in people with AD. However its effectiveness is considered controversial as it has no sufficient evidence of efficacy (Mullard, 2021).

1.1.6.1 AD risk factors

Several medical conditions, such as obesity, T2DM, IR, systemic inflammation, cardiovascular disease and others, are related to the development of AD and are therefore confirmed as AD risk factors. However, ageing is number one AD risk (Berger et al., 2007, Giannakopoulos et al., 2003).

1.1.6.1.1 Ageing

The greatest known AD risk factor is an increasing age. The incidence of AD increases dramatically with age: 5.3 % of people aged 65 to 73, 13.8 % of people aged 75 to 84 and 34.6 % of people aged 85 or older have AD. And due to the increasing age of the population about 100 milion people are estimated to be suffering from AD in 2050. However, it is important to note that AD is not a physiological part of ageing, and older age alone is not sufficient to cause AD (2021). If it affects a person below the age 65, AD can be considered an early onset. People with the early-onset AD can also be subdivided according to the level of AD development into the early, middle, or late stage of the disease.

1.1.6.1.2 Obesity

Obesity is defined as a medical condition in which excess body fat has accumulated to the extent that it may have an adverse effect on health. It is currently one of the most widespread health threats to have reached epidemic proportions worldwide and it is estimated to reach 573 million cases by 2030 (https://www.who.int/news-room/fact-

sheets/detail/obesity-and-overweight). Obesity arises from higher intake of calories than is their expenditure and it can be calculated by the body mass index (BMI). Obesity is associated with other metabolic disturbances, such as IR and peripheral inflammation; all of them are widely accepted as risk factors of age-related cognitive decline and AD (Tabassum et al., 2020, Whitmer et al., 2008).

However, it seems that it is important to differentiate between mid-life and late-life overweight (Xu et al., 2011). In fact, the scientists conclude that obesity below the age of 65 years (mid-life obesity) and weight loss in the preclinical phase characterize dementia (Singh-Manoux et al., 2018), but the late-life obesity (over 65 years) does not correlate with the incidence of dementia (Pedditzi et al., 2016). Very recently, Kivimäki et al. described that the risk of developing AD is even reversed in late-life and a higher BMI could even be protective (Kivimäki et al., 2018).

Obesity is associated with adverse alterations in adipose tissue (AT) that predispose metabolic dysregulation and lead to the development of IR. These adverse alterations include accumulation of activated macrophages, which constantly secrete pro-inflammatory cytokines such as IL-6, IL-1β, and TNF-α, and eventually lead to local and systemic inflammation (Kim et al., 2015, Sam and Mazzone, 2014).

An increase in AT could further promote a vascular injury leading to a decrease in the blood flow to the brain. A decrease in blood flow to the brain causes ischemia in the most vulnerable brain areas, such as the hippocampal regions CA1 and CA3, and parts of the caudate nucleus, cerebellum, and neocortex (Payabvash et al., 2011). The hippocampal areas, due to its high baseline metabolic activity, are extremely susceptible to reduced oxygen and glucose intake and it is believed that it can be one of the causes of increased memory loss (Kivipelto et al., 2005).

FGF21 is a hormonee considered as a major regulator of energy homeostasis that is associated with obesity-related metabolic complications in humans. Serum FGF21 is increased in obese individuals which may be explained by a compensatory response or resistance to FGF21. FGF21 is mainly secreted by the AT, liver, but it may also be expressed in skeletal muscle (Zhang et al., 2008).

Furthermore, chronic inflammation causes damage to the BBB that can have deleterious effects on the CNS, including hypothalamic dysfunction, loss of synapses, impaired cognition, and neurodegeneration (Wyss-Coray and Mucke, 2002, Gregor and Hotamisligil, 2011). The inflammation caused by obesity can, therefore, result in neuronal damage, usually beginning in adolescence.

Obesity also causes loss of gut microbial diversity that is associated with increased levels of pro-inflammatory bacterial species in the peripheral blood and thus could be viewed as factor contributing to AD risk (Le Chatelier et al., 2013). Moreover, obesity increases the propensity to acquire more bacterial or viral infections and thus directly increases the likelihood for systemic inflammation (Almond et al., 2013, Heneka et al., 2015). Together it seems possible that obesity increases the risk for AD by the systemic, chronic presence of pro-inflammatory cytokines.

1.1.6.1.3 Type 2 diabetes mellitus (T2DM)

Growing body of epidemiological studies suggest that people with T2DM as a possible consequence of obesity, are at a higher risk of developing AD. The salient features of T2DM are high levels of blood glucose (hyperglycemia), hyperinsulinemia, and IR (Taylor, 2012). Hyperinsulinemia can interrupt the physiological function of several vital organs by impairing insulin signaling and disrupting intracellular signaling transduction (Tabassum et al., 2020, Zhang et al., 2007). IR arises due to decreased sensitivity of muscle, liver, and AT to insulin.

T2DM is also considered as an islet amyloid polypeptide (IAPP)-associated pathology. IAPP is a hormone produced by pancreatic β-cells, similarly as insulin. It contributes to the maintenance of glucose physiological levels by inhibiting insulin and glucagon secretion as well as controlling adiposity and satiation. IAPP is a highly amyloidogenic polypeptide forming intracellular aggregates and amyloid structures that are associated with β-cell death (Raimundo et al., 2020).

Both these features ultimately result in a reduced uptake of circulating blood glucose for glycogenesis eventually leading to chronic hyperglycemia as one of the pathological hallmarks of T2DM. Likewise, AD brains are less capable of glucose uptake from the surroundings resembling a condition of brain IR.

In rodents, high-fat diet (HFD)-induced IR exhibited a cognitive decline with impaired insulin regulation, increased inflammation, mitochondrial dysfunction, increased oxidative stress, and apoptosis in the brain (Sripetchwandee et al., 2018, Tabassum et al., 2020). These results suggest that chronic peripheral IR can induce brain IR and brain dysfunction. Due to the same patterns of disturbance in insulin signaling and IR in the brain and periphery, AD is sometimes called Type 3 diabetes (de la Monte and Wands, 2008).

1.1.6.1.4 Disrupted blood-brain barrier

The BBB represents unique property of the CNS that regulates the entry of plasma components, red blood cells, leukocytes, and ions into the brain from the blood. And reversely it ensures the export of potentially neurotoxic molecules and ions from the brain to the blood. It is critical for maintaining brain homeostasis and for protecting the CNS from toxins, pathogens, and even the body's own immune system. BBB disruption is associated with inflammatory and immune responses and can initiate multiple pathways of neurodegeneration. Additionally, BBB breakdown can enable circulating pathogens to enter the brain and injure neurons, and it can also provoke an amyloid response that aggravates β-amyloidosis (Abbott et al., 2010, Sweeney et al., 2018, Zlokovic, 2011, Kacirova et al., 2020).

Recent studies have demonstrated that the paravascular glymphatic pathway driven by AQ4 constitutes a major clearance pathway of interstitial fluid solutes, including Aβ peptide, from the brain's parenchyma. In AD patients glymphatic function is reduced and perivascular space of penetrating arteries are subject to accumulation of Aβ peptides (Kress et al., 2014, Jessen et al., 2015).

Most of the properties of the BBB are exhibited by the endothelial cells that make up the walls of blood vessels, which are held together by tight junctions. They express proteins that selectively transport small molecules into the brain and express low levels of proteins, which are responsible for binding immune cells in other tissues (Daneman and Prat, 2015). The major components of tight junctions are the proteins claudin, which seems to regulate permeability, and occludin, which forms the backbone of tight junctions' strands and seems to be a sensitive indicator of structural changes in the BBB

during disease pathogenesis (Förster et al., 2008, Naik et al., 2014). These proteins are affected during acute and chronic CNS diseases (Bednarczyk and Lukasiuk, 2011, Gonçalves et al., 2013).

1.2 Models of neurodegeneration, obesity and T2DM

1.2.1 Models of neurodegeneration

1.2.1.1 Cellular models of neurodegeneration

1.2.1.1.1 SH-SY5Y cell line

SH-SY5Y is a subcloned cell line derived from SK-N-SH human neuroblastoma cell line, isolated from bone marrow biopsy taken from a four-year-old female of unknown ethnicity, with neuroblastoma. SH-SY5Y cells are often used as *in vitro* models for neurodegenerative disorders since they can be differentiated from a neuroblast-like state into mature human neurons through a variety of the different mechanisms including the use of retinoic acid, phorbol esters, and specific neurotrophins such as brain-derived neurotrophic factor. Prior evidence suggests that the use of the different methods can select for specific neuron subtypes such as adrenergic, cholinergic, and dopaminergic neurons (Påhlman et al., 1984, Xie et al., 2010). This latter aspect makes SH-SY5Y cells useful for a multitude of neurobiology experiments and they are therefore widely used in experimental neurological studies, including analysis of neuronal differentiation, metabolism, and function related to neurodegenerative processes, neurotoxicity, and neuroprotection (Ross et al., 1983, Biedler et al., 1973, Shipley et al., 2016).

Several studies have noted important differences between SH-SY5Y cells in their undifferentiated and differentiated states. When SH-SY5Y cells are undifferentiated, they rapidly proliferate and seem to be non-polarized, with very few, short processes. They often grow in clumps and express markers indicative of immature neurons (Shipley et al., 2016). When differentiated, these cells extend long, branched processes, decrease in proliferation, and in some cases polarize. Fully differentiated SH-SY5Y cells have been previously demonstrated to express a variety of different markers of mature neurons

including neuronal nuclei and synaptophysin, marker of synaptic plasticity (Shipley et al., 2016).

Neurotoxic agents such as methylglyoxal (MG) cause in neuroblastoma cells changes similar to the neurodegenerative ones (Amicarelli et al., 2003). MG is a highly reactive dicarbon metabolite formed during the metabolism of glucose, proteins, and fatty acids. MG levels are affected by hyperglycemia and its excess can increase the amount of oxygen radicals and cause oxidative stress. At the same time, it has been found that the enzyme responsible for the degradation of MG decreases and accumulates in older age (Desai et al., 2010).

In SH-SY5Y cells, MG causes an increase in oxygen radicals, a decrease in intracellular ATP and, above all, a loss of mitochondrial integrity. In addition, MG-induced apoptosis increases the levels of pro-apoptotic Bcl-2-associated X protein (Bax) protein, which is essential for the onset of apoptosis and is associated with an extended synapse disorder, which is an early sign of AD. The level of Bcl-2 protein, which is important for the cell viability, is reduced (D'Amelio et al., 2010, de Arriba et al., 2007, Tajes et al., 2014a). The ratio Bax/Bcl-2 is considered as marker of apoptosis.

1.2.1.1.2 Primary neuronal culture

Primary neuronal culture refers to *in vitro* maintenance of living neurons that have been extracted from animal nervous system tissue such as brain or spinal cord. Primary neuronal cultures are powerful model used to study neuronal morphology and differentiation, synaptic function and neurotransmitter release, neurotoxicity during preclinical drug development, and disease modeling. A primary neuron culture from embryonic rodent hippocampus or cortex has been one of the most fundamental methodologies for modern neurobiology (https://www.thermofisher.com/cz/en/home/life-science/cell-culture/primary-cell-culture/neuronal-cell-culture.html).

Primary neurons can be easily cultured and over a few days or weeks differentiated into neurons with clearly recognizable axons, dendrites, dendritic spines and synapses (Sahu et al., 2019). However, the disadvantage of primary cultures is that they do not divide in culture and need to be generated from embryonic or early postnatal brains for

each experiment. Furthermore, neuronal cultures vastly depend on source, age of derivation and culture conditions (Sahu et al., 2019).

1.2.1.2 Mouse models of AD

The animal models are an important and fundamental part of medical research. Several rodent models were designed to investigate the pathological processes leading to development of AD, obesity, or T2DM. In recent years, many models combining all of the above-mentioned diseases were used to examine the effect of obesity and related T2DM on the development of neurological disorders, such as dementia or AD.

1.2.1.2.1 APP/PS1 transgenic mouse model

This transgenic mouse model combined the Swedish mutation in APP (K670N/M671L), (SWE) and mutation in presenilin 1 ($PSEN1_{dE9}$). Mutation in APP leads to increased Aβ production and was observed in early-onset familial cases of AD in several families in Sweden, hence this mutation is called Swedish mutation. Mutation in PSEN1 (PS1) was discovered to enhance production of the Aβ fragments of 42-43 amino acids that are supposed to be more fibrillogenic (Borchelt, 1998). APP/PS1 mice are characterized by a pronounced increase in Aβ deposits in the hippocampus and cortex, compared to their littermates without mutations, impaired score in behavioral experiments and increased brain oxidative stress markers (Hulshof et al., 2022, Chen et al., 2019).

Aβ deposition starts at approximately 6 weeks of age in the neocortex. Deposits were reported in the hippocampus at 3 to 4 months, and in the striatum, thalamus, and brainstem at 4 to 5 months. Phosphorylated Tau-positive neuritic processes were observed in the vicinity of all congophilic amyloid deposits, but no fibrillar Tau inclusions (Maia et al., 2013). Global neuronal loss is not observed in APP/PS1 mice, but modest neuron loss was found in the granule cell layer of the dentate gyrus and other subregions with high neuron density at older ages, e.g. 17 months (Rupp et al., 2011).

1.2.1.2.2 3xTgAD mouse model

This widely used transgenic mouse model combines both pathological hallmarks of AD. Mice overexpress human mutated genes APPSWE and PSEN1dE9, which cause formation of Aβ plaques, and human TauP301L transgene, which leads to formation of NFT (Ramsden et al., 2005). Translation of the overexpressed transgenes appears restricted to the CNS, including the hippocampus and cerebral cortex. Aβ pathogenesis is progressive, with intracellular immunoreactivity and is observed prior to Tau pathology, from the age of 3 months (Oddo et al., 2003). Extracellular Aβ peptide deposits appear around 6 months of age. Changes in aggregation of phosphorylated Tau occur later, by 12 to 15 months in hippocampus. Mice are characterized by impaired memory, synaptic dysfunction, presence of Aβ plaques, and hyperphosphorylation of Tau protein (Billings et al., 2005, Oddo et al., 2003).

1.2.1.2.3 5xFAD mouse model

5xFAD mice express human APP and PSEN1 transgenes with a total of five AD-linked mutations: SWE, Florida (I716V), and London (V717I) mutations in APP, and the M146L and L286V mutations in PSEN1. 5xFAD mice have high APP expression correlating with high burden and accelerated accumulation of the Aβ42. 5xFAD mice generate Aβ42 almost exclusively, rapidly accumulating in cerebral cortex, intraneuronal Aβ42 accumulation is observed starting at the age of 1.5 months in hemizygotes, just prior to amyloid deposition and gliosis, which begins at the age of 2 months. In addition, these mice have reduced synaptic levels, increased neuronal loss, reduced anxiety and memory impairment (Richard et al., 2015).

1.2.2 Mouse models of obesity and T2DM

1.2.2.1.1 Model of diet-induced obesity

Rodents with diet induced obesity (DIO) are considered models of the most common human obesity, which is associated with the consumption of high energetic, mostly HF diet (Bagnol et al., 2012).

DIO model represents late onset obesity similar to the obesity, which spreads in developed countries due to over-consumption of HFD and lack of physical activity. Animals are fed with HFD since their young age. Already after two weeks of feeding HFD, increase in AT is observed, which consequently leads to hyperleptinemia, leptin resistance, and finally also to IR and hyperglycemia (Buettner et al., 2007, Youngren et al., 2001). Leptin dysfunction, or leptin resistance can further promote neurodegeneration (Flores-Cordero et al., 2022).

Moreover, in several mouse models of AD, such as Thy-Tau22 mice (Kacirova et al., 2021, Leboucher et al., 2013), 3xTg-AD mice (Knight et al., 2014), or APP/PS1 mice (Bracko et al., 2020, Fan et al., 2021), it was discovered that HFD feeding for several weeks worsened AD parameters, memory impairment in the spatial test, and increased phosphorylation of the Tau protein in Thy-Tau22 mice and 3xTg-AD mice. HFD also increased level of the neuroinflammation in Thy-Tau22 and APP/PS1 mice. Even though the exact mechanisms responsible of impact of HFD is not fully understood, there is a possible implication of neuronal IR, and neuroinflammation, but further research must be done (Knight et al., 2014, Leboucher et al., 2013, Kacirova et al., 2021, Fan et al., 2021).

1.3 Food intake regulating peptides as a potential treatment of AD

Recently discovered link between obesity, T2DM and obesity revealed new possible strategy for the treatment of neurodegenerative disorders. Analogs of food intake regulating peptides, such as glucagon-like peptide 1 (GLP-1), or prolactin-releasing peptide (PrRP) could increase insulin sensitivity and ameliorate neuroinflammation, and thus could be used for the AD treatment.

1.3.1 GLP-1 analogs

Glucose-dependent insulinotropic peptides (GIP) and GLP-1 are incretins decreasing blood glucose levels by enhancing the secretion of insulin and inhibiting the secretion of glucagon (Vilsbøll and Holst, 2004). GIP is secreted by K-cells of the upper intestine, GLP-1 by L-cells of the lower intestine. GIP and GLP-1 receptors belong to the family of G-protein coupled receptors. Recently, neuroprotective properties of GIP and GLP-1 were described as reviewed in (Hölscher and Li, 2010). However, naturally occuring

incretins have low stability, hence their structure had to be modified into analogs with prolonged stability. Structures of GLP-1 and its analogs are shown in Figure 7A.

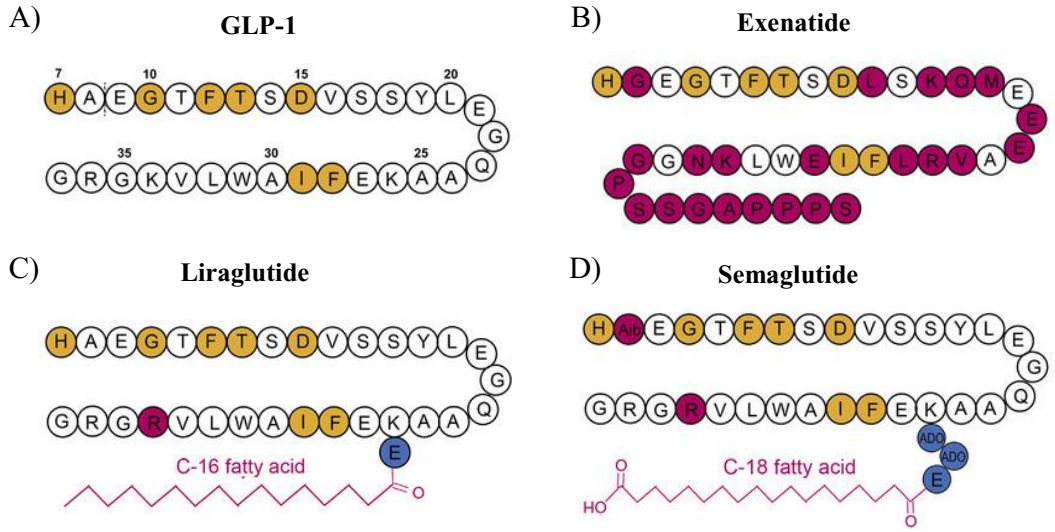

Figure 7. Amino acid structures of GLP-1, Exenatide, Liraglutide and Semaglutide. Key amino acids for potency highlighted in yellow, substituted amino acids in red and spacer in blue colour (Yu et al., 2018).
E = γ-Glu spacer, ADO = 8-amino-3,6-dioxaoctanoic acid.

1.3.1.1 Exenatide

Historically, exenatide was discovered as exendin-4, a protein originally isolated from the venom of Gila monster. It shares 53% sequence identity with GLP-1. Synthetically prepared exendin-4 (exenatide) has higher biological stability than GLP-1 (Drucker, 2006). Nowadays, it is a frequently prescribed medication used to treat T2DM that enhances pancreatic β-cell proliferation (Wang et al., 2015b). Exenatide has potential neuroprotective properties (Bomfim et al., 2012, Bonda et al., 2014, Chen et al., 2012) and it was tested as a treatment for AD in a pilot clinical trial (https://clinicaltrials.gov/ct2/show/NCT01255163; Holscher 2018). The treatment with exenatide induces improvement of impaired insulin signaling cascade mediated through activation of the PI3K/Akt pathway (Bomfim et al., 2012, Wang et al., 2015a). Moreover, the treatment reduced the number of Aβ plaques and the level of soluble Aβ, and improved memory in the Morris water maze (MWM) in several mouse models (Bomfim et al., 2012, Li et al., 2010). The treatment with exenatide further decreased

phosphorylation of Tau at different epitopes (Maletínská et al., 2019, Chen et al., 2012). Structure of exenatide is shown in Figure 7B.

1.3.1.2 Liraglutide

Liraglutide is a stable, long-lasting GLP-1 receptor agonist and the most used anti-T2DM drug (Victoze, NovoNordisk) and anti-obesity drug (Saxenda, NovoNordisk) and is now undergoing phase II clinical trial testing in AD patients (Hölscher, 2018). Its structure has 97% homology with natural GLP-1 (shown in Figure 7C), displaying only one amino acid substitution in which Lys34 is replaced with Arg and palmitoic acid attached to Lys20. Liraglutide has been widely assessed in animal models of AD. Initial studies with patients have shown modest beneficial effects in AD patients and it is currently under evaluation in the multi-centre, randomised, double-blind, placebo-controlled, phase IIb trial of liraglutide in participants with mild to moderate Alzheimer's dementia ELAD trial (Evaluating Liraglutide in Alzheimer's Disease NCT01843075). The treatment with liraglutide causes an overall improvement of brain metabolic alterations, insulin sensitivity, reduced level of Aβ plaques and attenuated Tau pathology and inflammation. Liraglutide further improved synaptogenesis and neurogenesis, impaired insulin signaling cascade and spatial memory in the MWM in mouse models of neurodegeneration (McClean et al., 2015, McClean and Hölscher, 2014, McClean et al., 2011, Parthsarathy and Hölscher, 2013). Liraglutide has also been tested in mouse models of obesity and/or diabetes. It improved metabolic parameters, including body weight and glucose levels (Maletínská et al., 2019, Porter et al., 2013, Porter et al., 2010).

1.3.1.3 Semaglutide

Semaglutide is a stable analog of GLP-1, with 94% similarity. Semaglutide improve sugar metabolism by increase in insulin secretion. It is distributed not only as a subcutaneous injection in a prefilled pen, but also as an oral form. One of its advantages over other antidiabetic drugs is that it has a long duration of action, so a once-a-week injection is sufficient (Kapitza et al., 2015).

Semaglutide improves motor impairment, reduced the oxidative injury, inflammation and apoptosis and neurogenesis in various murine models (Zhang et al., 2019, Yang et

al., 2019, Mahapatra et al., 2022). Semaglutide also protected dopaminergic neurons from injury by reducing the aggregation of α-synuclein (Zhang et al., 2019). Semaglutide in human neuroblastoma cell line SH-SY5Y reduced Aβ plaques, possibly mediated by enhanced autophagy and inhibition of apoptosis (Chang et al., 2020). Semaglutide is currently in two placebo-controlled phase-3 trial study (EVOKE NCT04777396 and EVOKE Plus NCT04777409) with patients with early AD, and the study will evaluate the efficacy and safety of oral semaglutide, compared with a placebo, taken once daily.

1.3.2 Prolactin-releasing peptide analogs

Other potential drugs for the treatment of obesity and associated T2DM are PrRP analogs. PrRP is a neuropeptide that belongs to the family of RF-amide peptides. PrRP immunoreactive fibers, as well as its receptor GPR10, can be found in the brain in nuclei implicated in food intake and energy balance regulation, such as in the nucleus of the solitary tract of the brainstem, and in several hypothalamic nuclei, where it acts as an anorexigenic compound (Prazienkova et al., 2019a, Kuneš et al., 2016). PrRP was also found to have high affinity to the neuropeptide FF 2 receptor, resulting in anorexigenic effect (Engström et al., 2003). Natural PrRP has two equally active isoforms with different lengths: the longer PrRP31 comprises 31 amino acids and the shorter PrRP20 comprises 20 C-terminal amino acids (Hinuma et al., 1998). None of the isoforms can decrease food intake after acute peripheral administration (Kuneš et al., 2016). Therefore, several PrRP substances modified with lipidization, increasing the stability of the peptide, and allowing it to exert its central anorexigenic and antidiabetic effects after peripheral administration, were designed and synthesized in our laboratory (Maletínská et al., 2015, Pražienková et al., 2017). Two PrRP analogs, PrRP31 palmitoylated at the N-terminus (palm^{1}-PrRP31) or through the γ-Glu-linker at Lys^{11} (instead of natural Arg^{11}, palm^{11}-PrRP31) were chosen as the most potent analogs, with strong specific binding to the GPR10 receptor and increased stability and bioavailability in blood plasma.

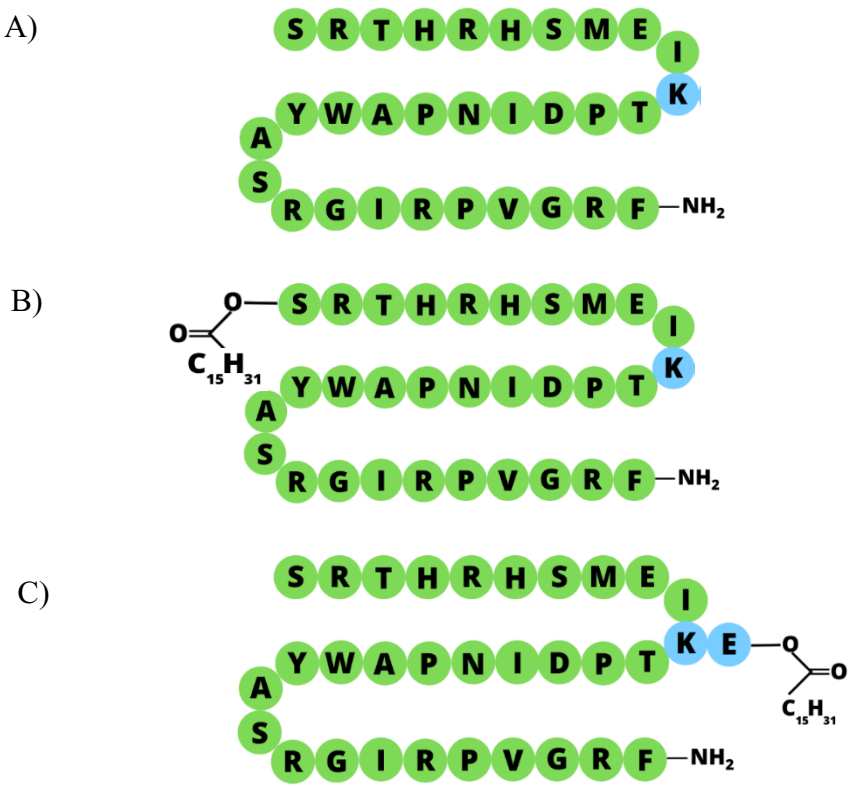

Figure 8: PrRP structures. PrRP31 (A) and it palmitoylated analogs: palmitoylated at the N-terminus (palm^{1}-PrRP31) (B) or through the γ-Glu-linker at Lys^{11} (instead of natural Arg^{11}, palm^{11}-PrRP31) (C).

In our previous studies, potential neuroprotective properties of palmitoylated PrRP analogs were tested in different mouse models of AD-like pathology and *in vitro*. Palm^{11}-PrRP31 attenuated hypothermia-induced Tau hyperphosphorylation in the SH-SY5Y neuroblastoma cell line and in rat primary cortical neurons (Prazienkova et al., 2019b). Furthermore, palm^{1}-PrRP31, ameliorated hippocampal insulin signaling pathways and attenuated Tau hyperphosphorylation at several epitopes in mice with monosodium glutamate (MSG)-induced obesity (Spolcova et al., 2015). Palm^{11}-PrRP31 also attenuated Tau hyperphosphorylation, improved short-term spatial memory and enhanced synaptic plasticity in transgenic Thy-Tau22 mice, a mouse model of Tau pathology (Popelova et al., 2018). Finally, palm^{11}-PrRP31 was shown to significantly reduce amyloid plaque deposition, neuroinflammation and Tau hyperphosphorylation in hippocampi and cortices of APP/PS1 mice (Holubova et al., 2019, Jankowsky et al., 2001).

2. AIMS OF THE THESIS

- **Cellular signaling and anti-apoptotic effect of PrRP and its palmitoylated analog palm^{11}-PrRP31 in SH-SY5Y cells**

In the first part of the thesis, we aimed to identify the signaling pathways activated by PrRP and its stable analog, with an emphasis on insulin pathways implicated in survival and growth of human neuroblastoma cell line SH-SY5Y and rat primary cortical neurons. Further, the effects of PrRP and its palmitoylated analog palm^{11}-PrRP31 were to examined in the prevention and after exposure to neurotoxic effect of MG, regarding cell viability and activation of pro- and anti-apoptotic enzymes.

- **Effect of palmitoylated PrRP analog on Aβ pathology and microgliosis in APP/PS1 mice**

In the second part, we aimed at the impact of the palm^{11}-PrRP31 treatment on pathological markers associated with AD: Aβ plaques, neuroinflammation, loss of synapses and apoptosis in the hippocampus, cortex and in the cerebellum in APP/PS1 mouse model of AD pathology.

- **Impact of HFD on metabolic parametres and AD-related pathology in APP/PS1 and WT mice**

In the third part of the thesis, we aimed to find out a potential relationship between obesity-induced insulin resistance, inflammation in the periphery and AD-like pathology in the brain of APP/PS1 mice fed with HFD, a model connecting obesity and AD-like pathology.

3. METHODS

3.1 Peptides

Human prolactin-releasing peptide (PrRP31) and its lipidized analog palmitoylated in position 11 (palm^{11}-PrRP31) (see Table 1 for structures) were synthesized and purified using the Fmoc strategy at the Institute of Organic Chemistry and Biochemistry, Czech Academy of Sciences, Prague, Czech Republic (IOCB CAS) as previously described (Pražienková et al., 2017, Maletínská et al., 2011). The scrambled-palm^{11}-PrRP31 peptide (scrambled) used in the *in vitro* study as a negative control was derived from the structure of palm^{11}-PrRP31, where arginines were substituted with citrullines (Cit) and the sequence of PrRP31 was randomly scrambled (Table 1). Purity of the analogs was determined by analytical high-performance liquid chromatography and by using a Q-TOF micro MS technique (Waters, Milford, MA, USA) and was higher than 95% (Pražienková et al., 2017, Maletínská et al., 2011).

Human insulin, used in *in vitro* studies as a positive control, was a gift from the group of Dr. Jiří Jiráček, IOCB CAS, Prague. All peptides used in *in vitro* studies were dissolved in deionized water. Palm^{11}-PrRP31 used in *in vivo* studies was dissolved in saline.

Table 1. Structure of human prolactin-releasing peptide 31 (PrRP31) and its analogs.

Analogs	Sequence
PrRP31	SRTHRHSMEI**R**^{11}TPDINPAWYASRGIRPVGRF-NH2
Palm^{11}-PrRP31	SRTHRHSMEI**K**^{11} (-E (N-palm))TPDINPAWYASRGIRPVGRF-NH2
Scrambled-palm^{11}-PrRP31	GHFTHSIRMI **K**^{11} (-E (N-palm))TPRNASVYARP Cit DWWGI Cit PES

Cit-citrullin.

3.2 *In vitro* studies

3.2.1 Cell lines

The SH-SY5Y (ATCC® CRL-2266.) neuroblastoma cell line, obtained from LGC standards (Teddington, London, UK), was grown in DMEM supplemented with 10% heat-inactivated fetal bovine serum, 1% nonessential amino acids, 1% streptomycin/penicillin, and 2 mM L-glutamine at 37℃ in a 5% CO_2 humidified

incubator. The medium was changed every 3–4 days, and the cells were subcultured as required.

Primary rat cortical neurons (A10840-02) obtained from Thermo Fisher Scientific (Waltham, MA, USA) were grown in neurobasal medium supplemented with 2% B27, 200 mM L-glutamine and 1% antibiotic-antimycotic agent. Cells were seeded at 80,000 cells/well in 96-well plates coated with poly-D-lysine (0.1 mg/ml) and laminin (20 g/ml), and the medium was changed every 3-4 days. The plates were maintained at 37℃ in a 5% CO_2 humidified incubator for 10 days.

3.2.2 Cellular signaling triggered by PrRP and palm^{11}-PrRP

The cells were cultured in 6-well plates at a density of 800,000 cells per well in growth medium, which was exchanged for serum-free medium 16 h before an experiment, and then, the cells were incubated with PrRP31, palm^{11}-PrRP31, or scrambled peptide at a final concentration of 1 x 10^{-5} M or insulin at a concentration of 1 x 10^{-7} M at 37℃ for 8 min. The cells were rapidly cooled on ice and lysed in 400 µl of Laemmli sample buffer (62.5 mM Tris-HCl with pH 6.8, 2% SDS, 10% glycerol, 0.01% bromophenol blue, 5% mercaptoethanol, 50 mM NaF, and 1 mM Na_3VO_4) and stored at -20℃. Eight minutes of incubation was performed as optimal time of incubation resulting from a series of experiments with different exposure times (5, 10, 15, 30, and 60 min) to PrRP31 and its palmitoylated analog. The PI3K/Akt pathway is one of the main signaling pathways of insulin; therefore, insulin was used as a positive control. Scrambled peptide was used as a negative control. The controls and compounds were tested in triplicate in three independent experiments.

For further research, inhibitors of signaling pathways were used. The growth medium was exchanged for serum-free DMEM 16 h before the experiment. On the day of the experiment, cells were incubated for 2 min with rapamycin, SB216736 or U0126 at a final concentration of 1 x 10^{-6} M; then, PrRP31, palm^{11}-PrRP31 or scrambled peptide at a final concentration of 1 x 10^{-5} M or insulin at a concentration of 1 x 10^{-7} M was added for 8 min. The plates were incubated at 37℃. The controls and compounds were tested in

triplicate. Rapamycin (m-Tor inhibitor), SB216736 (GSK-3β inhibitor), and U0126 (ERK inhibitor) were purchased from Tocris (Bristol, UK).

3.2.3 Western blotting

Signaling pathways were studied by Western blotting (WB). The cell lysates were sonicated for 1 minute, boiled for 2 minutes at 100 °C, centrifuged for 5 minutes, and finally resolved using 26-well 4-15% Criterion™ TGX™ Precast Midi Protein Gel (Bio-Rad, Hercules, CA, USA) at a constant voltage of 200 V. Proteins were transferred onto nitrocellulose membranes at constant voltage of 100 V. Nitrocellulose membranes were blocked in 5% nonfat milk or 5% BSA at room temperature (RT) for 1 h, as shown in Table 2. Subsequently, the membranes were incubated overnight with primary antibody (Ab) at 4℃, according to the manufacturer´s instructions (Table 2). The list of antibodies used and their appropriate dilutions in Tris-buffered saline (TBS)/0.1% tween-20 are shown in Table 2. The next day, the membranes were incubated with an HRP-linked secondary antibody for 1 h at RT. Chemiluminescence was visualized with a ChemiDoc™ System (Bio-Rad). Band intensities were normalized using glyceraldehyde 3-phosphate dehydrogenase (GAPDH) as an internal loading control. Activation is expressed as the ratio of the phosphorylated protein to the total amount of the protein.

3.2.4 Cell Viability Measurement

For this assay, cells were cultured in 96-well plates at a density of 40,000 cells per well. The growth medium was exchanged for serum-free DMEM 16 h before the experiment. First, the cells were pretreated with 1 x 10^{-5} M or 1 x 10^{-7} M PrRP31 or palm^{11}-PrRP31, or distilled water (vehicle) (in octuplicates) for 4 h to prevent MG cytotoxic effects; then, MG was added to a final concentration of 0.6 mM or 1.2 mM. The cells were incubated at 37℃ for 16 h. Second, cells were first incubated for 16 h at 37℃ with MG at a final concentration of 0.6 mM or 1.2 mM and subsequently treated with PrRP31 or palm^{11}-PrRP31 at a concentration of 1 x 10^{-5} M or 1 x 10^{-7} M for 4 h (in octuplicates). At the end of the experiment, the MTT (3-[4,5-dimethylthiazol-2-yl]-2,5-diphenyl tetrazolium bromide; thiazolyl blue) test was used to measure cell viability. The MTT reagent was dissolved in RPMI-1640 without phenol red. Cells were incubated for

2 h with a 10% solution of MTT at 37℃. Living cells converted soluble MTT to insoluble formazan, which was subsequently dissolved in dimethylsulfoxid (DMSO). The absorbance was measured at a wavelength of 560 nm.

3.2.4.1 Activation of apoptic pathways by MG and its prevention by PrRP31 and palm^{11}-PrRP31

For analysis of the molecular mechanism during MG-induced stress, the growth medium was exchanged for serum-free DMEM 16 h before the experiment. The cells were pretreated with 1 x 10^{-5} M PrRP31 or palm^{11}-PrRP31 for 4 h; then, MG was added to a final concentration of 0.6 mM, and the cells were incubated at 37℃ for 16 h. Cells were lysed in Laemmli buffer (described above in chapter 3.2.2) and stored at -20 °C. The controls and compounds were tested in triplicate.

3.2.5 Analysis of data and statistics

Data are presented as the means ± SEM and were analyzed with GraphPad Software (San Diego, CA, USA). Data from cell viability measurements and WB were analyzed using one-way ANOVA, followed by Dunnett´s post-hoc test or Student´s t-test, as stated in Figures. $P < 0.05$ was considered statistically significant.

3.3 Animal models – study designs, housing, and treatment

All animal experiments were performed following the ethical guidelines for animal experiments of the Czech Republic Act Nr. 246/1992 and were approved by the Committee for Experiments with Laboratory Animals of CAS of the Czech Republic.

3.3.1 Treatment of APP/PS1 mice on standard diet

APPswe/PSEN1dE9 (APP/PS1) male mice on the C57Bl/6J background and wild-type (WT) male controls of the same age were obtained at the age of 7 weeks from Jackson Laboratory (Bar Harbor, ME, USA), and they were housed in the animal facility of the IOCB CAS on a 12-h light/dark cycle (lights on at 5 a.m.) at a temperature of 23 ± 2 °C. The mice were housed 5 per cage until one week before the start of the treatment, at which point they were placed in separate cages and given free access to water and Ssniff®

Table 2: List of antibodies and their appropriate dilution used for WB

Antibody	Manufacturer and cat. no.	Blocking	Dilution
Akt, rabbit Ab	Cell Signaling Technology, Beverly, MA, USA, cat. no. 4691	5% milk	1:1 000, 5% BSA
p-Akt (Ser473), rabbit Ab	Cell Signaling Technology, Beverly, MA, USA, cat. no. 4060	5% milk	1:1 000, 5% BSA
p-Akt (Thr308), rabbit Ab	Cell Signaling Technology, Beverly, MA, USA, cat. no. 13038	5% milk	1:1 000, 5% BSA
Bad, rabbit Ab	Cell Signaling Technology, Beverly, MA, USA, cat. no. 9105	5% milk	1:1 000, 5% BSA
p-Bad (Ser136), rabbit Ab	Cell Signaling Technology, Beverly, MA, USA, cat. no. 9105	5% BSA	1:1 000, 5% BSA
p-Bad (Ser 112), rabbit Ab	Cell Signaling Technology, Beverly, MA, USA, cat. no. 9105	5% BSA	1:1 000, 5% BSA
Bax, rabbit Ab	Cell Signaling Technology, Beverly, MA, USA, cat. no. 14796	5% milk	1:1 000, 5% BSA
Bcl-2, rabbit Ab	Cell Signaling Technology, Beverly, MA, USA, cat. no. 3498	5% BSA	1:1 000, 5% BSA
CD68, mouse Ab	Abcam, Cambridge, GB, cat. no. ab31630	5% BSA	1:1 000, 5% BSA
c-Jun, rabbit Ab	Cell Signaling Technology, Beverly, MA, USA, cat. no. 9165	5% BSA	1:1 000, 5% BSA
p-c-Jun (Ser73), rabbit Ab	Cell Signaling Technology, Beverly, MA, USA, cat. no. 9164	5% BSA	1:1 000, 5% BSA
p44/42 MAPK (Erk1/2), mouse Ab	Cell Signaling Technology, Beverly, MA, USA, cat. no. 9107	5% milk	1:2 000, 5% milk
p-p44/42 MAPK (Erk1/2) (Thr202/Tyr204), mouse Ab	Cell Signaling Technology, Beverly, MA, USA, cat. no. 9106	5% milk	1:2 000, 5% milk
GAPDH, mouse Ab	Cell Signaling Technology, Beverly, MA, USA, cat. no. 97166	5% milk	1:1 000, 5% milk
GLUT4, mouse Ab	Cell Signaling Technology, Beverly, MA, USA, cat. no. 2213	5% milk	1:1 000, 5% milk
GSK 3β, rabbit Ab	Cell Signaling Technology, Beverly, MA, USA, cat. no. 9315	5% milk	1:1 000, 5% BSA
p-GSK 3β (Ser9), rabbit Ab	Cell Signaling Technology, Beverly, MA, USA, cat. no. 5558	5% milk	1:1 000, 5% BSA
IFNγ, rabbit Ab	Abcam, Cambridge, GB, cat. no. ab133566	5% milk	1:1 000, 5% milk
Insulin receptor β, rabbit Ab	Cell Signaling Technology, Beverly, MA, USA, cat. no. 3025	5% milk	1:1 000, 5% BSA
LRP1, rabbit Ab	Cell Signaling Technology, Beverly, MA, USA, cat. no. 64099	5% milk	1:1 000, 5% BSA
m-Tor, rabbit Ab	Cell Signaling Technology, Beverly, MA, USA, cat. no. 2983	5% BSA	1:1 000, 5% BSA
p-m-Tor, rabbit Ab	Cell Signaling Technology, Beverly, MA, USA, cat. no. 5536	5% BSA	1:1 000, 5% BSA
PDK1, rabbit Ab	Cell Signaling Technology, Beverly, MA, USA, cat. no. 3062	5% milk	1:1 000, 5% BSA
p-PDK1 (Ser241), rabbit Ab	Cell Signaling Technology, Beverly, MA, USA, cat. no. 3438	5% milk	1:1 000, 5% BSA
PI3K p85, rabbit Ab	Cell Signaling Technology, Beverly, MA, USA, cat. no. 4257	5% milk	1:1 000, 5% BSA
PSD95, mouse Ab	Cell Signaling Technology, Beverly, MA, USA, cat. no. 2507	5% BSA	1:1 000, 5% BSA
Synaptophysin, rabbit pAb	Santa Cruz Biotechnology, Dallas, TX, USA, cat. no. sc-9116	5% milk	1:5 000, 5% milk
Syntaxin 1A, rabbit Ab	Cell Signaling Technology, Beverly, MA, USA, cat. no. 18572	5% milk	1:1 000, 5% BSA
Tau 1	Merck Millipore, Burlington, USA, MAB3420	5% milk	1:10 000, 5% milk
Tau 5	Invitrogen/Thermo Fisher Scientific, Waltham, MA, USA, cat. no. AHB0042	5% milk	1:5 000, 5% milk
p-Tau (Ser396)	Invitrogen/Thermo Fisher Scientific, Waltham, MA, USA, cat. no. 44752G	5% BSA	1:10 000, 5% BSA
β-actin, mouse Ab	Sigma, St. Louis, MO, USA, cat. no. A5441	5% milk	1:10 000, 5% milk

R/M-H standard rodent chow (St) diet (Ssniff Spezialdiäten GmbH, Soest, Germany) containing 33%, 9% and 58% of calories from proteins, fats and carbohydrates, respectively. In the beginning of the treatment at 7 months of age, mice were randomly divided into groups of 9-10 animals.

APP/PS1 mice were subcutaneously (s.c.) injected with saline or palm^{11}-PrRP31 at a dose of 5 mg/kg of body weight (twice daily, injection volume of 0.15 ml per mouse) for 2 months (from the age of 7-8 months). WT mice (control mice) and APP/PS1 saline received s.c. injections of the same volume of saline. WT mice chronically injected with palm^{11}-PrRP31 exerted no significant difference compared to WT mice injected with saline (data not shown). This group was therefore not included in this study. The body weights of the mice were monitored once per week.

3.3.2 Impact of HFD on metabolic parametres and AD-related pathology in APP/PS1 and WT mice

In this experiment, APP/PS1 male mice on the C57Bl/6 background and WT male controls were obtained at the age of 7 weeks from the Biotechnology and Biomedicine Centre of the Academy of Sciences and Charles University (BIOCEV) (Vestec, Czech Republic) and they were housed in the animal facility of the IOCB CAS on a 12-h light/dark cycle (lights on at 5 a.m.) at a temperature of 23 ± 2 °C. The mice were housed 4-5 per cage until the end of the experiment and given free access to water and food. At the age of 8 weeks, mice were randomly divided into groups of 5-8 animals and according to Figure 9 they were fed either with St diet (STD), or high-fat diet (HFD) with caloric content percentage values 13% proteins, 60% fats and 27% carbohydrates. For the model characterization study, APP/PS1 and WT mice at the age 3, 6 and 10 months of age were used. The body weights of the mice were monitored once per week.

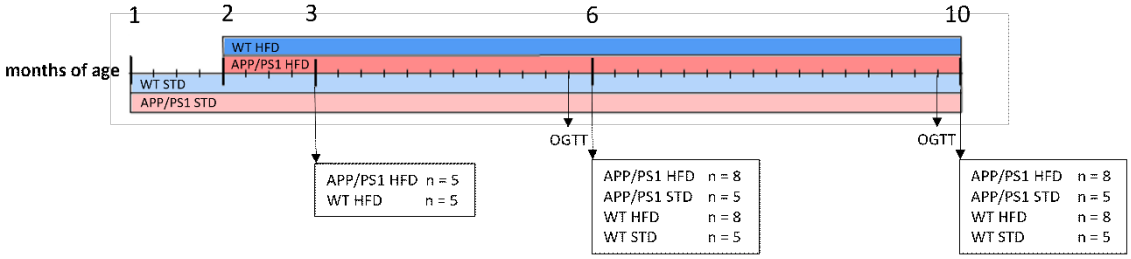

Figure 9: Experimental study design of treatment of APP/PS1 mice on HF diet.

3.4 Oral glucose tolerance test

Oral glucose tolerance test (OGTT) was performed in all studied groups one week prior to dissections. After 6 hours of fasting (time 0) blood glucose concentrations were measured in the blood from the tail vessel using Glucocard^{TM} X-meter (Arkray factory, Inc., Japan). 20% glucose solution at a dose of 2 g/kg of body weight was administred perorally and subsequentely blood glucose concentration was determined at 15, 30, 60, 90, 120, and 180 min after glucose administration. The areas under the curves (AUC) were calculated using GraphPad Prism 8.

3.5 Blood sampling

Blood samples were collected in the day of sacrification, from the tail vessels of overnight-fasted mice, and blood EDTA plasma was separated and stored at -80 °C. The mice were then deeply anesthetized with pentobarbital (50 mg/kg, intraperitoneally, Sigma Aldrich, St. Louis, MO, USA), the left heart ventricle was punctured, blood EDTA plasma was isolated and stored at − 80 °C. The mice were transcardially perfused with saline solution supplemented with heparin (10 U/ml, Zentiva, Prague, Czech Republic).

3.5.1 Determination of hormonal and biochemical parameters in fasting plasma

Blood glucose levels were measured using a glucometer (Arkray, Tokyo, Japan). Plasma insulin concentrations were measured using a RIA kit (Merck Millipore, Burlington, MA, USA), and plasma leptin concentrations were measured by using an ELISA kit (Merck Millipore, Burlington, USA). The concentrations of cholesterol and triacylglycerol in plasma were determined using enzymatic photometric assays (Erba, Mannheim, Germany). Concentration of fibroblast growth factor 21 (FGF21) in plasma was measured by using an ELISA kit (Merck Millipore, Burlington, USA). All measurements were performed by following the manufacturer's instructions.

3.5.2 Determination of CRP

The concentration of blood plasma c-reactive protein (CRP) in fasting plasma was determined by using a mouse CRP ELISA kit (Thermo Scientific, Frederick, MD, USA). The measurement was performed according to the protocols recommended by the manufacturers.

3.6 Organ dissections

The brains, livers, epididymal white adipose tissues (eWATs) and skeletal muscles were dissected, weighed, and maintained on ice prevent tissue degradation. While brains were studied in both studies with APP/PS1 mice, rest of the tissues were studied only in the characterization of APP/PS1 mice on HFD, decribed in the chapter 3.4.2.

3.6.1 Brains

The right hemisphere of each brain was postfixed in 4% paraformaldehyde in 0.1M phosphate-buffered saline, pH 7.4 (PBS) for 24 h and stored in a 30% sucrose solution supplemented with 0.1% sodium azide in PBS at 4 °C until cutting. The hippocampus was dissected from the left hemisphere of each brain for WB and prospectively for quantification of cytokine levels using ELISA kits; the hippocampi were frozen on dry ice immediately after dissection and stored at -80 °C until homogenization.

3.6.1.1 Immunohistochemistry

Paraformaldehyde-fixed right brain hemispheres were snap-frozen, and 30 μm coronal sections were cut throughout the hippocampus and cerebellum (an approximate depth of -0.9 to -3 and -5.5 to -7 from bregma) using a cryostat.

Detailed description of chromogenic staining protocol is described in the study of Holubová (Holubova et al., 2019). Briefly, the free-floating sections were incubated in citrate buffer to enhance antigen recognition and then in 0.6% H_2O_2 to quench endogenous peroxidase activity. Afterwards, the sections were permeabilized in TBS with 0.2% Triton X-100 (TBS-T) and blocked in 5% normal goat serum solution in TBS-T pH 7.4, to prevent nonspecific antibody binding. After blocking, the sections were incubated with the primary antibodies shown in Table 3 overnight at 4 °C. Subsequently, the

sections were incubated with biotinylated goat anti-rabbit IgG and then incubated with avidin-biotin peroxidase complex reagent. Finally, the samples were stained and mounted as described previously (Holubova et al., 2019). Stained sections were viewed and imaged under an Olympus IX83 inverted microscope (Olympus, Tokyo, Japan), using cellSens Imaging software (Olympus, Tokyo, Japan).

For the fluorescent immunohistochemistry, the free-floating sections were 3 times washed in 0.3% Triton X-100 with 0.25% BSA in PBS (PBS-T) pH 7.4, and then blocked in M.O.M (Vector Laboratories, Inc. Burlingame, CA, United States) in PBS to prevent nonspecific antibody binding (60 minutes in RT). After blocking, the sections were 3 times washed and incubated with the primary antibody against total Tau 9H12, or Tau 3-repeat isoform RD3 (Tau-3R) for 2 days at 4 °C; appropriate dilutions are provided in Table 3.

After three PBS-T washes, the sections were incubated with goat anti-mouse IgG2b heavy chain (Biotin) (Abcam, Cambridge, Great Britain) at RT for 60 minutes, 3 times washed with PBS-T and then incubated with Streptavidin, Alexa Fluor™ 568 conjugate (Invitrogen/Thermo Fisher Scientific, Waltham, MA, USA) at RT for 60 minutes. After 3 further washes in PBS, the sections were incubated either with the nuclear stain DAPI (Invitrogen/Thermo Fisher Scientific, Waltham, MA, USA), or with NeuroTrace™ 435/455 Blue Fluorescent Nissl Stain (Invitrogen/Thermo Fisher Scientific, Waltham, MA, USA) for visualizing neurons. Sections were washed 2 times in PBS, once in 0.9% NaCl (physiological serum), mounted on Superfrost® Plus slides (Invitrogen/Thermo Fisher Scientific, Waltham, MA, USA) and left dry.

Slides with air-dried sections were incubated with 1% Thioflavine S (Merck Millipore, Burlington, MA, USA) at RT for 30 minutes for staining fibrillar β-amyloid plaques and then washed for 3 minutes in 80% ethanol, in 90% ethanol and in tap water, respectively. Slides with stained sections were further washed in 70% ethanol for 5 minutes, incubated with Autofluorescence Eliminator Reagent (Merck Millipore, Burlington, MA, USA), washed in 70% ethanol for 1 minute and finally rinsed in physiological serum. Slides were coverslipped with VECTASHIELD® Antifade Mounting Medium (Vector Laboratories, Inc. Burlingame, CA, United States) and left to

dry up over night.

Stained sections were imaged by an IX83 P1ZF Olympus Microscope (Olympus Corporation, Tokyo, Japan) equipped with a DP74 camera with bright field or fluorescence CoolLed pE-Universal Collimator sources using OLYMPUS CellSens Dimension software.

For Aβ, Ionized calcium-binding adapter molecule 1 (Iba1), GFAP, syntaxin1A, spinophilin, Aquaporin 4 (AQ4), phospho-Tau (Ser202, Thr205) (AT8 Ab), total Tau (9H12 Ab), Neuronal Nuclear protein (NeuN), claudin and occludin staining, images of the whole area of the interest were taken at 10x magnification (approximately 8-10 sections per staining per mouse). The percentage of the area stained for the designated protein was analyzed using ImageJ software (NIH, Bethesda, MD, USA). The area of interest was selected manually according to the Paxinos and Franklin mouse brain atlas (Paxinos and Franklin, 2003). The threshold was kept constant, for all samples in each staining experiment. For doublecortin (DCX) and Tau-3R staining, the number of DCX+ and Tau 3R+, respectively, was counted manually using the ImageJ Multi-Point tool. The results are expressed as a percentage of the control group marked in every study to enable comparison of different staining series.

3.6.1.2 Tissue Preparation for WB

The left hippocampi were homogenized 1 minute in ice-cold lysis buffer A (62.5mM TRIS-HCl pH 6.8, 1% Triton X-100, 1% deoxycholate, 50mM NaF, 1mM Na3VO3, cOmpleteTM Protease Inhibitor Cocktail (CO-RO) (1 tablet/50 ml of solution), Roche, Mannheim, Germany) using a Bullet Blender homogenizer (Next Advance, Inc., Averill Park, NY, USA). The tissue samples were kept on ice during the homogenization to prevent the protein degradation. The homogenates were sonicated for 1 min, and the protein concentration was determined by using a Pierce BCA protein assay kit (Thermo Fisher Scientific, Waltham, MA, USA). The lysates were diluted to a final concentration of 1 μg/μl in Laemmli sample buffer (62.5 mM Tris-HCl (pH 6.8), 2% SDS, 10% glycerol, 0.01% bromphenol blue, 5% β-mercaptoethanol, 50 mM NaF, and 1 mM Na_3VO_4) and stored at -20 °C. In the study of HFD impact on metabolic parameters and AD-related pathology in APP/PS1 and WT mice, 3-month-old WT mice on HFD were

Table 3. List of antibodies and their appropriate dilution used for immunohistochemistry

Antibody	**Manufacturer and cat. no.**	**Dilution**
Aquaporin 4 rabbit pAb	Abcam, Cambridge, GB, cat. no. ab46182	1 : 300
AT8 (phospho-Tau pSer202 + pThr205) mouse mAb	Invitrogen/Thermo Fisher Scientific, Waltham, MA, USA, cat.no. MN1020	1 : 400
β-amyloid rabbit pAb	Invitrogen/Thermo Fisher Scientific, Waltham, MA, USA, cat. no. 715800	1 : 500
Claudin 5 rabbit mAb	Abcam, Cambridge, GB, cat. no. ab131259	1 : 600
Doublecortin rabbit pAb	Cell Signaling Technology, Beverly, MA, USA, cat. no. 4604	1 : 600
GFAP rabbit pAb	Invitrogen/Thermo Fisher Scientific, Waltham, MA, USA, cat. no. PA5-16291	1 : 500
Iba1 rabbit mAb	Fujifilm Wako Pure Chemical Corporation, Osaka, Japan, cat. no. 01919741	1 : 2 000
NeuN rabbit pAb	Invitrogen/Thermo Fisher Scientific, Waltham, MA, USA, cat.no. 711054	1 : 250
Occludin rabbit pAb	Abcam, Cambridge, GB, cat. no. ab222691	1 : 600
Tau-3R mouse mAb	Merck Millipore, Burlington, MA, USA, cat.no. 05803	1 : 200
Tau 9H12 (total Tau) mouse mAb	Generous gift from Dr. M.-C.Galas, INSERM, Lille, France	1 : 100
Spinophilin rabbit mAb	Cell Signaling Technology, Beverly, MA, USA, cat. no. 14136	1 : 800
Syntaxin 1A rabbit mAb	Cell Signaling Technology, Beverly, MA, USA, cat. no. 18572	1 : 800

chosen as a control group to enable the comparison of multiple staining series. WB was performed as described in chapter 3.2.3. The rest of the lysate was used for the quantification of cytokine level.

3.6.2 Livers

The hepatic caudate lobes were postfixed in 4% paraformaldehyde in PBS for 24 h and stored in a 70% etanol at 4 °C and stored until embending to parrafine. Approximately 100 mg of each hepatic left lobe was dissected and frozen on dry ice immediately after dissection and stored at -80 °C until homogenization in lysis buffer A.

3.6.2.1 Liver histology

Liver histology including qualification was made by Dr. Veronika Strnadová. For the hematoxylin/eosin staining marking steatosis, the liver samples were paraffined, cut and stained as described previously in (Kořínková et al., 2019). Briefly, liver samples in paraffin blocks were cut to slices of 5 μm thickness. Deparaffinization in xylene and rehydration in an ethanol range were performed. Slices were stained in hematoxylin using Weigert's iron hematoxylin solution set and subsequently stained in eosin. Level of liver steatosis was evaluated as % of fat droplets as in the study of Kleiner (Kleiner et al., 2005).

For the fibrotic liver staining, liver samples were deparaffinized in xylene and rehydrated in an ethanol range as described previously. Sample slides were then transfered into Weigert´s hematoxylin solution for 10 minutes and afterwards rinsed for 5 minutes in tap water to remove rest of the solution. Washed samples were stained with Pico-sirius red solution (0.25 g of Sirius Red, 250 ml of 1.3% Picric acid solution) for 15 minutes. Slices were then dehydrated 3 times for 5 minutes in 99.99% ethanol and afterwards 2 times for 2 minutes in xylene and mounted with DPX medium (Sigma Aldrich, St. Louis, MO, USA). Histological images were performed at 20× magnification. Level of fibrosis was scored according to Kleiner´s study (Kleiner et al., 2005).

3.6.2.2 Tissue preparation for WB

Liver homogenization was performed by following the procedure described in 2.6.1.2 with excerpted changes. Hepatic left lobes were homogenized for 5 minutes in ice-cold lysis buffer A using a Tissue Lyser II (Qiagen, Hilden, Germany). The lysates

were diluted to a final concentration of 2 µg/µl in Laemmli sample buffer and stored at -20 °C. WB was performed as described in chapter 3.2.3.

3.6.3 eWAT

300 mg of each eWAT was dissected and frozen on dry ice immediately after dissection and stored at -80 °C until homogenization in lysis buffer B (50mM TRIS-HCl pH 7.4, 150mM NaCl, 1mM EDTA, 1mM phenylmethylsulfonyl fluoride, 10µM leupeptin, 1mM Na_3VO_4, 1mM NaF, 0.5 % sodium deoxycholate, 0,1% sodium dodecyl sulfate).

3.6.3.1 Tissue preparation for WB

eWAT homogenization was performed following the procedure described in 2.6.1.2 with excerpted changes. eWATs were homogenized 3 times for 3 minutes and deeply freezed between every homogenization. Afterwards, an ice-cold lysis buffer B was added, and samples were further homogenized 2 times for 3 minutes using a Tissue Lyser II with metal beads (VWR, Radnor, Pennsylvania, USA) for better homogenization. The lysates were diluted to a final concentration of 2 µg/µl in Laemmli sample buffer and stored at -20 °C. WB was performed as described in chapter 3.2.3.

3.6.4 Muscles

Left gastrocnemius of each mouse was dissected and frozen on dry ice immediately after dissection and stored at -80 °C until homogenization in lysis buffer A.

3.6.4.1 Tissue Preparation for WB

Muscle homogenization was performed following the procedure described in 2.6.1.2 with excerpted changes. Samples of gastrocnemius were homogenized 5 times for 1 minute in ice-cold lysis buffer B using a Tissue Lyser II with metal beads, alternately with 30 s incubation on ice. The lysates were diluted to a final concentration of 2 µg/µl in Laemmli sample buffer and stored at -20 °C. WB was performed as described in chapter 3.2.3.

3.6.5 Quantification of cytokine level

Cytokine levels were quantified in hippocampi, livers, and blood plasma samples. The protein concentration of the hippocampi lysates (see section 3.6.1.2), liver lysates (see section 3.6.2.2) was determined by using a Pierce BCA protein assay kit. The lysates were diluted to a final concentration of 10 μg protein/μl in lysis buffer A. Blood plasma samples were not diluted. IL6 and TNFα concentrations were measured by using ELISA kits (Thermo Fisher Scientific, Waltham, MA, USA). All measurements were performed according to the protocols recommended by the manufacturers.

3.6.6 Statistical analyses

The data are presented as the means ± SEMs. In the study of effect of palmitoylated PrRP analog on Aβ pathology and microgliosis in APP/PS1 mice, statistical analysis was performed by using one-way ANOVA with Dunnett post-hoc test. In the study of HFD impact on metabolic parametres and neurodegeneration in APP/PS1 and WT mice, statistical analysis was performed by using one-way ANOVA with Bonferroni post-hoc test as only by this testing the comparison between all mouse groups was enabled. Statictical analyses was made with GraphPad Prism Software (San Diego, CA, USA) and $p<0.05$ was considered statistically significant.

The rate of insulin resistance was expressed with a homeostatic model assessment (HOMA-IR) index calculated as (fasting glucose level, mmol/l) x (fasting insulin level, pmol/l) divided by 22.5 (Lansang et al., 2001).

4. RESULTS

4.1 Cellular signaling and anti-apoptotic effects of PrRP and its lipidized analog palm^{11}-PrRP31 on SH-SY5Y cells

The results obtained in experiments performed in human neuroblastoma SH-SY5Y cells and primary rat cortical neurons presented in the following chapters were published in International Journal of Molecular Sciences (IJMS) (Zmeskalova et al., 2020).

4.1.1 PrRP31 and palm^{11}-PrRP31 activated the PI3K/Akt signaling pathway in SH-SY5Y cells

Both PrRP31 and palm^{11}-PrRP31 did not significantly affect PI3K level. Palm^{11}-PrRP31 significantly increased the level of p-PDK1 (Ser241)/PDK1 (Figure 11). Both peptides significantly increased the level of p-Akt (Ser473)/Akt, palm^{11}-PrRP31 also significantly enhanced the level of p-Akt (Thr308)/Akt (Figure 11). Both peptides subsequently significantly increased the levels of the p-GSK3β (Ser9)/GSK3β, and the p-m-Tor (Ser2448)/m-Tor. Scrambled-palm^{11}-PrRP31 analog (scrambled) with structure figured in the chapter 2.1, was used as a negative control, and did not affect the PI3K/Akt pathway (Figure 11). Insulin was used as a positive control and as expected, it significantly activated proteins of the insulin signaling cascade.

4.1.2 PrRP31 and palm^{11}-PrRP31 activated the ERK-CREB signaling pathway in SH-SY5Y cells

PrRP31 and palm^{11}-PrRP31 significantly increased both p-ERK (Thr 202/Tyr204)/, and p-CREB (Ser133)/CREB. Insulin was used as a positive control and proved activation of the mentioned signaling pathways in SH-SY5Y cells by PrRP31 and palm^{11}-PrRP31. On the other hand, scrambled-palm^{11}-PrRP31, as negative control, activated neither ERK, nor CREB. Representative immunoblots and their quantifications are shown in Figure 12.

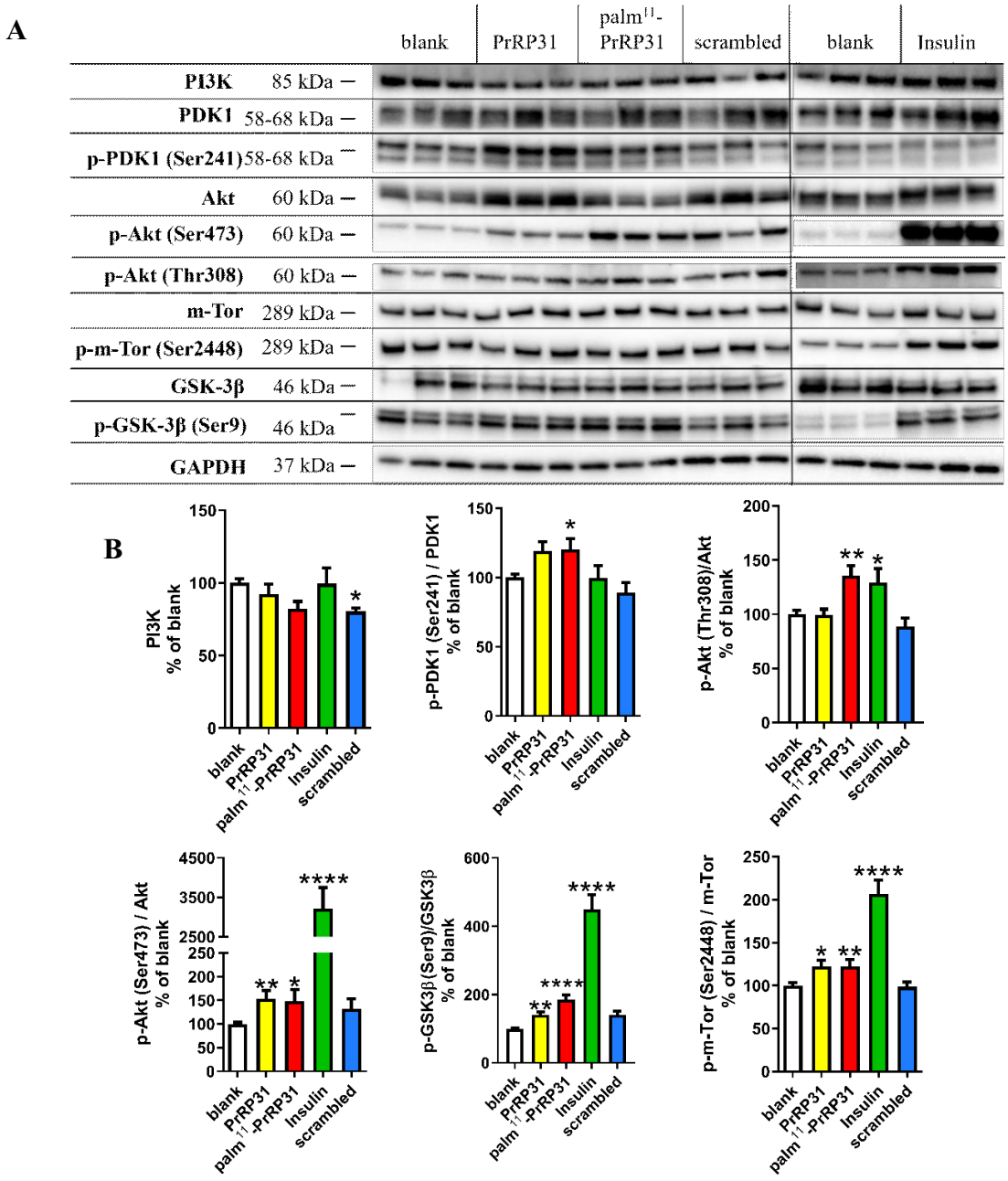

Figure 11. PrRP31 and palm^{11}-PrRP31 activated PI3K/Akt signaling pathway in SH-SY5Y cells. Immunoblots: (A) and their quantifications: (B). SH-SY5Y cells were incubated either with PrRP31 or palm^{11}-PrRP31 or scrambled palm^{11}-PrRP31 at a final concentration $1x10^{-5}$ M, or with insulin at the final concentration $1x10^{-7}$ M at 37°C for 8 minutes, or medium alone (blank). Activation was expressed as the ratio of the phosphorylated protein to the total protein, both normalized to loading control GAPDH. Data are presented as the means ± SEM as a percentage of control cells analysed by one-way ANOVA followed by Dunnett post-hoc test, *p<0.05, **p<0.01, ****p<0.0001 (dates of sampling n=3, each compound in triplicates).

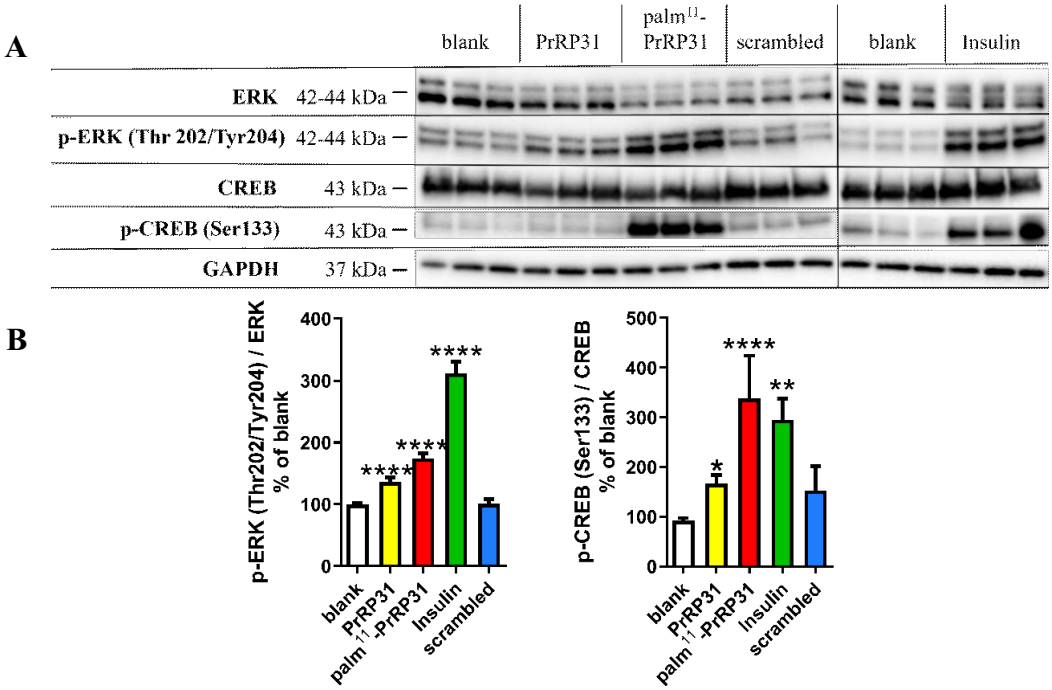

Figure 12. PrRP31 and palm^{11}-PrRP31 increased phosphorylation of ERK-CREB signaling pathway in SH-SY5Y cells. Immunoblots: (A) and their quantifications: (B) SH-SY5Y cells were incubated either with PrRP31 or palm^{11}-PrRP31 or scrambled-palm^{11}-PrRP31 at a final concentration 1x10^{-5} M, or with insulin at the final concentration 1x10^{-7} M at 37°C for 8 minutes, or medium alone (blank). Activation was expressed as the ratio of the phosphorylated protein to the total protein, both normalized to loading control GAPDH. Data are presented as the means ± SEM as a percentage of blank cells analysed by one-way ANOVA followed by Dunnett post-hoc test, *p<0.05, **p<0.01, ****p<0.0001 (dates of sampling n=3, each compound in triplicates).

4.1.3 Specific inhibitors of signaling proteins confirmed that PrRP31 and palm^{11}-PrRP31 activated m-Tor, ERK and GSK-3β in SH-SY5Y cells

From the results shown in Figure 13, it is evident that specific inhibitors significantly decreased the phosphorylation of relevant signaling proteins in the majority of experiments. After application of PrRP31, palm^{11}-PrRP31 or insulin as a positive control, p-m-Tor (Ser2448) was significantly increased; this increase was inhibited by the treatment with rapamycin, a selective inhibitor of m-TorC1 complex under the control level. A slight increase was also observed in p-GSK-3β (Ser9) after incubation with palm^{11}-PrRP31 and insulin. A selective inhibitor of GSK-3β, SB216736, significantly reversed the palm^{11}-PrRP31 effect and tended to decrease that of insulin. p-ERK and

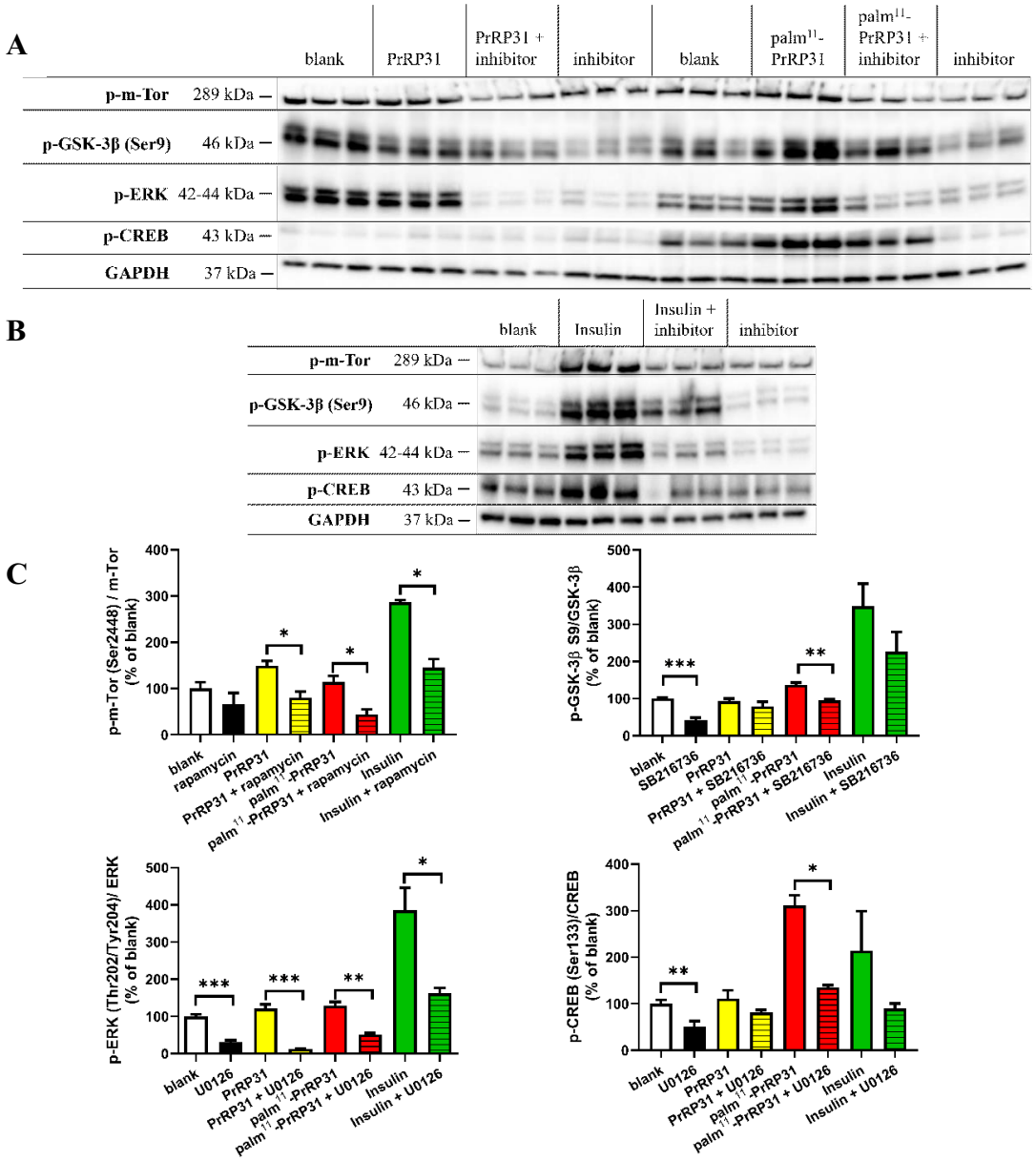

Figure 13. Inhibitors of m-Tor, ERK and GSK-3β (rapamycin, SB216736, U0126, respectively) proved that activation of these signaling pathways are mediated exclusively via PrRP31 and its palmitoylated analog. Immunoblots with (A) PrRP31 and palm^{11}-PrRP31 and (B) insulin and their quantifications: (C). SH-SY5Y cells were incubated first with selective inhibitors for 2 minutes and then either with PrRP31 and its palmitoylated analog at a final concentration $1x10^{-5}$ M, or with insulin in the final concentration $1x10^{-7}$ M at 37°C for 8 minutes, or inhibitors only in serum-free medium. Protein was normalized to loading control, GAPDH. Data are presented as the means ± SEM as a percentage of blank cells treated with medium alone. Analysis is made between groups as shown in the graphs by Student´s t-test, *p<0.05, **p<0.01, ***p<0.001 (dates of sampling n=3, each compound in triplicates).

p-CREB were increased after incubation with all three peptides similarly as in 4.1.2. This effect was significantly blocked under the blank level, by a selective inhibitor of MAPK kinase activity, U0126. This prove CREB being activated by ERK.

4.1.4 PrRP31 and its lipidized analog attenuated methylglyoxal-induced cytotoxicity in SH-SY5Y cells and rat cortical neurons

For optimization, increasing concentrations of MG (0.3 mM, 0.6 mM, and 1.2 mM) were used for its cytotoxic effect in SH-SY5Y cells (Figure 14A) or rat primary neurons (Figure 14B). DMSO was used as a comparator of MG-induced cytotoxicity. MG at concentration 0.3 mM did not decrease cell viability, however, MG at concentrations of 0.6 mM and 1.2 mM significantly decreased cell viability of SH-SY5Y cells and rat primary cortical neurons, compared to that treated with vehicle. MG at 0.6 and 1.2 mM was therefore used for further study.

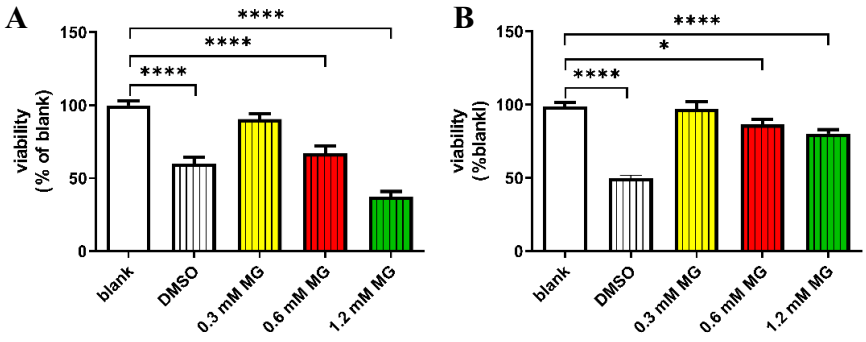

Figure 14. Optimization of methylglyoxal (MG) concentration for study of potential anti-apoptotic properties of PrRP. MG was incubated for 16 hours, and toxicity was measured with MTT assay: (A) in SH-SY5Y cells; (B) in rat primary neuronal culture. Data are presented as the means ± SEM as a percentage of blank cells treated with medium alone. Statistics: one-way ANOVA followed by Dunnett post-hoc test, *p<0.05, ****p<0.0001 (n=3, each concentration in octuplicates).

4.1.4.1 PrRP31 and palm^{11}-PrRP31 prevented SH-SY5Y cells from the cytotoxic effects of MG

MG at a concentration of 1.2 mM significantly decreased the cell viability compared to untreated cells in the MTT assay. 4h pretreatment with 1x10^{-5} M PrRP31 or palm^{11}-PRRP31 in SH-SY5Y cells resulted in significantly increased cell viability, compared the nonpretreated cells (Figure 15A). At concentration 1x10^{-7} M pretreatment with palm^{11}-PrRP31, but not PrRP31 significantly increased viability, compared to nonpretreated cells

affected with 1.2 mM MG (Figure 15B). At a concentration of 0.6 mM MG also significantly decreased cell viability compared to that of the vehicle-treated cells. Pretreatment with both PrRP31 and palm^{11}-PRRP31 at a concentration 1x10^{-5} M resulted in significantly increased cell viability (Figure 15C), pretreatment at a concentration 1x10^{-7} M significantly increased cell viability, compared to nonpretreated cells (Figure 15D).

Pretreatment with PrRP31 and palm^{11}-PrRP31 at a concentration 1x10^{-5} M in rat primary neuronal culture resulted in significantly enhanced cell viability, compared to nonpretreated cells administered with 0.6 mM MG (Figure 15E).

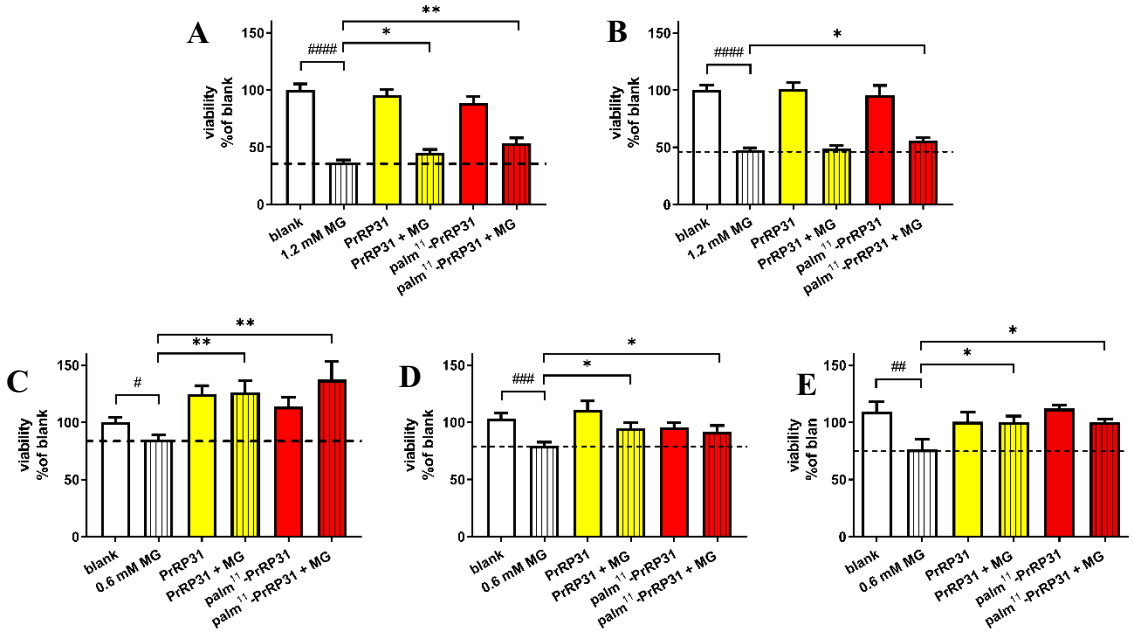

Figure 15. PrRP31 and palm^{11}-PrRP31 significantly increased cell viability during the MG-induced stress. Pretreatment for 4 h with PrRP31 and palm^{11}-PrRP31 at a concentration of: 1x10^{-5} M (A); or 1x10^{-7} M (B), followed by exposure to 1.2 mM MG for 16 h in SH-SY5Y cells. Pretreatment for 4 h with PrRP31 and palm^{11}-PrRP31 at a concentration of: 1x10^{-5} M (C); 1x10^{-7} M (D) in SH-SY5Y cells; or 1x10^{-5} M (E) in rat primary neuronal culture, followed by exposure to 0.6 mM MG for 16 h in SH-SY5Y cells. MG toxicity was measured with MTT assay. Data are presented as the means ± SEM as a percentage of blank cells treated with vehicle analysed by Student´s t-test vs 0.6 mM MG #p<0.5, ##p<0.01, ###p<0.001, ####p<0.0001 (dates of sampling n=3, each compound in octuplicates). MG vs treated cells analysed by Student´s t-test, *p<0.05, **p<0,01.

4.1.4.2 PrRP and palm^{11}-PrRP31 increased the viability of SH-SY5Y cells after 16 h of exposure to MG

MG at a concentration of 1.2 mM again significantly decreased cell viability compared to the control cells. 4h treatment with PrRP31 and its palmitoylated analog at

a concentration of $1x10^{-5}$ M in SH-SY5Y cells did not affect cell viability decreased by MG, compared to the cells administered only with 1.2 mM MG (Figure 16A).

MG at a concentration of 0.6 mM also significantly decreased cell viability compared to that of the control cells in the MTT test; treatment with PrRP31 and palm^{11}-PrRP31 at concentrations $1x10^{-5}$ M (Figure 16B) or $1x10^{-7}$ M (Figure 16C) in SH-SY5Y cells resulted in significantly increased cell viability compared to the nontreated cells treated with 0.6 mM MG.

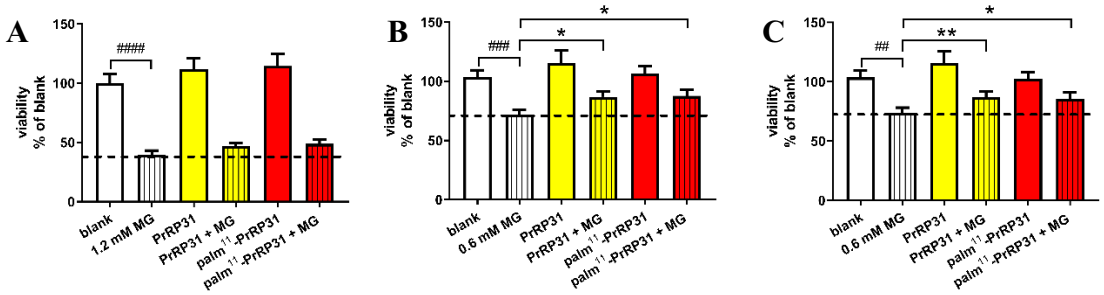

Figure 16. PrRP31 and palm^{11}-PrRP31 increased cell viability of SH-SY5Y cells after 16-hour exposure to MG. Treatment for 4 h with PrRP31 and palm^{11}-PrRP31 at a concentration of: $1x10^{-5}$ M (A); after exposure to 1.2 mM MG for 16 h in SH-SY5Y cells. Treatment for 4 h with PrRP31 and palm^{11}-PrRP31 at a concentration of: $1x10^{-5}$ M (B); $1x10^{-7}$ M (C), after exposure to 0.6 mM MG for 16 h in SH-SY5Y cells. MG toxicity measured with MTT assay. Data are presented as the means ± SEM as a percentage of blank cells treated with vehicle analysed by Student´s t-test vs 0.6 mM MG ##p<0.01, ###p<0.001, ####p<0.0001 (n=3, each sample in octuplicates). MG vs treated cells analysed by Student´s t-test, *p<0.05, **p<0,01.

4.1.4.3 PrRP31 and palm^{11}-PrRP31 induced anti-apoptotic signaling in SH-SY5Y cells

Representative immunoblots of SH-SY5Y cells pretreated with the peptides and then stressed with MG, and their quantification are shown in Figure 17. The levels of pro-apoptotic p-Bcl-2-associated death promoter (Bad) (Ser112)/Bad and p-Bad (Ser136)/Bad were increased after MG, tended to decrease in the cells pretreated with

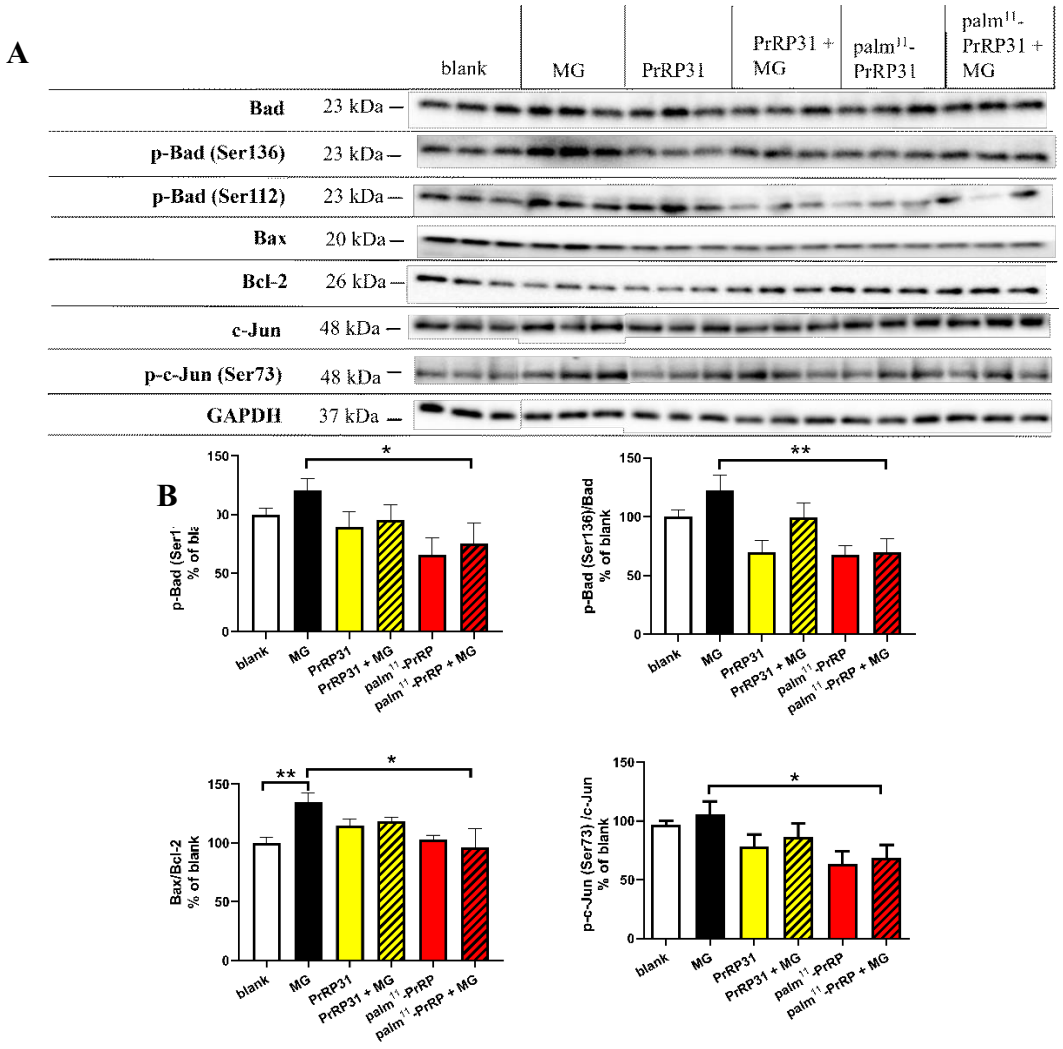

Figure 17. PrRP31 and palm^{11}-PrRP31 improved anti-apoptotic signaling in SH-SY5Y cells. Immunoblots: (A) and their quantifications: (B). SH-SY5Y cells were pretreated with PrRP31 and palm^{11}-PrRP31 at a concentration of $1x10^{-5}$ M for 4 h and then stressed with 0.6 mM MG for 16 h. Activation was expressed as the ratio of the activated protein to the total amount of the protein both normalized to loading control, GAPDH. Data are presented as the means ± SEM as a percentage of blank cells treated with medium alone. Analysis is made vs MG by Student´s t-test, *p<0.05, **p<0.01 (each sample in triplicates).

PrRP31 and were significantly decreased in the cells pretreated with palm^{11}-PrRP31. The pro-apoptotic ratio of Bax/Bcl-2 regulators significantly increased after MG exposure was attenuated significantly in the cells pretreated with palm^{11}-PrRP31. MG increased the level of p-c-Jun (Ser73)/c-Jun, which tended to decrease in SH-SY5Y treated with PrRP31, and significantly decreased in the SH-SY5Y cells pretreated with palm^{11}-PrRP31.

4.1.4.4 PrRP31 and palm^{11}-PrRP31 attenuated Tau hyperphosphorylation at different epitopes in SH-SY5Y cells

MG increased Tau phosphorylation at Ser396 (Figure 18). Pretreatment with either PrRP31 or palm^{11}-PrRP31 significantly attenuated this phosphorylation. Tau 1 antibody detects unphosphorylated Tau at Ser198/199/202. The level of Tau 1/total Tau (Tau 5 antibody) tended to decrease after MG, pointing to increase phosphorylation of Tau. Pretreatment with PrRP31 tended to, while palm^{11}-PrRP31 significantly attenuated Tau phosphorylation shown by increase in unphosphorylated Tau labeled by Tau 1 antibody.

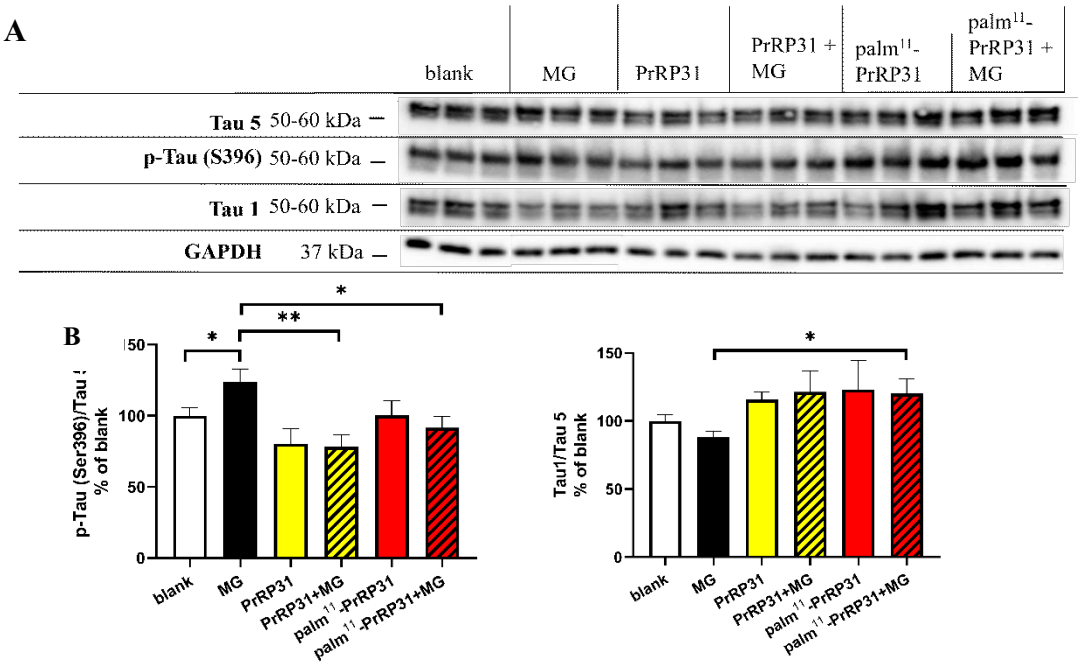

Figure 18. PrRP31 and palm^{11}-PrRP31 attenuated Tau hyperphosphorylation induced by MG at the epitopes Ser396 and Ser198/199/202 (Tau1) in SH-SY5Y. Immunoblots: (A) and their quantifications: (B). SH-SY5Y cells were pretreated with PrRP31 and palm^{11}-PrRP31 at a concentration of 1x10^{-5} M for 4 h and then stressed with 0.6 mM MG for 16 h. Phosphorylation was expressed as the ratio of the phosphorylated protein to the total amount of the protein both normalized to loading control, GAPDH. Data are presented as the means ± SEM as a percentage of blank cells treated with medium alone. Analysis is made vs MG by Student´s t-test, *p<0.05, **p<0.01 (each sample replicate in triplicate).

4.2 Effect of palm^{11}-PrRP31 analog on pathological markers connected to AD in APP/PS1 mice on standard diet

Results obtained in experiments performed with APP/PS1 mouse model presented in the following chapters were published in Current Alzheimer Research (CAR) (Mengr et

al., 2021). Results confirm and extend previous study from our laboratory (Holubová et al., 2019).

4.2.1 Effects of palm^{11}-PrRP31 on body weight and metabolic parameters

Throughout the two months of treatment, palm^{11}-PrRP31 did not significantly reduce the body weights (BW) of APP/PS1 mice, or affect metabolic parameters measured at the end of the experiment (Table 4), such as glucose, insulin, or leptin blood levels.

Table 4: BW and metabolic parameters in the APP/PS1 mice and their age-matched controls.

Parameter	APP/PS1 saline	APP/PS1 palm^{11}-PrRP31	control saline
BW change [% of initial BW]	-1.32 ± 0.81	-4,59 ± 1.10	-0.21 ± 1.04
Glucose [mmol/l]	7.29 ± 0.55	9.00 ± 0.78	6.86 ± 0.26
Insulin [ng/ml]	0.26 ± 0.04	0.28 ± 0.04	0.24 ± 0.03
Leptin [ng/ml]	1.87 ± 0.42	1.01 ± 0.33	1.89 ± 0.71

The data are presented as the means ± SEM. Statistical analysis is made between groups as shown in the graphs by by one-way ANOVA with Dunnett post-hoc test (n = 9-10 mice per group).

4.2.2 Palm^{11}-PrRP31 reduced the Aβ plaque load, microgliosis and astrocytosis in the hippocampi and cortices of APP/PS1 mice

Photomicrographs of immunohistochemically stained brain sections showed the development of extensive Aβ plaque loads in the hippocampi of APP/PS1 mice (Figure 19), whereas age-matched control mice (Figure 19C) did not develop any plaques. As expected according to our previous study (Holubova et al., 2019), two months of treatment with palm^{11}-PrRP31 (Figure 19B) reduced the number of Aβ plaques in both the hippocampus and the cortex.

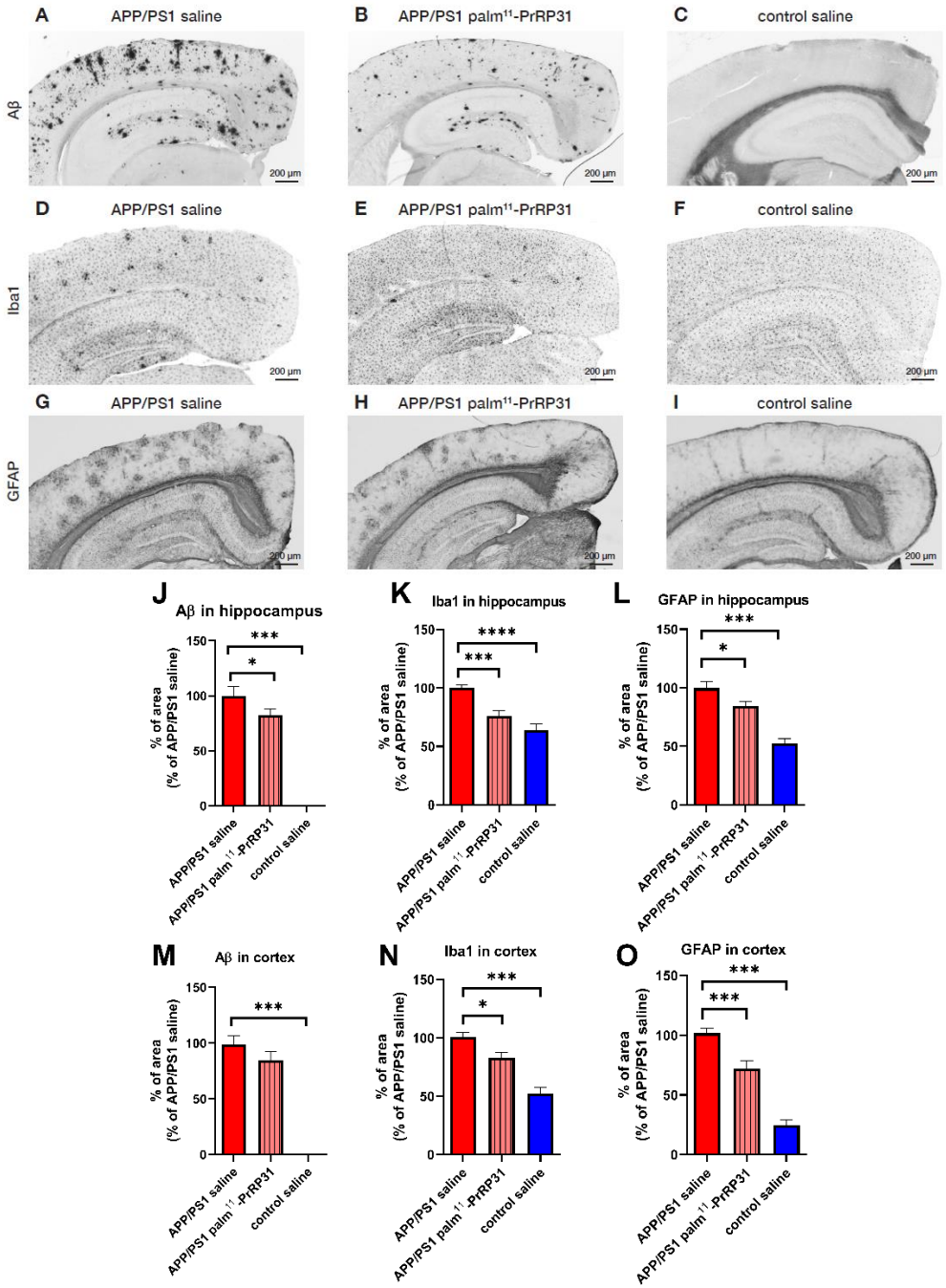

Figure 19: Aβ plaque load, microgliosis and astrocytosis in the hippocampus and cortex of the APP/PS1 mice. Reduction of β-amyloid plaque load, microgliosis and astrocytosis in the hippocampus and cortex of the APP/PS1 mice after treatment with palm^{11}-PrRP31. Representative photomicrographs of the saline and palm^{11}-PrRP31 treated APP/PS1 mice, and their age-matched controls immunohistochemically stained for human Aβ peptide (A-C), for microglial marker Iba1 (D-F) and for astrocyte marker GFAP (G-I) and their quantification (J-O). Percentage of the stained area is expressed as a % of the saline-treated APP/PS1 group to enable the comparison of multiple staining series. The data are presented as the means ± SEM. Statistical analysis is made between groups as shown in the graphs by one-way ANOVA with Dunnett post-hoc test, *p<0.05, ***p<0.001 (n = 9-10 mice per group).

Immunohistochemical staining of Iba1, a marker specifically expressed by both resting and activated microglia and macrophages, revealed visible clusters of activated microglia in the hippocampi and cortices of APP/PS1 mice (Figure 19D) but not the hippocampi and cortices of control mice, where only resting microglia were visible (Figure 19F). Activated microglia exhibit differences in morphology; activated cells are less ramified, possess fewer branches and are more widely hypertrophic than ramified microglia in control tissue. Two months of treatment with palm^{11}-PrRP31 (Figure 19E) reduced microgliosis in both the hippocampus and the cortex.

Immunohistochemical staining of GFAP, a marker of astrocytes, revealed clusters of reactive astrocytes, which were visible mainly in the cortex, but also found in the hippocampus in APP/PS1 mice (Figure 19G) but not in control mice (Figure 19I). The number of reactive astrocytes was reduced after two months of palm^{11}-PrRP31 treatment, both in hippocampi and cortices (Figure 19H).

4.2.3 Palm^{11}-PrRP31 reduced the Aβ plaque load and microgliosis in the cerebella of APP/PS1 mice

To further study the effects of palm^{11}-PrRP31, we performed immunohistochemical staining of the cerebellum to assess Aβ plaque load, microgliosis and astrocytosis. Widespread Aβ plaques were found in the cerebella of APP/PS1 mice (Figure 20A), whereas plaques did not develop in the cerebella of control mice (Figure 20C). The number of Aβ plaques was significantly reduced after two months of treatment with palm^{11}-PrRP31 (Figure 20B).

In the cerebella of APP/PS1 mice, clusters of activated microglia were also visible (Figure 20E). The percentage of the area stained with Iba1 was significantly increased in the APP/PS1 mice compared to their controls, where only resting microglia were visible (Figure 20G). Treatment with palm^{11}-PrRP31 (Figure 20F) significantly reduced cerebellar microgliosis. We did not observe any difference in the percentage of area stained for astrocytes between APP/PS1 mice and control mice (Figure 20I).

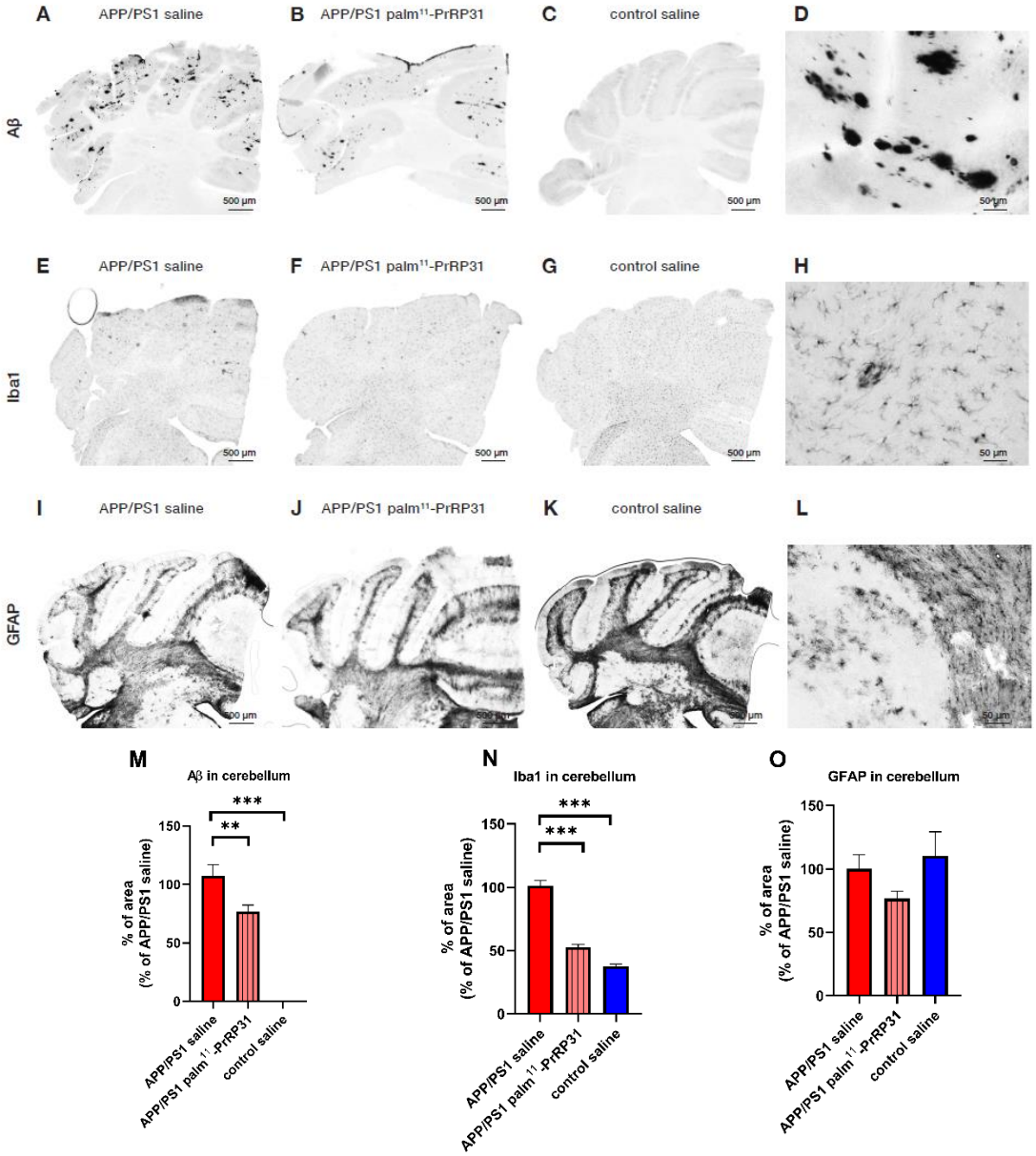

Figure 20: Reduction of β-amyloid plaque load and microgliosis in the cerebellum of the APP/PS1 mice after treatment with palm^{11}-PrRP31. Representative photomicrographs of the saline and palm^{11}-PrRP31 treated APP/PS1 mice and their age-matched controls immunohistochemically stained (A-C) for human Aβ, (E-G) for microglial marker Iba1 and (I-K) for astrocyte marker GFAP. M-O, quantification of immunohistochemical staining (M) of human Aβ, (N) of microglial marker Iba1 and (O) of astrocyte marker GFAP in cerebellum. (D,H,L) Detailed photomicrographs illustrating (D) Aβ plaques, (H) microglial activation and (L) astroglial activation in APP/PS1 saline mice. Percentage of the stained area is expressed as a % of the saline-treated APP/PS1 group to enable the comparison of multiple staining series. The data are presented as the means ± SEM. Statistical analysis is made between groups as shown in the graphs by one-way ANOVA with Dunnett post-hoc test, **p<0.01, ***p<0.001 (n = 9-10 mice per group).

4.2.4 Palm^{11}-PrRP31 reduced neuroinflammation in the hippocampi of APP/PS1 mice

We observed increased protein levels of neuroinflammation markers in the hippocampi of APP/PS1 mice, as shown in Figure 21. APP/PS1 mice had slightly increased CD68 (Figure 21B) and significantly increased pro-inflammatory IFNγ (Figure 21C), a commonly used marker of inflammation. Treatment with palm^{11}-PrRP31 significantly decreased both CD68 and IFNγ.

Compared to control mice, APP/PS1 mice showed slightly increased protein levels of the pro-inflammatory cytokine TNFα (Figure 21D) and significantly increased protein levels of the pro-inflammatory cytokine IL6 (Figure 21E); two months of treatment with palm^{11}-PrRP31 tended to attenuate the both of them.

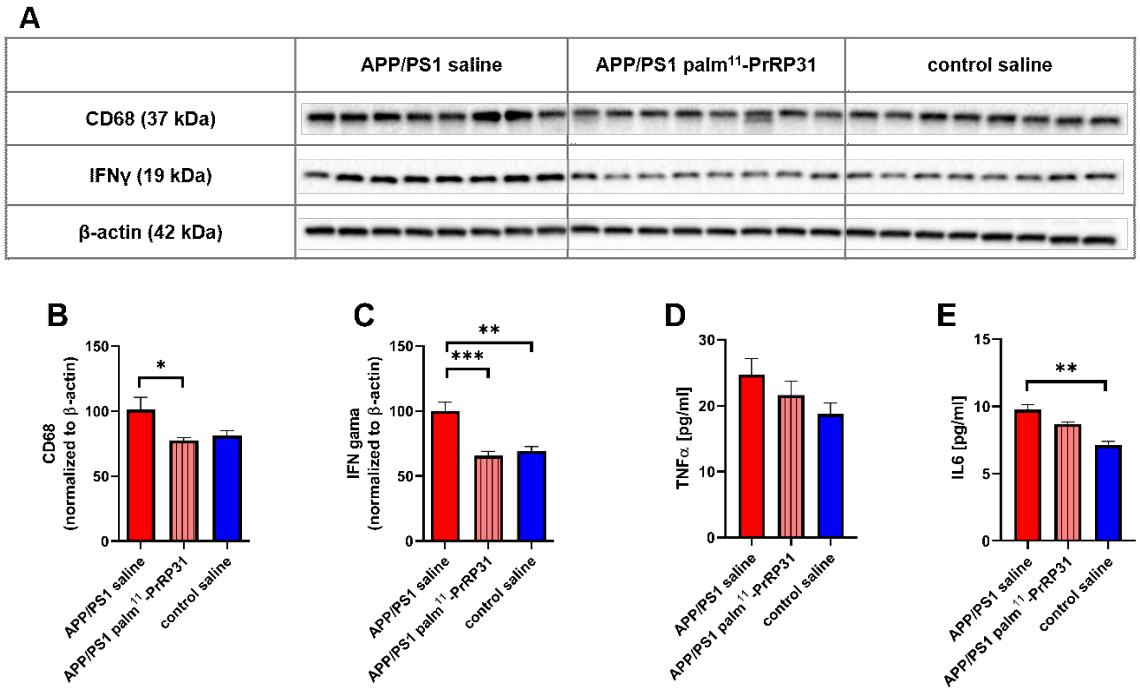

Figure 21: Decreased level of pro-inflammatory proteins in the hippocampi of the APP/PS1 mice after treatment with palm^{11}-PrRP31. Protein levels of CD68 and IFNγ were determined by WB. Immunoblots (A), quantification of protein levels (B-C): CD68 (B), IFNγ (C) (n = 8 mice per group). Cytokines TNFα (D) and IL6 (E) were determined by ELISA kit (n = 5 mice per group). The data are presented as the means ± SEM. Statistical analysis is made between groups as shown in the graphs by one-way ANOVA with Dunnett post-hoc test, *p<0.05, **p<0.01, ***p<0.001.

4.2.5 Palm^{11}-PrRP31 decreased apoptosis in the hippocampi of APP/PS1 mice

APP/PS1 mice had significantly increased the pro-apoptotic regulator Bax (Figure 22B) in the hippocampus. Two months of treatment with palm^{11}-PrRP31 significantly decreased the level of Bax. Furthermore, the treatment tended to increase the anti-apoptotic regulator Bcl-2 (Figure 22C) therefore, the pro-apoptotic Bax/Bcl-2 ratio significantly decreased after the treatment, as shown in Figure 22E.

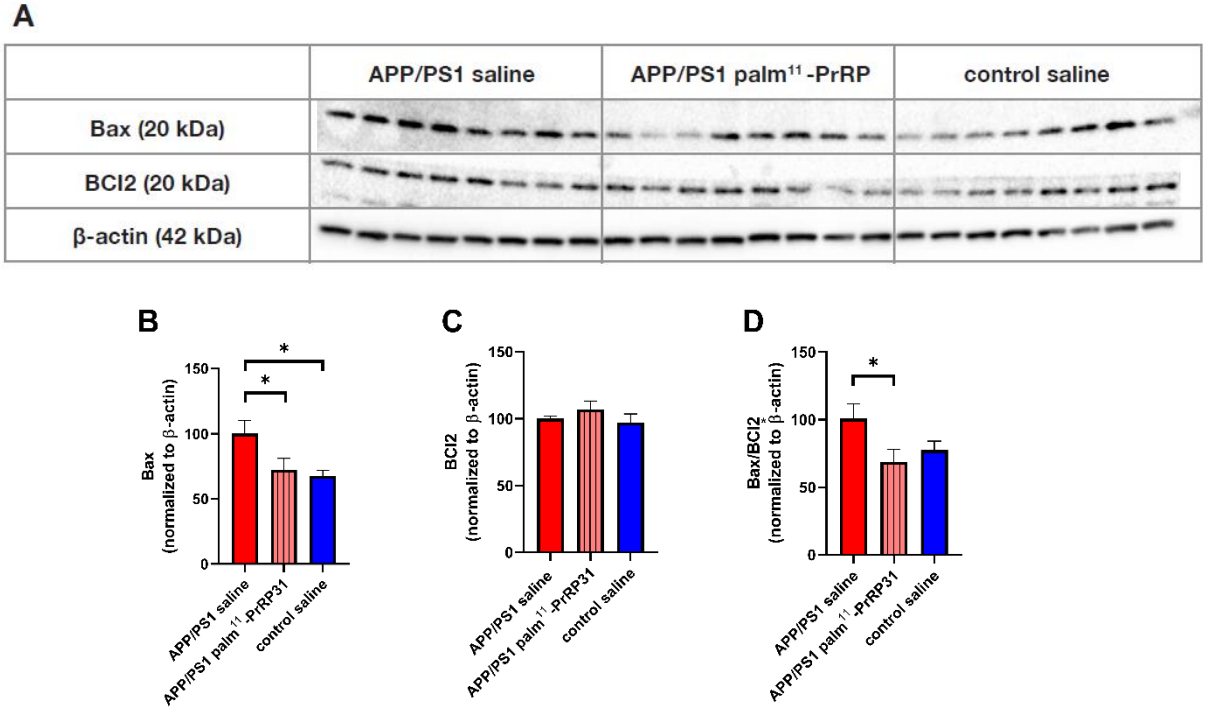

Figure 22: Decreased level of pro-apoptotic ratio in the hippocampi of the APP/PS1 mice after treatment with palm^{11}-PrRP31. Markers were determined by Western blotting. Immunoblots (A), quantification of protein levels (B-E): Bax (B), Bcl-2 (C) and the the pro-apoptotic ratio Bax/Bcl-2 (D). The data are presented as the means ± SEM. Statistical analysis is made between groups as shown in the graphs by one-way ANOVA with Dunnett post-hoc test, *p<0.05, (n = 8 mice per group).

4.2.6 Palm^{11}-PrRP31 increased synaptogenesis in APP/PS1 mice

Photomicrographs of immunohistochemically stained brain sections showed a decrease in the presynaptic protein syntaxin1A, mainly in the cortex but also in the hippocampus in APP/PS1 mice compared to age-matched control mice (Fig. 23A-F) and a decrease in the postsynaptic marker spinophilin in the cortex and in the hippocampus in APP/PS1 mice compared to age-matched control mice (Figure 23G-L).

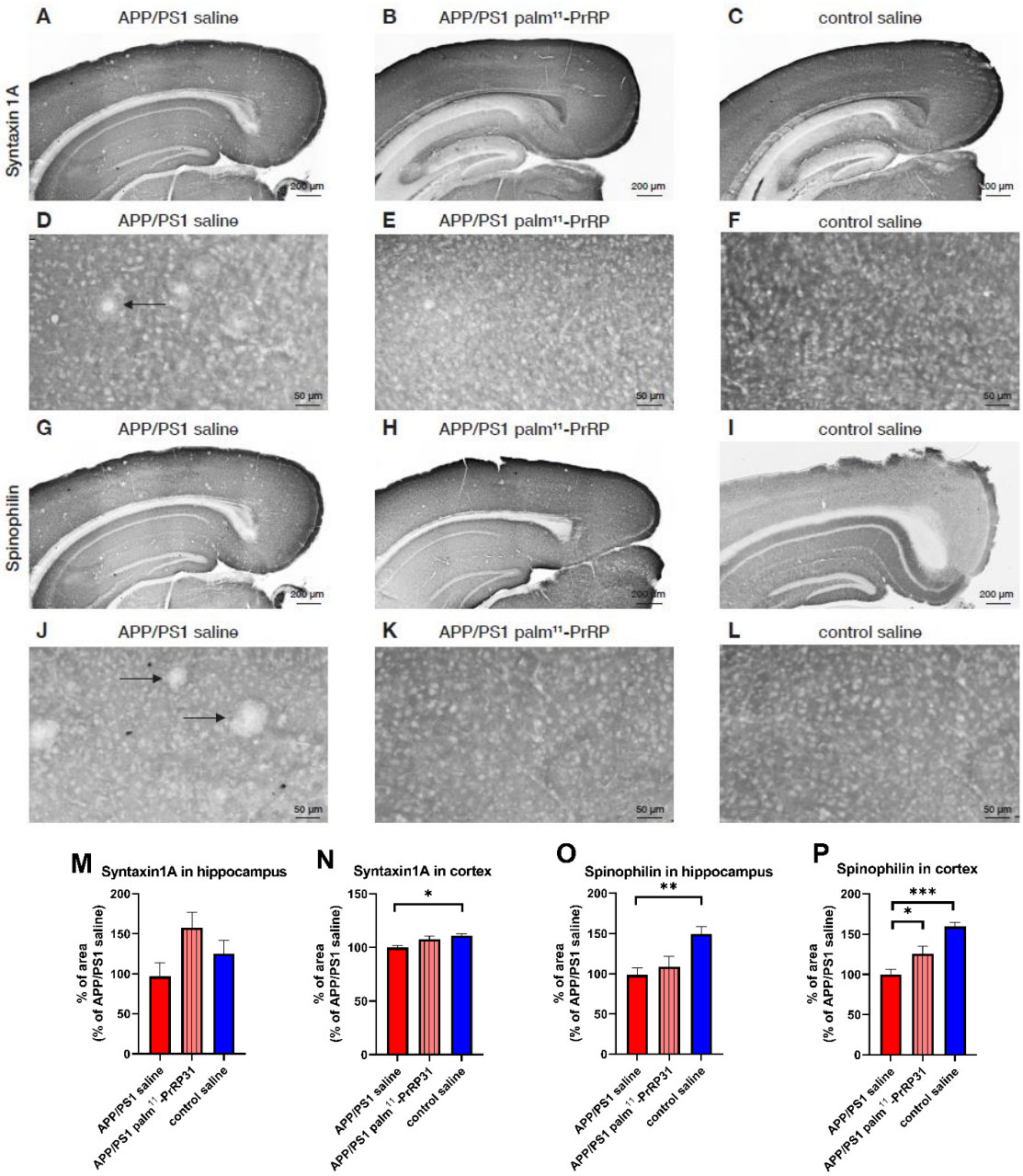

Figure 23: Increase in synaptogenesis in the brains of the APP/PS1 mice after treatment with palm^{11}-PrRP31, regarding IHC. Representative photomicrographs of the saline and palm^{11}-PrRP31 treated APP/PS1 mice, and their age-matched controls immunohistochemically stained for presynaptic marker syntaxin1A (A-C) and postsynaptic marker spinophilin (G-I), and their quantification (M-P). Detailed photomicrographs illustrating difference in synaptic density (pointed by black arrows) by syntaxin1A (D-F) and spinophilin (J-L). Percentage of the stained area is expressed as a % of the saline-treated APP/PS1 group to enable the comparison of multiple staining series. The data are presented as the means ± SEM. Statistical analysis is made between groups as shown in the graphs by one-way ANOVA with Dunnett post-hoc test, *p<0.05, **p<0.01, ***p<0.001 (n = 5 mice per group).

Two months of treatment with palm[11]-PrRP31 (Figure 23B) tended to increase the number of the presynaptic protein syntaxin1A in the hippocampus (Figure 23M), and also significantly increased the postsynaptic protein spinophilin in the cortex (Figure 23P) and nonsignificantly increased the postsynaptic protein in the hippocampus. No difference was found in the presynaptic protein syntaxin1A and the postsynaptic protein spinophilin in the cerebella of APP/PS1 mice compared to their age-matched controls (Figure 24).

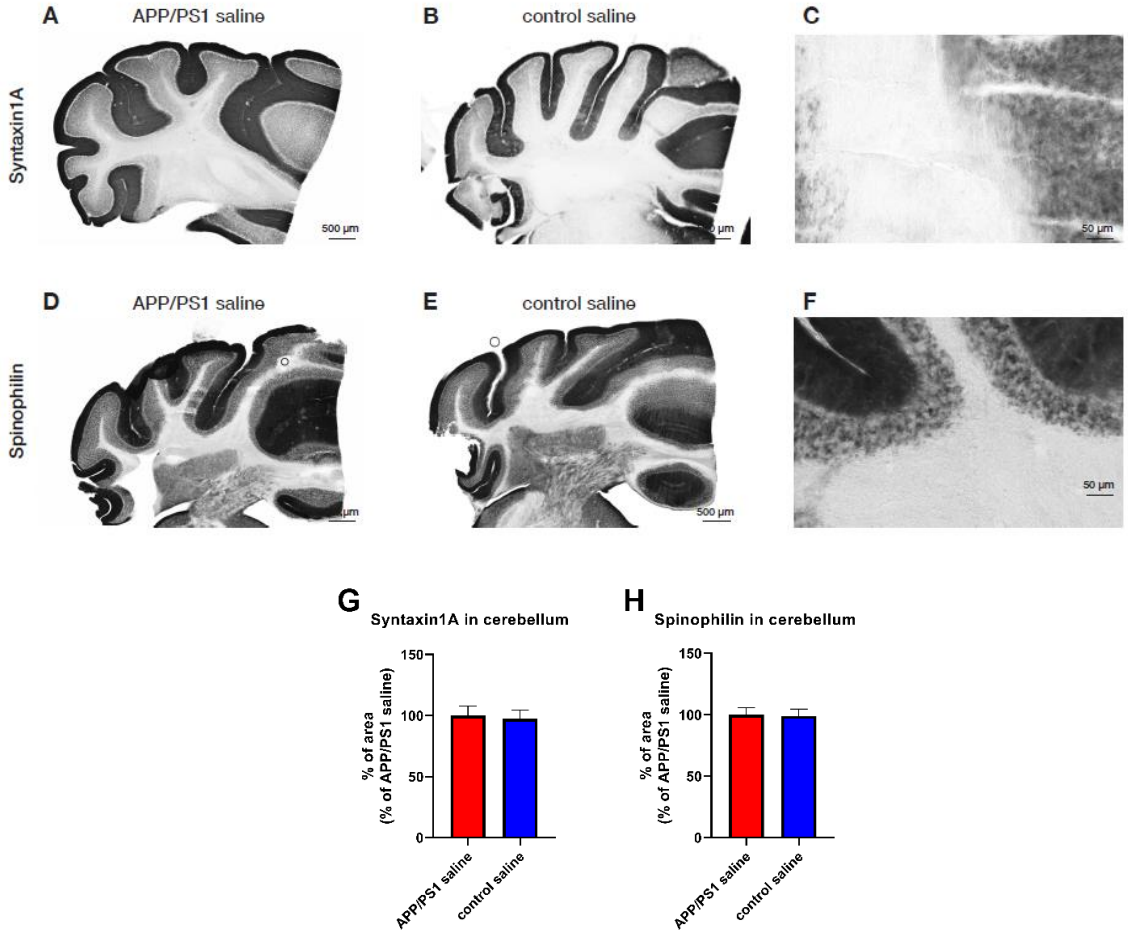

Figure 24: No difference in synaptic proteins in the cerebella of the APP/PS1 mice and the controls. Representative photomicrographs of the saline treated APP/PS1 mice and their age-matched controls immunohistochemically stained for presynaptic marker syntaxin1A (A-C) and postsynaptic marker Spinophilin (D-F) and their quantification (G,H). Detailed photomicrographs (C,F). Percentage of the stained area is expressed as a % of the saline-treated APP/PS1 group to enable the comparison of multiple staining series. The data are presented as the means ± SEM. Statistical analysis is made between groups as shown in the graphs by one-way ANOVA with Dunnett post-hoc test (n = 5 mice per group).

The levels of synaptic markers were further determined in hippocampal lysates using WB. Compared to age-matched control mice, APP/PS1 mice showed significantly reduced protein levels of the postsynaptic density protein 95 (PSD95) (Figure 25B) and the presynaptic markers synaptophysin (Figure 25C) and syntaxin1A. After two months of treatment, the protein levels of PSD95, synaptophysin and syntaxin1A were significantly improved in the palm^{11}-PrRP31-treated group compared to the APP/PS1 saline-treated group, as shown in Figure 25. WB confirmed the results from IHC.

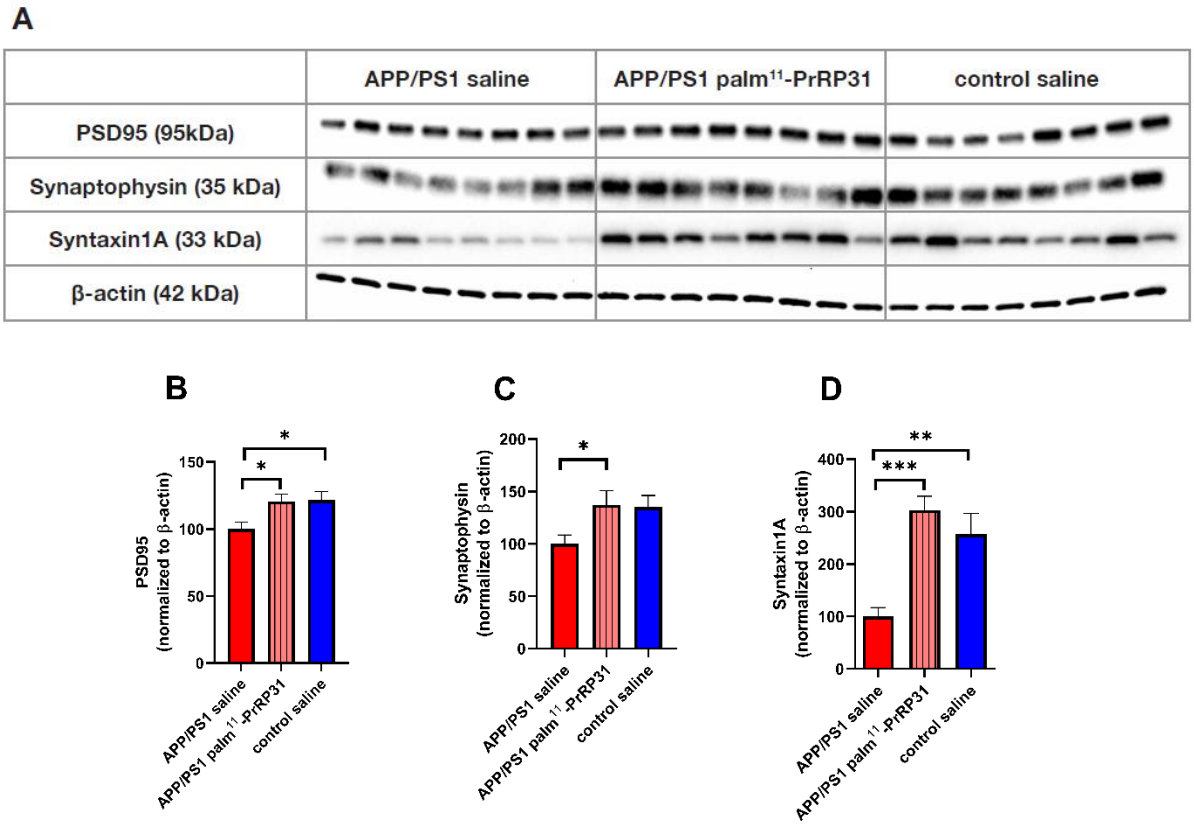

Figure 25: Increase in synaptogenesis in the hippocampi of the APP/PS1 mice after treatment with palm^{11}-PrRP31, determined by WB. Levels of postsynaptic marker PSD95 and presynaptic markers synaptophysin and syntaxin1A were determined by western blotting. Immunoblots (A), quantification of protein levels of PSD95 (B), synaptophysin (C) and syntaxin1A (D). The data are presented as the means ± SEM. Statistical analysis is made between groups as shown in the graphs by one-way ANOVA with Dunnett post-hoc test, *p<0.05, **p<0.01, ***p<0.001 (n = 8 mice per group).

4.2.7 Palm^{11}-PrRP31 improved the glymphatic system in APP/PS1 mice

We used the astroglial water channel AQ4 as a marker of Aβ clearance via the paravascular glymphatic pathway. Compared to control saline mice (Figure 26C),

APP/PS1 mice (Figure 26A) exhibited a nonsignificant decrease in the density of AQ4 in the hippocampus and a significantly decreased density of AQ4 in the cortex. Two months of treatment with palm^{11}-PrRP31 significantly increased the density of this water channel in the cortex (Figure 26H) and tended to increase its density in the hippocampus.

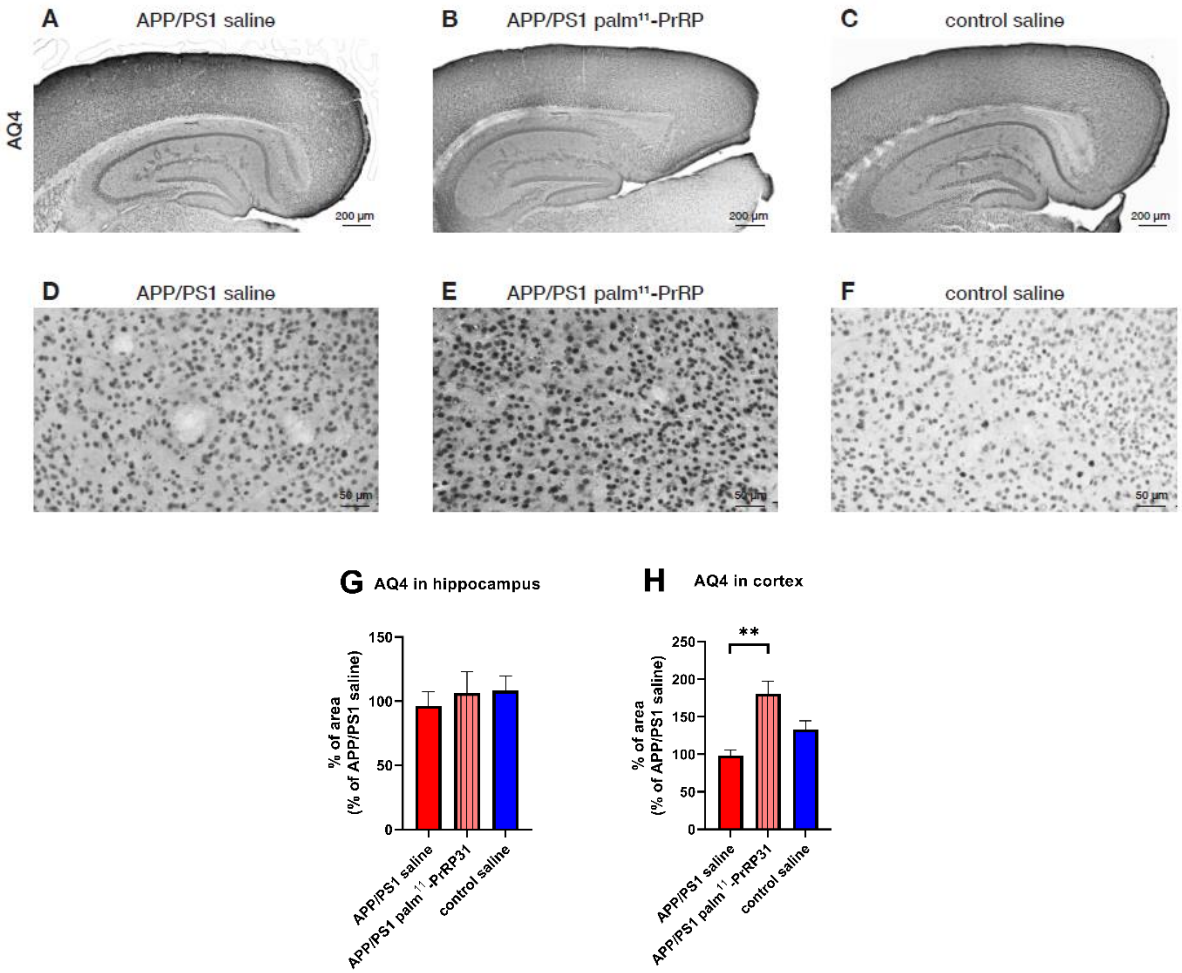

Figure 26: Improvement in glymphatic system in the brains of the APP/PS1 mice after treatment with palm^{11}-PrRP31. Representative photomicrographs (A-C) of the saline and palm^{11}-PrRP31 treated APP/PS1 mice, and their age-matched controls immunohistochemically stained for marker of paravascular glymphatic pathway Aquaporin 4. Detailed photomicrographs illustrating improvement in glymphatic system (D-F). Quantification (G-H) of immunohistochemical staining in the hippocampus (G) and cortex (H). Percentage of the stained area is expressed as a % of the saline-treated APP/PS1 group to enable the comparison of multiple staining series. The data are presented as the means ± SEM. Statistical analysis is made between groups as shown in the graphs by one-way ANOVA with Dunnett post-hoc test, **p<0.01 (n = 5 mice per group).

4.2.8 Palm[11]-PrRP31 decreased the protein levels of p-m-Tor and LRP1 in the brains of APP/PS1 mice

Treatment with palm[11]-PrRP31 affected level of m-Tor and low-density lipoprotein receptor-related protein 1 (LRP1), both supporting the metabolism of Aβ peptide. Palm[11]-PrRP31 significantly decreased the p-m-Tor (Ser2448)/m-Tor in the hippocampus in APP/PS1 mice compared to the age-matched control mice, as shown in Figure 27. APP/PS1 mice had significantly increased LRP1 (Figure 27B), which was attenuated after the treatment with palm[11]-PrRP31. All results from this study are summarized in Table 5.

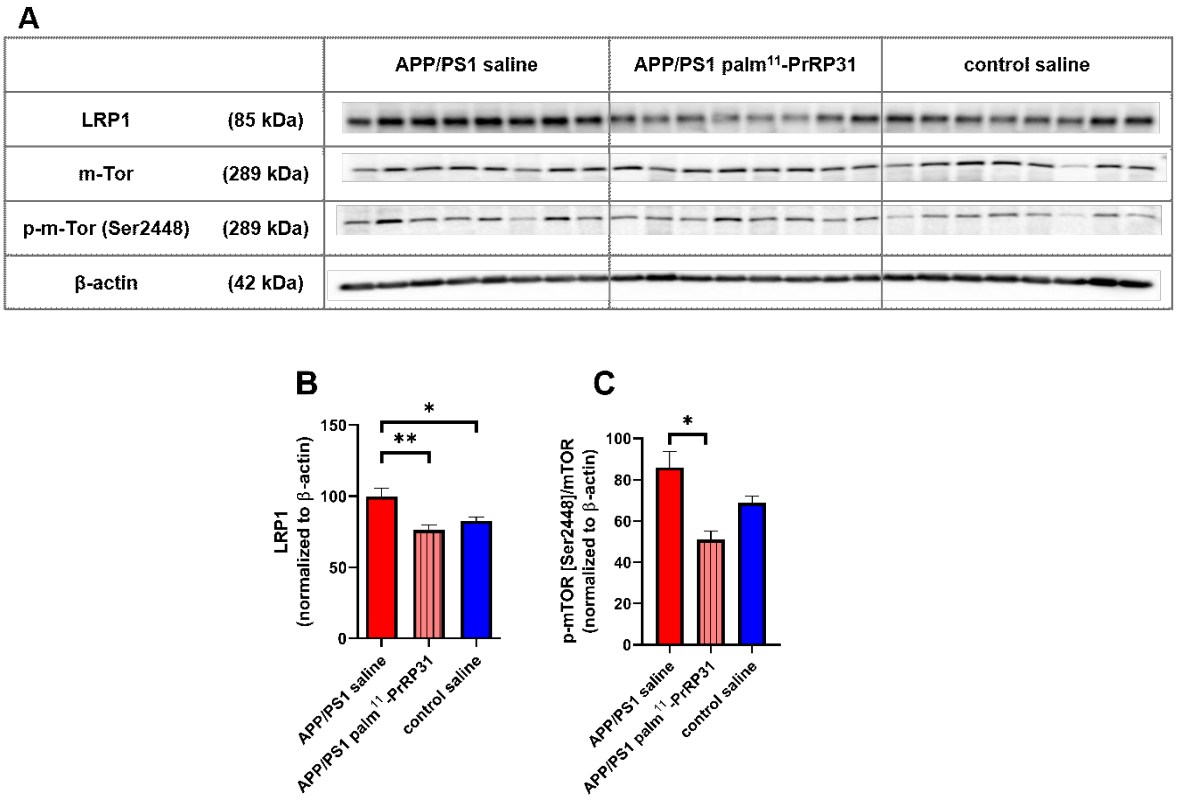

Figure 27: Decreased level of p-m-Tor and LRP1 in the hippocampi of the APP/PS1 mice after treatment with palm[11]-PrRP31. Markers were determined by western blotting. (A) Immunoblots, (B-C) quantification of protein levels: (B) LRP1 (C) p-m-Tor (Ser2448)/m-Tor. The data are presented as the means ± SEM. Statistical analysis is made between groups as shown in the graphs by one-way ANOVA with Dunnett post-hoc test, *p<0.05, **p<0.01 (n = 8 mice per group).

Table 5: Summary of measured parameters

Parameter	Brain region	APP/PS1 vs. control mice	Palm^{11}-PrRP31 vs saline
Body Weight change	-	-	-
Glucose	-	-	-
Insulin	-	-	-
Leptin	-	-	-
Aβ plaques	hippocampus	↑***	↓*
	cortex	↑***	↓
	brainstem	-	-
	cerebellum	↑***	↓*
Iba1	hippocampus	↑***	↓***
	cortex	↑***	↓*
	brainstem	-	-
	cerebellum	↑***	↓***
GFAP	hippocampus	↑***	↓*
	cortex	↑***	↓***
	brainstem	-	-
	cerebellum	-	-
CD68	hippocampus	↑*	↓*
IFNγ	hippocampus	↑***	↓***
TNFα	hippocampus	↑	↓
IL6	hippocampus	↑***	↓ p=0.075
Bax/Bcl-2	hippocampus	↑	↓*
Spinophilin	hippocampus	↓**	↑
	cortex	↓***	↑*
	cerebellum	-	-
Syntaxin1A	hippocampus	↓**	↑***
	cortex	↓*	↑
	cerebellum	-	-
Synaptophysin	hippocampus	↓	↑*
PSD95	hippocampus	↓*	↑*
Aquaporin 4	hippocampus	↓	↑
	cortex	↓	↑**
LRP1	hippocampus	↑*	↓**
p-m-Tor/m-Tor	hippocampus	↑	↓*

The data are presented as the means ± SEM. Statistical analysis is made by one-way ANOVA with Dunnett post-hoc test, *p<0.05, **p<0.01, ***p<0.001 (n = 8-10 mice per group).

↑ increase, ↓ decrease

4.3 Impact of HFD on metabolic parametres and neurodegeneration in APP/PS1 and WT mice

4.3.1 Effect of HFD on BW, eWAT weight and metabolic parametres

APP/PS1 and WT mice fed with HFD developed severe obesity, compared to their age-matched controls on STD. As shown in Figure 28, HFD significantly increased BW in 6 and 10 months old both APP/PS1 mice and WT mice, compared to their respective STD controls that did not gain weight throughout the whole experiment. Moreover, the BW of 10-month-old APP/PS1 male mice on HFD was significantly higher than the ones of their respective age-matched WT controls on HFD (Figure 28A). Accordingly, the weights of eWAT were significantly increased by the HFD in 6 and 10 months of age in both mouse strains (Figure 28B).

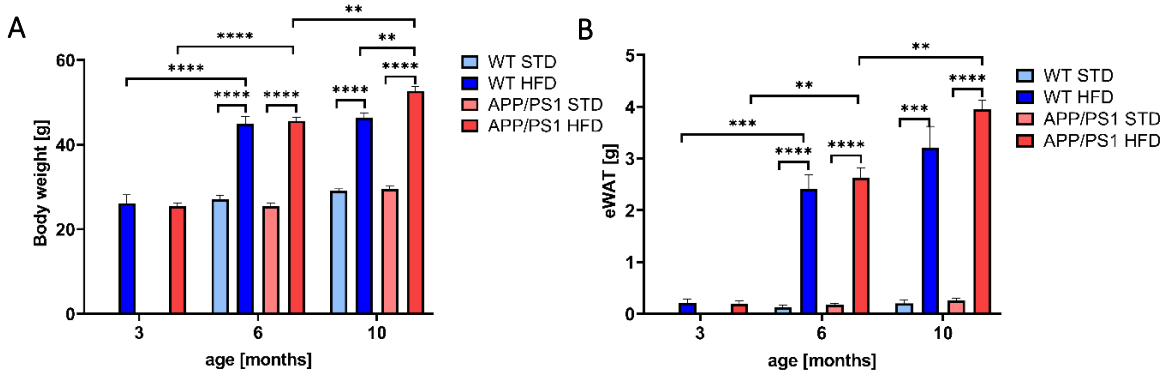

Figure 28: HFD significantly increased BW and eWAT weight. Quantification of body weights (A) and eWAT weights (B) in the APP/PS1 mice and their age-matched controls on STD or HFD in 3, 6, or 10 months of age. The data are presented as the means ± SEM. Statistical analysis is made between groups as shown in the graphs by one-way ANOVA with Bonferroni post-hoc test **p<0.01, ***p<0.001, ****p<0.0001 (n = 5-8 mice per group)

Along with an excess in an adipose tissue, HFD significantly increased plasma level of leptin in all 6- and 10-month-old mice (Table 6). Similar trend was observed for plasma cholesterol and plasma triacylglycerols. Fasting glucose levels were increased above the normoglycemic value (the value for WT mice) in mice on HFD at all ages, but significantly only at the age of 6 months.

Obesity was also accompanied by hyperinsulinemia, represented by increased plasma insulin levels in both 6 and 10 months of age. 10-month-old APP/PS1 mice on HFD reached 38-fold those of their controls on STD and 3-fold those of age-matched WT controls on HFD (Table 6).

Table 6: Metabolic parameters in the APP/PS1 mice and their age-matched controls on STD or HFD in 3, 6, or 10 months of age.

Parameter		Glucose [mmol/l]	Insulin [ng/ml]	Leptin [ng/ml]	Cholesterol [mmol/l]	Triacylglycerol [mmol/l]	FGF21 [pg/ml]	HOMA-IR index
3 months	WT HFD	7.68 ± 0.87	0.38 ± 0.09	0.49 ± 0.15	5.26 ± 0.19	0.86 ± 0.04	537.53 ± 136.65	23.61 ± 7.61
	APP/PS1 HFD	7.28 ± 0.77	0.38 ± 0.10	0.98 ± 0.49	5.12 ± 0.63	0.85 ± 0.19	900.48 ± 202.13	22.98 ± 7.25
6 months	WT STD	4.96 ± 0.46	0.08 ± 0.03	1.18 ± 0.59	3.40 ± 0.14	0.55 ± 0.06	541.55 ± 169.42	3.24 ± 1.05
	WT HFD	6.96 ± 0.34	1.36 ± 0.16	55.09 ± 5.30	6.25 ± 0.54	0.97 ± 0.10	804.94 ± 128.84	73.14 ± 10.76
	APP/PS1 STD	4.88 ± 0.26	0.13 ± 0.01	1.72 ± 0.71	3.32 ± 0.35	0.57 ± 0.05	891.75 ± 324.21	4.50 ± 0.53
	APP/PS1 HFD	7.78 ± 0.21	1.95 ± 0.32	67.39 ± 6.15	7.85 ± 0.53	1.23 ± 0.08	1279.26 ± 282.41	117.24 ± 21.00
10 months	WT STD	6.16 ± 0.32	0.27 ± 0.14	1.04 ± 0.39	2.54 ± 0.49	0.90 ± 0.16	615.40 ± 113.28	12.35 ± 6.31
	WT HFD	7.85 ± 0.44	1.51 ± 0.33	67.92 ± 6.29	4.18 ± 0.42	1.51 ± 0.15	1013.95 ± 168.00	93.48 ± 21.99
	APP/PS1 STD	6.32 ± 0.86	0.12 ± 0.04	0.78 ± 0.14	2.47 ± 0.22	1.06 ± 0.17	824.23 ± 232.00	6.83 ± 3.08
	APP/PS1 HFD	6.95 ± 0.39	4.64 ± 0.42	86.12 ± 8.73	5.32 ± 0.37	1.65 ± 0.12	1999.93 ± 390.17	254.85 ± 31.88

Parametres measured from blood plasma collected from overnight-fasted mice. The data are presented as the means ± SEM. Statistical analysis is made between groups fed with STD and HFD as shown in the Table by one-way ANOVA with Bonferroni post-hoc test, *p<0.05, **p<0.01, ***p<0.001, ****p<0,0001 (n = 5-8 mice per group). * Statistical analysis between APP/PS1 and WT mice on HFD.

HFD – high fat diet, STD – standard diet, FGF21 – fibroblast growth factor 21, HOMA-IR - homeostatic model assessment for insulin resistance

All mice fed with HFD showed a significantly higher HOMA-IR index than their age- and genotype-matched STD-fed mice (Table 6), which indicates increased peripheral IR. HOMA-IR of 10 months-old APP/PS1 mice on HFD was also significantly increased in comparison with their age-matched WT controls on HFD. Moreover, 10-month-old APP/PS1 mice on HFD had significantly increased levels of FGF21 in comparison not only with their age-matched APP/PS1 on STD, but also with their age-matched WT mice on HFD. These parameters indicate APP/PS1 and WT mice on HFD to be in a pre-diabetic state.

At the age of 6 and 10 months, OGTT was performed. The HFD significantly increased AUC in 6 months in both strains, suggesting glucose intolerance of the mice (Figure 29). In addition, APP/PS1 mice on HFD showed significantly increased glucose intolerance in comparison with WT mice of the same age on HFD and APP/PS1 on STD showed significant increase in glucose level in comparison with WT mice on STD (Figure 29C). However, at 10 months of age, no difference was obvious among the groups.

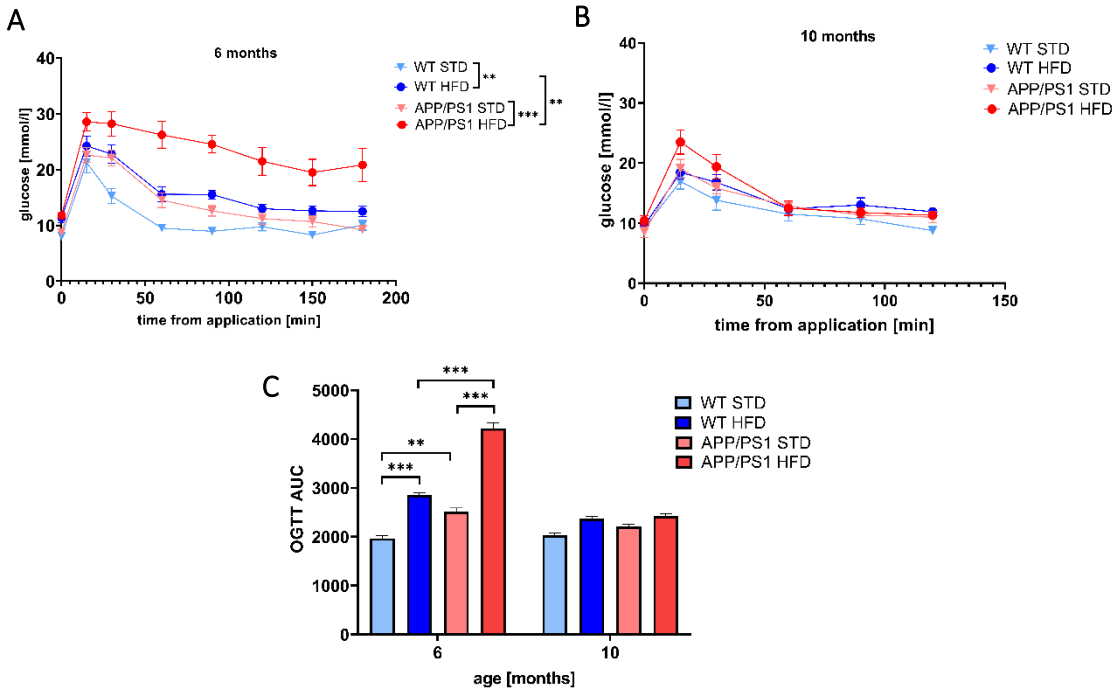

Figure 29: Oral glucose tolerance test in 6- and 10-month-old mice on STD and HFD. Time course of OGTT after orally administered glucose at a dose 2g/kg at 6 months (A) and 10 months (B) of age and area under curve (AUC) (C). The data are presented as the means ± SEM. Statistical analysis is made between groups as shown in the graphs by one-way ANOVA with Bonferroni post-hoc test, **p<0.01, ***p<0.001, (n = 5-8 mice per group).

4.3.2 HFD caused peripheral inflammation

The HFD-induced obesity led to a significant increase of CRP, marker of peripheral inflammation, in the fasted plasma of APP/PS1 mice in 6 and 10 months of age (Figure 30) in comparison with their age-matched controls on STD. HFD feeding of WT mice did not result in a significant increase of CRP.

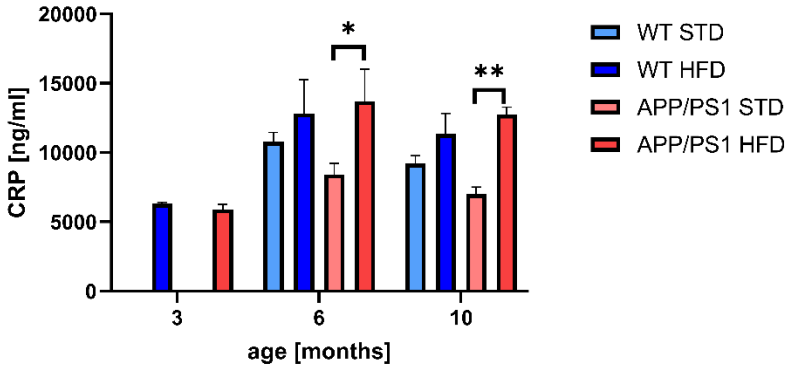

Figure 30: HFD caused peripheral inflammation in APP/PS1 mice. Quantification of CRP in fasted plasma. The data are presented as the means ± SEM. Statistical analysis is made between groups as shown in the graphs by one-way ANOVA with Bonferroni post-hoc test, *p<0.05, **p<0.01 (n = 5-8 mice per group).

4.3.3 HFD caused liver steatosis

HFD feeding caused a significant increase in liver weight in 6- and 10-month-old APP/PS1 mice, while it only tended to increase the liver weight of WT mice as shown in Figure 31Q. Furthermore, livers of 10-month-old APP/PS1 mice on HFD were significantly heavier than those of their respective WT controls on HFD (Figure 31Q). Increase in liver weight was mainly caused by abnormal retention of fat within the livers, an obvious liver steatosis. Representative figures of steatotic liver slices are shown in Figure 31 (A-H). Mice in 3 months of age did not develop any signs of steatosis and no significant difference was found between the strains. At the age of 6 and 10 months, both APP/PS1 and WT mice on HFD developed micro- and macrosteatosis as shown in Figure 31L. Macrosteatosis is characterized by a single, bulky fat vacuole in hepatocytes, displacing the nucleus to the edge of the cell. In microsteatosis, the cytoplasm of the hepatocytes contains tiny lipid vesicles without nuclear dislocation. Microsteatosis is

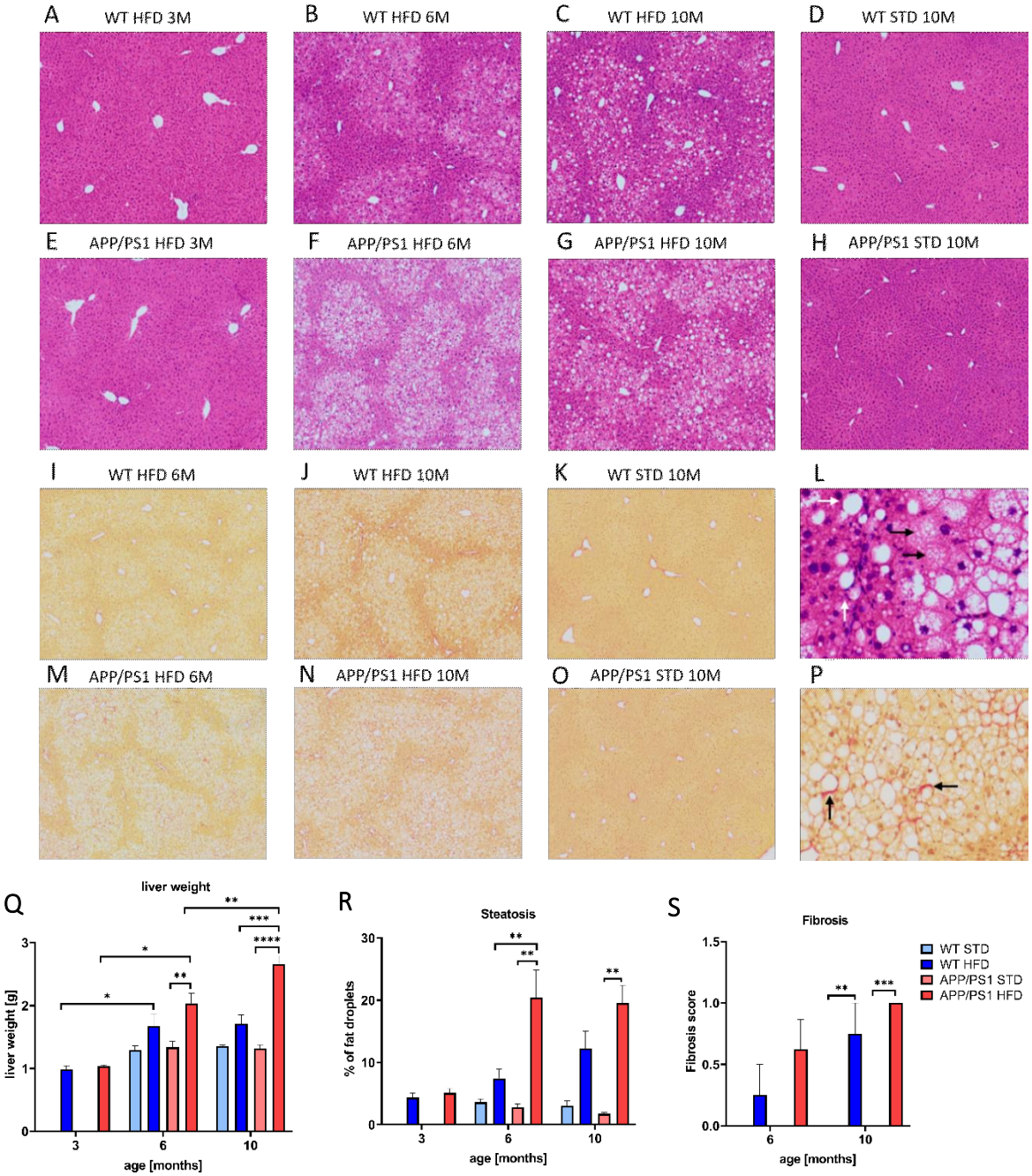

Figure 31: HFD caused liver steatosis and fibrosis. Quantification of liver weights (Q) and representative photomicrographs of the APP/PS1 mice on HFD and their controls on STD. Livers stained by hematoxylin-eosin for (A-H) steatosis and by the fibrotic liver staining (I-K, M-O), and their quantification (R,S). Detailed photomicrographs (L,P). White arrows in (L), show macrosteatosis and black arrows microsteatosis of the liver. Black arrows in (P) point on fibrotic scarring. The data are presented as the means ± SEM. Statistical analysis is made between groups as shown in the graphs by one-way ANOVA with Bonferroni post-hoc test, *p<0.05, **p<0.01, ***p<0.001, ****p<0.0001 (n = 5-8 mice per group).

considered as more damaging. However, only in APP/PS1 mice fed HFD the increase in steatosis was statistically significant. Furthermore, APP/PS1 mice on HFD developed significant gain in steatosis in 6 months in comparison to WT on HFD as shown in Figure 31R. STD-fed mice did not show any evidence of liver steatosis, even at a late age.

Level of fibrosis was measured only in 6- and 10-months old mice, after they developed the steatosis. APP/PS1 and WT mice on HFD developed mild fibrosis already in 6 months of age, compared to their age-matched controls on STD that was significantly pronounced in both strains in 10 months of age as shown in the Figure 31S. Mice on STD did not develop any fibrosis. Representative figures of fibrotic liver slices are shown in Figure 31 (I-K, M-P).

4.3.4 Markers related to peripheral insulin resistance

4.3.4.1 HFD and age attenuated the PI3K/Akt signaling pathway in the liver

HFD significantly decreased the level of insulin receptor β (IRβ**)** in the liver of APP/PS1 mice in both 6 and 10 months of age in comparison with APP/PS1 mice on STD and tended to decrease level of IRβ in 6-month-old WT mice compared to age-matched WT mice on STD (Figure 32E). PI3K level significantly increased in the liver of WT on HFD compared to those on STD, however, its levels significantly decreased with age; level of Akt also decreased with ageing. No significant changes were observed in p-Akt (Ser473).

4.3.4.2 HFD reduced the PI3K/Akt signaling pathway in eWAT

HFD significantly decreased level of IRβ in eWAT in 6- and 10-month-old APP/PS1 mice and 6-month-old WT mice and also tended to decrease level of IRβ in 10-month-old WT mice as shown in Figure 33. PI3K p85 tended to be lowered by HFD in all of the mice. HFD significantly decreased level of Akt in 10-month-old APP/PS1 mice and tended to decrease Akt in 10-month-old WT mice and furthermore, it significantly decreased level of p-Akt (Ser473) in 10-month-old WT mice and tended to decrease level of p-Akt (Ser473) in 10-month-old APP/PS1 mice. HFD also significantly decreased level of GLUT4 in 6-month-old WT mice and tended to decrease the level of GLUT4 in all the other mice (Figure 33).

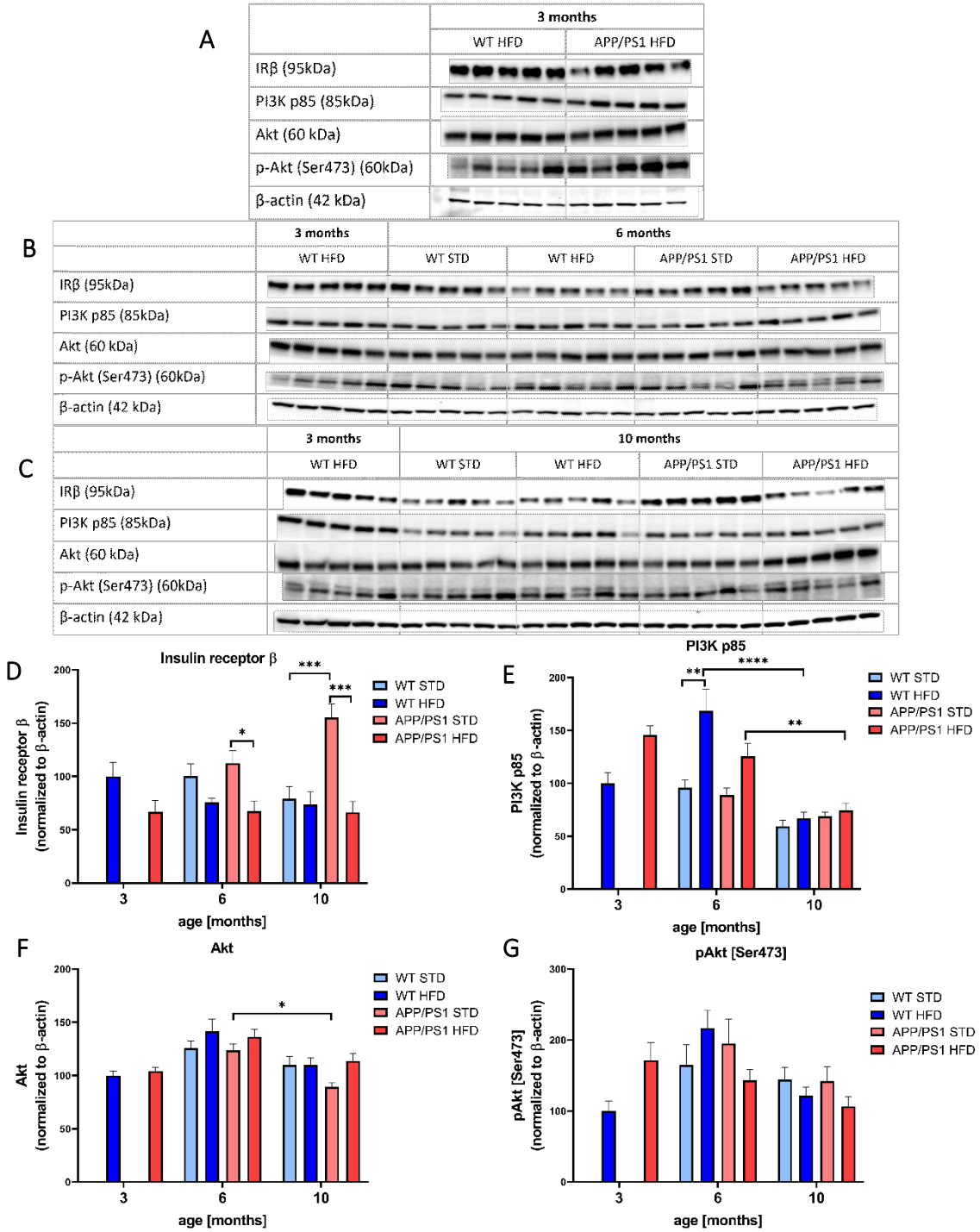

Figure 32: HFD and age attenuated the PI3K/Akt signaling pathway in liver. Proteins levels were determined by western blotting. Immunoblots in 3 months (A), 6 months (B) and 10 months (C) of age, quantification of protein levels (D-G): Insulin receptor β (D) PI3K p85 (E) Akt (F) p-Akt (Ser473) (G). Percentage of the stained area is expressed as a % of 3-month-old WT on HFD to enable the comparison of multiple staining series. The data are presented as the means ± SEM. Statistical analysis is made between groups as shown in the graphs by one-way ANOVA with Bonferroni post-hoc test, *p<0.05, **p<0.01, ***p<0.001, ****p<0.0001 (n = 5 mice per group).

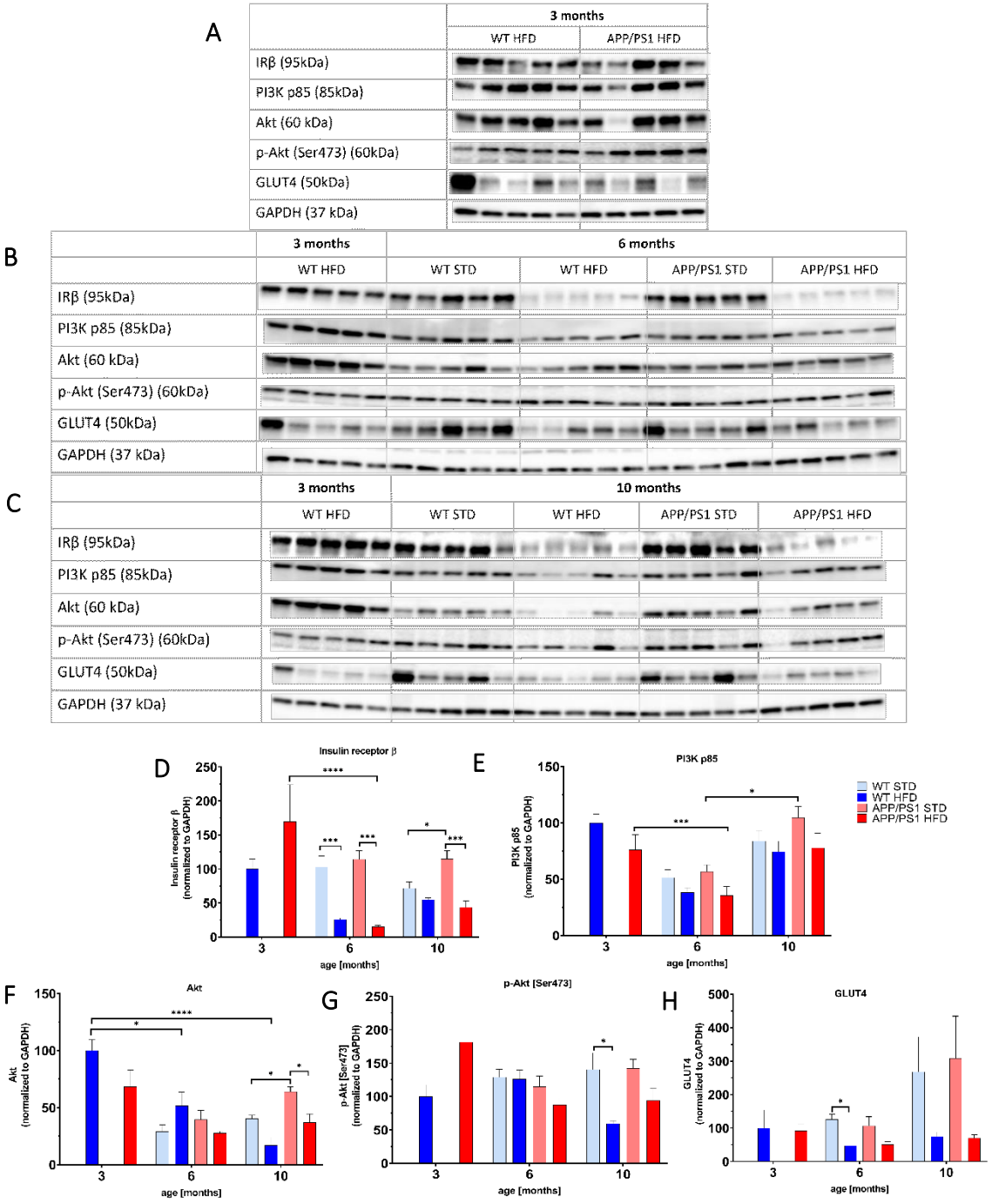

Figure 33: HFD reduced the PI3K/AKT signaling pathway in eWAT. Proteins were determined by western blotting. Immunoblots in 3 months (A), 6 months (B) and 10 months of age (C), quantification of protein levels (D-G): Insulin receptor β (D) PI3K p85 (E) Akt (F) p-Akt (Ser473) (G) GLUT4 (H). Percentage of the stained area is expressed as a % of 3-month-old WT on HFD to enable the comparison of multiple staining series. The data are presented as the means ± SEM. Statistical analysis is made between groups as shown in the graphs by one-way ANOVA with Bonferroni post-hoc test, *p<0.05, ***p<0.001, ****p<0.0001 (n = 5 mice per group).

4.3.4.3 HFD attenuated the PI3K/Akt signaling pathway in the skeletal muscle

HFD significantly decreased levels of IRβ in the skeletal muscles of APP/PS1 mice at the age of 6 and 10 months and it tended to decrease level of IRβ in the muscles of 6-month-old WT mice (Figure 34). HFD also significantly decreased levels of PI3K p85 in the muscles of 6-month-old APP/PS1 mice and 10-month-old WT mice and tended to decrease the level in 10-month-old APP/PS1 mice. Level of Akt tended to decrease in the muscle of 6- and 10-month-old APP/PS1 on HFD mice and 10-month-old WT mice on HFD, but it significantly increased in 6-month-old WT mice on HFD. Furthermore, HFD decreased level of GLUT4 in muscle in 10-month-old APP/PS mice and their age-matched WT controls. GLUT4 significantly increased in STD fed WT and APP/PS1 mice between 6^{th} to 10^{th} months of age. All results from the peripheral parametres affected by age, HFD and APP/PS1 genotype are summarized in Table 7.

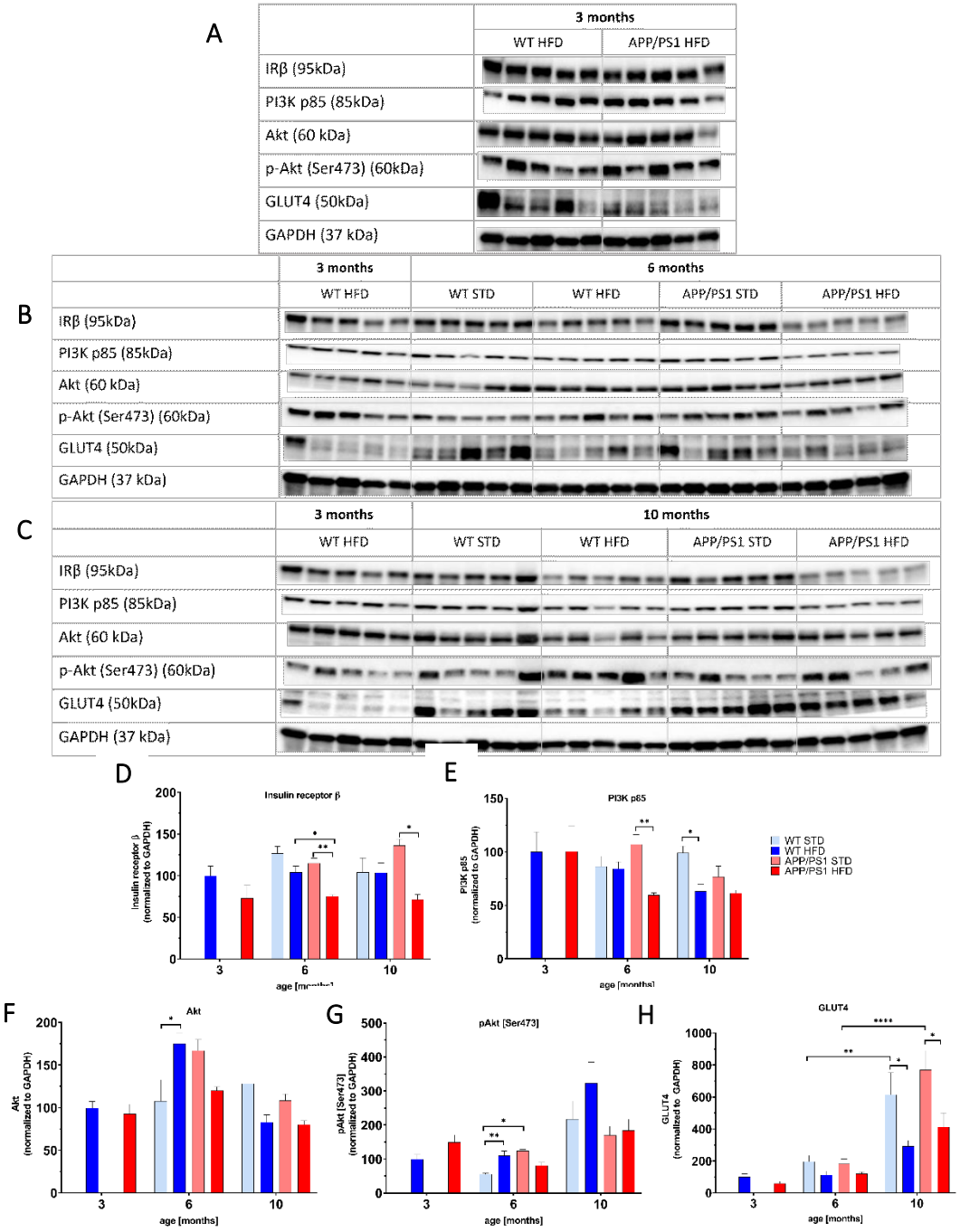

Figure 34: HFD attenuated the PI3K/Akt signaling pathway in the skeletal muscle. Proteins were determined by western blotting. Immunoblots in 3 months (A), 6 months (B) and 10 months of age (C), quantification of protein levels (D-H): Insulin receptor β (D) PI3K p85 (E) Akt (F) p-Akt (Ser473) (G) GLUT4 (H). Percentage of the stained area is expressed as a % of 3-month-old WT on HFD to enable the comparison of multiple staining series. The data are presented as the means ± SEM. Statistical analysis is made between groups as shown in the graphs by one-way ANOVA with Bonferroni post-hoc test, *p<0.05, ****p<0.0001 (n = 5 mice per group).

Table 7. Summary of peripheral parametres affected by age, HFD and APP/PS1 genotype

	Plasma/Tissue	3 months	6 months				10 months				
		APP/PS1 vs WT on HFD	HFD vs STD		APP/PS1 vs WT on HFD	Age 6M vs 3M on HFD		HFD vs STD		APP/PS1 vs WT on HFD	Age 10M vs 6M on HFD	
Body Weight		-	↑****	↑****	-	↑****	↑****	↑****	↑****	↑**	-	↑**
eWAT		-	↑****	↑****	-	↑***	↑**	↑***	↑****	-	-	↑**
Leptin	plasma	-	↑***	↑****	-	↑****	↑****	↑****	↑****	-	-	-
Glucose	plasma	-	↑**	↑****	-	-	↑**	-	-	-	-	-
OGTT AUC	plasma	-	↑***	↑***	↑***	-	-	-	-		-	-
Insulin	plasma	-	↑***	↑***	-	-	↑*	↑***	↑***	↑***	-	↑****
FGF21	plasma	-	-	-	-	-	-	-	↑*	↑*	-	-
HOMA-IR index		-	↑*	↑***	-	-	-	-	-	↑***	-	↑***
Cholesterol	plasma	-	↑**	↑****	-	-	↑**	↑*	↑***	-	-	↓**
Triacylglycerol	plasma	-	↑**	↑***	-	-	-	-	↑*	-	↑*	↑**
CRP	plasma	-	-	↑*	-	-	-	-	↑**	-	-	-
LIVER WEIGHT		-	-	↑**	-	↑*	↑*	-	↑****	↑***	-	↑**
Steatosis	liver	-	-	↑**	↑**	-	-	-	↑**	-	-	-
Fibrosis	liver	-	-	-	-	-	-	↑**	↑***	-	-	-
IRbeta	liver	-	-	↓*	-	-	-	-	↓***	-	-	-
PI3K	liver	-	↑**	-	-	-	-	-	-	-	↓****	↓**
p-Akt (Ser473)	liver	-	-	-	-	-	-	-	-	-	-	-
IRbeta	eWAT	-	↓***	↓***	-	-	↓****	↓*	↓***	-	-	-
PI3K	eWAT	-	-	-	-	-	↓***	-	-	-	-	-
p-Akt (Ser473)	eWAT	-	-	-	-	-	-	↓*	-	-	-	-
GLUT4	eWAT	-	↓*	-	-	-	-	-	-	-	-	-
IRbeta	muscle	-	-	↓**	↓**	-	-	-	↓*	-	-	-
PI3K	muscle	-	-	↓**	-	-	-	↓*	-	-	-	-
p-Akt (Ser473)	muscle	-	↑**	-	-	-	-	-	-	-	-	-
GLUT4	muscle	-	-	-	-	-	-	↓*	↓*	-	-	-

The data are presented as the means ± SEM. Statistical analysis is made by one-way ANOVA with Bonferroni test, *p<0.05, **p<0.01, ***p<0.001, ****p<0.0001 (n = 5-8 mice per group). Difference between the WT mice on HFD and STD pointed up by blue colour, difference between the APP/PS1 mice on HFD and STD pointed up by red colour.

↑ - increase; ↓ - decrease; HFD - high-fat diet; STD – standard diet; eWAT – epididymal white adipose tissue; OGTT - oral glucose tolerance test; FGF21 – fibroblast growth factor 21; HOMA-IR - homeostatic model assessment for insulin resistance ; CRP – c-reactive protei

4.3.5 Effects of HFD on the development of AD-like pathology

4.3.5.1 HFD exacerbated the Aβ plaque load in the hippocampi and cortices of APP/PS1 mice

Photomicrographs of immunohistochemically stained brain sections showed the development of extensive Aβ plaque loads both in the hippocampi and cortices of APP/PS1 mice (Figure 35), starting in 3 months (Figure 35D) and developing with age. Whereas control mice (Figure 35A) did not develop any plaques, not even at 10 months of age. HFD significantly exacerbated

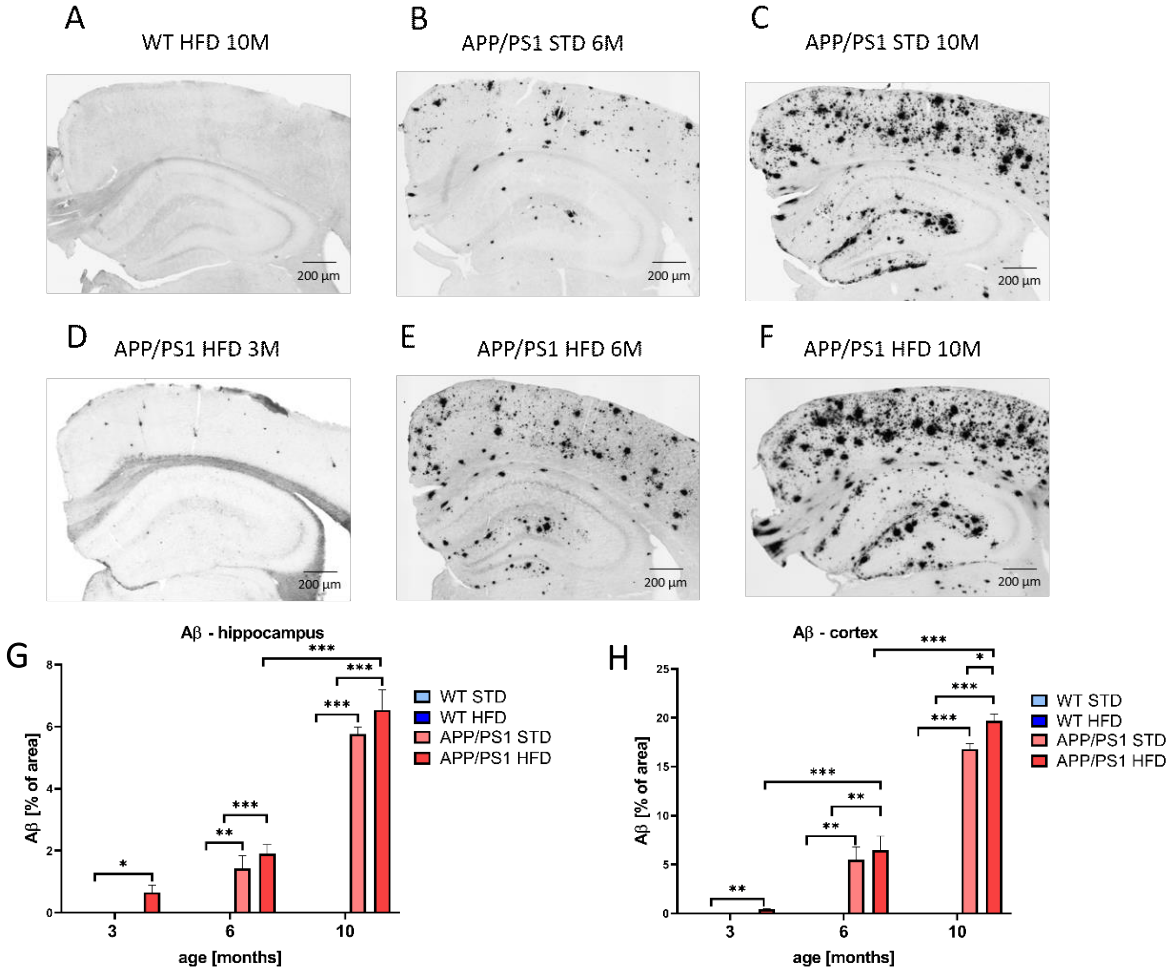

Figure 35: HFD exacerbated Aβ plaque load in the cortices of 10-month-old APP/PS1 mice. Representative photomicrographs of the APP/PS1 mice fed either with STD in 6 months (B) 10 months (C), or HFD in 3 months (D) 6 months (E) and 10 months (F) of age and the WT control in 10 months of age (G) immunohistochemically stained (A-F) for human Aβ and their quantification (G, H). Aβ plaque load is expressed as a percentage of the stained area. The data are presented as the means ± SEM. Statistical analysis is made between groups as shown in the graphs by one-way ANOVA with Bonferroni post-hoc test, *p<0.05, **p<0.01, ***p<0.001 (n = 5-8 mice per group).

the Aβ plaque loads in cortices of 10-month-old APP/PS1 mice as shown in Figure 35F, compared to APP/PS1 mice on STD (35C).

4.3.5.2 HFD worsened neuroinflammation in the brains of APP/PS1 mice

Immunohistochemical microglial staining of Iba1 revealed visible clusters of activated microglia in the hippocampi and cortices of APP/PS1 mice on STD of both ages (Figure 36) but not in the brains of WT control mice, where only resting microglia were visible (Figure 36A). HFD significantly increased level of microgliosis in both

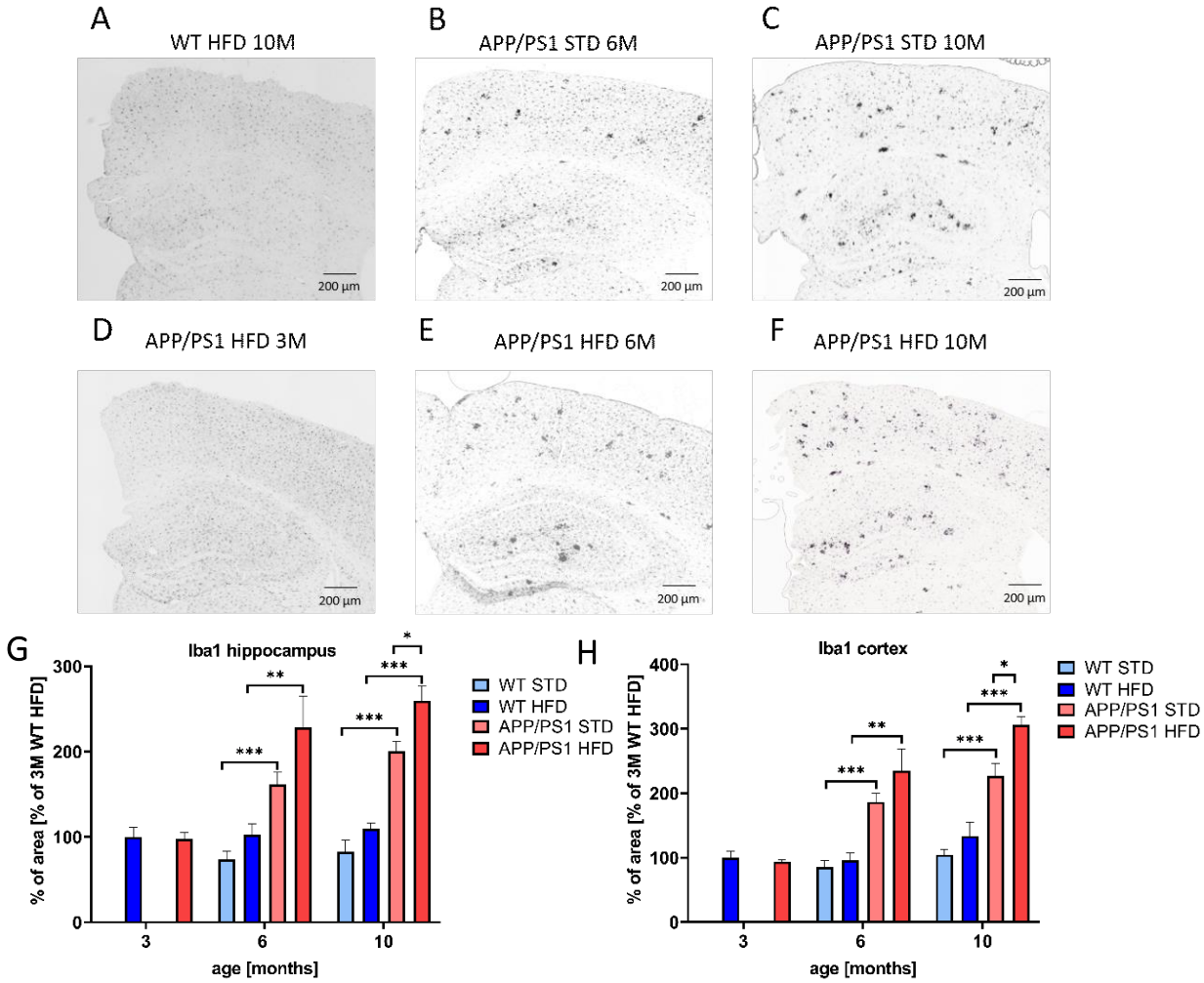

Figure 36: Effect of HFD on microgliosis in the hippocampi and cortices of the APP/PS1 mice. Representative photomicrographs of the APP/PS1 mice fed either with STD in 6 months (B) 10 months (C), or HFD in 3 months (D) 6 months (E) and 10 months (F) of age and the WT control in 10 months of age (A) immunohistochemically stained (A-F) and their quantification (G, H). Percentage of the stained area is expressed as a % of the 3-month-old WT mice on HFD to enable the comparison of multiple staining series. The data are presented as the means ± SEM. Statistical analysis is made between groups as shown in the graphs by one-way ANOVA with Bonferroni post-hoc test, *p<0.05, **p<0.01, ***p<0.001 (n = 5-8 mice per group).

hippocampi and cortices of 10-month-old APP/PS1 mice compared to APP/PS1 on STD as shown in Figure 36.

Immunohistochemical staining of astrocytic marker GFAP revealed clusters of reactive astrocytes in hippocampi and cortices of APP/PS1 mice on both diets (Figure 37); HFD did not affect number of reactive astrocytes in any age. However, the astrogliosis significantly increased with age in both hippocampi and cortices.

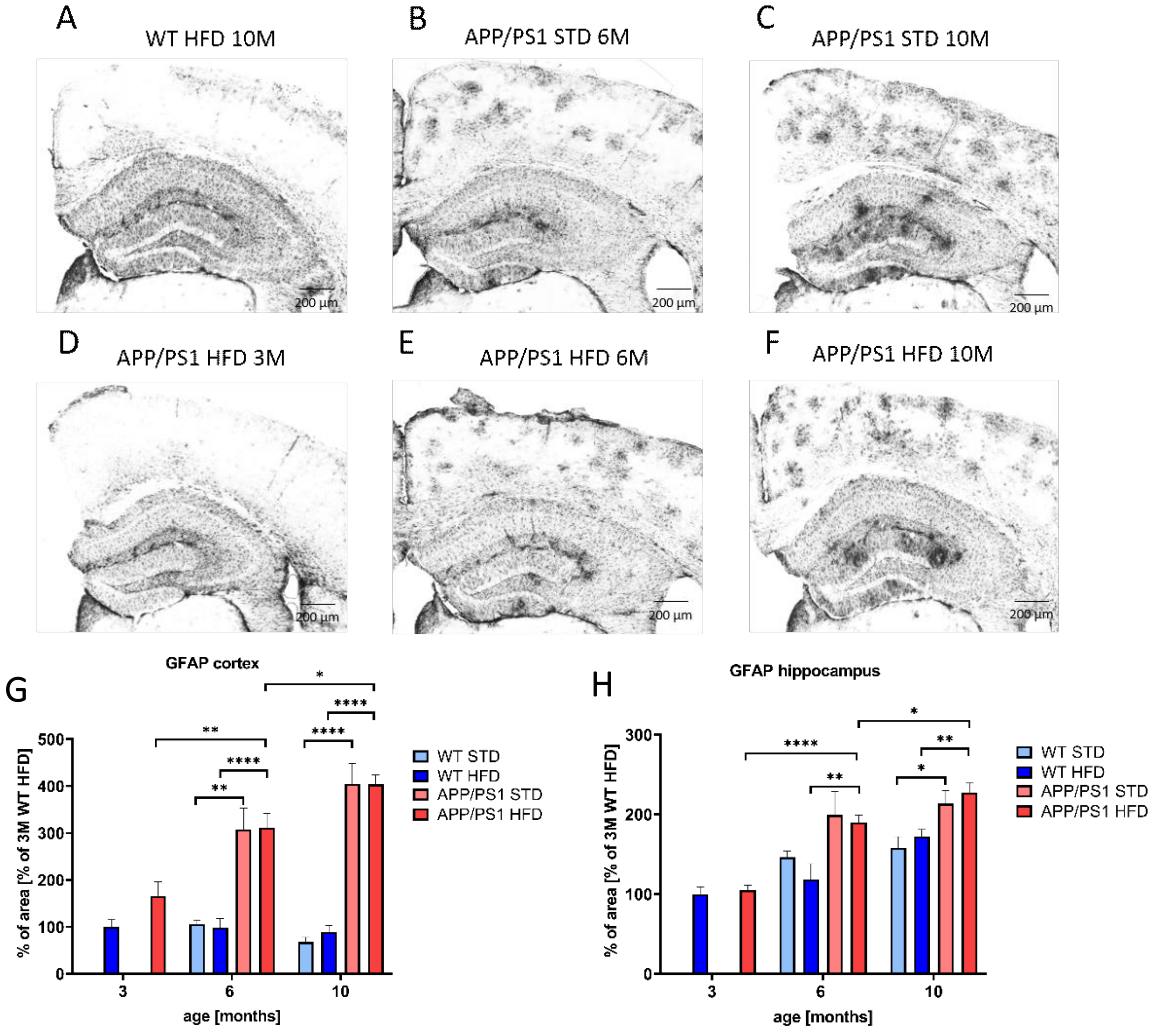

Figure 37: Effect of HFD on astrocytosis in the hippocampi and cortices of the APP/PS1 mice. Representative photomicrographs of the APP/PS1 mice fed either with STD in (B) 6 months (C) 10 months, or HFD in (D) 3 months (E) 6 months and (F) 10 months of age and (A) the WT control in 10 months of age immunohistochemically stained (A-F) for GFAP and their quantification (G, H). Percentage of the stained area is expressed as a % of the 3-month-old WT mice on HFD to enable the comparison of multiple staining series. The data are presented as the means ± SEM. Statistical analysis is made between groups as shown in the graphs by one-way ANOVA with Bonferroni post-hoc test, *p<0.05, **p<0.01, ***p<0.001, ****p<0.0001 (n = 5-8 mice per group).

4.3.5.3 Increased Tau phosphorylation in the hippocampi and cortices of APP/PS1 mice

Double staining of total Tau (antibody 9H12) in red, that recognizes the central region of Tau protein (aa162-175), and NeuroTrace™ visualizing neurons in blue, revealed an increasing trend in accumulation of Tau protein in neurons of CA1 part of hippocampus in 10-month-old APP/PS1 mice on both types of diet (Figure 38); HFD did not affect accumulation of Tau.

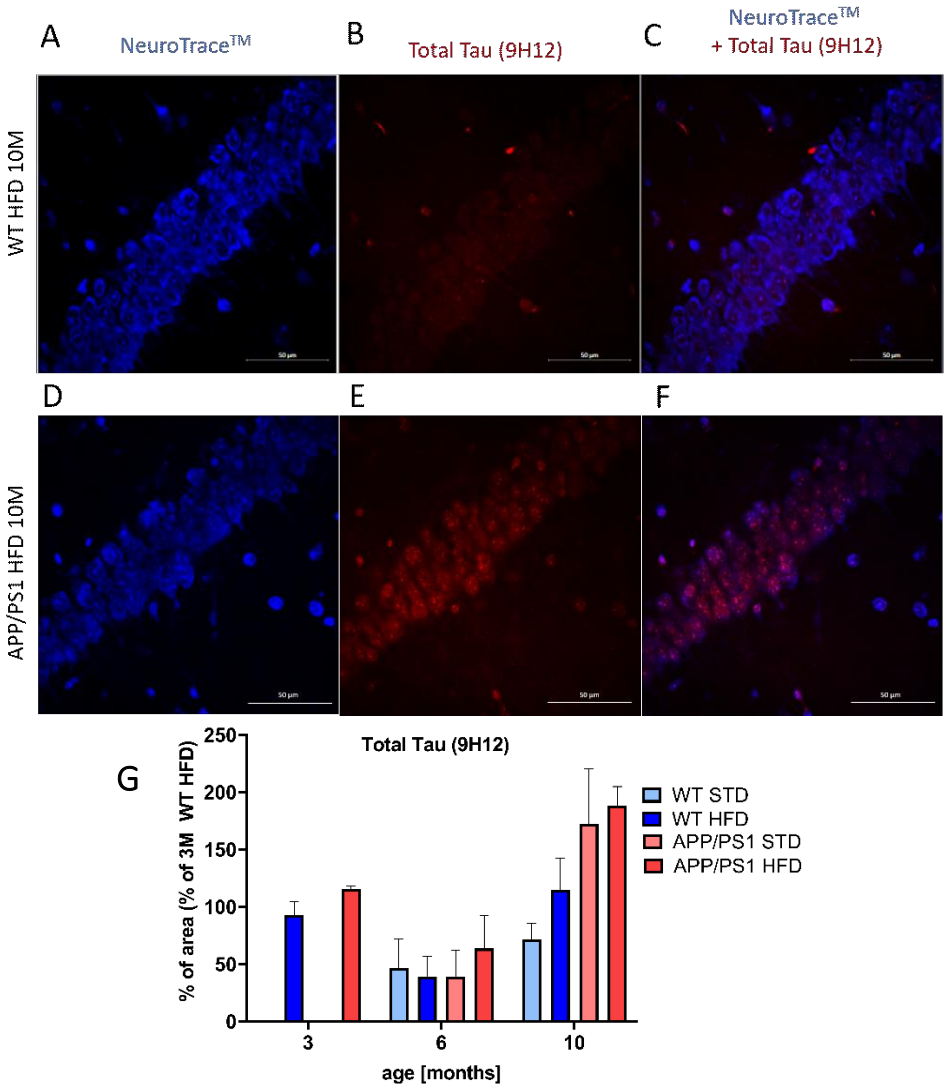

Figure 38: Increased accumulation of Tau in the CA1 part of hippocampi of the 10-month-old APP/PS1 mice. Representative photomicrographs of total Tau (9H12) and neurons in 10-month-old WT mice fed with HFD (A) NeuroTrace™ (B) total Tau (9H12) (C) their merge, and their age-matched APP/PS1 mice on HFD (D) NeuroTrace™ (E) total Tau (9H12) and (F) their merge. Percentage of the stained area is expressed as a % of the 3-month-old WT mice on HFD to enable the comparison of multiple staining series. The data are presented as the means ± SEM. Statistical analysis is made between groups as shown in the graphs by one-way ANOVA with Bonferroni post-hoc test (n = 5-8 mice per group).

Immunohistochemical staining revealed increased number of phosphorylated Tau at Ser202 and Thr205 (AT8 antibody) in dystrophic neurites (Figure 39) in hippocampi and cortices of APP/PS1 mice. The Tau phosphorylation is detectable already in 3 months (Figure 39A) and increases with the age and spreading of Aβ pathology; as it is obvious in the Figure 39G, where pTau labeled with AT8 antibody (red colour) is detectable around Aβ plaques labeled with Thioflavin S (green colour).

HFD significantly increased number of AT8 clusters formed around the Aβ plaques in the cortices and hippocampi of 6-month-old APP/PS1 mice. HFD also significantly increased size of the AT8 clusters in the hippocampi and cortices of 6-month-old APP/PS1 mice (Figure 39 J-K).

4.3.5.4 HFD and age attenuated the PI3K/Akt signaling pathway in the hippocampus

Level of IRβ significantly increased in time in hippocampi of WT and APP/PS1 mice, however, HFD reversed this effect; significantly decreased IRβ was observed in the hippocampus of 10-month-old APP/PS1 on HFD compared to APP/PS1 mice on STD (Figure 40D). Furthermore, levels of PI3K p85 also significantly decreased in 10-month-old APP/PS1 mice on HFD compared to their age-matched controls on STD, but also compared to 10-month-old WT mice on HFD. No differences were observed in levels of Akt, nevertheless, its phosphorylation at Ser473 tended to decrease with HFD at 6 months old WT and AP/PS1 mice, and significantly decreased between 6th and 10th month of age, as indicated in Figure 40G.

4.3.5.5 Decreased neuronal density and neurogenesis with age of mice

Immunohistochemical staining of neuronal nuclei (NeuN), a marker of mature neurons, detected significant decrease in neuronal density in the hippocampus of WT and APP/PS1 mice on HFD between 3rd and 6th month of age (Figure 41G), and in the cortex of WT on HFD (Figure 41H).

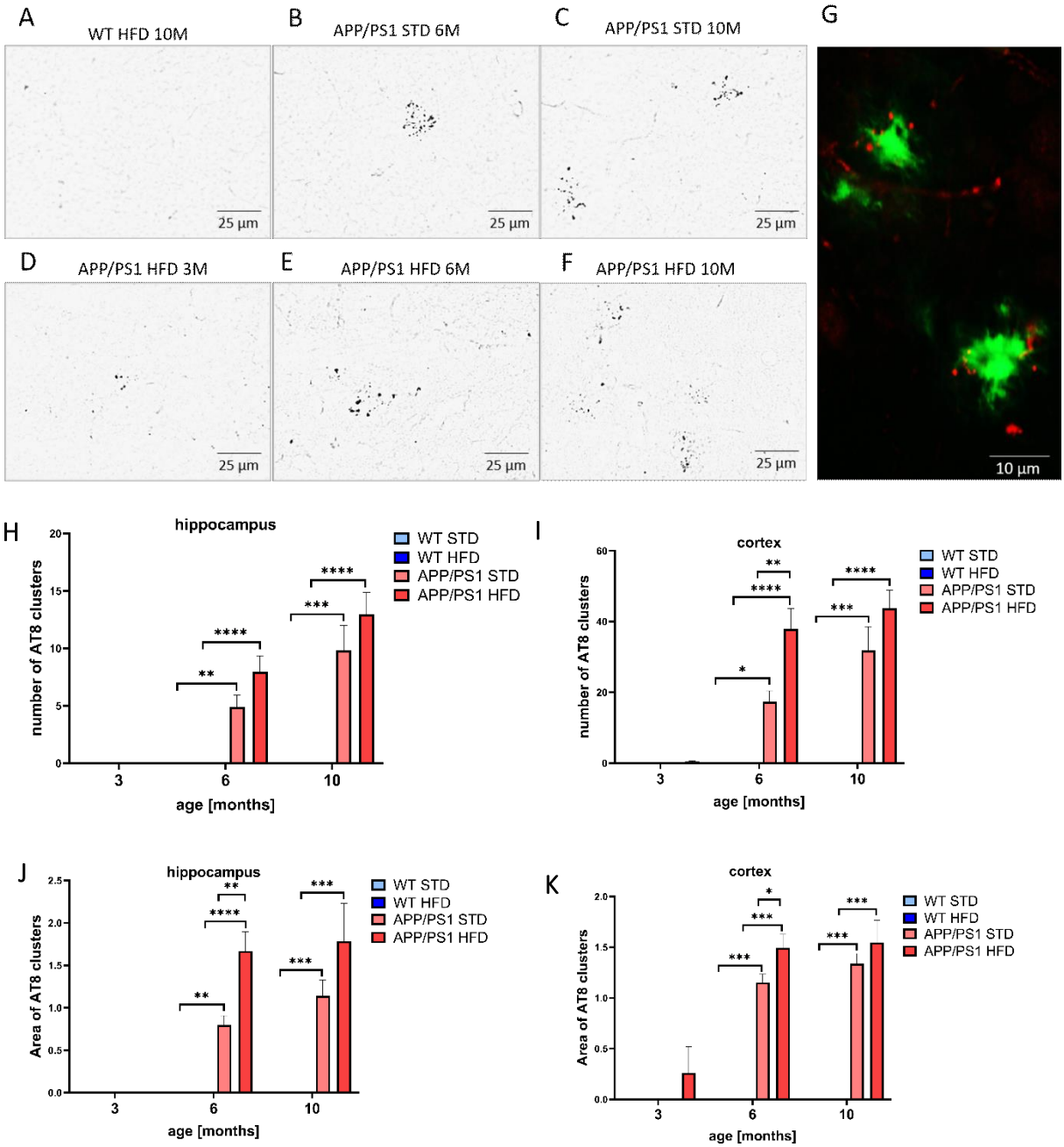

Figure 39: Increased Tau phosphorylation around Aβ plaques in hippocampi and cortices of APP/PS1 mice. Representative photomicrographs of the APP/PS1 mice fed either with STD in (B) 6 months (C) 10 months or HFD in (A) 3 months (E) 6 months and (F) 10 months of age and (D) the WT control in 10 months of age immunohistochemically stained (A-C) with AT8 antibody recognizing p-Tau at Ser202 and Thr205 and their quantification (H-K). (G) Representative figure of double staining of Aβ plaque (Thioflavin S) and p-Tau (AT8 antibody) in 10-month-old APP/PS1 mouse. Percentage of the stained area is expressed as a % of the 3-month-old WT mice on HFD to enable the comparison of multiple staining series. The data are presented as the means ± SEM. Statistical analysis is made between groups as shown in the graphs by one-way ANOVA with Bonferroni post-hoc test, *p<0.05, **p<0.01, ***p<0.001, ****p<0.0001 (n = 5-8 mice per group).

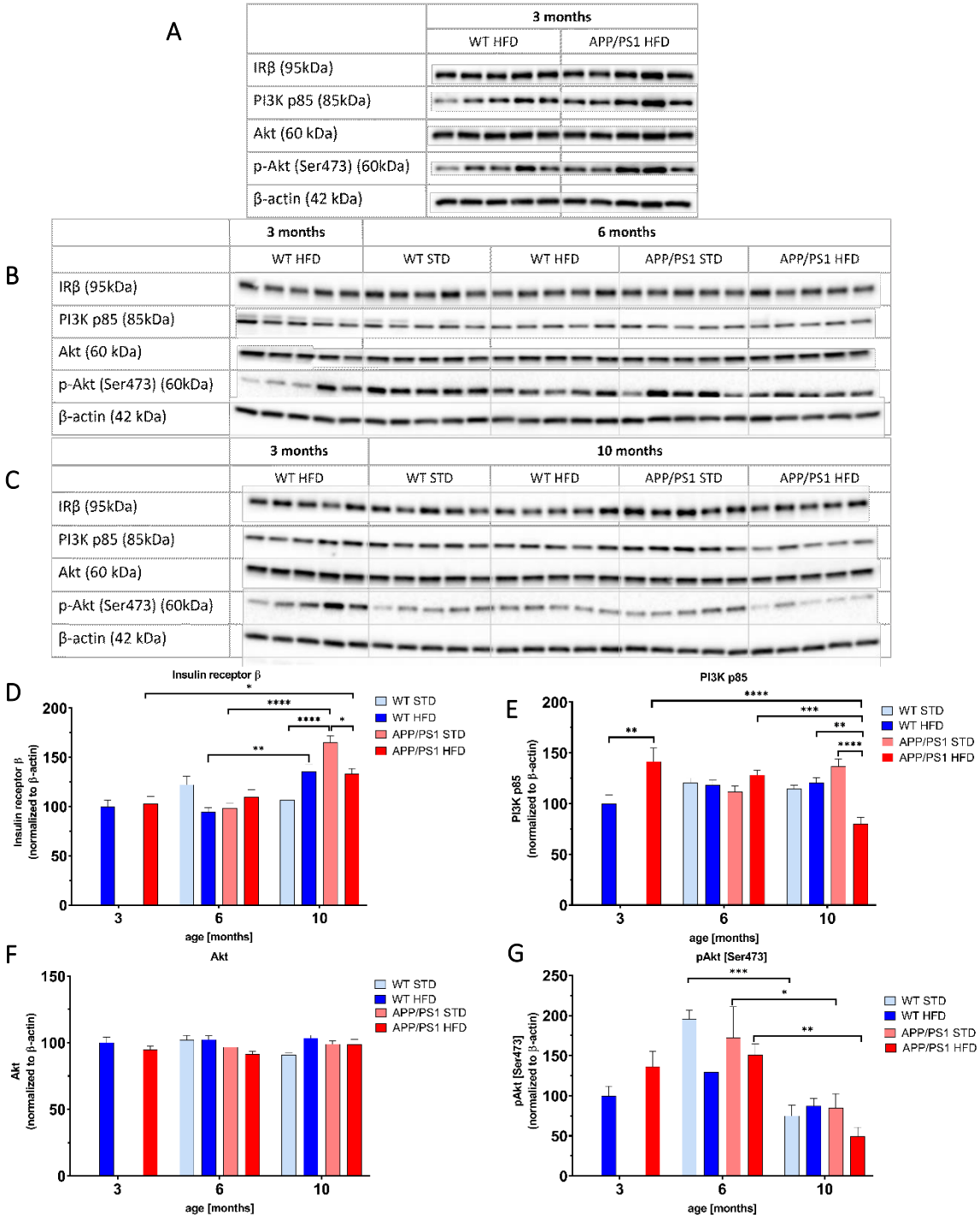

Figure 40: HFD and age attenuated the PI3K/Akt signaling pathway in the hippocampus. Proteins were determined by western blotting. Immunoblots in (A) 3 months, (B) 6 months and (C) 10 months of age, (D-G) quantification of protein levels: (D) Insulin receptor β (E) PI3K p85 (F) Akt (G) p-Akt (Ser473). Percentage of the stained area is expressed as a % of 3-month-old WT on HFD to enable the comparison of multiple staining series. The data are presented as the means ± SEM. Statistical analysis is made between groups as shown in the graphs by one-way ANOVA with Bonferroni post-hoc test, *p<0.05, **p<0.01, ***p<0.001, and ****p<0.0001 (n = 5 mice per group).

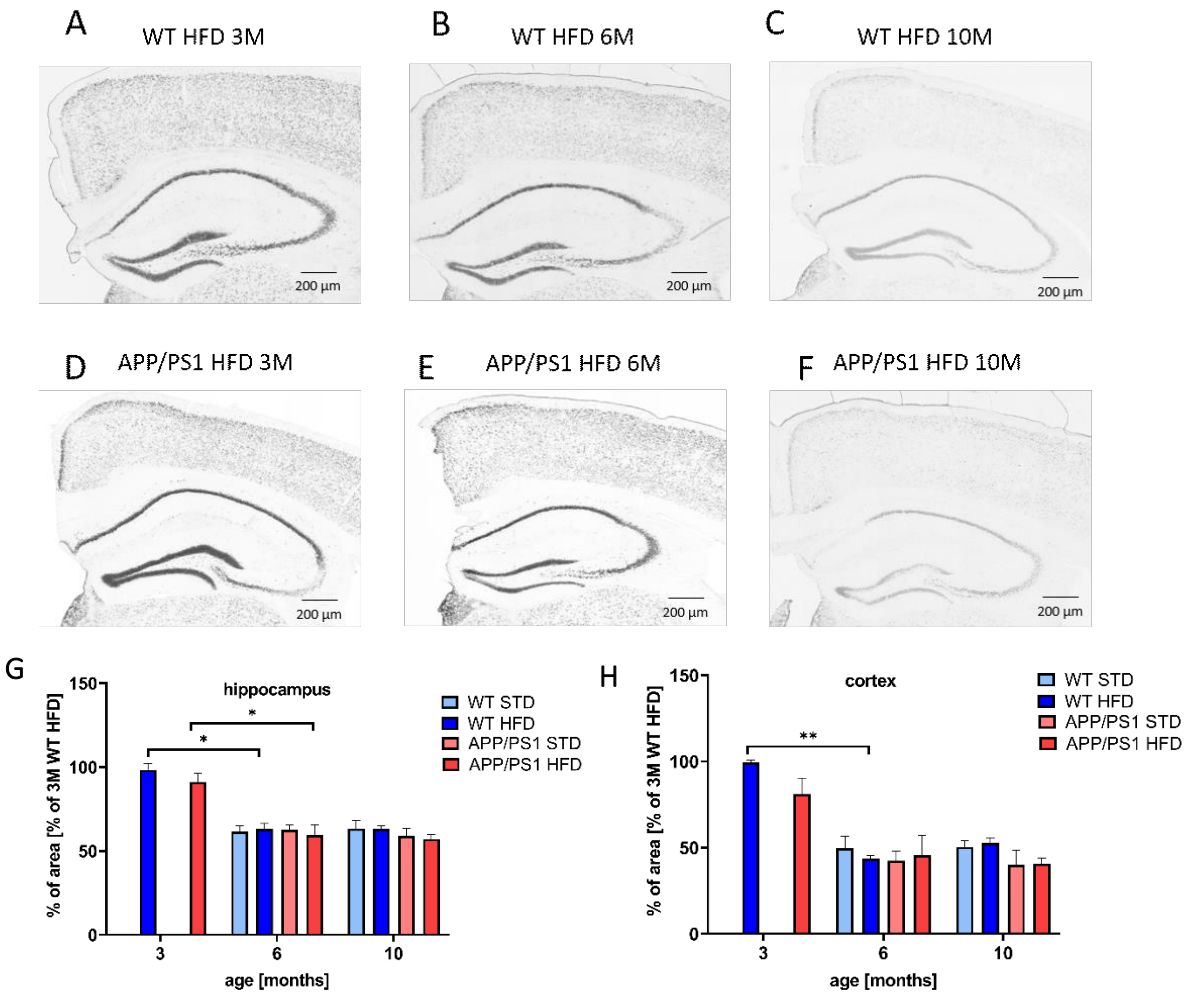

Figure 41: Decreased neuronal density with age of mice. Representative photomicrographs of the WT mice fed with HFD in (A) 3 months, (B) 6 months and (C) 10 months of age and APP/PS1 mice fed with HFD in (D) 3 months, (E) 6 months and (F) 10 months, and their quantification (G,H). Percentage of the stained area is expressed as a % of the 3-month-old WT mice on HFD to enable the comparison of multiple staining series. The data are presented as the means ± SEM. Statistical analysis is made between groups as shown in the graphs by one-way ANOVA with Bonferroni post-hoc test, *p<0.05, **p<0.01 (n = 5 mice per group).

Immunohistochemical staining of DCX, a marker of early neurogenesis, revealed a significant sharp decrease in production of new neurons in dentate gyrus (DG) of APP/PS1 and WT mice between 3- and 6-month-old mice on STD or HFD, which further decreased between 6th and 10th month (Figure 42G). Similarly staining of Tau 3R, a marker of late neurogenesis, showed a significantly decreased number of newly born neurons in DG between 3rd and 6th month of age in APP/PS1, as well as WT mice (Figure 42H).

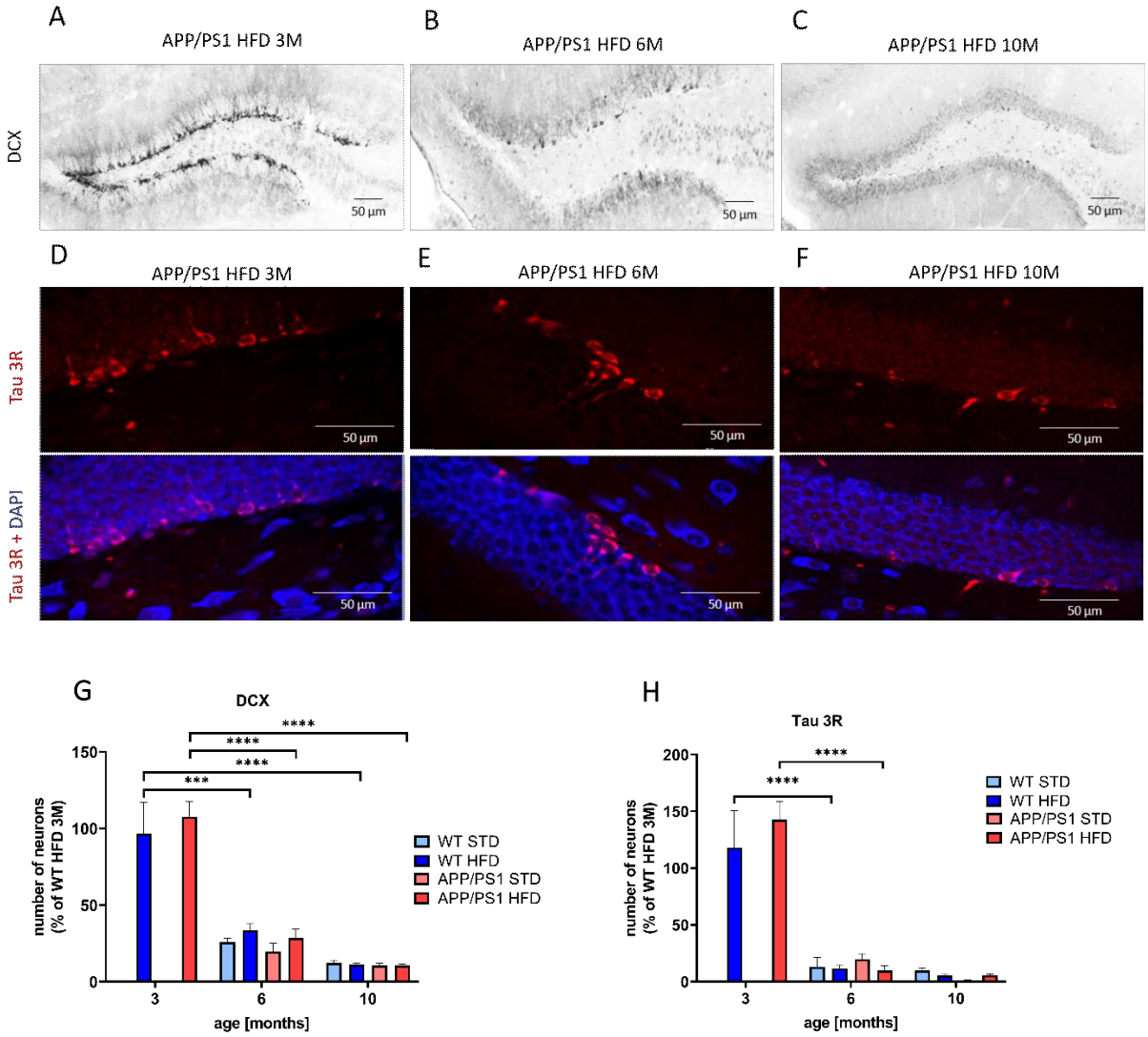

Figure 42: Decreased neurogenesis in mice with age. Representative photomicrographs of the APP/PS1 mice fed with HFD in (A,D) 3 months (B,E) 6 months and (C,F) 10 months of age immunohistochemically stained either for (A-C) doublecortin (DCX), or for (D-F) double staining Tau3R and DAPI. Percentage of the stained area is expressed as a % of the 3-month-old WT mice on HFD to enable the comparison of multiple staining series. The data are presented as the means ± SEM. Statistical analysis is made between groups as shown in the graphs by one-way ANOVA with Bonferroni post-hoc test, ***p<0.001, ****p<0.0001 (n = 5-8 mice per group).

4.3.5.6 HFD decreased synaptogenesis in the hippocampus of APP/PS1 mice

Presynaptic marker synaptophysin tended to decrease at 6-month-old APP/PS1 compared to WT mice, whereas significantly decreased at 10-month-old APP/PS1 mice on either STD, or HFD compared to their diet-matched WT controls (Figure 43D). Compared to APP/PS1 on STD, HFD further tended to decrease a level of synaptophysin

in 6-month-old APP/PS1, but also tended to decrease a level of postsynaptic marker spinophilin in 6-month-old APP/PS1 as shown in Figure 43E.

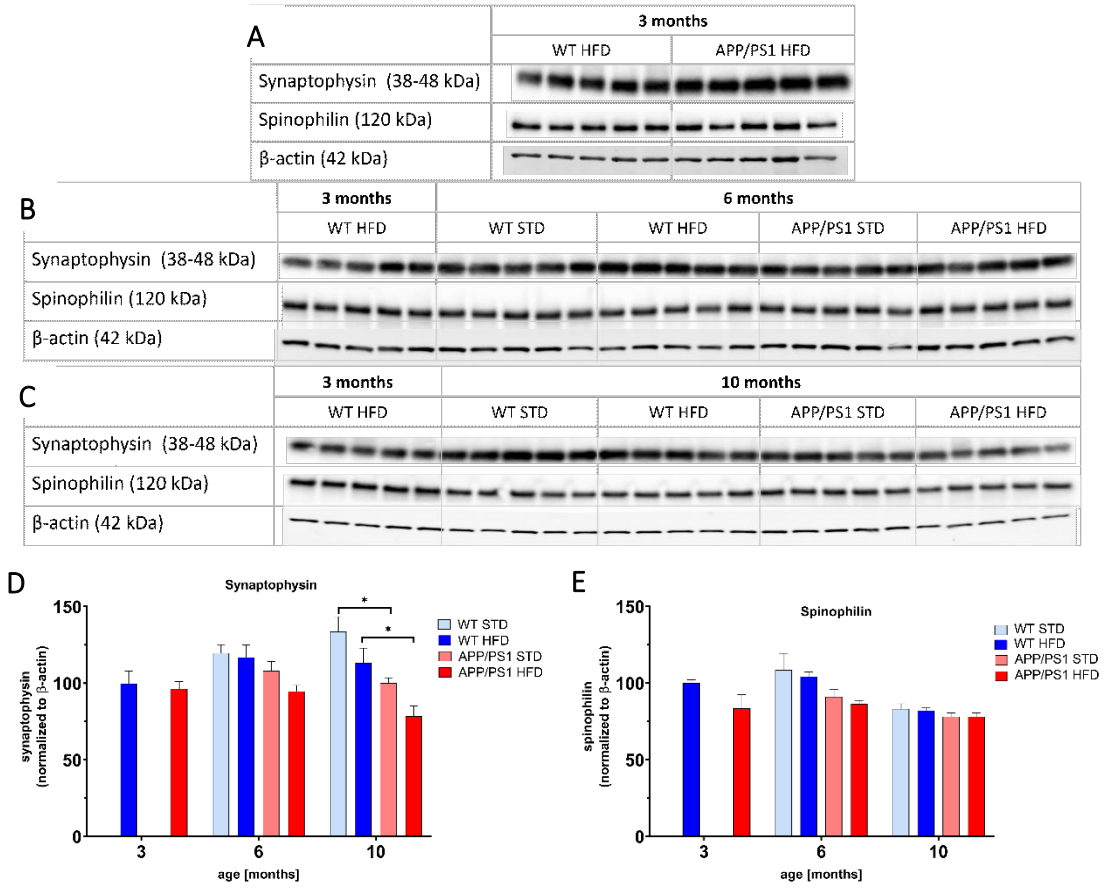

Figure 43: HFD decreased synaptogenesis in the hippocampi. Markers were determined by western blotting. Immunoblots in (A) 3 months, (B) 6 months and (C) 10 months of age, (D-E) quantification of protein levels: (D) synaptophysin (E) spinophilin. The data are presented as the means ± SEM. Statistical analysis is made between groups as shown in the graphs by one-way ANOVA with Bonferroni post-hoc test, *p<0.05 (n = 5 mice per group).

4.3.6 Decrease in markers connected to disrupted BBB in APP/PS1 mice

To search for the effect of HFD on the disruption of BBB, immunohistochemical staining of claudin-5 and occludin was made in hippocampi of APP/PS1 and WT mice. As shown in the Figure 44G, no difference was observed in the level of claudin-5 in APP/PS1 mice compared to their age-matched WT mice.

Immunohistochemical staining of occludin revealed significant decrease in hippocampi of all of the mice between 6th and 10th month of age as shown in the Figure 44H. However, no difference was observed in between APP/PS1 and WT mice, neither

between STD, and HFD-fed mice. All results from the AD-like pathology parametres affected by age, HFD and APP/PS1 genotype are summarized in Table 8.

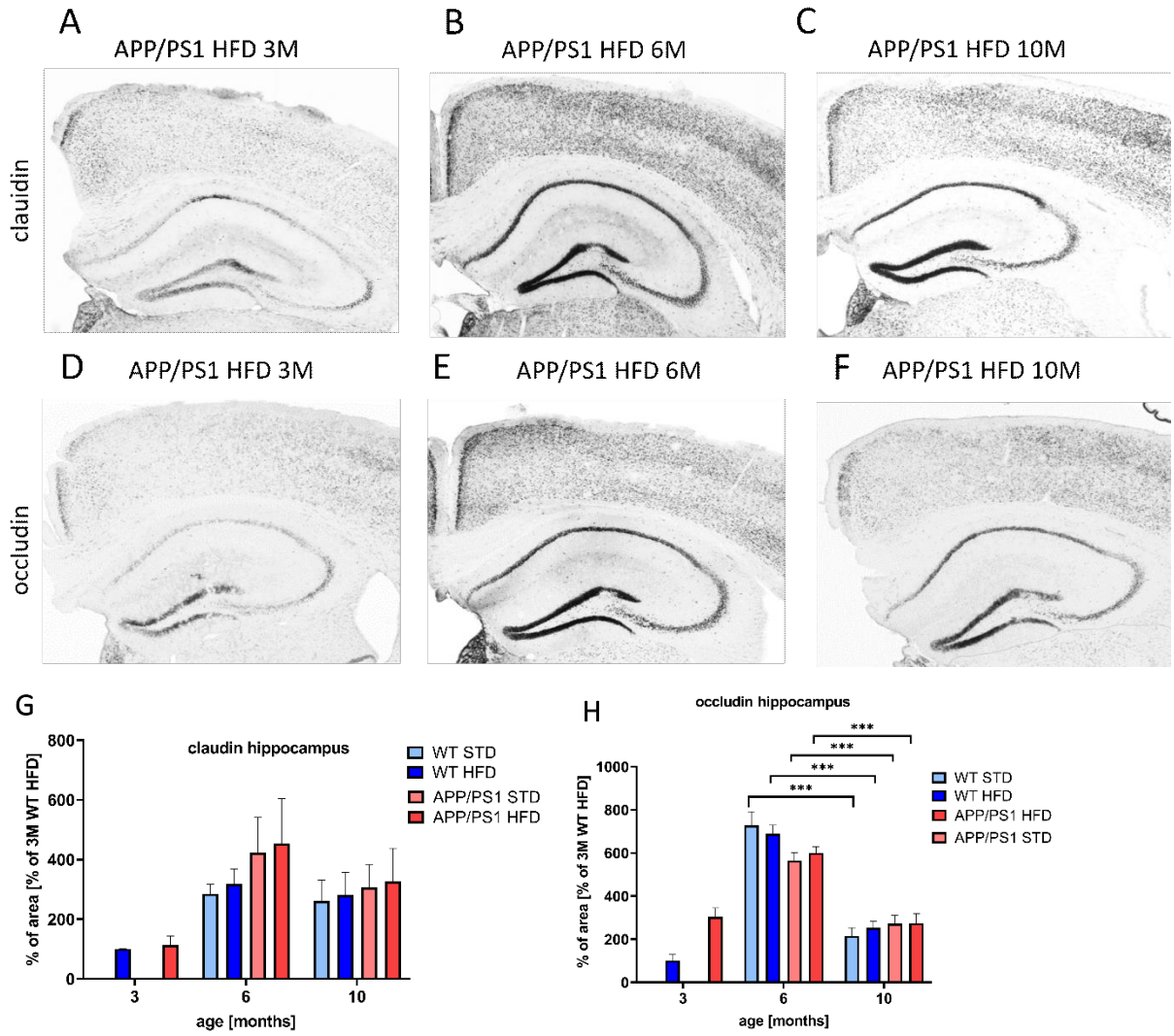

Figure 44: Disturbed BBB manifested by decrease in occludin with age. Representative photomicrographs of APP/PS1 mice fed with HFD in 3 months, 6 months and 10 months of age, immunohistochemically stained (A-C) for claudin-5 and (D-F) for occludin and their quantification in hippocampus (G,H). Percentage of the stained area is expressed as a % of the 3-month-old WT mice on HFD to enable the comparison of multiple staining series. The data are presented as the means ± SEM. Statistical analysis is made between groups as shown in the graphs by one-way ANOVA with Bonferroni post-hoc test. ***p<0.001 (n = 5-8 mice per group).

Table 8. Summary of AD-like pathology parametres affected by age, HFD and APP/PS1 genotype

	Brain region	3 months	6 months				10 months			
		APP/PS1 vs WT on HFD	HFD vs STD		APP/PS1 vs WT on HFD	Age 6M vs 3M on HFD		HFD vs STD	APP/PS1 vs WT on HFD	Age 10M vs 6M on HFD	
Aβ plaques	hippocampus	↑*	-	-	↑***	-	-	-	-	↑***	-	↑***
	cortex	↑**	-	-	↑**	-	↑***	-	↑*	↑***	-	↑***
Microgliosis (Iba1)	hippocampus	-	-	-	↑**	-	-	-	↑*	↑***	-	-
	cortex	-	-	-	↑**	-	-	-	↑*	↑***	-	-
Astrocytosis (GFAP)	hippocampus	-	-	-	↑****	-	↑**	-	-	↑**	-	↑*
	cortex	-	-	-	↑**	-	↑****	-	-	↑**	-	↑*
Total Tau (9H12)	Hippocampus (CA1)	-	-	-	-	-	-	-	-	-	-	-
p-Tau (Ser202, Thr205) (AT8)	hippocampus	-	-	↑*	↑****	-	-	-	-	↑***	-	-
	cortex	-	-	↑**	↑****	-	-	-	-	↑***	-	-
Insulin receptor β	hippocampus	-	-	-	-	↑**	-	-	↓****	↓**	-	↓***
PI3K	hippocampus	↑**	-	-	-	-	-	-	↓*	-	-	-
p-Akt (Ser473)	hippocampus	-	-	-	-	-	-	-	-	-	-	↓**
Neuronal density (NeuN)	hippocampus	-	-	-	↑**	↓*	↓*	-	-	-	-	-
	cortex	-	-	-	-	-	↓**	-	-	-	-	-
Neurogenesis (DCX)	hippocampus (DG)	-	-	-	-	↓***	↓****	-	-	-	-	-
Neurogenesis (Tau 3R)	hippocampus (DG)	-	-	-	-	↓****	↓****	-	-	-	-	-
Synaptophysin	hippocampus	-	-	-	-	-	-	-	-	↓*	-	-
Spinophilin	hippocampus	-	-	-	-	-	-	-	-	-	-	-
Claudin	hippocampus	-	-	-	-	-	-	-	-	-	-	-
Occludin	hippocampus	-	-	-	-	-	-	-	-	-	↓***	↓***

The data are presented as the means ± SEM. Statistical analysis is made by one-way ANOVA with Bonferroni test, *p<0.05, **p<0.01, ***p<0.001, ****p<0.0001 (n = 5-8 mice per group). Difference between the WT mice on HFD and STD pointed up by blue colour, difference between the APP/PS1 mice on HFD and STD pointed up by red colour.

↑ - increase, ↓ - decrease, HFD - high-fat diet, STD – standard diet, CA1 - cornu ammonis, DG – dentate gyrus

5. DISCUSSION

Obesity and related IR have been established as risk factors for the development of AD, resulting in intensive research of metabolic and pathological changes, which are caused by both diseases in the CNS (Tabassum et al., 2020). Currently, there is no sufficient AD treatment because the exact mechanisms leading to AD progression are still not fully elucidated. However, increasing evidence shows that anorexigenic and antidiabetic peptides could be potential powerful neuroprotective agents, but their mechanism of action is poorly understood.

First part of my PhD thesis describes the cellular signaling of the anorexigenic neuropeptide PrRP31 and its lipidized analog palm^{11}-PrRP31, with emphasis to activation of insulin signaling pathways as insulin signaling pathway is vital for both metabolism and CNS function. The potential neuroprotective and anti-apoptotic effects of PrRP are shown in two neuronal models stressed with neurotoxic MG: the human neuroblastoma cell line SH-SY5Y and rat primary cortical neurons. In the second part, an AD mouse model APP/PS1 mice were 2 months s.c. treated with palm^{11}-PrRP31; neuroprotective effects on pathological markers associated with AD, such as Aβ plaques, neuroinflammation, loss of synapses and apoptosis were followed in the hippocampi, cortices and in the cerebella. Finally, a relationship among the diet-induced obesity, IR, and inflammation in the periphery and development of neuropathological changes in the brain was demonstrated in WT or APP/PS1 mice fed with HFD.

5.1 Cell signaling pathways induced by PrRP31 and palm^{11}-PrRP31 in SH-SY5Y cells

Tracking of cell signaling pathways can help elucidate the molecular mechanism underlying the anorexigenic and antidiabetic effect of PrRP. From our previous *in vitro* (Maixnerová et al., 2011) and *in vivo* (Holubova et al., 2019, Kořínková et al., 2019) studies, PI3K/Akt and ERK-CREB signaling pathways are known to be activated by PrRP and its analogs. In this study, incubation of the SH-SY5Y cells with PrRP31 and palm^{11}-

PrRP31 increased the activation of proteins involved in insulin signaling pathways, as shown in Figure 45.

Namely, PDK1 and Akt kinases were activated by PrRP, similarly as by insulin in the study of Varghese et al (Varghese et al., 2013). In the brain, the PI3K/Akt signaling pathway activated by insulin plays a significant role as a neuromodulator, influencing the release and re-uptake of neurotransmitters (Sauter et al., 1983), neuronal survival (Yamaguchi et al., 2001, Zheng et al., 2002), synapse formation and plasticity (Beattie et al., 2000, Man et al., 2000, Chiu et al., 2008) and learning and memory (Zhao et al., 1999); hence, insulin was chosen as a positive neuroprotective control in other (Summers and Birnbaum, 1997, Lee et al., 2011) and this studies. Impaired activation of PI3K/Akt pathway is often linked to neurodegenerative changes (Xu et al., 2020). In this study, it is proved that PrRP and its lipidized analog participate in the activation of an insulin signaling pathway, which could be linked to a neuroprotective effect of PrRP31.

Furthermore, PrRP31 and its analog significantly increased the phosphorylation of m-Tor, which belongs to the PI3K-related kinase protein family (Swiech et al., 2008, Jung et al., 2010). m-Tor may exist as m-Tor complex 1 (m-TorC1) or m-Tor complex 2 (m-TorC2). The key component of m-TorC2 is rapamycin-insensitive companion of mammalian target of rapamycin (RICTOR), which, unlike m-TorC1, is not directly inhibited by rapamycin. In our study, rapamycin reduced the activation of m-Tor induced by PrRP31 and palm^{11}-PrRP31. Therefore, we assume that PrRP31 and palm^{11}-PrRP31 increased the activation of m-TorC1, which is involved in the molecular mechanism of dendritic branching and is important for the enhancement of synaptic transmission (Jaworski and Sheng, 2006). m-TorC1 plays an important role in the growth and differentiation of neural tissue and a decrease in its activation can lead to memory impairment and an inhibition of the ability to learn (Franco et al., 2017).

Kinases implicated in the regulation of a cellular metabolism include GSK-3β, a main kinase of glycogen synthase and Tau protein. In our study, PrRP31 and palm^{11}-PrRP31 increased phosphorylation of GSK-3β at Ser9, resulting in inhibition of kinase activity of GSK-3β towards Tau protein, manifested by a decreased phosphorylation of Tau protein, similarly as in our previous study with MSG mice (Spolcova et al., 2015). Therefore, the

inhibition of GSK-3β kinase activity can have a potential to attenuate Tau hyperphosphorylation (Nicolia et al., 2010, Baum et al., 1996, Plattner et al., 2006). A selective inhibitor of GSK-3β, SB216736, confirmed that PrRP31 and its palmitoylated analog inhibited specifically PrRP-activated phosphorylation of GSK-3β at Ser9.

Decreased activation of the ERK-CREB pathway, which physiologically promotes cell survival, growth, cell proliferation and differentiation (Wen et al., 2010), can play an important role in the development of neurodegenerative diseases such as AD (Scott Bitner, 2012). Insulin-induced activation of ERK has been suggested as a crucial player in synaptic and neuronal plasticity (Sweatt, 2001). ERK is also an essential component of the signal transduction mechanisms subserving behavioral memory formation (Wu et al., 1999, Zhao et al., 1999, Sweatt, 2001, Kimura et al., 2000). Our results showed that PrRP31 and palm^{11}-PrRP31 rapidly increased the activation of ERK and CREB kinases, similar to our and other studies (Maixnerova et al., 2011, Maletinska et al., 2015, Kimura et al., 2000), which again confirmed the potential neuroprotective properties of PrRP31 and its palmitoylated analog, similarly to insulin. U0126, a selective inhibitor of ERK kinase activity, proved that activation of the ERK-CREB signaling pathway is induced specifically by PrRP or its palmitoylated analog, as the inhibitor attenuated PrRP-mediated phosphorylation of both ERK and CREB.

PrRP and its lipidized analog increased phosphorylation of PDK1 and Akt which are part of the insulin signaling pathway, increased an activation of m-TorC1 and phosphorylation of GSK-3β at Ser9 and furthermore, it increased activation of ERK-CREB pathway in the same manner, as insulin, which is required for neuronal synaptic and dendritic plasticity, for learning, and for memory formation. We observed the activation of these signaling pathways in our previous *in vivo* models of neurodegeneration, hence these could be the main pathways contributing to the potential neuroprotective effect of PrRP. Therefore, PrRP can have similar positive effects on neuropathological processes as insulin, thereby eventually curbing the development and progression of AD (Maletínská et al., 2019).

To conclude, PrRP and its lipidized analog increased PI3K/Akt and ERK-CREB insulin signaling in the same manner, as insulin, which is required for neuronal synaptic

and dendritic plasticity, for learning, and for memory formation, hence these could be the main pathways contributing to the potential neuroprotective effect of PrRP.

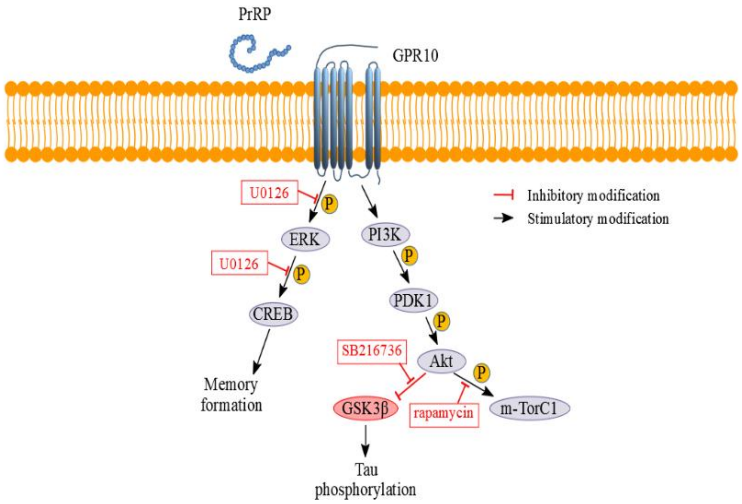

Figure 45. Schematic view of PrRP signaling pathways (Zmeskalova et al., 2020)**.**
CREB - cAMP response element binding protein; ERK - extracellular signal-regulated kinase; GSK-3β - glycogen synthase kinase 3β; GPR10 - G-protein coupled receptor 10; m-TorC1 - mammalian target of rapamycin complex 1; PDK1 - phosphoinositide-dependent kinase 1; PI3K - phosphoinositide 3-kinase; PrRP – prolactin-releasing peptide; U0126 – mitogen-activated protein kinases inhibitor; SB216736 - GSK-3β inhibitor; rapamycin – m-TorC1 inhibitor

5.2 Potential neuroprotective and anti-apoptotic effects of PrRP31 and palm^{11}-PrRP31 in SH-SY5Y cells and rat cortical neurons

MG, a reactive intermediate of cellular metabolism, is the most potent precursor of the advanced glycation end products and is strictly correlated with an increase in oxidative stress in AD (Angeloni et al., 2014). Therefore, MG can be useful for screening of potential neuroprotective compounds that could ameliorate oxidative stress (Bellier et al., 2019). Similarly as in the study with the GLP-1 analog liraglutide, where liraglutide enhanced SH-SY5Y cell viability (Sharma et al., 2014), PrRP31 and palm^{11}-PrRP31 increased viability determined by the MTT test in the MG-stressed SH-SY5Y cells.

Pretreatment of SH-SY5Y and primary cortical neurons with both PrRP31 and palm^{11}-PrRP31 significantly enhanced viability of the cells affected with MG.

Following proteins of the Bcl-2 protein family, whose members act as anti- or pro-apoptotic agents showed that increase in the apoptotic activator Bax induced by the MG

treatment was attenuated by PrRP31 and palm^{11}-PrRP31, similar to our and others studies as shown in Figure 46 (Tajes et al., 2014b, Popelová et al., 2018). On the other hand, the decrease in the prosurvival protein Bcl-2 induced by MG was reversed by PrRP31 and palm^{11}-PrRP31. Bcl-2 directly binds to Bax, forming a nonactive heterodimer and blocking the formation of the active pro-apoptotic Bax homodimer. The Bax/Bcl-2 ratio is regarded as an apoptotic marker (Salakou et al., 2007); its decrease in the cells treated with PrRP31 and palm^{11}-PrRP31 signifies decreased apoptosis. MG induces the phosphorylation of the pro-apoptotic protein Bad (Stickles et al., 2015), a key regulator for neuronal apoptosis, neuroinflammation and Aβ clearance (Zhang et al., 2021). The Bad phosphorylation at several epitopes was decreased by both PrRP and palm^{11}-PrRP31.

c-Jun is a component of the transcription factor activator protein-1 (AP-1); its transcriptional activity is regulated by phosphorylation at Ser63 and Ser73 through SAPK/JNK (Vogt, 2002). AP-1-regulated genes, are involved in diverse biological functions, including cell proliferation, differentiation, and apoptosis, as well as transformation, invasion and metastasis, depending on cell type and context (Leppa and Bohmann, 1999, Shaulian and Karin, 2002). Similarly, as in the study of Du (Du et al., 2000), p-c-Jun (Ser73) was increased after incubation with MG and was reduced by pretreatment with PrRP31 and palm^{11}-PrRP31, which further points to anti-apoptotic properties of PrRP.

In accordance with a previous study (Li et al., 2012), we confirmed MG-induced Tau hyperphosphorylation at Ser396 and at Ser198/199/202 (Tau 1 antibody) in SH-SY5Y cells as in (Li et al., 2012). This increased phosphorylation was attenuated by both PrRP31 and palm^{11}-PrRP31 in this study. Furthermore, the decreased Tau phosphorylation after palm^{11}-PrRP31 was consistent with our previous *in vivo* study, which showed that palm^{11}-PrRP31 inhibited the phosphorylation of Tau (Ser396/Ser404) in THY-Tau22 mice overexpressing mutated human Tau (Popelova et al., 2018), and with our previous *in vitro* study, which showed that palm^{11}-PrRP31 attenuated hypothermia-induced phosphorylation of Tau (Ser396) in SH-SY5Y cells (Prazienkova et al., 2019b). All mentioned phosphorylation epitopes contribute to the pathological phosphorylation of Tau protein.

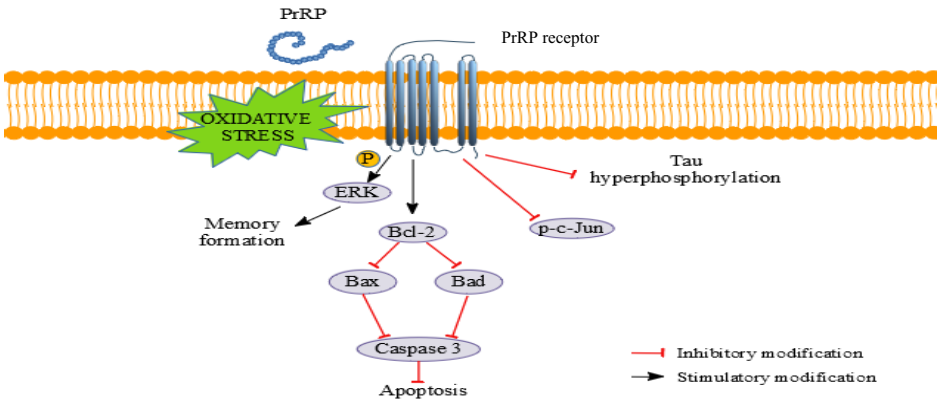

Figure 46. Schematic view of signaling pathways involved in PrRP neuroprotective and anti-apoptotic effect (Zmeskalova et al., 2020)**.**
Bad - The Bcl-2 associated agonist of cell death protein; Bax - Bcl-2-associated X protein; ERK - extracellular signal-regulated kinase; GPR10 - G-protein coupled receptor 10; PrRP – prolactin-releasing peptide

In summary, PrRP and its lipidized analog decreased the oxidative stress and increased viability in the MG-stressed SH-SY5Y cells and primary cortical cells. PrRP and palm^{11}-PrRP31 decreased apoptosis in the cells and prevented pathological hyperphosphorylation of Tau supporting the thought of their potential neuroprotectivity.

5.3 Effect of palm^{11}-PrRP31 analog on pathological markers connected to AD in APP/PS1 mice on standard diet

In our previous *in vivo* studies, we tested the potential neuroprotective properties of the palmitoylated PrRP analogs in the different mouse models of AD-like pathology. Palm^{1}-PrRP31, an analog of PrRP palmitoylated at the N-terminus, ameliorated hippocampal insulin signaling pathways and attenuated Tau hyperphosphorylation at several epitopes in mice with monosodium glutamate (MSG)-induced obesity (Spolcova et al., 2015). Palm^{11}-PrRP31 also attenuated Tau hyperphosphorylation, improved a short-term spatial memory and enhanced synaptic plasticity in transgenic THY-Tau22 mice, a mouse model of AD-like Tau pathology (Popelova et al., 2018). Finally, palm^{11}-PrRP31 was shown to significantly reduce an amyloid plaque deposition, neuroinflammation and Tau phosphorylation in hippocampi and cortices of APP/PS1

mice, a transgenic mouse model of amyloidosis (Holubova et al., 2019). In this study, we wanted to further extend our knowledge of possible neuroptotective effect of palm^{11}-PrRP31 for cerebellum and explore its potential neuroprotective effects on further pathological markers associated with AD.

As shown previously, chronic administration of palm^{11}-PrRP31 significantly decreased cumulative food intake and BW in rodents with HFD-induced obesity (Maletínská et al., 2015, Mikulaskova et al., 2018, Pražienková et al., 2017) but similarly as in our study on APP/PS1 mice no decrease in BW was observed in lean mice (Popelová et al., 2018, Holubova et al., 2019). In view of no significant BW changes, we did not observe any significant differences in the circulating leptin levels, an indicator of adipose tissue balkiness, in fasted blood glucose or insulin levels after the treatment, similar to the result of our previous studies on lean mice (Holubova et al., 2019, Popelová et al., 2018). Nevertheless, no differences in glucose and insulin levels were expected after treatment, as there were no differences between APP/PS1 mice and their controls.

Research on AD has focused on the characterization of the toxicity of Aβ peptide and Tau protein in the hippocampus and the cerebral cortex since they are regarded as the main regions affected during memory loss (Scheff et al., 2007, Miniaci and De Leonibus, 2018), but the role of the cerebellum has been neglected for a long time. The cerebellum was considered a plaque-free region and was used as a reference for Aβ peptide accumulation in the hippocampi and cortex, mainly for imaging. However, recent studies using transgenic AD mouse models have revealed deposits of Aβ plaques in the cerebellum and their effect on the synaptic plasticity (Mitew et al., 2013, Yousefi et al., 2015). Also, this study showed multiple Aβ plaques in the cerebella of APP/PS1 mice, while controls had none. Furthermore, significant visual or motor impairment in both patients with AD and mouse models of AD suggests that Aβ pathology extends beyond the hippocampus (Caine and Hodges, 2001, Lambon Ralph et al., 2003, Albers et al., 2015, Hoxha et al., 2018).

In this study, we confirmed the effect of palm^{11}-PrRP31 to reduce the number of Aβ plaques in the hippocampi and cortices of APP/PS1 mice, similarly as in our previous study (Holubova et al., 2019). Protective palm^{11}-PrRP31 effect was further confirmed in

the cerebella of APP/PS1 mice, where widespread Aβ plaques were significantly decreased after a chronic treatment with palm^{11}-PrRP31.

Neuroinflammation, the main indicator of AD progression is characterized by reactive astrocytes and microglia surrounding Aβ plaques (Fakhoury, 2018, Holubova et al., 2019). Glial cells play an important role in protecting and repairing the central nervous system from damage, oxidative stress and inflammation induced by toxic Aβ (Hansen et al., 2018, Frost and Li, 2017). However, in the context of chronic inflammation, microglia and astrocytes lose their neurosupportive functions, become reactive and make neurons vulnerable to excitotoxicity and metabolic and oxidative stress (Steele and Robinson, 2012). Therefore, reducing chronic inflammation seems to be a potential neuroprotective strategy. Palm^{11}-PrRP31 was previously shown to suppress neuroinflammation, as indicated by decreased numbers of reactive astrocytes and microglia in both the hippocampi and cortices of APP/PS1 mice (Holubova et al., 2019). In this study, clusters of reactive microglia, indicated by Iba1-positive microglia with altered morphology, were found in the cerebella of APP/PS1 mice, and the number of these microglia was significantly decreased after treatment with palm^{11}-PrRP31. It seems that microglial changes are vital contributors to AD progression within the cerebellum, which occur in the absence of major features of traditional AD neuropathology. This suggests that microglial changes occur independent of neuronal loss and Tau tangle formation during cerebellar AD pathogenesis (Singh-Bains et al., 2019, Serrano-Pozo et al., 2013). However, similarly as in the study of Singh-Bains (Singh-Bains et al., 2019), no differences were found between APP/PS1 mice and their controls in the cerebral GFAP, suggesting an absence of reactive astrocytes in the cerebellum (Singh-Bains et al., 2019).

This study aimed to define more precisely the potential anti-inflammatory effect of palm^{11}-PrRP31. CD68, scavenger receptor promoting phagocytosis of cellular debris extensively increased in highly reactive microglia (Belfiore et al., 2019, Zotova et al., 2011), was decreased after treatment with palm^{11}-PrRP31 in hippocampi of APP/PS1 mice.

Activated glial cells, and neurons produce a large number of inflammatory mediators, such as pro-inflammatory cytokines, increasing inflammation and further contributing to

neuronal dysfunction and cell death (Zhang et al., 2018, Tuppo and Arias, 2005, Rubio-Perez and Morillas-Ruiz, 2012). Hippocampi of APP/PS1 mice showed increased levels of the pro-inflammatory cytokines IL6 and IFNγ. Chronic treatment with palm^{11}-PrRP31 decreased very significantly IFNγ.

Changes in proteins of Bcl-2 family involve primarily apoptosis. The expression of pro-apoptotic protein Bax, present in both neurons and microglia is upregulated in AD (Su et al., 1997). Bax protein was increased in APP/PS1 mice and attenuated by palm^{11}-PrRP31, similarly as in our previous *in vitro* study using SH-SY5Y cells (Popelová et al., 2018). An increase in the ratio of Bax/Bcl-2 indicates an increase in apoptosis (Salakou et al., 2007), and this ratio was decreased after palm^{11}-PrRP31 treatment in APP/PS1 mice, in this study.

As synaptic failure is the pathological hallmark of cognitive deficits in AD, we further aimed to examine the effect of palm^{11}-PrRP31 on synaptogenesis (Scheff et al., 2007). As previously reported, APP/PS1 mice exhibit a decrease in synaptophysin, a presynaptic marker, which was prevented by treatment with palm^{11}-PrRP31, suggesting that this agent prevents synapse loss or increases synaptogenesis (Holubova et al., 2019, Tai et al., 2018). Syntaxin1A, a protein found at presynaptic neuronal terminals that mediates the fusion of synaptic vesicles (Jordà-Siquier et al., 2020, Yang et al., 2015), was found around Aβ plaques, and was decreased in both the hippocampi and cortices of APP/PS1 mice and significantly increased after treatment with palm^{11}-PrRP31. Additionally, the levels of both PSD95, a crucial marker of synaptic density of neurons that is involved in anchoring synaptic proteins (Hunt et al., 1996), and spinophilin, a postsynaptic marker localized in dendritic spines that is involved in synaptic plasticity, learning, and memory (Carmody et al., 2008, Allen et al., 2006), were decreased in APP/PS1 mice and increased after treatment with palm^{11}-PrRP31. Elevated levels of either the presynaptic markers synaptophysin and syntaxin1A or the postsynaptic markers PSD95 and spinophilin in both the hippocampus and cortex after the treatment indicated that palm^{11}-PrRP31 provided synaptic protection. No difference in synaptic markers was found in the cerebella of APP/PS1 mice or their controls, suggesting that there was no

change in synaptic plasticity in 8-month-old APP/PS1 mice, similarly as in the study of Hoxha (Hoxha et al., 2018).

In order to elucidate the possible mechanism of Aβ peptide clearance in APP/PS1 mice treated with palm^{11}-PrRP31, its potential beneficial effect was followed on the paravascular glymphatic pathway driven by AQ4, a major pathway responsible for the clearance of interstitial fluid solutes, such as Aβ peptide, from the brain parenchyma. In AD patients, glymphatic function is reduced, and Aβ peptide accumulates (Kress et al., 2014). APP/PS1 mice showed decreased number of the astrocytic water channels AQ4, resulting in decreased clearance via the glymphatic pathway (Iliff et al., 2012, Rasmussen et al., 2018). Palm^{11}-PrRP31 increased the AQ4, suggesting that it improved Aβ clearance.

LRP1 has a dual role in the metabolism of Aβ peptide in the brain. The inactivation of LRP1 causes both a decreased Aβ clearance from the brain and an impairment of Aβ generation, resulting in an overall reduced Aβ pathology (Van Gool et al., 2019, Shinohara et al., 2017). The level of LRP1 is increased in APP/PS1 mice and was significantly decreased after treatment with palm^{11}-PrRP31, suggesting that a decrease in LRP1 is a possible mechanism by which the number of Aβ plaques was decreased after palm^{11}-PrRP31 treatment.

m-Tor plays a crucial role in Aβ pathology. Its activation contributes to Aβ production and accumulation by directly inhibiting autophagy (Oddo, 2012, Caccamo et al., 2010). As in a study by Zhou (Zhou et al., 2008), 8-month-old APP/PS1 mice with widespread Aβ plaque deposits exhibited more hyperactive m-Tor signaling than their age-matched control mice. Similar findings of increased m-Tor signaling were shown in the brains of human patients with AD (Tramutola et al., 2015, Lafay-Chebassier et al., 2005). Palm^{11}-PrRP31 restored m-Tor signaling to normal levels in APP/PS1 mice and decreased Aβ pathology similarly as in the studies of others (Talboom et al., 2015, Mueed et al., 2018).

Results from the study on APP/PS1 mice support previous findings that palm^{11}-PrRP31 exhibited multiple beneficial neuroprotective effects. Palm^{11}-PrRP31 significantly reduced the Aβ plaque load by improving clearance via glymphatic pathway.

It further attenuated microgliosis not only in the hippocampi and cortices of a mouse model of AD-like Aβ pathology, but also in the cerebella of APP/PS1 mice. Treatment with palm^{11}-PrRP31 also decreased the levels of pro-inflammatory cytokines and pro-apoptotic proteins and increased the number of synapses.

5.4 Impact of HFD on metabolic parametres and development of AD-like pathology in APP/PS1 and WT mice

5.4.1 Peripheral effects of HFD

A growing body of evidence supports the idea of clinical connection between obesity, T2DM and AD with common pathogenic mechanisms. One of them could be low-grade chronic inflammation leading to peripheral IR, which could trigger tissue deterioration and overal health decline (De Felice et al., 2014). HFD induced obesity may lead to IR and cause inflammation not only in the periphery, but also in the CNS.

Chronic intake of HFD significantly increased BW of the mice and induced obesity. At the age of 6 months (4 months of HFD) no difference was observed between APP/PS1 and WT mice, similarly to previous studies (Ramos-Rodriguez et al., 2014, Graham et al., 2016). However, at the age of 10 months (8 months on HFD) significant weight gain was measured in HFD-fed APP/PS1 mice compared to HFD-fed WT mice. HFD induced obesity increased the weight of eWAT, resulted in increase in plasma leptin, cholesterol, and triacylglycerols in 6 and 10 months.

A large body of evidence have indicated that obesity is associated with a mild chronic inflammation, characterized by slightly increased levels of CRP, that is further linked to the development of IR (Misiak et al., 2012, Festa et al., 2003). In our study, HFD-obesity induced significant increase in CRP only in APP/PS1 mice in both, at the age of 6 and 10 months, suggesting AD-related pathology interacts with HFD in aggravating the chronic inflammation in the mice.

To reveal the impact of AD-related pathology on the glycemic regulation, the fasting glucose levels of mice were measured. Blood glucose measurements were significantly increased in HFD mice independently of genotype, but neither APP/PS1, nor WT mice turned diabetic, but only pre-diabetic, since glucose levels did not reach the indicative

level for diabetes (Clee and Attie, 2007, Ramos-Rodriguez et al., 2014, Lechuga-Sancho et al., 2006). However, the OGTT showed that an elevated glucose level was sustained in APP/PS1 mice compared to WT mice, not only on HFD, similarly as in the study of Lee (Lee et al., 2018), but also on STD. Insulin and FGF21 plasma levels as well as HOMA-IR index were significantly increased in HFD-fed mice in both 6 and 10 months and further worsening effect was observed in 10-month-old APP/PS1 mice, similarly as in the studies of others (Ramos-Rodriguez et al., 2014, Lee et al., 2018). These data support more severe glucose intolerance and IR when both AD and obesity are set together.

The livers of both APP/PS1 and WT mice on HFD exhibited significant liver abnormality, characterized by severe hepatomegaly, fat accumulation (steatosis), liver scarring (fibrosis), beginning from the age of 6 months. Interestingly, 8 months of HFD caused significant gain in liver weight of APP/PS1 mice compared to the WT mice. Furthermore, after 4 months on HFD, APP/PS1 mice developed significantly pronounced higher liver steatosis, and also started to develop liver fibrosis, compared to WT mice on HFD, which developed only mild steatosis and fibrosis, mainly at the age of 10 months. These results support increasing evidence of the involvement of liver disease in AD pathogenesis as the liver are thought to be a major player in the clearance of Aβ at the periphery. Imbalance in the peripheral Aβ clearance could lead to the disruption of Aβ clearance from the brain toward the brain accumulation, but the mechanism needs to be further studied (Kim et al., 2016, Kim et al., 2022, Estrada et al., 2019).

Skeletal muscle, liver, and eWAT are major insulin-responsive tissues that control glucose homeostasis (Huang et al., 2018). Glucose uptake in the muscle and adipose tissue is based on the insulin dependent GLUT4 whose malfunction is known to be involved in obesity-induced IR (Américo-Da-Silva et al., 2021, Abel et al., 2001). In this study, HFD significantly decreased level of muscular and adipose GLUT4, similarly as in the studies of others (Favaretto et al., 2014, Gaster et al., 2001, Seraphim et al., 2001), in both APP/PS1 and WT mice, suggesting reduction of glucose uptake. In obese patients, cellular insulin receptors are decreased and the magnitude of this decrease is inversely related to the degree of hyperinsulinemia (Huang et al., 2018). HFD reduced peripheral insulin signaling resulting in IR by the decrease of IRβ level in eWAT of both APP/PS1

and WT mice and, also in the livers and mucles of APP/PS1 mice. Levels of PI3K in the muscles and eWAT were mighty decreased similarly as reported in previous studies (Nelson et al., 2014, Huang et al., 2018, Kruszynska et al., 2002). Beyond, HFD caused decrease in activation of Akt in livers and eWAT, further confirming impairment of peripheral PI3K/Akt signaling pathway (Maletinska et al., 2015, Kimura et al., 2000). Impaired insulin pathway in peripheral tissues, caused by HFD and even more pronounced in APP/PS1 mice, could lead to obesity and T2DM as the result of IR, similarly as described in the study of Huang (Huang et al., 2018).

5.4.2 Central effects of HFD

Next, the burden of senile plaques and astrocytic and microglial reactivity were examined. 4 months of HFD did not induce any significant difference in the development of Aβ pathology compared to STD fed APP/PS1 mice, similarly as in previous studies (Aso et al., 2013, Beckett et al., 2013). However, consistently with other studies maintained for longer periods of time, (Ramos-Rodriguez et al., 2014), we observed a significant increase of Aβ plaque load in cortices of APP/PS1 mice fed with HFD for 8 months. Similarly, as in the previous study, APP/PS1 mice developed number of reactive astrocytes, and microglia in close proximity of Aβ plaques. HFD did not affect a level of astrocytosis. However, in accordance with previous study (Ramos-Rodriguez et al., 2014), higher number of reactive microglia was found in the hippocampi and cortices of HFD-fed APP/PS1 mice, supporting a role for neuroinflammation in this animal model. Furthermore, in our study, strong correlation was found between peripheral (CRP) and central (GFAP) inflammation that was calculated in the whole set of mice (Pearson r: 0.3924, p=0.0028 **), but also separately in WT mice (Pearson r: 0.4634, p=0.0130 *), providing a strong evidence suggesting that inflammation is one of the main denominators of obesity and AD.

Further, our study was aimed at revealing effect of HFD on Tau pathology. Level of total Tau was increased in 10-month-old APP/PS1 mice either on STD, or HFD although it was not statistically significant mainly because of a large variation between mice. However, in contrast to the study on 3xTg-AD mice (Julien et al., 2010), no progressive

increase in total Tau was revealed in HFD-fed mice. The amyloid cascade theory of AD etiology states that the accumulation of Aβ plaque accelerates the progression of Tau pathology (Selkoe and Hardy, 2016). In this study, Aβ plaques induced the accumulation of endogenous phosphorylated Tau within dystrophic neurites surrounding the plaques of APP/PS1 mice, similarly as in the study of Chen (Chen et al., 2021). HFD significantly aggravated both number and size of Tau clusters surrounding the plaques already in 6 months. Tau is considered to be responsible for the cytotoxic, dystrophic, and functional effects of Aβ (Bloom, 2014, Chabrier et al., 2014, Roberson et al., 2007, Jin et al., 2011), suggesting that huge Tau pathology increase in 6 months could further support neuroinflammatory and neurodegenerative effect of Aβ in APP/PS1 mice. Aβ and Tau pathologies and neuroinflammation are worsened in HFD-fed APP/PS1 mice, pointing towards the idea that metabolic disturbances related to obesity exacerbate the pathological hallmarks of AD (De Felice et al., 2014, Terzo et al., 2021, Bracko et al., 2020).

PI3K/Akt signaling is impaired in the brains of obese subjects with IR (Tabassum et al., 2020). HFD decreased level of IRβ and PI3K p85 in the hippocampus of 10-month-old APP/PS1 mice, suggesting development of central IR. Moreover, activation of Akt protein decreased in an age-dependent manner, supporting the most important role of age in the development of neurodegenerative diseases such as AD (Scott Bitner, 2012). In our study, strong negative correlations were computed between peripheral IR (HOMA-IR index) and hippocampal level of PI3K (Pearson r: -0.3226, p=0.0253) and p-Akt (Ser473) (Pearson r: -0.2941, p=0.0448) as markers of central IR. These data show that hyperinsulinemia, which can be induced by obesity, could lead to reduced activation of insulin signaling in the brain and prove strong evidence of IR being an interconnection between obesity, and AD-like pathology development

Loss of synapses and neuronal loss have been correlated with dementia in AD as an early event during the disease progression (Tabassum et al., 2020). To study contribution of obesity on neuronal changes, markers of synaptogenesis, neurogenesis and neuronal density were measured. In this study, previously reported decrease in synaptophysin in APP/PS1 mice (Holubova et al., 2019) was confirmed. Furthemore, decrease in synaptic markers was further pronounced in HFD-fed mice, similarly as in the studies of others

(Crispino et al., 2020, Arnold et al., 2014). However, although several studies report impaired hippocampal neurogenesis in HFD-fed murine models (Lindqvist et al., 2006, Bracke et al., 2019), any significant difference was found neither in neuronal density nor in early and late neurogenesis of APP/PS1 and WT mice on HFD. Similarly as in the study of Rupp (Rupp et al., 2011), where no changes in neuronal density or neurogenesis were observed between the APP/PS1 and WT mice.

Chronic inflammation inflicted by obesity can further cause a damage to the BBB that can have deleterious effects on the CNS (Rhea et al., 2017). To search for a possible effect of HFD on BBB disruption, claudin-5 and occludin, major components of tight junctions that are often affected during acute and chronic CNS diseases, such as AD (Kacirova et al., 2020), were measured. Unlike in previous studies, where hippocampal decrease of claudin and occludin was found in AD murine models (Sántha et al., 2015, Zhu et al., 2022, Kurz et al., 2022), no difference showing disruption of BBB were found between the strains in our study. The only difference observed was the age-related decrease of occludin, suggesting decrease in functionality of BBB.

In summary, HFD-related obesity worsened metabolic parametres connected to obesity, leading to glucose intolerance, insulin resistance and chronic peripheral inflammation as summed up in Figure 47. These dysregulations further promote disturbance in the hippocampal insulin signaling and neuroinflammation, leading to worsened Aβ and Tau pathology in APP/PS1 mice. Moreover, mice on HFD developed significant increase in liver weight and its abnormality, such as liver steatosis, or fibrosis. While slight decrease in synaptogenesis was observed in HFD-fed mice, no difference was seen in neurogenesis.

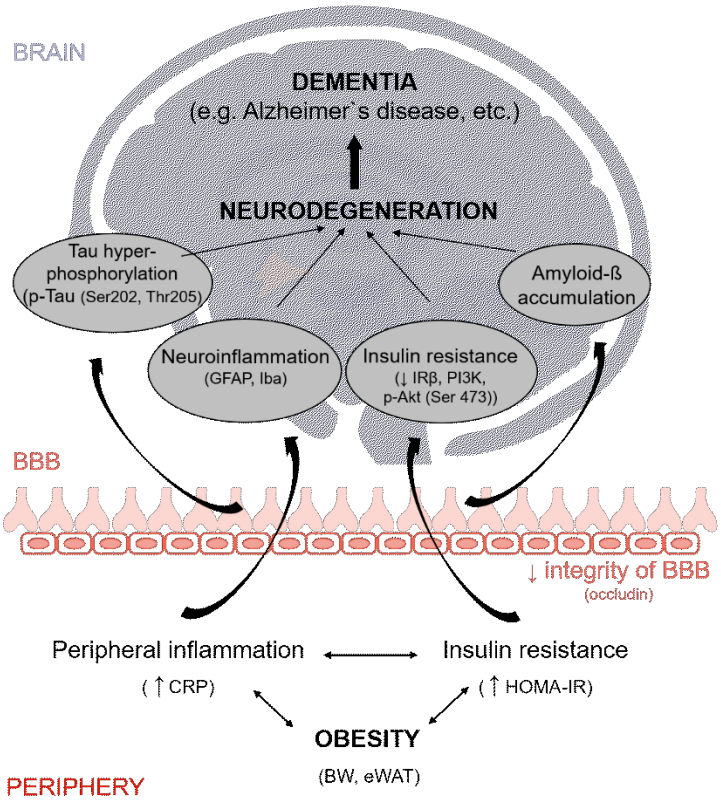

Figure 47: Summary of results from the study of HFD impact on metabolic parametres and development of AD-like pathology in APP/PS1 and WT mice.

BW – body weight; CRP – c-reactive protein; eWAT – epididymal white adipose tissue; GFAP – glial fibrillary acidic protein; HOMA-IR - homeostatic model assessment for insulin resistance; Iba - ionized calcium-binding adapter molecule; IRβ – insulin receptor β; PI3K - phosphoinositide 3-kinase

6. SUMMARY

In general, obesity is defined as a medical condition in which excess body fat has accumulated to the extent that it may have an adverse effect on health. Since obesity and related metabolic disturbances, such as IR and peripheral inflammation are widely accepted as risk factors of cognitive decline and AD, anorexigenic and antidiabetic peptides, such as PrRP seem to be potential neuroprotective agents.

In this study, a potential relationship between IR and AD was followed in the brains and periphery of APP/PS1 mice fed with a HFD, the model connecting obesity and AD-like pathology. The study revealed a deleterious effect of obesity-related inflammation and pre-diabetes on the development of Aβ pathology and neuroinflammation and confirmed peripheral and central inflammation and IR as potential mediators of brain dysfunction in AD.

Furthermore, potential neuroprotective effects of PrRP were studied in *in vitro* and *in vivo* models of neurodegeneration. PrRP31 and palm^{11}-PrRP31 exhibit neuroprotective effects in methylglyoxal-stressed SH-SY5Y cells and rat primary cortical neurons. These were confirmed in chronic administration of APP/PS1, a model of Aβ pathology, where palm^{11}-PrRP31significantly reduced the Aβ plaque load and microgliosis in the hippocampi, cortices, and cerebella. Furthermore, palm^{11}-PrRP31 increased the synaptogenesis and attenuated neuroinflammation and apoptosis in the hippocampus of APP/PS1 mice.

In conclusion, my thesis proves deleterious effectof HFD on AD-like pathology, and beneficial effect of PrRP in the AD-like pathology, suggesting palm^{11}-PrRP31 as a promising agent for the treatment of AD (Figure 48).

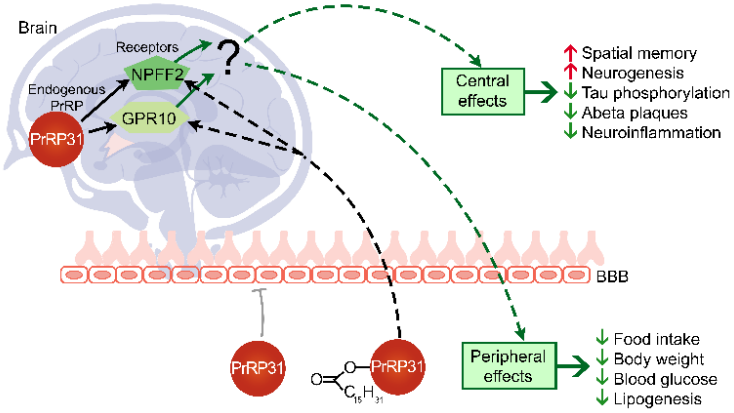

Figure 48: Central and peripheral effect of palm^{11}-PrRP31.

7. CONCLUSIONS

Neuroprotective effects of anorexigenic neuropeptide PrRP and its palmitoylated analog palm^{11}-PrRP31were studied in models of neurodegeneration *in vitro* in SH-SY5Y cells and rat primary cortical neurons and *in vivo* in APP/PS1 mice.

To conclude, the *in vitro* studies, PrRP and its lipidized analog palm^{11}-PrRP31 increased insulin signaling pathways in the same manner as insulin which is required for neuronal synaptic and dendritic plasticity, for learning, and for memory formation. We observed activation of these signaling pathways in our previous *in vivo* models of neurodegeneration, hence these could be the main pathways contributing to the potential neuroprotective effect of PrRP.

Furthermore, PrRP and its lipidized analog decreased the oxidative stress and increased viability in the MG-stressed SH-SY5Y cells and primary cortical cells. PrRP and palm^{11}-PrRP31 decreased apoptosis in the cells and Tau hyperphosphorylation, confirming our previous *in vivo* study (Popelova et al., 2018) and clarifying the potential mechanisms implicated in the neuroprotective properties of PrRP.

In conclusion of the *in vivo* studies, palm^{11}-PrRP31 exhibited multiple beneficial neuroprotective effects for APP/PS1 mice, which supports our previous findings. Palm^{11}-PrRP31 significantly reduced the Aβ plaque load by improved clearance via glymphatic pathway and attenuated microgliosis not only in the hippocampi and cortices of a mouse model of AD-like Aβ pathology, but also in the cerebella of APP/PS1 mice. Treatment with palm^{11}-PrRP31 also decreased the levels of pro-inflammatory cytokines and pro-apoptotic proteins and increased the number of synapses.

Based on the results from my PhD thesis, we would like to conclude that PrRP is a promising agent for alleviating different changes that occur in neurodegenerative disorders and it might be a potential drug against neurodegenerative disorders including Alzheimer´s disease.

To conclude our study of possible relationship among diet-induced obesity, IR, and inflammation in the periphery and development of neuropathological changes in the brain, HFD-related obesity worsened metabolic parameters connected to obesity, leading to glucose intolerance, insulin resistance and chronic peripheral inflammation. These

dysregulations further promote disturbance in hippocampal insulin signaling and neuroinflammation, leading to a worsening of Aβ and Tau pathology in APP/PS1 mice. Moreover, mice on HFD developed significant increase in liver weight and its abnormality, such as liver steatosis, or fibrosis.

Furthermore, we found a strong correlation not only between the peripheral and central insulin resistance, but also between the peripheral and central inflammation, both in APP/PS1 and WT mice. These results support the theory of inflammation and insulin resistance being the main common factors between obesity and AD.

8. REFERENCES

2021. 2021 Alzheimer's disease facts and figures. *Alzheimer's & Dementia,* 17**,** 327-406.

ABBOTT, N. J., PATABENDIGE, A. A., DOLMAN, D. E., YUSOF, S. R. & BEGLEY, D. J. 2010. Structure and function of the blood-brain barrier. *Neurobiol Dis,* 37**,** 13-25.

ABEL, E. D., PERONI, O., KIM, J. K., KIM, Y. B., BOSS, O., HADRO, E., MINNEMANN, T., SHULMAN, G. I. & KAHN, B. B. 2001. Adipose-selective targeting of the GLUT4 gene impairs insulin action in muscle and liver. *Nature,* 409**,** 729-33.

ACKERMAN, S. 1992. *Discovering the Brain.* Washington (DC): National Academies Press (US)

Copyright © 1992 by the National Academy of Sciences.

ALBERS, M. W., GILMORE, G. C., KAYE, J., MURPHY, C., WINGFIELD, A., BENNETT, D. A., BOXER, A. L., BUCHMAN, A. S., CRUICKSHANKS, K. J., DEVANAND, D. P., DUFFY, C. J., GALL, C. M., GATES, G. A., GRANHOLM, A. C., HENSCH, T., HOLTZER, R., HYMAN, B. T., LIN, F. R., MCKEE, A. C., MORRIS, J. C., PETERSEN, R. C., SILBERT, L. C., STRUBLE, R. G., TROJANOWSKI, J. Q., VERGHESE, J., WILSON, D. A., XU, S. & ZHANG, L. I. 2015. At the interface of sensory and motor dysfunctions and Alzheimer's disease. *Alzheimers Dement,* 11**,** 70-98.

ALLEN, P. B., ZACHARIOU, V., SVENNINGSSON, P., LEPORE, A. C., CENTONZE, D., COSTA, C., ROSSI, S., BENDER, G., CHEN, G., FENG, J., SNYDER, G. L., BERNARDI, G., NESTLER, E. J., YAN, Z., CALABRESI, P. & GREENGARD, P. 2006. Distinct roles for spinophilin and neurabin in dopamine-mediated plasticity. *Neuroscience,* 140**,** 897-911.

ALMOND, M. H., EDWARDS, M. R., BARCLAY, W. S. & JOHNSTON, S. L. 2013. Obesity and susceptibility to severe outcomes following respiratory viral infection. *Thorax,* 68**,** 684-6.

ALONSO, A. D., DI CLERICO, J., LI, B., CORBO, C. P., ALANIZ, M. E., GRUNDKE-IQBAL, I. & IQBAL, K. 2010. Phosphorylation of tau at Thr212, Thr231, and Ser262 combined causes neurodegeneration. *J Biol Chem,* 285**,** 30851-60.

ALVAREZ, A., MUÑOZ, J. P. & MACCIONI, R. B. 2001. A Cdk5-p35 stable complex is involved in the beta-amyloid-induced deregulation of Cdk5 activity in hippocampal neurons. *Exp Cell Res,* 264**,** 266-74.

AMÉRICO-DA-SILVA, L., AGUILERA, J., QUINTEROS-WALTEMATH, O., SÁNCHEZ-AGUILERA, P., RUSSELL, J., CADAGAN, C., MENESES-VALDÉS, R., SÁNCHEZ, G., ESTRADA, M., JORQUERA, G., BARRIENTOS, G. & LLANOS, P. 2021. Activation of the NLRP3 Inflammasome Increases the IL-1β Level and Decreases GLUT4 Translocation in Skeletal Muscle during Insulin Resistance. *Int J Mol Sci,* 22.

AMICARELLI, F., COLAFARINA, S., CATTANI, F., CIMINI, A., DI ILIO, C., CERU, M. P. & MIRANDA, M. 2003. Scavenging system efficiency is crucial for cell

resistance to ROS-mediated methylglyoxal injury. *Free Radical Biology and Medicine,* 35**,** 856-871.

ANAND, K. S. & DHIKAV, V. 2012. Hippocampus in health and disease: An overview. *Ann Indian Acad Neurol,* 15**,** 239-46.

ANGELONI, C., ZAMBONIN, L. & HRELIA, S. 2014. Role of methylglyoxal in Alzheimer's disease. *BioMed research international,* 2014**,** 238485-238485.

ARNOLD, S. E., LUCKI, I., BROOKSHIRE, B. R., CARLSON, G. C., BROWNE, C. A., KAZI, H., BANG, S., CHOI, B. R., CHEN, Y., MCMULLEN, M. F. & KIM, S. F. 2014. High fat diet produces brain insulin resistance, synaptodendritic abnormalities and altered behavior in mice. *Neurobiol Dis,* 67**,** 79-87.

ASO, E., SEMAKOVA, J., JODA, L., SEMAK, V., HALBAUT, L., CALPENA, A., ESCOLANO, C., PERALES, J. C. & FERRER, I. 2013. Triheptanoin supplementation to ketogenic diet curbs cognitive impairment in APP/PS1 mice used as a model of familial Alzheimer's disease. *Curr Alzheimer Res,* 10**,** 290-7.

ATZORI, C., GHETTI, B., PIVA, R., SRINIVASAN, A. N., ZOLO, P., DELISLE, M. B., MIRRA, S. S. & MIGHELI, A. 2001. Activation of the JNK/p38 pathway occurs in diseases characterized by tau protein pathology and is related to tau phosphorylation but not to apoptosis. *J Neuropathol Exp Neurol,* 60**,** 1190-7.

BAGNOL, D., AL-SHAMMA, H. A., BEHAN, D., WHELAN, K. & GROTTICK, A. J. 2012. Diet-induced models of obesity (DIO) in rodents. *Curr Protoc Neurosci,* Chapter 9**,** Unit 9.38.1-13.

BALLARD, C., GAUTHIER, S., CORBETT, A., BRAYNE, C., AARSLAND, D. & JONES, E. 2011. Alzheimer's disease. *Lancet,* 377**,** 1019-31.

BALOYANNIS, S. J., MAVROUDIS, I., MITILINEOS, D., BALOYANNIS, I. S. & COSTA, V. G. 2015. The hypothalamus in Alzheimer's disease: a Golgi and electron microscope study. *Am J Alzheimers Dis Other Demen,* 30**,** 478-87.

BAMBERGER, M. E., HARRIS, M. E., MCDONALD, D. R., HUSEMANN, J. & LANDRETH, G. E. 2003. A cell surface receptor complex for fibrillar beta-amyloid mediates microglial activation. *J Neurosci,* 23**,** 2665-74.

BAUM, L., HANSEN, L., MASLIAH, E. & SAITOH, T. 1996. Glycogen synthase kinase 3 alteration in alzheimer disease is related to neurofibrillary tangle formation. *Molecular and Chemical Neuropathology,* 29**,** 253-261.

BEATTIE, M. S., LI, Q. & BRESNAHAN, J. C. 2000. Cell death and plasticity after experimental spinal cord injury. *Prog Brain Res,* 128**,** 9-21.

BEAUQUIS, J., PAVÍA, P., POMILIO, C., VINUESA, A., PODLUTSKAYA, N., GALVAN, V. & SARAVIA, F. 2013. Environmental enrichment prevents astroglial pathological changes in the hippocampus of APP transgenic mice, model of Alzheimer's disease. *Exp Neurol,* 239**,** 28-37.

BECKETT, T. L., STUDZINSKI, C. M., KELLER, J. N., PAUL MURPHY, M. & NIEDOWICZ, D. M. 2013. A ketogenic diet improves motor performance but does not affect β-amyloid levels in a mouse model of Alzheimer's Disease. *Brain Research,* 1505**,** 61-67.

BEDNARCZYK, J. & LUKASIUK, K. 2011. Tight junctions in neurological diseases. *Acta Neurobiol Exp (Wars),* 71**,** 393-408.

BELFIORE, R., RODIN, A., FERREIRA, E., VELAZQUEZ, R., BRANCA, C., CACCAMO, A. & ODDO, S. 2019. Temporal and regional progression of Alzheimer's disease-like pathology in 3xTg-AD mice. *Aging Cell,* 18**,** e12873.

BELLIER, J., NOKIN, M. J., LARDE, E., KAROYAN, P., PEULEN, O., CASTRONOVO, V. & BELLAHCENE, A. 2019. Methylglyoxal, a potent inducer of AGEs, connects between diabetes and cancer. *Diabetes Res Clin Pract,* 148**,** 200-211.

BERGER, Z., RODER, H., HANNA, A., CARLSON, A., RANGACHARI, V., YUE, M., WSZOLEK, Z., ASHE, K., KNIGHT, J., DICKSON, D., ANDORFER, C., ROSENBERRY, T. L., LEWIS, J., HUTTON, M. & JANUS, C. 2007. Accumulation of pathological tau species and memory loss in a conditional model of tauopathy. *J Neurosci,* 27**,** 3650-62.

BERCHTOLD, N. C. & COTMAN, C. W. 1998. Evolution in the Conceptualization of Dementia and Alzheimer's Disease: Greco-Roman Period to the 1960s. *Neurobiology of Aging,* 19**,** 173-189.

BIEDLER, J. L., HELSON, L. & SPENGLER, B. A. 1973. Morphology and growth, tumorigenicity, and cytogenetics of human neuroblastoma cells in continuous culture. *Cancer Res,* 33**,** 2643-52.

BILLINGS, L. M., ODDO, S., GREEN, K. N., MCGAUGH, J. L. & LAFERLA, F. M. 2005. Intraneuronal Abeta causes the onset of early Alzheimer's disease-related cognitive deficits in transgenic mice. *Neuron,* 45**,** 675-88.

BLISS, T. V. & LOMO, T. 1973. Long-lasting potentiation of synaptic transmission in the dentate area of the anaesthetized rabbit following stimulation of the perforant path. *J Physiol,* 232**,** 331-56.

BLOOM, G. S. 2014. Amyloid-beta and tau: the trigger and bullet in Alzheimer disease pathogenesis. *JAMA Neurol,* 71**,** 505-8.

BOMFIM, T. R., FORNY-GERMANO, L., SATHLER, L. B., BRITO-MOREIRA, J., HOUZEL, J. C., DECKER, H., SILVERMAN, M. A., KAZI, H., MELO, H. M., MCCLEAN, P. L., HOLSCHER, C., ARNOLD, S. E., TALBOT, K., KLEIN, W. L., MUNOZ, D. P., FERREIRA, S. T. & DE FELICE, F. G. 2012. An anti-diabetes agent protects the mouse brain from defective insulin signaling caused by Alzheimer's disease- associated Aβ oligomers. *J Clin Invest,* 122**,** 1339-53.

BONDA, D. J., STONE, J. G., TORRES, S. L., SIEDLAK, S. L., PERRY, G., KRYSCIO, R., JICHA, G., CASADESUS, G., SMITH, M. A., ZHU, X. & LEE, H.-G. 2014. Dysregulation of leptin signaling in Alzheimer disease: evidence for neuronal leptin resistance. *Journal of Neurochemistry,* 128**,** 162-172.

BORCHELT, D. R. 1998. Metabolism of Presenilin 1: Influence of Presenilin 1 on Amyloid Precursor Protein Processing. *Neurobiology of Aging,* 19**,** S15-S18.

BOXER, A. L., RABINOVICI, G. D., KEPE, V., GOLDMAN, J., FURST, A. J., HUANG, S. C., BAKER, S. L., O'NEIL, J. P., CHUI, H., GESCHWIND, M. D., SMALL, G. W., BARRIO, J. R., JAGUST, W. & MILLER, B. L. 2007. Amyloid imaging in distinguishing atypical prion disease from Alzheimer disease. *Neurology,* 69**,** 283.

BRAAK, H., BRAAK, E. & BOHL, J. 1993. Staging of Alzheimer-related cortical destruction. *Eur Neurol,* 33**,** 403-8.

BRAAK, H., THAL, D. R., GHEBREMEDHIN, E. & DEL TREDICI, K. 2011. Stages of the pathologic process in Alzheimer disease: age categories from 1 to 100 years. *J Neuropathol Exp Neurol,* 70**,** 960-9.

BRACKE, A., DOMANSKA, G., BRACKE, K., HARZSCH, S., VAN DEN BRANDT, J., BRÖKER, B. & VON BOHLEN UND HALBACH, O. 2019. Obesity Impairs Mobility and Adult Hippocampal Neurogenesis. *J Exp Neurosci,* 13**,** 1179069519883580.

BRACKO, O., VINARCSIK, L. K., CRUZ HERNÁNDEZ, J. C., RUIZ-URIBE, N. E., HAFT-JAVAHERIAN, M., FALKENHAIN, K., RAMANAUSKAITE, E. M., ALI, M., MOHAPATRA, A., SWALLOW, M. A., NJIRU, B. N., MUSE, V., MICHELUCCI, P. E., NISHIMURA, N. & SCHAFFER, C. B. 2020. High fat diet worsens Alzheimer's disease-related behavioral abnormalities and neuropathology in APP/PS1 mice, but not by synergistically decreasing cerebral blood flow. *Scientific reports,* 10**,** 9884-9884.

BUETTNER, R., SCHÖLMERICH, J. & BOLLHEIMER, L. C. 2007. High-fat diets: modeling the metabolic disorders of human obesity in rodents. *Obesity (Silver Spring),* 15**,** 798-808.

BUKAR MAINA, M., AL-HILALY, Y. K. & SERPELL, L. C. 2016. Nuclear Tau and Its Potential Role in Alzheimer's Disease. *Biomolecules,* 6**,** 9.

CACCAMO, A., MAJUMDER, S., RICHARDSON, A., STRONG, R. & ODDO, S. 2010. Molecular interplay between mammalian target of rapamycin (mTOR), amyloid-beta, and Tau: effects on cognitive impairments. *J Biol Chem,* 285**,** 13107-20.

CAINE, D. & HODGES, J. R. 2001. Heterogeneity of semantic and visuospatial deficits in early Alzheimer's disease. *Neuropsychology,* 15**,** 155-64.

CARMODY, L. C., BAUCUM, A. J., 2ND, BASS, M. A. & COLBRAN, R. J. 2008. Selective targeting of the gamma1 isoform of protein phosphatase 1 to F-actin in intact cells requires multiple domains in spinophilin and neurabin. *Faseb j,* 22**,** 1660-71.

CLEE, S. M. & ATTIE, A. D. 2007. The genetic landscape of type 2 diabetes in mice. *Endocr Rev,* 28**,** 48-83.

CRISPINO, M., TRINCHESE, G., PENNA, E., CIMMINO, F., CATAPANO, A., VILLANO, I., PERRONE-CAPANO, C. & MOLLICA, M. P. 2020. Interplay between Peripheral and Central Inflammation in Obesity-Promoted Disorders: The Impact on Synaptic Mitochondrial Functions. *Int J Mol Sci,* 21.

CUÉNOD, C. A., DENYS, A., MICHOT, J. L., JEHENSON, P., FORETTE, F., KAPLAN, D., SYROTA, A. & BOLLER, F. 1993. Amygdala atrophy in Alzheimer's disease. An in vivo magnetic resonance imaging study. *Arch Neurol,* 50**,** 941-5.

CUMMINGS, J. 2021. New approaches to symptomatic treatments for Alzheimer’s disease. *Molecular Neurodegeneration,* 16**,** 2.

D'AMELIO, M., CAVALLUCCI, V., MIDDEI, S., MARCHETTI, C., PACIONI, S., FERRI, A., DIAMANTINI, A., DE ZIO, D., CARRARA, P., BATTISTINI, L., MORENO, S., BACCI, A., AMMASSARI-TEULE, M., MARIE, H. &

CECCONI, F. 2010. Caspase-3 triggers early synaptic dysfunction in a mouse model of Alzheimer's disease. *Nature Neuroscience,* 14**,** 69.
DANEMAN, R. & PRAT, A. 2015. The blood-brain barrier. *Cold Spring Harbor perspectives in biology,* 7**,** a020412-a020412.
DE ARRIBA, S. G., STUCHBURY, G., YARIN, J., BURNELL, J., LOSKE, C. & MÜNCH, G. 2007. Methylglyoxal impairs glucose metabolism and leads to energy depletion in neuronal cells—protection by carbonyl scavengers. *Neurobiology of Aging,* 28**,** 1044-1050.
DE FELICE, F. G., LOURENCO, M. V. & FERREIRA, S. T. 2014. How does brain insulin resistance develop in Alzheimer's disease? *Alzheimers Dement,* 10**,** S26-32.
DE LA MONTE, S. M. & WANDS, J. R. 2008. Alzheimer's disease is type 3 diabetes-evidence reviewed. *J Diabetes Sci Technol,* 2**,** 1101-13.
DESAI, K. M., CHANG, T., WANG, H., BANIGESH, A., DHAR, A., LIU, J., UNTEREINER, A. & WU, L. 2010. Oxidative stress and aging: Is methylglyoxal the hidden enemy?This review is one of a selection of papers published in a Special Issue on Oxidative Stress in Health and Disease. *Canadian Journal of Physiology and Pharmacology,* 88**,** 273-284.
DING, H., MATTHEWS, T. A. & JOHNSON, G. V. 2006. Site-specific phosphorylation and caspase cleavage differentially impact tau-microtubule interactions and tau aggregation. *J Biol Chem,* 281**,** 19107-14.
DRUCKER, D. J. 2006. The biology of incretin hormones. *Cell Metabolism,* 3**,** 153-165.
DU, J., SUZUKI, H., NAGASE, F., AKHAND, A. A., YOKOYAMA, T., MIYATA, T., KUROKAWA, K. & NAKASHIMA, I. 2000. Methylglyoxal induces apoptosis in Jurkat leukemia T cells by activating c-Jun N-terminal kinase. *J Cell Biochem,* 77**,** 333-44.
DUONG, S., PATEL, T. & CHANG, F. 2017. Dementia: What pharmacists need to know. *Canadian pharmacists journal : CPJ = Revue des pharmaciens du Canada : RPC,* 150**,** 118-129.
EKINCI, F. J. & SHEA, T. B. 1999. Hyperactivation of mitogen-activated protein kinase increases phospho-tau immunoreactivity within human neuroblastoma: additive and synergistic influence of alteration of additional kinase activities. *Cell Mol Neurobiol,* 19**,** 249-60.
EL KHOURY, J. B., MOORE, K. J., MEANS, T. K., LEUNG, J., TERADA, K., TOFT, M., FREEMAN, M. W. & LUSTER, A. D. 2003. CD36 mediates the innate host response to beta-amyloid. *J Exp Med,* 197**,** 1657-66.
ENGSTRÖM, M., BRANDT, A., WURSTER, S., SAVOLA, J. M. & PANULA, P. 2003. Prolactin releasing peptide has high affinity and efficacy at neuropeptide FF2 receptors. *Journal of Pharmacology and Experimental Therapeutics,* 305**,** 825-832.
ESTRADA, L. D., AHUMADA, P., CABRERA, D. & ARAB, J. P. 2019. Liver Dysfunction as a Novel Player in Alzheimer's Progression: Looking Outside the Brain. *Front Aging Neurosci,* 11**,** 174.
FAKHOURY, M. 2018. Microglia and Astrocytes in Alzheimer's Disease: Implications for Therapy. *Curr Neuropharmacol,* 16**,** 508-518.

FAN, X., LIU, B., ZHOU, J., GU, X., ZHOU, Y., YANG, Y., GUO, F., WEI, X., WANG, H., SI, N., YANG, J., BIAN, B. & ZHAO, H. 2021. High-Fat Diet Alleviates Neuroinflammation and Metabolic Disorders of APP/PS1 Mice and the Intervention With Chinese Medicine. *Front Aging Neurosci,* 13**,** 658376.

FAVARETTO, F., MILAN, G., COLLIN, G. B., MARSHALL, J. D., STASI, F., MAFFEI, P., VETTOR, R. & NAGGERT, J. K. 2014. GLUT4 defects in adipose tissue are early signs of metabolic alterations in Alms1GT/GT, a mouse model for obesity and insulin resistance. *PLoS One,* 9**,** e109540.

FEIN, J. A., SOKOLOW, S., MILLER, C. A., VINTERS, H. V., YANG, F., COLE, G. M. & GYLYS, K. H. 2008. Co-localization of amyloid beta and tau pathology in Alzheimer's disease synaptosomes. *Am J Pathol,* 172**,** 1683-92.

FESTA, A., HANLEY, A. J., TRACY, R. P., D'AGOSTINO, R., JR. & HAFFNER, S. M. 2003. Inflammation in the prediabetic state is related to increased insulin resistance rather than decreased insulin secretion. *Circulation,* 108**,** 1822-30.

FLORES-CORDERO, J. A., PÉREZ-PÉREZ, A., JIMÉNEZ-CORTEGANA, C., ALBA, G., FLORES-BARRAGÁN, A. & SÁNCHEZ-MARGALET, V. 2022. Obesity as a Risk Factor for Dementia and Alzheimer's Disease: The Role of Leptin. *Int J Mol Sci,* 23.

FÖRSTER, C., BUREK, M., ROMERO, I. A., WEKSLER, B., COURAUD, P. O. & DRENCKHAHN, D. 2008. Differential effects of hydrocortisone and TNFalpha on tight junction proteins in an in vitro model of the human blood-brain barrier. *J Physiol,* 586**,** 1937-49.

FRANCO, R., MARTINEZ-PINILLA, E., NAVARRO, G. & ZAMARBIDE, M. 2017. Potential of GPCRs to modulate MAPK and mTOR pathways in Alzheimer's disease. *Prog Neurobiol,* 149-150**,** 21-38.

FRANK, S., BURBACH, G. J., BONIN, M., WALTER, M., STREIT, W., BECHMANN, I. & DELLER, T. 2008. TREM2 is upregulated in amyloid plaque-associated microglia in aged APP23 transgenic mice. *Glia,* 56**,** 1438-47.

FREEMAN, M. R. & ROWITCH, D. H. 2013. Evolving concepts of gliogenesis: a look way back and ahead to the next 25 years. *Neuron,* 80**,** 613-23.

FROST, G. R. & LI, Y. M. 2017. The role of astrocytes in amyloid production and Alzheimer's disease. *Open Biol,* 7.

GASPARINI, L., GOURAS, G. K., WANG, R., GROSS, R. S., BEAL, M. F., GREENGARD, P. & XU, H. 2001. Stimulation of beta-amyloid precursor protein trafficking by insulin reduces intraneuronal beta-amyloid and requires mitogen-activated protein kinase signaling. *J Neurosci,* 21**,** 2561-70.

GASTER, M., STAEHR, P., BECK-NIELSEN, H., SCHRØDER, H. D. & HANDBERG, A. 2001. GLUT4 Is Reduced in Slow Muscle Fibers of Type 2 Diabetic Patients: Is Insulin Resistance in Type 2 Diabetes a Slow, Type 1 Fiber Disease? *Diabetes,* 50**,** 1324-1329.

GIANNAKOPOULOS, P., HERRMANN, F. R., BUSSIÈRE, T., BOURAS, C., KÖVARI, E., PERL, D. P., MORRISON, J. H., GOLD, G. & HOF, P. R. 2003. Tangle and neuron numbers, but not amyloid load, predict cognitive status in Alzheimer's disease. *Neurology,* 60**,** 1495-500.

GOEDERT, M., SPILLANTINI, M. G., JAKES, R., RUTHERFORD, D. & CROWTHER, R. A. 1989. Multiple isoforms of human microtubule-associated protein tau: sequences and localization in neurofibrillary tangles of Alzheimer's disease. *Neuron,* 3**,** 519-26.

GONÇALVES, A., AMBRÓSIO, A. F. & FERNANDES, R. 2013. Regulation of claudins in blood-tissue barriers under physiological and pathological states. *Tissue Barriers,* 1**,** e24782.

GONG, C. X., LIU, F., GRUNDKE-IQBAL, I. & IQBAL, K. 2006. Impaired brain glucose metabolism leads to Alzheimer neurofibrillary degeneration through a decrease in tau O-GlcNAcylation. *J Alzheimers Dis,* 9**,** 1-12.

GRAHAM, L. C., HARDER, J. M., SOTO, I., DE VRIES, W. N., JOHN, S. W. M. & HOWELL, G. R. 2016. Chronic consumption of a western diet induces robust glial activation in aging mice and in a mouse model of Alzheimer's disease. *Scientific Reports,* 6**,** 21568.

GREGOR, M. F. & HOTAMISLIGIL, G. S. 2011. Inflammatory Mechanisms in Obesity. *Annual Review of Immunology,* 29**,** 415-445.

GRUNDKE-IQBAL, I., IQBAL, K., TUNG, Y. C., QUINLAN, M., WISNIEWSKI, H. M. & BINDER, L. I. 1986. Abnormal phosphorylation of the microtubule-associated protein tau (tau) in Alzheimer cytoskeletal pathology. *Proc Natl Acad Sci U S A,* 83**,** 4913-7.

HAASS, C. & SELKOE, D. J. 2007. Soluble protein oligomers in neurodegeneration: lessons from the Alzheimer's amyloid beta-peptide. *Nat Rev Mol Cell Biol,* 8**,** 101-12.

HANSEN, D. V., HANSON, J. E. & SHENG, M. 2018. Microglia in Alzheimer's disease. *J Cell Biol,* 217**,** 459-472.

HENEKA, M. T., CARSON, M. J., EL KHOURY, J., LANDRETH, G. E., BROSSERON, F., FEINSTEIN, D. L., JACOBS, A. H., WYSS-CORAY, T., VITORICA, J., RANSOHOFF, R. M., HERRUP, K., FRAUTSCHY, S. A., FINSEN, B., BROWN, G. C., VERKHRATSKY, A., YAMANAKA, K., KOISTINAHO, J., LATZ, E., HALLE, A., PETZOLD, G. C., TOWN, T., MORGAN, D., SHINOHARA, M. L., PERRY, V. H., HOLMES, C., BAZAN, N. G., BROOKS, D. J., HUNOT, S., JOSEPH, B., DEIGENDESCH, N., GARASCHUK, O., BODDEKE, E., DINARELLO, C. A., BREITNER, J. C., COLE, G. M., GOLENBOCK, D. T. & KUMMER, M. P. 2015. Neuroinflammation in Alzheimer's disease. *Lancet Neurol,* 14**,** 388-405.

HERSOM, M., HELMS, H. C., SCHMALZ, C., PEDERSEN, T., BUCKLEY, S. T. & BRODIN, B. 2018. The insulin receptor is expressed and functional in cultured blood-brain barrier endothelial cells but does not mediate insulin entry from blood to brain. *Am J Physiol Endocrinol Metab,* 315**,** E531-e542.

HICKMAN, S. E., ALLISON, E. K. & EL KHOURY, J. 2008. Microglial dysfunction and defective beta-amyloid clearance pathways in aging Alzheimer's disease mice. *The Journal of neuroscience : the official journal of the Society for Neuroscience,* 28**,** 8354-8360.

HICKMAN, S. E., KINGERY, N. D., OHSUMI, T. K., BOROWSKY, M. L., WANG, L. C., MEANS, T. K. & EL KHOURY, J. 2013. The microglial sensome revealed by direct RNA sequencing. *Nat Neurosci,* 16**,** 1896-905.

HILLER, A. J. & ISHII, M. 2018. Disorders of Body Weight, Sleep and Circadian Rhythm as Manifestations of Hypothalamic Dysfunction in Alzheimer's Disease. *Frontiers in Cellular Neuroscience,* 12.

HINUMA, S., HABATA, Y., FUJII, R., KAWAMATAYUJI, HOSOYA, M., FUKUSUMI, S., KITADA, C., MASUO, Y., ASANO, T., MATSUMOTO, H., SEKIGUCHI, M., KUROKAWA, T., NISHIMURA, O., ONDA, H. & FUJINO, M. 1998. A prolactin-releasing peptide in the brain. *Nature,* 393**,** 272-276.

HIPPIUS, H. & NEUNDÖRFER, G. 2003. The discovery of Alzheimer's disease. *Dialogues Clin Neurosci,* 5**,** 101-8.

HIRONO, N., MORI, E., ISHII, K., IKEJIRI, Y., IMAMURA, T., SHIMOMURA, T., HASHIMOTO, M., YAMASHITA, H. & SASAKI, M. 1998. Frontal lobe hypometabolism and depression in Alzheimer's disease. *Neurology,* 50**,** 380.

HOLROYD, S., SHEPHERD, M. L. & DOWNS, J. H., 3RD 2000. Occipital atrophy is associated with visual hallucinations in Alzheimer's disease. *J Neuropsychiatry Clin Neurosci,* 12**,** 25-8.

HÖLSCHER, C. 2018. Novel dual GLP-1/GIP receptor agonists show neuroprotective effects in Alzheimer's and Parkinson's disease models. *Neuropharmacology,* 136**,** 251-259.

HÖLSCHER, C. & LI, L. 2010. New roles for insulin-like hormones in neuronal signalling and protection: new hopes for novel treatments of Alzheimer's disease? *Neurobiol Aging,* 31**,** 1495-502.

HOLUBOVA, M., HRUBA, L., POPELOVA, A., BENCZE, M., PRAZIENKOVA, V., GENGLER, S., KRATOCHVILOVA, H., HALUZIK, M., ZELEZNA, B., KUNES, J., HOLSCHER, C. & MALETINSKA, L. 2019. Liraglutide and a lipidized analog of prolactin-releasing peptide show neuroprotective effects in a mouse model of beta-amyloid pathology. *Neuropharmacology,* 144**,** 377-387.

HONG, S., BEJA-GLASSER, V. F., NFONOYIM, B. M., FROUIN, A., LI, S., RAMAKRISHNAN, S., MERRY, K. M., SHI, Q., ROSENTHAL, A., BARRES, B. A., LEMERE, C. A., SELKOE, D. J. & STEVENS, B. 2016. Complement and microglia mediate early synapse loss in Alzheimer mouse models. *Science,* 352**,** 712-716.

HORNG, S., THERATTIL, A., MOYON, S., GORDON, A., KIM, K., ARGAW, A. T., HARA, Y., MARIANI, J. N., SAWAI, S., FLODBY, P., CRANDALL, E. D., BOROK, Z., SOFRONIEW, M. V., CHAPOULY, C. & JOHN, G. R. 2017. Astrocytic tight junctions control inflammatory CNS lesion pathogenesis. *J Clin Invest,* 127**,** 3136-3151.

HOXHA, E., LIPPIELLO, P., ZURLO, F., BALBO, I., SANTAMARIA, R., TEMPIA, F. & MINIACI, M. C. 2018. The Emerging Role of Altered Cerebellar Synaptic Processing in Alzheimer's Disease. *Front Aging Neurosci,* 10**,** 396.

HSIEH, C. L., KOIKE, M., SPUSTA, S. C., NIEMI, E. C., YENARI, M., NAKAMURA, M. C. & SEAMAN, W. E. 2009. A role for TREM2 ligands in the phagocytosis of apoptotic neuronal cells by microglia. *J Neurochem,* 109**,** 1144-56.

HUANG, X., LIU, G., GUO, J. & SU, Z. 2018. The PI3K/AKT pathway in obesity and type 2 diabetes. *International journal of biological sciences,* 14**,** 1483-1496.

HULSHOF, L. A., FRAJMUND, L. A., VAN NUIJS, D., VAN DER HEIJDEN, D. C. N., MIDDELDORP, J. & HOL, E. M. 2022. Both male and female APPswe/PSEN1dE9 mice are impaired in spatial memory and cognitive flexibility at 9 months of age. *Neurobiology of Aging,* 113**,** 28-38.

HUNT, C. A., SCHENKER, L. J. & KENNEDY, M. B. 1996. PSD-95 is associated with the postsynaptic density and not with the presynaptic membrane at forebrain synapses. *J Neurosci,* 16**,** 1380-8.

CHABRIER, M. A., CHENG, D., CASTELLO, N. A., GREEN, K. N. & LAFERLA, F. M. 2014. Synergistic effects of amyloid-beta and wild-type human tau on dendritic spine loss in a floxed double transgenic model of Alzheimer's disease. *Neurobiol Dis,* 64**,** 107-17.

CHANG, Y. F., ZHANG, D., HU, W. M., LIU, D. X. & LI, L. 2020. Semaglutide-mediated protection against Aβ correlated with enhancement of autophagy and inhibition of apotosis. *J Clin Neurosci,* 81**,** 234-239.

CHEN, L., XU, S., WU, T., SHAO, Y., LUO, L., ZHOU, L., OU, S., TANG, H., HUANG, W., GUO, K. & XU, J. 2019. Studies on APP metabolism related to age-associated mitochondrial dysfunction in APP/PS1 transgenic mice. *Aging (Albany NY),* 11**,** 10242-10251.

CHEN, S., LIU, A.-R., AN, F.-M., YAO, W.-B. & GAO, X.-D. 2012. Amelioration of neurodegenerative changes in cellular and rat models of diabetes-related Alzheimer's disease by exendin-4. *AGE,* 34**,** 1211-1224.

CHEN, Y., ZHAO, S., FAN, Z., LI, Z., ZHU, Y., SHEN, T., LI, K., YAN, Y., TIAN, J., LIU, Z. & ZHANG, B. 2021. Metformin attenuates plaque-associated tau pathology and reduces amyloid-β burden in APP/PS1 mice. *Alzheimer's Research & Therapy,* 13**,** 40.

CHIU, S. L., CHEN, C. M. & CLINE, H. T. 2008. Insulin receptor signaling regulates synapse number, dendritic plasticity, and circuit function in vivo. *Neuron,* 58**,** 708-19.

CHO, J. H. & JOHNSON, G. V. 2004. Primed phosphorylation of tau at Thr231 by glycogen synthase kinase 3beta (GSK3beta) plays a critical role in regulating tau's ability to bind and stabilize microtubules. *J Neurochem,* 88**,** 349-58.

ILIFF, J. J., WANG, M., LIAO, Y., PLOGG, B. A., PENG, W., GUNDERSEN, G. A., BENVENISTE, H., VATES, G. E., DEANE, R., GOLDMAN, S. A., NAGELHUS, E. A. & NEDERGAARD, M. 2012. A Paravascular Pathway Facilitates CSF Flow Through the Brain Parenchyma and the Clearance of Interstitial Solutes, Including Amyloid β. *Science Translational Medicine,* 4**,** 147ra111.

JACK, C. R., JR., KNOPMAN, D. S., JAGUST, W. J., SHAW, L. M., AISEN, P. S., WEINER, M. W., PETERSEN, R. C. & TROJANOWSKI, J. Q. 2010.

Hypothetical model of dynamic biomarkers of the Alzheimer's pathological cascade. *Lancet Neurol,* 9**,** 119-28.

JACKSON, J., JAMBRINA, E., LI, J., MARSTON, H., MENZIES, F., PHILLIPS, K. & GILMOUR, G. 2019. Targeting the Synapse in Alzheimer's Disease. *Front Neurosci,* 13**,** 735.

JACOBS, H. I. L., VAN BOXTEL, M. P. J., JOLLES, J., VERHEY, F. R. J. & UYLINGS, H. B. M. 2012. Parietal cortex matters in Alzheimer's disease: An overview of structural, functional and metabolic findings. *Neuroscience & Biobehavioral Reviews,* 36**,** 297-309.

JANKOWSKY, J. L., SLUNT, H. H., RATOVITSKI, T., JENKINS, N. A., COPELAND, N. G. & BORCHELT, D. R. 2001. Co-expression of multiple transgenes in mouse CNS: a comparison of strategies. *Biomol Eng,* 17**,** 157-65.

JAWORSKI, J. & SHENG, M. 2006. The growing role of mTOR in neuronal development and plasticity. *Mol Neurobiol,* 34**,** 205-19.

JESSEN, N. A., MUNK, A. S. F., LUNDGAARD, I. & NEDERGAARD, M. 2015. The Glymphatic System: A Beginner's Guide. *Neurochemical Research,* 40**,** 2583-2599.

JI, K., AKGUL, G., WOLLMUTH, L. P. & TSIRKA, S. E. 2013. Microglia actively regulate the number of functional synapses. *PLoS One,* 8**,** e56293.

JICHA, G. A., WEAVER, C., LANE, E., VIANNA, C., KRESS, Y., ROCKWOOD, J. & DAVIES, P. 1999. cAMP-dependent protein kinase phosphorylations on tau in Alzheimer's disease. *J Neurosci,* 19**,** 7486-94.

JIN, M., SHEPARDSON, N., YANG, T., CHEN, G., WALSH, D. & SELKOE, D. J. 2011. Soluble amyloid beta-protein dimers isolated from Alzheimer cortex directly induce Tau hyperphosphorylation and neuritic degeneration. *Proc Natl Acad Sci U S A,* 108**,** 5819-24.

JOHNSON, G. V. & STOOTHOFF, W. H. 2004. Tau phosphorylation in neuronal cell function and dysfunction. *J Cell Sci,* 117**,** 5721-9.

JOHNSON, J. W. & KOTERMANSKI, S. E. 2006. Mechanism of action of memantine. *Curr Opin Pharmacol,* 6**,** 61-7.

JOLIVALT, C. G., LEE, C. A., BEISWENGER, K. K., SMITH, J. L., ORLOV, M., TORRANCE, M. A. & MASLIAH, E. 2008. Defective insulin signaling pathway and increased glycogen synthase kinase-3 activity in the brain of diabetic mice: Parallels with Alzheimer's disease and correction by insulin. *Journal of Neuroscience Research,* 86**,** 3265-3274.

JORDÀ-SIQUIER, T., PETREL, M., KOUSKOFF, V., CORDELIÈRES, F., FRYKMAN, S., MÜLLER, U., MULLE, C. & BARTHET, G. 2020. APP accumulates around dense-core amyloid plaques with presynaptic proteins in Alzheimer's disease brain. *bioRxiv***,** 2020.10.16.342196.

JULIEN, C., TREMBLAY, C., PHIVILAY, A., BERTHIAUME, L., EMOND, V., JULIEN, P. & CALON, F. 2010. High-fat diet aggravates amyloid-beta and tau pathologies in the 3xTg-AD mouse model. *Neurobiol Aging,* 31**,** 1516-31.

JUNG, C. H., RO, S. H., CAO, J., OTTO, N. M. & KIM, D. H. 2010. mTOR regulation of autophagy. *FEBS Lett,* 584**,** 1287-95.

KACIROVA, M., ZELEZNA, B., BLAZKOVA, M., HOLUBOVA, M., POPELOVA, A., KUNES, J., SEDIVA, B. & MALETINSKA, L. 2021. Aging and high-fat diet feeding lead to peripheral insulin resistance and sex-dependent changes in brain of mouse model of tau pathology THY-Tau22. *J Neuroinflammation,* 18**,** 141.

KACIROVA, M., ZMESKALOVA, A., KORINKOVA, L., ZELEZNA, B., KUNES, J. & MALETINSKA, L. 2020. Inflammation: major denominator of obesity, Type 2 diabetes and Alzheimer's disease-like pathology? *Clin Sci (Lond),* 134**,** 547-570.

KAPITZA, C., NOSEK, L., JENSEN, L., HARTVIG, H., JENSEN, C. B. & FLINT, A. 2015. Semaglutide, a once-weekly human GLP-1 analog, does not reduce the bioavailability of the combined oral contraceptive, ethinylestradiol/levonorgestrel. *J Clin Pharmacol,* 55**,** 497-504.

KHAN, U. A., LIU, L., PROVENZANO, F. A., BERMAN, D. E., PROFACI, C. P., SLOAN, R., MAYEUX, R., DUFF, K. E. & SMALL, S. A. 2014. Molecular drivers and cortical spread of lateral entorhinal cortex dysfunction in preclinical Alzheimer's disease. *Nat Neurosci,* 17**,** 304-11.

KIM, B., FIGUEROA-ROMERO, C., PACUT, C., BACKUS, C. & FELDMAN, E. L. 2015. Insulin Resistance Prevents AMPK-induced Tau Dephosphorylation through Akt-mediated Increase in AMPKSer-485 Phosphorylation. *J Biol Chem,* 290**,** 19146-57.

KIM, D. G., KRENZ, A., TOUSSAINT, L. E., MAURER, K. J., ROBINSON, S. A., YAN, A., TORRES, L. & BYNOE, M. S. 2016. Non-alcoholic fatty liver disease induces signs of Alzheimer's disease (AD) in wild-type mice and accelerates pathological signs of AD in an AD model. *J Neuroinflammation,* 13**,** 1.

KIM, G. A., OH, C. H., KIM, J. W., JEONG, S. J., OH, I. H., LEE, J. S., PARK, K. C. & SHIM, J. J. 2022. Association between non-alcoholic fatty liver disease and the risk of dementia: A nationwide cohort study. *Liver Int,* 42**,** 1027-1036.

KIM, S. H. & REAVEN, G. M. 2008. Insulin resistance and hyperinsulinemia: you can't have one without the other. *Diabetes Care,* 31**,** 1433-8.

KIMURA, A., OHMICHI, M., TASAKA, K., KANDA, Y., IKEGAMI, H., HAYAKAWA, J., HISAMOTO, K., MORISHIGE, K., HINUMA, S., KURACHI, H. & MURATA, Y. 2000. Prolactin-releasing peptide activation of the prolactin promoter is differentially mediated by extracellular signal-regulated protein kinase and c-Jun N-terminal protein kinase. *J Biol Chem,* 275**,** 3667-74.

KIVIMÄKI, M., LUUKKONEN, R., BATTY, G. D., FERRIE, J. E., PENTTI, J., NYBERG, S. T., SHIPLEY, M. J., ALFREDSSON, L., FRANSSON, E. I., GOLDBERG, M., KNUTSSON, A., KOSKENVUO, M., KUOSMA, E., NORDIN, M., SUOMINEN, S. B., THEORELL, T., VUOKSIMAA, E., WESTERHOLM, P., WESTERLUND, H., ZINS, M., KIVIPELTO, M., VAHTERA, J., KAPRIO, J., SINGH-MANOUX, A. & JOKELA, M. 2018. Body mass index and risk of dementia: Analysis of individual-level data from 1.3 million individuals. *Alzheimers Dement,* 14**,** 601-609.

KIVIPELTO, M., NGANDU, T., FRATIGLIONI, L., VIITANEN, M., KAREHOLT, I., WINBLAD, B., HELKALA, E. L., TUOMILEHTO, J., SOININEN, H. & NISSINEN, A. 2005. Obesity and vascular risk factors at midlife and the risk of dementia and Alzheimer disease. *Arch Neurol,* 62**,** 1556-60.

KLEINER, D. E., BRUNT, E. M., VAN NATTA, M., BEHLING, C., CONTOS, M. J., CUMMINGS, O. W., FERRELL, L. D., LIU, Y. C., TORBENSON, M. S., UNALP-ARIDA, A., YEH, M., MCCULLOUGH, A. J. & SANYAL, A. J. 2005. Design and validation of a histological scoring system for nonalcoholic fatty liver disease. *Hepatology,* 41**,** 1313-21.

KNIGHT, E. M., MARTINS, I. V., GÜMÜSGÖZ, S., ALLAN, S. M. & LAWRENCE, C. B. 2014. High-fat diet-induced memory impairment in triple-transgenic Alzheimer's disease (3xTgAD) mice is independent of changes in amyloid and tau pathology. *Neurobiol Aging,* 35**,** 1821-32.

KOŘÍNKOVÁ, L., HOLUBOVÁ, M., NEPRAŠOVÁ, B., HRUBÁ, L., STRNADOVÁ, V., BENCZE, M., HALUZIK, M., KUNES, J., MALETINSKA, L. & ZELEZNÁ, B. 2019. Synergistic effect of leptin and lipidized PrRP on metabolic pathways in ob/ob mice. *Journal of Molecular Endocrinology,* 64.

KRABBE, G., HALLE, A., MATYASH, V., RINNENTHAL, J. L., EOM, G. D., BERNHARDT, U., MILLER, K. R., PROKOP, S., KETTENMANN, H. & HEPPNER, F. L. 2013. Functional impairment of microglia coincides with Beta-amyloid deposition in mice with Alzheimer-like pathology. *PLoS One,* 8**,** e60921.

KRESS, B. T., ILIFF, J. J., XIA, M., WANG, M., WEI, H. S., ZEPPENFELD, D., XIE, L., KANG, H., XU, Q., LIEW, J. A., PLOG, B. A., DING, F., DEANE, R. & NEDERGAARD, M. 2014. Impairment of paravascular clearance pathways in the aging brain. *Annals of Neurology,* 76**,** 845-861.

KRUSZYNSKA, Y. T., WORRALL, D. S., OFRECIO, J., FRIAS, J. P., MACARAEG, G. & OLEFSKY, J. M. 2002. Fatty Acid-Induced Insulin Resistance: Decreased Muscle PI3K Activation But Unchanged Akt Phosphorylation. *The Journal of Clinical Endocrinology & Metabolism,* 87**,** 226-234.

KUEHN, B. M. 2020. In Alzheimer Research, Glucose Metabolism Moves to Center Stage. *JAMA,* 323**,** 297-299.

KUMMER, M. P., HAMMERSCHMIDT, T., MARTINEZ, A., TERWEL, D., EICHELE, G., WITTEN, A., FIGURA, S., STOLL, M., SCHWARTZ, S., PAPE, H.-C., SCHULTZE, J. L., WEINSHENKER, D., HENEKA, M. T. & URBAN, I. 2014. Ear2 deletion causes early memory and learning deficits in APP/PS1 mice. *The Journal of neuroscience : the official journal of the Society for Neuroscience,* 34**,** 8845-8854.

KUNEŠ, J., PRAŽIENKOVÁ, V., POPELOVÁ, A., MIKULÁŠKOVÁ, B., ZEMENOVÁ, J. & MALETÍNSKÁ, L. 2016. Prolactin-releasing peptide: a new tool for obesity treatment. *Journal of Endocrinology,* 230**,** R51-R58.

KURZ, C., WALKER, L., RAUCHMANN, B. S. & PERNECZKY, R. 2022. Dysfunction of the blood-brain barrier in Alzheimer's disease: Evidence from human studies. *Neuropathol Appl Neurobiol,* 48**,** e12782.

LAFAY-CHEBASSIER, C., PACCALIN, M., PAGE, G., BARC-PAIN, S., PERAULT-POCHAT, M. C., GIL, R., PRADIER, L. & HUGON, J. 2005. mTOR/p70S6k signalling alteration by Abeta exposure as well as in APP-PS1 transgenic models and in patients with Alzheimer's disease. *J Neurochem,* 94**,** 215-25.

LAMBON RALPH, M. A., PATTERSON, K., GRAHAM, N., DAWSON, K. & HODGES, J. R. 2003. Homogeneity and heterogeneity in mild cognitive

impairment and Alzheimer's disease: a cross-sectional and longitudinal study of 55 cases. *Brain,* 126**,** 2350-62.
LANSANG, M. C., WILLIAMS, G. H. & CARROLL, J. S. 2001. Correlation between the glucose clamp technique and the homeostasis model assessment in hypertension*. *American Journal of Hypertension,* 14**,** 51-53.
LAURENT, C., BUÉE, L. & BLUM, D. 2018. Tau and neuroinflammation: What impact for Alzheimer's Disease and Tauopathies? *Biomed J,* 41**,** 21-33.
LE CHATELIER, E., NIELSEN, T., QIN, J., PRIFTI, E., HILDEBRAND, F., FALONY, G., ALMEIDA, M., ARUMUGAM, M., BATTO, J. M., KENNEDY, S., LEONARD, P., LI, J., BURGDORF, K., GRARUP, N., JØRGENSEN, T., BRANDSLUND, I., NIELSEN, H. B., JUNCKER, A. S., BERTALAN, M., LEVENEZ, F., PONS, N., RASMUSSEN, S., SUNAGAWA, S., TAP, J., TIMS, S., ZOETENDAL, E. G., BRUNAK, S., CLÉMENT, K., DORÉ, J., KLEEREBEZEM, M., KRISTIANSEN, K., RENAULT, P., SICHERITZ-PONTEN, T., DE VOS, W. M., ZUCKER, J. D., RAES, J., HANSEN, T., BORK, P., WANG, J., EHRLICH, S. D. & PEDERSEN, O. 2013. Richness of human gut microbiome correlates with metabolic markers. *Nature,* 500**,** 541-6.
LEBOUCHER, A., LAURENT, C., FERNANDEZ-GOMEZ, F. J., BURNOUF, S., TROQUIER, L., EDDARKAOUI, S., DEMEYER, D., CAILLIEREZ, R., ZOMMER, N., VALLEZ, E., BANTUBUNGI, K., BRETON, C., PIGNY, P., BUÉE-SCHERRER, V., STAELS, B., HAMDANE, M., TAILLEUX, A., BUÉE, L. & BLUM, D. 2013. Detrimental effects of diet-induced obesity on τ pathology are independent of insulin resistance in τ transgenic mice. *Diabetes,* 62**,** 1681-8.
LEE, C. C., HUANG, C. C. & HSU, K. S. 2011. Insulin promotes dendritic spine and synapse formation by the PI3K/Akt/mTOR and Rac1 signaling pathways. *Neuropharmacology,* 61**,** 867-79.
LEE, C. Y. & LANDRETH, G. E. 2010. The role of microglia in amyloid clearance from the AD brain. *J Neural Transm (Vienna),* 117**,** 949-60.
LEE, G. & LEUGERS, C. J. 2012. Tau and tauopathies. *Prog Mol Biol Transl Sci,* 107**,** 263-93.
LEE, J. H., RYAN, J., ANDREESCU, C., AIZENSTEIN, H. & LIM, H. K. 2015. Brainstem morphological changes in Alzheimer's disease. *Neuroreport,* 26**,** 411-415.
LEE, Y. H., HSU, H. C., KAO, P. C., SHIAO, Y. J., YEH, S. H., SHIE, F. S., HSU, S. M., YEH, C. W., LIU, H. K., YANG, S. B. & TSAY, H. J. 2018. Augmented Insulin and Leptin Resistance of High Fat Diet-Fed APPswe/PS1dE9 Transgenic Mice Exacerbate Obesity and Glycemic Dysregulation. *Int J Mol Sci,* 19.
LECHUGA-SANCHO, A. M., ARROBA, A. I., FRAGO, L. M., PAÑEDA, C., GARCÍA-CÁCERES, C., DELGADO RUBÍN DE CÉLIX, A., ARGENTE, J. & CHOWEN, J. A. 2006. Activation of the intrinsic cell death pathway, increased apoptosis and modulation of astrocytes in the cerebellum of diabetic rats. *Neurobiol Dis,* 23**,** 290-9.
LEPPA, S. & BOHMANN, D. 1999. Diverse functions of JNK signaling and c-Jun in stress response and apoptosis. *Oncogene,* 18**,** 6158-62.

LEUZY, A., CHIOTIS, K., LEMOINE, L., GILLBERG, P. G., ALMKVIST, O., RODRIGUEZ-VIEITEZ, E. & NORDBERG, A. 2019. Tau PET imaging in neurodegenerative tauopathies-still a challenge. *Mol Psychiatry,* 24**,** 1112-1134.

LI, X. H., XIE, J. Z., JIANG, X., LV, B. L., CHENG, X. S., DU, L. L., ZHANG, J. Y., WANG, J. Z. & ZHOU, X. W. 2012. Methylglyoxal induces tau hyperphosphorylation via promoting AGEs formation. *Neuromolecular Med,* 14**,** 338-48.

LI, Y., DUFFY, K. B., OTTINGER, M. A., RAY, B., BAILEY, J. A., HOLLOWAY, H. W., TWEEDIE, D., PERRY, T., MATTSON, M. P., KAPOGIANNIS, D., SAMBAMURTI, K., LAHIRI, D. K. & GREIG, N. H. 2010. GLP-1 Receptor Stimulation Reduces Amyloid-β Peptide Accumulation and Cytotoxicity in Cellular and Animal Models of Alzheimer's Disease. *Journal of Alzheimer's Disease,* 19**,** 1205-1219.

LIDDELOW, S. A., GUTTENPLAN, K. A., CLARKE, L. E., BENNETT, F. C., BOHLEN, C. J., SCHIRMER, L., BENNETT, M. L., MÜNCH, A. E., CHUNG, W.-S., PETERSON, T. C., WILTON, D. K., FROUIN, A., NAPIER, B. A., PANICKER, N., KUMAR, M., BUCKWALTER, M. S., ROWITCH, D. H., DAWSON, V. L., DAWSON, T. M., STEVENS, B. & BARRES, B. A. 2017. Neurotoxic reactive astrocytes are induced by activated microglia. *Nature,* 541**,** 481-487.

LINDQVIST, A., MOHAPEL, P., BOUTER, B., FRIELINGSDORF, H., PIZZO, D., BRUNDIN, P. & ERLANSON-ALBERTSSON, C. 2006. High-fat diet impairs hippocampal neurogenesis in male rats. *Eur J Neurol,* 13**,** 1385-8.

LINDWALL, G. & COLE, R. D. 1984. Phosphorylation affects the ability of tau protein to promote microtubule assembly. *J Biol Chem,* 259**,** 5301-5.

LIU, Y., LIU, F., GRUNDKE-IQBAL, I., IQBAL, K. & GONG, C.-X. 2011. *Deficient brain insulin signaling pathway in Alzheimer's disease and diabetes*.

LIU, Y., LIU, F., GRUNDKE-IQBAL, I., IQBAL, K. & GONG, C. X. 2009. Brain glucose transporters, O-GlcNAcylation and phosphorylation of tau in diabetes and Alzheimer's disease. *J Neurochem,* 111**,** 242-9.

MAHAPATRA, M. K., KARUPPASAMY, M. & SAHOO, B. M. 2022. Therapeutic Potential of Semaglutide, a Newer GLP-1 Receptor Agonist, in Abating Obesity, Non-Alcoholic Steatohepatitis and Neurodegenerative diseases: A Narrative Review. *Pharm Res,* 39**,** 1233-1248.

MAIA, L. F., KAESER, S. A., REICHWALD, J., HRUSCHA, M., MARTUS, P., STAUFENBIEL, M. & JUCKER, M. 2013. Changes in amyloid-β and Tau in the cerebrospinal fluid of transgenic mice overexpressing amyloid precursor protein. *Sci Transl Med,* 5**,** 194re2.

MAIXNEROVA, J., SPOLCOVA, A., PYCHOVA, M., BLECHOVA, M., ELBERT, T., REZACOVA, M., ZELEZNA, B. & MALETINSKA, L. 2011. Characterization of prolactin-releasing peptide: binding, signaling and hormone secretion in rodent pituitary cell lines endogenously expressing its receptor. *Peptides,* 32**,** 811-7.

MAIXNEROVÁ, J., ŠPOLCOVÁ, A., PÝCHOVÁ, M., BLECHOVÁ, M., ELBERT, T., ŘEZÁČOVÁ, M., ŽELEZNÁ, B. & MALETÍNSKÁ, L. 2011. Characterization

of prolactin-releasing peptide: Binding, signaling and hormone secretion in rodent pituitary cell lines endogenously expressing its receptor. *Peptides,* 32**,** 811-817.
MALEK-AHMADI, M. & SABBAGH, M. N. 2015. Development and Validation of the Alzheimer's Questionnaire (AQ). *J Nat Sci,* 1**,** e104.
MALETINSKA, L., NAGELOVA, V., TICHA, A., ZEMENOVA, J., PIRNIK, Z., HOLUBOVA, M., SPOLCOVA, A., MIKULASKOVA, B., BLECHOVA, M., SYKORA, D., LACINOVA, Z., HALUZIK, M., ZELEZNA, B. & KUNES, J. 2015. Novel lipidized analogs of prolactin-releasing peptide have prolonged half-lives and exert anti-obesity effects after peripheral administration. *Int J Obes (Lond)*.
MALETÍNSKÁ, L., NAGELOVÁ, V., TICHÁ, A., ZEMENOVÁ, J., PIRNÍK, Z., HOLUBOVÁ, M., ŠPOLCOVÁ, A., MIKULÁŠKOVÁ, B., BLECHOVÁ, M., SÝKORA, D., LACINOVÁ, Z., HALUZÍK, M., ŽELEZNÁ, B. & KUNEŠ, J. 2015. Novel lipidized analogs of prolactin-releasing peptide have prolonged half-lives and exert anti-obesity effects after peripheral administration. *International Journal Of Obesity,* 39**,** 986.
MALETÍNSKÁ, L., POPELOVÁ, A., ŽELEZNÁ, B., BENCZE, M. & KUNEŠ, J. 2019. The impact of anorexigenic peptides in experimental models of Alzheimer's disease pathology. *Journal of Endocrinology,* 240**,** R47-R72.
MALETÍNSKÁ, L., ŠPOLCOVÁ, A., MAIXNEROVÁ, J., BLECHOVÁ, M. & ŽELEZNÁ, B. 2011. Biological properties of prolactin-releasing peptide analogs with a modified aromatic ring of a C-terminal phenylalanine amide. *Peptides,* 32**,** 1887-1892.
MAN, H. Y., LIN, J. W., JU, W. H., AHMADIAN, G., LIU, L., BECKER, L. E., SHENG, M. & WANG, Y. T. 2000. Regulation of AMPA receptor-mediated synaptic transmission by clathrin-dependent receptor internalization. *Neuron,* 25**,** 649-62.
MANTOVANI, A., SOZZANI, S., LOCATI, M., ALLAVENA, P. & SICA, A. 2002. Macrophage polarization: tumor-associated macrophages as a paradigm for polarized M2 mononuclear phagocytes. *Trends Immunol,* 23**,** 549-55.
MARTIN, L., LATYPOVA, X., WILSON, C. M., MAGNAUDEIX, A., PERRIN, M. L. & TERRO, F. 2013. Tau protein phosphatases in Alzheimer's disease: the leading role of PP2A. *Ageing Res Rev,* 12**,** 39-49.
MARTTINEN, M., TAKALO, M., NATUNEN, T., WITTRAHM, R., GABBOUJ, S., KEMPPAINEN, S., LEINONEN, V., TANILA, H., HAAPASALO, A. & HILTUNEN, M. 2018. Molecular Mechanisms of Synaptotoxicity and Neuroinflammation in Alzheimer's Disease. *Frontiers in Neuroscience,* 12.
MARUCCI, G., BUCCIONI, M., BEN, D. D., LAMBERTUCCI, C., VOLPINI, R. & AMENTA, F. 2021. Efficacy of acetylcholinesterase inhibitors in Alzheimer's disease. *Neuropharmacology,* 190**,** 108352.
MATSUZAKI, M., HONKURA, N., ELLIS-DAVIES, G. C. R. & KASAI, H. 2004. Structural basis of long-term potentiation in single dendritic spines. *Nature,* 429**,** 761-766.
MAWUENYEGA, K. G., SIGURDSON, W., OVOD, V., MUNSELL, L., KASTEN, T., MORRIS, J. C., YARASHESKI, K. E. & BATEMAN, R. J. 2010. Decreased clearance of CNS beta-amyloid in Alzheimer's disease. *Science,* 330**,** 1774.

MCCLEAN, P. L. & HÖLSCHER, C. 2014. Liraglutide can reverse memory impairment, synaptic loss and reduce plaque load in aged APP/PS1 mice, a model of Alzheimer's disease. *Neuropharmacology,* 76**,** 57-67.

MCCLEAN, P. L., JALEWA, J. & HÖLSCHER, C. 2015. Prophylactic liraglutide treatment prevents amyloid plaque deposition, chronic inflammation and memory impairment in APP/PS1 mice. *Behavioural Brain Research,* 293**,** 96-106.

MCCLEAN, P. L., PARTHSARATHY, V., FAIVRE, E. & HÖLSCHER, C. 2011. The Diabetes Drug Liraglutide Prevents Degenerative Processes in a Mouse Model of Alzheimer's Disease. *The Journal of Neuroscience,* 31**,** 6587-6594.

MEDEIROS, R. & LAFERLA, F. M. 2013. Astrocytes: conductors of the Alzheimer disease neuroinflammatory symphony. *Exp Neurol,* 239**,** 133-8.

MENGR, A., HRUBÁ, L., EXNEROVÁ, A., HOLUBOVÁ, M., POPELOVÁ, A., ŽELEZNÁ, B., KUNEŠ, J. & MALETÍNSKÁ, L. 2021. Palmitoylated Prolactin-releasing Peptide Reduced Aβ Plaques and Microgliosis in the Cerebellum: APP/PS1 Mice Study. *Curr Alzheimer Res,* 18**,** 607-622.

MIKULASKOVA, B., HOLUBOVA, M., PRAZIENKOVA, V., ZEMENOVA, J., HRUBA, L., HALUZIK, M., ZELEZNA, B., KUNES, J. & MALETINSKA, L. 2018. Lipidized prolactin-releasing peptide improved glucose tolerance in metabolic syndrome: Koletsky and spontaneously hypertensive rat study. *Nutr Diabetes,* 8**,** 5.

MINIACI, M. C. & DE LEONIBUS, E. 2018. Missing the egocentric spatial reference: a blank on the map. *F1000Res,* 7**,** 168.

MISIAK, B., LESZEK, J. & KIEJNA, A. 2012. Metabolic syndrome, mild cognitive impairment and Alzheimer's disease--the emerging role of systemic low-grade inflammation and adiposity. *Brain Res Bull,* 89**,** 144-9.

MITEW, S., KIRKCALDIE, M. T., DICKSON, T. C. & VICKERS, J. C. 2013. Altered synapses and gliotransmission in Alzheimer's disease and AD model mice. *Neurobiol Aging,* 34**,** 2341-51.

MONTPLAISIR, J., PETIT, D., LORRAIN, D., GAUTHIER, S. & NIELSEN, T. 1995. Sleep in Alzheimer's disease: further considerations on the role of brainstem and forebrain cholinergic populations in sleep-wake mechanisms. *Sleep,* 18**,** 145-8.

MU, Y. & GAGE, F. H. 2011. Adult hippocampal neurogenesis and its role in Alzheimer's disease. *Molecular Neurodegeneration,* 6**,** 85.

MUEED, Z., TANDON, P., MAURYA, S. K., DEVAL, R., KAMAL, M. A. & PODDAR, N. K. 2018. Tau and mTOR: The Hotspots for Multifarious Diseases in Alzheimer's Development. *Front Neurosci,* 12**,** 1017.

MULLARD, A. 2021. Controversial Alzheimer's drug approval could affect other diseases. *Nature,* 595**,** 162-163.

NAIK, P., FOFARIA, N., PRASAD, S., SAJJA, R. K., WEKSLER, B., COURAUD, P.-O., ROMERO, I. A. & CUCULLO, L. 2014. Oxidative and pro-inflammatory impact of regular and denicotinized cigarettes on blood brain barrier endothelial cells: is smoking reduced or nicotine-free products really safe? *BMC Neuroscience,* 15**,** 51.

NELSON, V. L., JIANG, Y. P., DICKMAN, K. G., BALLOU, L. M. & LIN, R. Z. 2014. Adipose tissue insulin resistance due to loss of PI3K p110α leads to decreased energy expenditure and obesity. *Am J Physiol Endocrinol Metab,* 306**,** E1205-16.

NEWCOMBE, E. A., CAMATS-PERNA, J., SILVA, M. L., VALMAS, N., HUAT, T. J. & MEDEIROS, R. 2018. Inflammation: the link between comorbidities, genetics, and Alzheimer's disease. *J Neuroinflammation,* 15**,** 276.

NICOLIA, V., FUSO, A., CAVALLARO, R. A., DI LUZIO, A. & SCARPA, S. 2010. B vitamin deficiency promotes tau phosphorylation through regulation of GSK3beta and PP2A. *J Alzheimers Dis,* 19**,** 895-907.

ODDO, S. 2012. The role of mTOR signaling in Alzheimer disease. *Frontiers in bioscience (Scholar edition),* 4**,** 941-952.

ODDO, S., CACCAMO, A., SHEPHERD, J. D., MURPHY, M. P., GOLDE, T. E., KAYED, R., METHERATE, R., MATTSON, M. P., AKBARI, Y. & LAFERLA, F. M. 2003. Triple-transgenic model of Alzheimer's disease with plaques and tangles: intracellular Abeta and synaptic dysfunction. *Neuron,* 39**,** 409-21.

OLABARRIA, M., NORISTANI, H. N., VERKHRATSKY, A. & RODRÍGUEZ, J. J. 2010. Concomitant astroglial atrophy and astrogliosis in a triple transgenic animal model of Alzheimer's disease. *Glia,* 58**,** 831-8.

OLABARRIA, M., NORISTANI, H. N., VERKHRATSKY, A. & RODRÍGUEZ, J. J. 2011. Age-dependent decrease in glutamine synthetase expression in the hippocampal astroglia of the triple transgenic Alzheimer's disease mouse model: mechanism for deficient glutamatergic transmission? *Molecular Neurodegeneration,* 6**,** 55.

PÅHLMAN, S., RUUSALA, A. I., ABRAHAMSSON, L., MATTSSON, M. E. & ESSCHER, T. 1984. Retinoic acid-induced differentiation of cultured human neuroblastoma cells: a comparison with phorbolester-induced differentiation. *Cell Differ,* 14**,** 135-44.

PARTHSARATHY, V. & HÖLSCHER, C. 2013. Chronic treatment with the GLP1 analogue liraglutide increases cell proliferation and differentiation into neurons in an AD mouse model. *PLoS One,* 8**,** e58784.

PAXINOS, G. & FRANKLIN, K. B. J. 2003. *The Mouse Brain In Stereotaxic Coordinates*.

PAYABVASH, S., SOUZA, L. C., WANG, Y., SCHAEFER, P. W., FURIE, K. L., HALPERN, E. F., GONZALEZ, R. G. & LEV, M. H. 2011. Regional ischemic vulnerability of the brain to hypoperfusion: the need for location specific computed tomography perfusion thresholds in acute stroke patients. *Stroke,* 42**,** 1255-60.

PEARSON, H. A. & PEERS, C. 2006. Physiological roles for amyloid beta peptides. *The Journal of physiology,* 575**,** 5-10.

PEDDITZI, E., PETERS, R. & BECKETT, N. 2016. The risk of overweight/obesity in mid-life and late life for the development of dementia: a systematic review and meta-analysis of longitudinal studies. *Age Ageing,* 45**,** 14-21.

PIHLAJA, R., KOISTINAHO, J., KAUPPINEN, R., SANDHOLM, J., TANILA, H. & KOISTINAHO, M. 2011. Multiple cellular and molecular mechanisms are

involved in human Aβ clearance by transplanted adult astrocytes. *Glia,* 59**,** 1643-57.
PIVOVAROVA, O., HÖHN, A., GRUNE, T., PFEIFFER, A. F. H. & RUDOVICH, N. 2016. Insulin-degrading enzyme: new therapeutic target for diabetes and Alzheimer's disease? *Annals of Medicine,* 48**,** 614-624.
PLATTNER, F., ANGELO, M. & GIESE, K. P. 2006. The roles of cyclin-dependent kinase 5 and glycogen synthase kinase 3 in tau hyperphosphorylation. *J Biol Chem,* 281**,** 25457-65.
PLUM, L., SCHUBERT, M. & BRÜNING, J. C. 2005. The role of insulin receptor signaling in the brain. *Trends Endocrinol Metab,* 16**,** 59-65.
POMYTKIN, I., COSTA-NUNES, J. P., KASATKIN, V., VENIAMINOVA, E., DEMCHENKO, A., LYUNDUP, A., LESCH, K. P., PONOMAREV, E. D. & STREKALOVA, T. 2018. Insulin receptor in the brain: Mechanisms of activation and the role in the CNS pathology and treatment. *CNS Neurosci Ther,* 24**,** 763-774.
POPELOVÁ, A., KÁKONOVÁ, A., HRUBÁ, L., KUNEŠ, J., MALETÍNSKÁ, L. & ŽELEZNÁ, B. 2018. Potential neuroprotective and anti-apoptotic properties of a long-lasting stable analog of ghrelin: an in vitro study using SH-SY5Y cells. *Physiol Res,* 67**,** 339-346.
POPELOVA, A., PRAZIENKOVA, V., NEPRASOVA, B., KASPEROVA, B. J., HRUBA, L., HOLUBOVA, M., ZEMENOVA, J., BLUM, D., ZELEZNA, B., GALAS, M. C., KUNES, J. & MALETINSKA, L. 2018. Novel Lipidized Analog of Prolactin-Releasing Peptide Improves Memory Impairment and Attenuates Hyperphosphorylation of Tau Protein in a Mouse Model of Tauopathy. *J Alzheimers Dis,* 62**,** 1725-1736.
PORTER, D. W., KERR, B. D., FLATT, P. R., HOLSCHER, C. & GAULT, V. A. 2010. Four weeks administration of Liraglutide improves memory and learning as well as glycaemic control in mice with high fat dietary-induced obesity and insulin resistance. *Diabetes, Obesity and Metabolism,* 12**,** 891-899.
PORTER, W. D., FLATT, P. R., HÖLSCHER, C. & GAULT, V. A. 2013. Liraglutide improves hippocampal synaptic plasticity associated with increased expression of Mash1 in ob/ob mice. *International Journal of Obesity,* 37**,** 678-684.
PRAZIENKOVA, V., POPELOVA, A., KUNES, J. & MALETINSKA, L. 2019a. Prolactin-Releasing Peptide: Physiological and Pharmacological Properties. *Int J Mol Sci,* 20.
PRAZIENKOVA, V., SCHIRMER, C., HOLUBOVA, M., ZELEZNA, B., KUNES, J., GALAS, M. C. & MALETINSKA, L. 2019b. Lipidized Prolactin-Releasing Peptide Agonist Attenuates Hypothermia-Induced Tau Hyperphosphorylation in Neurons. *J Alzheimers Dis,* 67**,** 1187-1200.
PRAŽIENKOVÁ, V., HOLUBOVÁ, M., PELANTOVÁ, H., BUGÁŇOVÁ, M., PIRNÍK, Z., MIKULÁŠKOVÁ, B., POPELOVÁ, A., BLECHOVÁ, M., HALUZÍK, M., ŽELEZNÁ, B., KUZMA, M., KUNEŠ, J. & MALETÍNSKÁ, L. 2017. Impact of novel palmitoylated prolactin-releasing peptide analogs on metabolic changes in mice with diet-induced obesity. *PLOS ONE,* 12**,** e0183449.

RAIMUNDO, A. F., FERREIRA, S., MARTINS, I. C. & MENEZES, R. 2020. Islet Amyloid Polypeptide: A Partner in Crime With Aβ in the Pathology of Alzheimer's Disease. *Front Mol Neurosci,* 13**,** 35.

RAMOS-RODRIGUEZ, J. J., ORTIZ-BARAJAS, O., GAMERO-CARRASCO, C., DE LA ROSA, P. R., INFANTE-GARCIA, C., ZOPEQUE-GARCIA, N., LECHUGA-SANCHO, A. M. & GARCIA-ALLOZA, M. 2014. Prediabetes-induced vascular alterations exacerbate central pathology in APPswe/PS1dE9 mice. *Psychoneuroendocrinology,* 48**,** 123-135.

RAMSDEN, M., KOTILINEK, L., FORSTER, C., PAULSON, J., MCGOWAN, E., SANTACRUZ, K., GUIMARAES, A., YUE, M., LEWIS, J., CARLSON, G., HUTTON, M. & ASHE, K. H. 2005. Age-Dependent Neurofibrillary Tangle Formation, Neuron Loss, and Memory Impairment in a Mouse Model of Human Tauopathy (P301L). *The Journal of Neuroscience,* 25**,** 10637.

RASMUSSEN, M. K., MESTRE, H. & NEDERGAARD, M. 2018. The glymphatic pathway in neurological disorders. *Lancet Neurol,* 17**,** 1016-1024.

RHEA, E., SALAMEH, T., LOGSDON, A., HANSON, A., ERICKSON, M. & BANKS, W. 2017. Blood-Brain Barriers in Obesity. *The AAPS Journal,* 19.

RICHARD, B. C., KURDAKOVA, A., BACHES, S., BAYER, T. A., WEGGEN, S. & WIRTHS, O. 2015. Gene Dosage Dependent Aggravation of the Neurological Phenotype in the 5XFAD Mouse Model of Alzheimer's Disease. *Journal of Alzheimer's Disease,* 45**,** 1223-1236.

ROBERSON, E. D., SCEARCE-LEVIE, K., PALOP, J. J., YAN, F., CHENG, I. H., WU, T., GERSTEIN, H., YU, G. Q. & MUCKE, L. 2007. Reducing endogenous tau ameliorates amyloid beta-induced deficits in an Alzheimer's disease mouse model. *Science,* 316**,** 750-4.

ROSS, R. A., SPENGLER, B. A. & BIEDLER, J. L. 1983. Coordinate morphological and biochemical interconversion of human neuroblastoma cells. *J Natl Cancer Inst,* 71**,** 741-7.

ROTHERMUNDT, M. & AROLT, V. 2007. CHAPTER 27 - Schizophrenia and Immunity. *In:* ADER, R. (ed.) *Psychoneuroimmunology (Fourth Edition).* Burlington: Academic Press.

RÜB, U., DEL TREDICI, K., SCHULTZ, C., THAL, D. R., BRAAK, E. & BRAAK, H. 2001. The autonomic higher order processing nuclei of the lower brain stem are among the early targets of the Alzheimer's disease-related cytoskeletal pathology. *Acta Neuropathol,* 101**,** 555-64.

RUBIO-PEREZ, J. M. & MORILLAS-RUIZ, J. M. 2012. A review: inflammatory process in Alzheimer's disease, role of cytokines. *TheScientificWorldJournal,* 2012**,** 756357-756357.

RUKMANGADACHAR, L. A. & BOLLU, P. C. 2022. Amyloid Beta Peptide. *StatPearls.* Treasure Island (FL): StatPearls Publishing

RUPP, N. J., WEGENAST-BRAUN, B. M., RADDE, R., CALHOUN, M. E. & JUCKER, M. 2011. Early onset amyloid lesions lead to severe neuritic abnormalities and local, but not global neuron loss in APPPS1 transgenic mice. *Neurobiol Aging,* 32**,** 2324.e1-6.

SAHU, M. P., NIKKILÄ, O., LÅGAS, S., KOLEHMAINEN, S. & CASTRÉN, E. 2019. Culturing primary neurons from rat hippocampus and cortex. *Neuronal Signal,* 3**,** Ns20180207.

SAIDO, T. & LEISSRING, M. A. 2012. Proteolytic degradation of amyloid β-protein. *Cold Spring Harb Perspect Med,* 2**,** a006379.

SALAKOU, S., KARDAMAKIS, D., TSAMANDAS, A. C., ZOLOTA, V., APOSTOLAKIS, E., TZELEPI, V., PAPATHANASOPOULOS, P., BONIKOS, D. S., PAPAPETROPOULOS, T., PETSAS, T. & DOUGENIS, D. 2007. Increased Bax/Bcl-2 ratio up-regulates caspase-3 and increases apoptosis in the thymus of patients with myasthenia gravis. *In Vivo,* 21**,** 123-32.

SAM, S. & MAZZONE, T. 2014. Adipose tissue changes in obesity and the impact on metabolic function. *Transl Res,* 164**,** 284-92.

SÁNTHA, P., VESZELKA, S., HOYK, Z., MÉSZÁROS, M., WALTER, F. R., TÓTH, A. E., KISS, L., KINCSES, A., OLÁH, Z., SEPRÉNYI, G., RÁKHELY, G., DÉR, A., PÁKÁSKI, M., KÁLMÁN, J., KITTEL, Á. & DELI, M. A. 2015. Restraint Stress-Induced Morphological Changes at the Blood-Brain Barrier in Adult Rats. *Front Mol Neurosci,* 8**,** 88.

SAPER, C. B. & GERMAN, D. C. 1987. Hypothalamic pathology in Alzheimer's disease. *Neuroscience Letters,* 74**,** 364-370.

SASMITA, A. O. 2019. Current viral-mediated gene transfer research for treatment of Alzheimer's disease. *Biotechnol Genet Eng Rev,* 35**,** 26-45.

SAUTER, A., GOLDSTEIN, M., ENGEL, J. & UETA, K. 1983. Effect of insulin on central catecholamines. *Brain Res,* 260**,** 330-3.

SCOTT BITNER, R. 2012. Cyclic AMP response element-binding protein (CREB) phosphorylation: a mechanistic marker in the development of memory enhancing Alzheimer's disease therapeutics. *Biochem Pharmacol,* 83**,** 705-14.

SELKOE, D. J. & HARDY, J. 2016. The amyloid hypothesis of Alzheimer's disease at 25 years. *EMBO Mol Med,* 8**,** 595-608.

SERAPHIM, P. M., NUNES, M. T. & MACHADO, U. F. 2001. GLUT4 protein expression in obese and lean 12-month-old rats: insights from different types of data analysis. *Braz J Med Biol Res,* 34**,** 1353-62.

SERRANO-POZO, A., GÓMEZ-ISLA, T., GROWDON, J. H., FROSCH, M. P. & HYMAN, B. T. 2013. A Phenotypic Change But Not Proliferation Underlies Glial Responses in Alzheimer Disease. *The American Journal of Pathology,* 182**,** 2332-2344.

SERRANO-POZO, A., MIELKE, M. L., GOMEZ-ISLA, T., BETENSKY, R. A., GROWDON, J. H., FROSCH, M. P. & HYMAN, B. T. 2011. Reactive glia not only associates with plaques but also parallels tangles in Alzheimer's disease. *Am J Pathol,* 179**,** 1373-84.

SHAHIDEHPOUR, R. K., HIGDON, R. E., CRAWFORD, N. G., NELTNER, J. H., IGHODARO, E. T., PATEL, E., PRICE, D., NELSON, P. T. & BACHSTETTER, A. D. 2021. Dystrophic microglia are associated with neurodegenerative disease and not healthy aging in the human brain. *Neurobiology of Aging,* 99**,** 19-27.

SHARMA, M. K., JALEWA, J. & HÖLSCHER, C. 2014. Neuroprotective and anti-apoptotic effects of liraglutide on SH-SY5Y cells exposed to methylglyoxal stress. *Journal of Neurochemistry,* 128**,** 459-471.

SHAULIAN, E. & KARIN, M. 2002. AP-1 as a regulator of cell life and death. *Nat Cell Biol,* 4**,** E131-6.

SHINOHARA, M., TACHIBANA, M., KANEKIYO, T. & BU, G. 2017. Role of LRP1 in the pathogenesis of Alzheimer's disease: evidence from clinical and preclinical studies. *Journal of lipid research,* 58**,** 1267-1281.

SHIPLEY, M. M., MANGOLD, C. A. & SZPARA, M. L. 2016. Differentiation of the SH-SY5Y Human Neuroblastoma Cell Line. *Journal of visualized experiments : JoVE***,** 53193-53193.

SCHAFE, G. E., DOYÈRE, V. & LEDOUX, J. E. 2005. Tracking the fear engram: the lateral amygdala is an essential locus of fear memory storage. *J Neurosci,* 25**,** 10010-4.

SCHEFF, S. W., PRICE, D. A., SCHMITT, F. A., DEKOSKY, S. T. & MUFSON, E. J. 2007. Synaptic alterations in CA1 in mild Alzheimer disease and mild cognitive impairment. *Neurology,* 68**,** 1501-8.

SCHEFF, S. W., PRICE, D. A., SCHMITT, F. A. & MUFSON, E. J. 2006. Hippocampal synaptic loss in early Alzheimer's disease and mild cognitive impairment. *Neurobiol Aging,* 27**,** 1372-84.

SIERRA-FILARDI, E., PUIG-KRÖGER, A., BLANCO, F. J., NIETO, C., BRAGADO, R., PALOMERO, M. I., BERNABÉU, C., VEGA, M. A. & CORBÍ, A. L. 2011. Activin A skews macrophage polarization by promoting a proinflammatory phenotype and inhibiting the acquisition of anti-inflammatory macrophage markers. *Blood,* 117**,** 5092-101.

SINGH-BAINS, M. K., LINKE, V., AUSTRIA, M. D. R., TAN, A. Y. S., SCOTTER, E. L., MEHRABI, N. F., FAULL, R. L. M. & DRAGUNOW, M. 2019. Altered microglia and neurovasculature in the Alzheimer's disease cerebellum. *Neurobiol Dis,* 132**,** 104589.

SINGH-MANOUX, A., DUGRAVOT, A., SHIPLEY, M., BRUNNER, E. J., ELBAZ, A., SABIA, S. & KIVIMAKI, M. 2018. Obesity trajectories and risk of dementia: 28 years of follow-up in the Whitehall II Study. *Alzheimers Dement,* 14**,** 178-186.

SMALL, G. W., ERCOLI, L. M., SILVERMAN, D. H., HUANG, S. C., KOMO, S., BOOKHEIMER, S. Y., LAVRETSKY, H., MILLER, K., SIDDARTH, P., RASGON, N. L., MAZZIOTTA, J. C., SAXENA, S., WU, H. M., MEGA, M. S., CUMMINGS, J. L., SAUNDERS, A. M., PERICAK-VANCE, M. A., ROSES, A. D., BARRIO, J. R. & PHELPS, M. E. 2000. Cerebral metabolic and cognitive decline in persons at genetic risk for Alzheimer's disease. *Proc Natl Acad Sci U S A,* 97**,** 6037-42.

SOFRONIEW, M. V. 2009. Molecular dissection of reactive astrogliosis and glial scar formation. *Trends Neurosci,* 32**,** 638-47.

SOFRONIEW, M. V. & VINTERS, H. V. 2010. Astrocytes: biology and pathology. *Acta Neuropathol,* 119**,** 7-35.

SPOLCOVA, A., MIKULASKOVA, B., HOLUBOVA, M., NAGELOVA, V., PIRNIK, Z., ZEMENOVA, J., HALUZIK, M., ZELEZNA, B., GALAS, M. C. &

MALETINSKA, L. 2015. Anorexigenic lipopeptides ameliorate central insulin signaling and attenuate tau phosphorylation in hippocampi of mice with monosodium glutamate-induced obesity. *J Alzheimers Dis,* 45**,** 823-35.

SQUIRE, L. R. 1992. Memory and the hippocampus: a synthesis from findings with rats, monkeys, and humans. *Psychol Rev,* 99**,** 195-231.

SRIPETCHWANDEE, J., CHATTIPAKORN, N. & CHATTIPAKORN, S. C. 2018. Links Between Obesity-Induced Brain Insulin Resistance, Brain Mitochondrial Dysfunction, and Dementia. *Front Endocrinol (Lausanne),* 9**,** 496.

STEELE, M. L. & ROBINSON, S. R. 2012. Reactive astrocytes give neurons less support: implications for Alzheimer's disease. *Neurobiol Aging,* 33**,** 423.e1-13.

STEWART, C. R., STUART, L. M., WILKINSON, K., VAN GILS, J. M., DENG, J., HALLE, A., RAYNER, K. J., BOYER, L., ZHONG, R., FRAZIER, W. A., LACY-HULBERT, A., EL KHOURY, J., GOLENBOCK, D. T. & MOORE, K. J. 2010. CD36 ligands promote sterile inflammation through assembly of a Toll-like receptor 4 and 6 heterodimer. *Nat Immunol,* 11**,** 155-61.

STICKLES, X. B., MARCHION, D. C., BICAKU, E., AL SAWAH, E., ABBASI, F., XIONG, Y., BOU ZGHEIB, N., BOAC, B. M., ORR, B. C., JUDSON, P. L., BERRY, A., HAKAM, A., WENHAM, R. M., APTE, S. M., BERGLUND, A. E. & LANCASTER, J. M. 2015. BAD-mediated apoptotic pathway is associated with human cancer development. *International journal of molecular medicine,* 35**,** 1081-1087.

SU, J. H., DENG, G. & COTMAN, C. W. 1997. Bax protein expression is increased in Alzheimer's brain: correlations with DNA damage, Bcl-2 expression, and brain pathology. *J Neuropathol Exp Neurol,* 56**,** 86-93.

SUMMERS, S. A. & BIRNBAUM, M. J. 1997. A role for the serine/threonine kinase, Akt, in insulin-stimulated glucose uptake. *Biochem Soc Trans,* 25**,** 981-8.

SWEATT, J. D. 2001. The neuronal MAP kinase cascade: a biochemical signal integration system subserving synaptic plasticity and memory. *J Neurochem,* 76**,** 1-10.

SWEENEY, M. D., SAGARE, A. P. & ZLOKOVIC, B. V. 2018. Blood–brain barrier breakdown in Alzheimer disease and other neurodegenerative disorders. *Nature Reviews Neurology,* 14**,** 133-150.

SWIECH, L., PERYCZ, M., MALIK, A. & JAWORSKI, J. 2008. Role of mTOR in physiology and pathology of the nervous system. *Biochim Biophys Acta,* 1784**,** 116-32.

ŠPOLCOVÁ, A. 2015. Impact of different types of antidiabetic interventions on the development of neurodegenerative changes in brains of diabetic mice and rats. Praha, 2015. Dizertační práce. Univerzita Karlova, 1. lékařská fakulta.

TABASSUM, S., MISRANI, A. & YANG, L. 2020. Exploiting Common Aspects of Obesity and Alzheimer's Disease. *Frontiers in human neuroscience,* 14**,** 602360-602360.

TABATON, M., ZHU, X., PERRY, G., SMITH, M. A. & GILIBERTO, L. 2010. Signaling effect of amyloid-beta(42) on the processing of AbetaPP. *Exp Neurol,* 221**,** 18-25.

TAI, J., LIU, W., LI, Y., LI, L. & HÖLSCHER, C. 2018. Neuroprotective effects of a triple GLP-1/GIP/glucagon receptor agonist in the APP/PS1 transgenic mouse model of Alzheimer's disease. *Brain Res,* 1678**,** 64-74.

TAJES, M., ERASO-PICHOT, A., RUBIO-MOSCARDÓ, F., GUIVERNAU, B., BOSCH-MORATÓ, M., VALLS-COMAMALA, V. & MUÑOZ, F. J. 2014a. Methylglyoxal reduces mitochondrial potential and activates Bax and caspase-3 in neurons: Implications for Alzheimer's disease. *Neuroscience Letters,* 580**,** 78-82.

TAJES, M., ERASO-PICHOT, A., RUBIO-MOSCARDÓ, F., GUIVERNAU, B., BOSCH-MORATÓ, M., VALLS-COMAMALA, V. & MUÑOZ, F. J. 2014b. Methylglyoxal reduces mitochondrial potential and activates Bax and caspase-3 in neurons: Implications for Alzheimer's disease. *Neurosci Lett,* 580**,** 78-82.

TAKASHIMA, A. 2006. GSK-3 is essential in the pathogenesis of Alzheimer's disease. *J Alzheimers Dis,* 9**,** 309-17.

TAKEDA, S., SATO, N., RAKUGI, H. & MORISHITA, R. 2011. Molecular mechanisms linking diabetes mellitus and Alzheimer disease: beta-amyloid peptide, insulin signaling, and neuronal function. *Mol Biosyst,* 7**,** 1822-7.

TALBOOM, J. S., VELAZQUEZ, R. & ODDO, S. 2015. The mammalian target of rapamycin at the crossroad between cognitive aging and Alzheimer's disease. *npj Aging and Mechanisms of Disease,* 1**,** 15008.

TAYLOR, R. 2012. Insulin resistance and type 2 diabetes. *Diabetes,* 61**,** 778-9.

TERZO, S., AMATO, A. & MULÈ, F. 2021. From obesity to Alzheimer's disease through insulin resistance. *J Diabetes Complications,* 35**,** 108026.

THAL, D. R., RONISZ, A., TOUSSEYN, T., RIJAL UPADHAYA, A., BALAKRISHNAN, K., VANDENBERGHE, R., VANDENBULCKE, M., VON ARNIM, C. A. F., OTTO, M., BEACH, T. G., LILJA, J., HEURLING, K., CHAKRABARTY, A., ISMAIL, A., BUCKLEY, C., SMITH, A. P. L., KUMAR, S., FARRAR, G. & WALTER, J. 2019. Different aspects of Alzheimer's disease-related amyloid β-peptide pathology and their relationship to amyloid positron emission tomography imaging and dementia. *Acta Neuropathologica Communications,* 7**,** 178.

TRAMUTOLA, A., TRIPLETT, J. C., DI DOMENICO, F., NIEDOWICZ, D. M., MURPHY, M. P., COCCIA, R., PERLUIGI, M. & BUTTERFIELD, D. A. 2015. Alteration of mTOR signaling occurs early in the progression of Alzheimer disease (AD): analysis of brain from subjects with pre-clinical AD, amnestic mild cognitive impairment and late-stage AD. *J Neurochem,* 133**,** 739-49.

TUPPO, E. E. & ARIAS, H. R. 2005. The role of inflammation in Alzheimer's disease. *Int J Biochem Cell Biol,* 37**,** 289-305.

VAN GOOL, B., STORCK, S. E., REEKMANS, S. M., LECHAT, B., GORDTS, P. L. S. M., PRADIER, L., PIETRZIK, C. U. & ROEBROEK, A. J. M. 2019. LRP1 Has a Predominant Role in Production over Clearance of Aβ in a Mouse Model of Alzheimer's Disease. *Molecular Neurobiology,* 56**,** 7234-7245.

VAN HOESEN, G. W., HYMAN, B. T. & DAMASIO, A. R. 1991. Entorhinal cortex pathology in Alzheimer's disease. *Hippocampus,* 1**,** 1-8.

VARGHESE, B. V., KOOHESTANI, F., MCWILLIAMS, M., COLVIN, A., GUNEWARDENA, S., KINSEY, W. H., NOWAK, R. A., NOTHNICK, W. B. & CHENNATHUKUZHI, V. M. 2013. Loss of the repressor REST in uterine fibroids promotes aberrant G protein-coupled receptor 10 expression and activates mammalian target of rapamycin pathway. *Proc Natl Acad Sci U S A,* 110**,** 2187-92.

VILSBØLL, T. & HOLST, J. J. 2004. Incretins, insulin secretion and Type 2 diabetes mellitus. *Diabetologia,* 47**,** 357-366.

VOGT, P. K. 2002. Fortuitous convergences: the beginnings of JUN. *Nature Reviews Cancer,* 2**,** 465-469.

WALSH, D. M., KLYUBIN, I., FADEEVA, J. V., CULLEN, W. K., ANWYL, R., WOLFE, M. S., ROWAN, M. J. & SELKOE, D. J. 2002. Naturally secreted oligomers of amyloid beta protein potently inhibit hippocampal long-term potentiation in vivo. *Nature,* 416**,** 535-9.

WANG, C., CHEN, X., DING, X., HE, Y., GU, C. & ZHOU, L. 2015a. Exendin-4 Promotes Beta Cell Proliferation via PI3k/Akt Signalling Pathway. *Cellular Physiology and Biochemistry,* 35**,** 2223-2232.

WANG, J., TAN, L., WANG, H. F., TAN, C. C., MENG, X. F., WANG, C., TANG, S. W. & YU, J. T. 2015b. Anti-inflammatory drugs and risk of Alzheimer's disease: an updated systematic review and meta-analysis. *J Alzheimers Dis,* 44**,** 385-96.

WANG, W. Y., TAN, M. S., YU, J. T. & TAN, L. 2015c. Role of pro-inflammatory cytokines released from microglia in Alzheimer's disease. *Ann Transl Med,* 3**,** 136.

WATSON, G. S. & CRAFT, S. 2004. Modulation of memory by insulin and glucose: neuropsychological observations in Alzheimer's disease. *Eur J Pharmacol,* 490**,** 97-113.

WEINGARTEN, M. D., LOCKWOOD, A. H., HWO, S. Y. & KIRSCHNER, M. W. 1975. A protein factor essential for microtubule assembly. *Proceedings of the National Academy of Sciences of the United States of America,* 72**,** 1858-1862.

WEN, A. Y., SAKAMOTO, K. M. & MILLER, L. S. 2010. The role of the transcription factor CREB in immune function. *J Immunol,* 185**,** 6413-9.

WHITMER, R. A., GUSTAFSON, D. R., BARRETT-CONNOR, E., HAAN, M. N., GUNDERSON, E. P. & YAFFE, K. 2008. Central obesity and increased risk of dementia more than three decades later. *Neurology,* 71**,** 1057-64.

WINSLOW, B. T., ONYSKO, M. K., STOB, C. M. & HAZLEWOOD, K. A. 2011. Treatment of Alzheimer disease. *Am Fam Physician,* 83**,** 1403-12.

WU, C. J., QIAN, X. & O'ROURKE, D. M. 1999. Sustained mitogen-activated protein kinase activation is induced by transforming erbB receptor complexes. *DNA Cell Biol,* 18**,** 731-41.

WYSS-CORAY, T., LOIKE, J. D., BRIONNE, T. C., LU, E., ANANKOV, R., YAN, F., SILVERSTEIN, S. C. & HUSEMANN, J. 2003. Adult mouse astrocytes degrade amyloid-beta in vitro and in situ. *Nat Med,* 9**,** 453-7.

WYSS-CORAY, T. & MUCKE, L. 2002. Inflammation in neurodegenerative disease--a double-edged sword. *Neuron,* 35**,** 419-32.

XIE, H. R., HU, L. S. & LI, G. Y. 2010. SH-SY5Y human neuroblastoma cell line: in vitro cell model of dopaminergic neurons in Parkinson's disease. *Chin Med J (Engl),* 123**,** 1086-92.

XU, F., NA, L., LI, Y. & CHEN, L. 2020. Roles of the PI3K/AKT/mTOR signalling pathways in neurodegenerative diseases and tumours. *Cell & bioscience,* 10**,** 54-54.

XU, W. L., ATTI, A. R., GATZ, M., PEDERSEN, N. L., JOHANSSON, B. & FRATIGLIONI, L. 2011. Midlife overweight and obesity increase late-life dementia risk: a population-based twin study. *Neurology,* 76**,** 1568-74.

XUE, J., SCHMIDT, S. V., SANDER, J., DRAFFEHN, A., KREBS, W., QUESTER, I., DE NARDO, D., GOHEL, T. D., EMDE, M., SCHMIDLEITHNER, L., GANESAN, H., NINO-CASTRO, A., MALLMANN, M. R., LABZIN, L., THEIS, H., KRAUT, M., BEYER, M., LATZ, E., FREEMAN, T. C., ULAS, T. & SCHULTZE, J. L. 2014. Transcriptome-based network analysis reveals a spectrum model of human macrophage activation. *Immunity,* 40**,** 274-88.

YAMAGUCHI, A., TAMATANI, M., MATSUZAKI, H., NAMIKAWA, K., KIYAMA, H., VITEK, M. P., MITSUDA, N. & TOHYAMA, M. 2001. Akt activation protects hippocampal neurons from apoptosis by inhibiting transcriptional activity of p53. *J Biol Chem,* 276**,** 5256-64.

YANG, X., FENG, P., ZHANG, X., LI, D., WANG, R., JI, C., LI, G. & HÖLSCHER, C. 2019. The diabetes drug semaglutide reduces infarct size, inflammation, and apoptosis, and normalizes neurogenesis in a rat model of stroke. *Neuropharmacology,* 158**,** 107748.

YANG, Y., KIM, J., KIM, H. Y., RYOO, N., LEE, S., KIM, Y., RHIM, H. & SHIN, Y.-K. 2015. Amyloid-β Oligomers May Impair SNARE-Mediated Exocytosis by Direct Binding to Syntaxin 1a. *Cell reports,* 12**,** 1244-1251.

YOUNGREN, J. F., PAIK, J. & BARNARD, R. J. 2001. Impaired insulin-receptor autophosphorylation is an early defect in fat-fed, insulin-resistant rats. *J Appl Physiol (1985),* 91**,** 2240-7.

YOUSEFI, B. H., VON REUTERN, B., SCHERUBL, D., MANOOK, A., SCHWAIGER, M., GRIMMER, T., HENRIKSEN, G., FORSTER, S., DRZEZGA, A. & WESTER, H. J. 2015. FIBT versus florbetaben and PiB: a preclinical comparison study with amyloid-PET in transgenic mice. *EJNMMI Res,* 5**,** 20.

YU, M., BENJAMIN, M. M., SRINIVASAN, S., MORIN, E. E., SHISHATSKAYA, E. I., SCHWENDEMAN, S. P. & SCHWENDEMAN, A. 2018. Battle of GLP-1 delivery technologies. *Adv Drug Deliv Rev,* 130**,** 113-130.

ZHANG, D., LIU, Z. X., CHOI, C. S., TIAN, L., KIBBEY, R., DONG, J., CLINE, G. W., WOOD, P. A. & SHULMAN, G. I. 2007. Mitochondrial dysfunction due to long-chain Acyl-CoA dehydrogenase deficiency causes hepatic steatosis and hepatic insulin resistance. *Proc Natl Acad Sci U S A,* 104**,** 17075-80.

ZHANG, L., QIAN, Y., LI, J., ZHOU, X., XU, H., YAN, J., XIANG, J., YUAN, X., SUN, B., SISODIA, S. S., JIANG, Y. H., CAO, X., JING, N. & LIN, A. 2021. BAD-mediated neuronal apoptosis and neuroinflammation contribute to Alzheimer's disease pathology. *iScience,* 24**,** 102942.

ZHANG, L., XIE, H. & CUI, L. 2018. Activation of astrocytes and expression of inflammatory cytokines in rats with experimental autoimmune encephalomyelitis. *Exp Ther Med,* 16**,** 4401-4406.

ZHANG, L., ZHANG, L., LI, L. & HÖLSCHER, C. 2019. Semaglutide is Neuroprotective and Reduces α-Synuclein Levels in the Chronic MPTP Mouse Model of Parkinson's Disease. *Journal of Parkinson's Disease,* 9**,** 157-171.

ZHANG, X., YEUNG, D. C., KARPISEK, M., STEJSKAL, D., ZHOU, Z. G., LIU, F., WONG, R. L., CHOW, W. S., TSO, A. W., LAM, K. S. & XU, A. 2008. Serum FGF21 levels are increased in obesity and are independently associated with the metabolic syndrome in humans. *Diabetes,* 57**,** 1246-53.

ZHAO, W., CHEN, H., XU, H., MOORE, E., MEIRI, N., QUON, M. J. & ALKON, D. L. 1999. Brain insulin receptors and spatial memory. Correlated changes in gene expression, tyrosine phosphorylation, and signaling molecules in the hippocampus of water maze trained rats. *J Biol Chem,* 274**,** 34893-902.

ZHENG, W. H., KAR, S. & QUIRION, R. 2002. Insulin-like growth factor-1-induced phosphorylation of transcription factor FKHRL1 is mediated by phosphatidylinositol 3-kinase/Akt kinase and role of this pathway in insulin-like growth factor-1-induced survival of cultured hippocampal neurons. *Mol Pharmacol,* 62**,** 225-33.

ZHOU, X. W., TANILA, H. & PEI, J. J. 2008. Parallel increase in p70 kinase activation and tau phosphorylation (S262) with Abeta overproduction. *FEBS Lett,* 582**,** 159-64.

ZHU, N., WEI, M., YUAN, L., HE, X., CHEN, C., JI, A. & ZHANG, G. 2022. Claudin-5 relieves cognitive decline in Alzheimer's disease mice through suppression of inhibitory GABAergic neurotransmission. *Aging (Albany NY),* 14**,** 3554-3568.

ZILBERTER, Y. & ZILBERTER, M. 2017. The vicious circle of hypometabolism in neurodegenerative diseases: Ways and mechanisms of metabolic correction. *J Neurosci Res,* 95**,** 2217-2235.

ZLOKOVIC, B. V. 2011. Neurovascular pathways to neurodegeneration in Alzheimer's disease and other disorders. *Nature Reviews Neuroscience,* 12**,** 723-738.

ZMESKALOVA, A., POPELOVA, A., EXNEROVA, A., ZELEZNA, B., KUNES, J. & MALETINSKA, L. 2020. Cellular Signaling and Anti-Apoptotic Effects of Prolactin-Releasing Peptide and Its Analog on SH-SY5Y Cells. *Int J Mol Sci,* 21.

ZOTOVA, E., HOLMES, C., JOHNSTON, D., NEAL, J. W., NICOLL, J. A. & BOCHE, D. 2011. Microglial alterations in human Alzheimer's disease following Aβ42 immunization. *Neuropathol Appl Neurobiol,* 37**,** 513-24.

WEB SITES

https://www.alz.org/alzheimers-dementia/research_progress/earlier-diagnosis

https://www.who.int/news-room/fact-sheets/detail/dementia

https://clinicaltrials.gov/ct2/show/NCT01255163

https://www.alzheimers.org.uk/about-dementia/treatments/drugs/antipsychotic-drugs

https://www.who.int/news-room/fact-sheets/detail/obesity-and-overweight

https://www.thermofisher.com/cz/en/home/life-science/cell-culture/primary-cell-culture/neuronal-cell-culture.html